

*Politehnica University Timișoara
Mechanics Faculty
Mechatronics Department*



***Modeling, simulation and experimental research
on technical and biological systems***

Argeșanu Veronica

2016

Table of Contents

Abstract.....	3
Rezumat	7
I Scientific achievements.....	11
1.Constructive and functional optimization of the mechanical face seals through modeling, simulation and experimental work.....	11
1.1.Basic topics of mechanical seals	11
1.2. Lipseals and mechanical face seals performance criteria.....	15
1.3. The flowing-friction dependency at a mechanical face seal.....	19
1.4. The elastohydrodynamic (EHD) lubrication of a mechanical face seal.....	23
1.5.Model and analysis of a mechanical seal by finite element method. Interface tension distribution.....	29
1.6. Interface contact pressure distribution in dynamic contact face seals; Analyzed by FEM.....	33
1.7.Automotive Mechanical Face Seals – Tribological Simulation.....	38
1.8. Calculation by Finite Element Method (FEM) of Temperature Distribution in the Components of a Mechanical Face Seal.....	48
2. Constructive and functional analysis of machine parts used in road vehicles	55
2.1 Rectangular section circlips / retaining rings axial load - carrying capacity considerations.....	55
2.2 Considerations upon the circular section of the circlips/retaining rings axial load-carrying capacity.....	62
2.3 On the priority of the modulus versus the center distance predimensioning of the evolventical gear calculus.....	66
2.4 Determination of the optimum variant of shaft-hub joint for gears.....	70
2.5 Hydraulic and thermographical test rig for automatic gearboxes.....	75
2.6 The energetic balance of the friction clutches used in automotive.....	80
2.7 Active suspension LQ control for improving riding comfort.....	85
3. Modeling, simulation and experimental work on biological systems.....	91
3.1 Car seats ergonomic evaluation.....	91
3.2 The drivers spine analytical model.....	102
3.3 The drivers spine movement equation in the coronal plane.....	115

3.4.Experimental determination of the intervertebral stress.....124

3.5. Modeling, simulation and experimental determination of the spine muscles activities of the driver.....132

3.6. Human body posture before and after maxillofacial surgery.....140

II. Academic and professional achievements.....143

III. Career evolution and development plans.....149

IV. References.....152

Abstract

The current thesis is the consequence of the author's research efforts during the 2000-2016 period at Politehnica University Timișoara, being focused on: 1. Constructive and functional optimization of the mechanical face seals through modeling, simulation and experimental work; 2. Constructive and functional analysis of machine parts used in road vehicles; 3. Modeling, simulation and experimental work on biological systems.

This holds only a part of the research in mechanical systems design, road vehicles design and ergonomics during the time mentioned, research that embedded diverse areas from analytical modeling, finite model modeling and experimental work to application fields such as road vehicles ergonomics and medicine and maxillofacial ergonomics.

In the recent years it has become more clear that the technical systems evolution is strongly influenced by the outbreak from materials science domain, advanced technologies, information technology and electronics and mechatronics.

This allows the increase of research and optimizations in mechanical construction domain.

Since the *Phd* thesis elaborated in 1998 the professional activities in the field of research and education had the topics related to mechanical engineering, flow and heat transfer in mechanical face seals and ergonomics. Until 2007 the topics were mostly in the field of mechanical engineering, specifically mechanical face seals, joints, clutches, gears as a result of research contracts from the national level (CEEX 21 I 03/07.10.2005/, *Research about the possibilities of using robotic systems with the ai of increasing Romanian industry*; 36/1999 cod CNCSU 204/1999, *Means and methods for mechanical transmissions and its components research :Results implementation in education units and economic units with industrial profile*, 36/1998 cod CNCSU 280/1998, *Means and methods for mechanical transmissions and its components research Experimental research*), international -FP7 250485/2010 ThinkMotion or with private partners. - S.C. ROSEAL S.A and because the activity was oriented in the machine design field –applications and teaching, construction and design of road vehicles teaching.

So, this was the reason for making the experimental research. The research results were published in 6 ISI Journals, 16 ISI Proceedings and IEEE Explore papers, 39 in Scopus database, 53 in other database-Google (Scholar) Academic.

The issues that were considered were

1. *Constructive and functional optimization of the mechanical face seals through modeling, simulation and experimental work*;
- 1.1. Argeșanu, V.; Popa, A., The elasto-hydrodynamics (EHD) lubrication of a mechanical face seal, The revue of Tribology Fascicle VIII, „The Annals of University Dunărea de Jos of Galați”, ISSN 1221-4590, 2004, pp. 136 – 139.
- 1.2. Argeșanu, V.; Mădăras, L., Model and analysis of a Mechanical seal by Finit Element Method. Interface Tension Distribution, Facta universitatis-series Mechanics; Automatic control and robots, ISSN 0354-2009, 2003, Vol. 3, no. 15
- 1.3. Argeșanu, V.; Popa, A., Interface contact pressure distribution in Dynamic contact face seals, analyzed by FEM, 3rd International Conference With International Scientific Comitee Research and Development in Mechanical Industry, RaDMI, ISBN 86-83803-10-4, 2003

- 1.4. Argeşanu, V. ; Kulcsar, R.M.; Borozan, I.S., Automotive Mechanical Face Seals Tribological Simulation, Journal of the Balkan Tribological Association, ISSN 1310-4772, 2011, Vol. 17, no. 1, pp. 1 -12.
- 1.5. Argeşanu, V.; Kulcsar, R.M.; Farkaş, I.A., Calculation by Finite Element Method(FEM) of Temperature Distribution in the Components of a Mechanical Face Seal, Journal of the Balkan Tribological Association, ISSN 1310-4772, 2011, vol. 17, no.1, pp.13-20.
2. *Constructive and functional analysis of machine parts used in road vehicles;*
 - 2.1. Argeşanu, V.; Luchin, M.; Jula, M.; Mărgineanu, D., Considerations Upon the Circular Section Circlips/Retaining Rings Axial Load-Carrying Capacity, ANNALS of DAAAM for 2008 & Proceedings of the 19th International DAAAM Symposium, ISBN 978-3-901509-68-1, 2008, pp. 33-34.
 - 2.2. Argeşanu, V.; Jula, M.; Cărăbas, I., Determination of the Optimum Variant of Shaft-Hub Joint for Gears, ANNALS of DAAAM for 2009 & Proceedings of the 20th international DAAAM Symposium, ISBN 978-3-901509-70-4, 2009, vol. 20, pp. 1881-1882.
3. *Modeling, simulation and experimental work on biological systems;*
 - 3.1. Argeşanu, V.; Kulcsar R.M.; Borozan I.S., The drivers spine analytical model International Journal of Biology and Biomedical Engineering, ISSN 19984510, 2014, vol. 8, pp. 172-178
 - 3.2. Kulcsar R.M.; Borozan I.S.; Argeşanu V., Experimental determination of the intervertebral stress, 12th IEEE International Symposium on Intelligent Systems and Informatics (SISY), 2014, pp. 303-307.
 - 3.3. Streian, F.; Argeşanu, V.; Kulcsar, R.M.; Borozan, I.S.; Jula, M.; Talpoş-Niculescu, C., Human Body Posture before and after Maxillofacial Surgery, Procedia Engineering, ISBN 1877-7058, 2014, Vol. 69, 508-511.

The first part refers to the optimization of the mechanical face seals from the point of view of construction criteria and functioning, the specific conditions concerning the environment and the durability have a great impact on the construction of the mechanical equipment. The complete adjustment of all the types of mechanical seals implies additional anticorrosive and calorific protection of the elastic pre-tensioned component, the cooling of the surface, which are in contact, and recirculation and/or the evacuation of the discharge flow.

A great diversity of contact-seals designs, materials, operating conditions, and factor that affect their performance have not yet allowed the general conclusions on friction and wear of these seals to be drawn.

The simple model of the complex friction between the surfaces in contact, when taking into account the hydrostatic theory of lubrication, is functional both for convergent surfaces and for divergent ones, with the necessary particularities. If the hydrostatic effect of lubrication is combined with the mechanical effect of the solid contact with friction, the problem of mixed friction that appears at mechanical face seals can be solved. Afterwards, the hydrodynamic effect of lubrication can also be introduced.

There are various causes for face seal leaks. Leakage normally takes place through the radial seal gap formed by the two sliding surfaces. Calculations are based on the assumption that a hydrodynamic film exists in face seals and that the leakage can be calculated in accordance with the known equations for laminar flow through a radial annular gap. The form of the surfaces can, however, be altered by heating and wear, for instance.

Modeling to access solutions is the goal of predictive engineering. The research deals with the boundary element analysis or the numerical simulation of the behavior of a mechanical face

seal. The present boundary element analysis is a particularly one for it contains the nonlinear effect due to changes in boundary conditions resulting from the contact of the static ring and the sealing head of the face seal. These all have significant influence on the behavior of the system. The results can be used for optimizing designs, predicting limits or investigating failures.

In the second part the focus is on the constructive and functional analysis of machine parts used in road vehicles:

Some interesting aspects about the strength of helical gears are presented: the beam strength and the surface strength. A "minimum modulus" that guarantees the resistance of the gear at both strength, the beam strength and the contact strength as a "remedy" is proposed. The PC is utilized in order to ensure the arguments;

The analysis is devoted primarily to the design of helical gears to resist bending failure of the teeth and to resist pitting of failure of the tooth surface;

the evolution of the constructive solutions of the joint that form the cylindrical fitting specific to the gears determined the occurrence of some typified families whose carrying capacity tend to equal the performances obtained by the joint by shrinking joints;

Experimental data regarding operational stats and thermal stats of an automatic gearbox are presented. Experimental data regarding the operating pressure and the command of the solenoid actuators is being expressed in percentage and current, is being recorded on the hydraulic test rig for establishment and optimization of the clutches, and brakes operations from an automatic gearbox;

The purpose of the research is to point out a controlled vibration quarter car model of a human body in seated position. Its importance is mostly due to the vertical accelerations impact of the human body and be able to control these vibrations. It marks these vertical accelerations based on a concentrated mass mathematical damped model. This is first established mathematically and then simulated in Matlab software, its results clarifying the differences between accelerations at different parts of the model and their range.

The third part is about ergonomics as a human centered design and presents the candidate contributions in the biological systems area. This is the main area in which the candidate has made the latest research as a result of research contracts at the national level- Manager- Contract CNMP/PNCI 2, Nr 91-022/18.09.2007 – 2010: *Workplace ergoengineering. Dental medicine applications*, or with enterprise partners-Honeywell, researcher key-expert researcher, in contract AMPOSDRU 1477/24.03.2010, ID 55651- *Ergonomics, prevention and performant management in dental medicine by alignment to European standards*, CNMP/ PNCI 2 no 41-034/14.09.2007 MICRODENT-*Clinical protocols in dental microscopy applications*, CEEX 116/04.08.2006 with Medical Science Academy Bucharest –*Studies regarding the modular dental equipment based on mechatronics systems; ergonomic solutions for the double prevention of medical diseases*, CEEX 88/2006 –*Development and implement of performant systems of spine deformities on school population and professional categories with sedentary lifestyle investigation and recovery*, the great collaboration on national and international scale with SRED (*Romanian Dental Ergonomics Society-Societatea Română de Ergonomie Dentară*) –founding member and vicepresident, ESDE (*European Society of Dental Ergonomics*), specially with Prof. Rotgans Jerome from Medical Faculty, RWTH Aachen University –the president of ESDE and Chairman of the Study Group 'Dental Ergonomics' of the German Dental Association, founding member and president of SRE (*Ergonomic Romanian Society -Societatea Română de Ergonomie-*) and material base development through personal effort.

Another contribution has been the involvement in POSDRU contract-Potential future PhD leaders, Contract AMPOSDRU/21/1,5/G/13798 *Doctoral school in research aid through European context "Școala doctorală în sprijinul cercetării în context european"* in which I guided two doctorate students, As. Dr. Eng. Kulcsar Raul-Miklos (*Ergonomic research regarding the spine behaviour during the drive*) and As. Dr. Eng. Borozan Ion-Silviu (*Automatic gearboxes parametric quality analysis regarding the improvement of the technical and functional characteristics*).

Rezumat

Teza curentă este urmarea eforturilor de cercetare ale autoarei din perioada 2000-2016 la Universitatea Politehnica Timișoara, fiind focalizată pe: 1. Optimizarea funcțional constructivă a etanșărilor frontale prin modelare, simulare și încercări experimentale; 2- Analiza funcțional-constructivă a unor organe de mașini utilizate în autovehicule rutiere, 3- Modelarea, simularea și încercarea experimentală a sistemelor biologice.

Aceasta constituie doar o parte a cercetărilor în construcția sistemelor mecanice, a autovehiculelor rutiere și ergonomie din această perioadă, cercetare care a vizat diverse direcții de la modelare analitică, modelare cu element finit și încercări experimentale până la zone aplicative precum ergonomia autovehiculelor rutiere și cea în domeniul medicinei dentare respectiv chirurgiei maxilo-faciale.

În anii recentii a devenit din ce în ce mai evident că evoluția sistemelor tehnice este puternic influențată de explozia noutăților din domeniul științei materialelor, al tehnologiilor avansate, al tehnologiei informației și electronicii, precum și cea din domeniul mecatronic.

Aceasta obligă la a realiza cercetări și optimizări ale construcțiilor mecanice.

De la elaborarea tezei de doctorat din anul 1998 activitățile profesionale în domeniul cercetării și au avut ca bază domenii ale ingineriei mecanice, curgeri și transfer termic ale etanșărilor frontale și ergonomie. Până în 2007 temele s-au axat mai mult în domeniul inginerie mecanice, în special etanșări frontale, lagăre, cuplaje, angrenaje ca urmare a unor contracte de cercetare la nivel național (CEEX 21 I 03/07.10.2005/, *Cercetări privind posibilitățile de utilizare ale sistemelor robotice în scopul creșterii competitivității tehnico-economice a industriei românești*; 36/1999 cod CNCSU 204/1999, *Metode și mijloace pentru încercarea transmisiilor mecanice și a componentelor acestora. Etapa: „Implementarea rezultatelor cercetării în unități de învățământ și unități economice cu profil industrial”*, 36/1998 cod CNCSU 280/1998, *Metode și mijloace pentru încercarea transmisiilor mecanice și a componentelor acestora. Etapa: „Cercetări experimentale”*), internațional -FP7 250485/2010 ThinkMotion sau cu parteneri privați. - S.C. ROSEAL S.A și pentru că activitatea didactică era orientată prioritar în domeniul “organe de mașini”- predare, aplicații, construcția și cal culul autovehiculelor rutiere-predare.

Prin urmare acesta a fost scopul efectuării cercetărilor experimentale. Rezultatele cercetărilor au fost publicate în 6 lucrări Reviste ISI, 16 lucrări ISI Proceedings și IEEE Explore, 39 în baza de date Scopus, 53 în alte baze de date Google (Scholar) Academic.

Temele principale analizate au fost:

1. *Optimizarea funcțional constructivă a etanșărilor frontale prin modelare, simulare și încercări experimentale*
 - 1.1. Argeșanu, V.; Popa, A., The elastohydrodynamics (EHD) lubrication of a mechanical face seal , The revue of Tribology Fascicle VIII, „The Annals of University Dunărea de Jos of Galați”, ISSN 1221-4590, 2004, pp. 136 – 139.
 - 1.2. Argeșanu, V.; Mădăras, L., Model and analysis of a Mechanical seal by Finit Element Method. Interface Tension Distribution, Facta universitatis-series Mechanics; Automatic control and robots, ISSN 0354-2009, 2003, Vol. 3, no. 15
 - 1.3. Argeșanu, V.; Popa, A., Interface contact pressure distribution in Dynamic contact face seals, analyzed by FEM, 3rd International Conference With International Scientific Comitee Research and Development in Mechanical Industry, RaDMI, ISBN 86-83803-10-4, 2003

- 1.4. Argeşanu, V. ; Kulcsar, R.M.; Borozan, I.S., Automotive Mechanical Face Seals Tribological Simulation, Journal of the Balkan Tribological Association, ISSN 1310-4772, 2011, Vol. 17, no. 1, pp. 1 -12.
- 1.5. Argeşanu, V.; Kulcsar, R.M.; Farkaş, I.A., Calculation by Finite Element Method(FEM) of Temperature Distribution in the Components of a Mechanical Face Seal, Journal of the Balkan Tribological Association, ISSN 1310-4772, 2011, vol. 17, no.1, pp.13-20.
2. *Analiza funcțional-constructivă a unor organe de mașini utilizate în autovehicule rutiere*
- 2.1. Argeşanu, V.; Luchin, M.; Jula, M.; Mărgineanu, D., Considerations Upon the Circular Section Circlips/Retaining Rings Axial Load-Carrying Capacity, ANNALS of DAAAM for 2008 & Proceedings of the 19th International DAAAM Symposium, ISBN 978-3-901509-68-1, 2008, pp. 33-34.
- 2.2. Argeşanu, V.; Jula, M.; Cărăbas, I., Determination of the Optimum Variant of Shaft-Hub Joint for Gears, ANNALS of DAAAM for 2009 & Proceedings of the 20th international DAAAM Symposium, ISBN 978-3-901509-70-4, 2009, vol. 20, pp. 1881-1882.
3. *Modelarea, simularea și încercarea experimentală a sistemelor biologice*
- 3.1. Argeşanu, V.; Kulcsar R.M.; Borozan I.S., The drivers spine analytical model International Journal of Biology and Biomedical Engineering, ISSN 19984510, 2014, vol. 8, pp. 172-178
- 3.2. Kulcsar R.M.; Borozan I.S.; Argeşanu V., Experimental determination of the intervertebral stress, 12th IEEE International Symposium on Intelligent Systems and Informatics (SISY), 2014, pp. 303-307.
- 3.3. Streian, F.; Argeşanu, V.; Kulcsar, R.M.; Borozan, I.S.; Jula, M.; Talpoş-Niculescu, C., Human Body Posture before and after Maxillofacial Surgery, Procedia Engineering, ISBN 1877-7058, 2014, Vol. 69, 508-511.

Prima parte se referă la optimizarea etanșărilor frontale din punctul de vedere al criteriului de construcție și al funcționării acestora condițiile specifice de mediu și durabilitate având un impact însemnat în construcția de echipamente mecanice.

Completa ajustare a tuturor tipurilor de etanșări frontale implică protecție anticorozivă și calorică suplimentară a elementului elastic pretensionat, răcirea suprafeței ce intră în contact și recircularea și/sau evacuarea fluxului evacuat.

O mare diversitate a construcției și calculului etanșărilor de contact, a materialelor, condițiilor de operare și a altor factori ce afectează performanța acestora nu au permis încă trasarea concluziilor referitoare la frecare și uzură.

Modelul simplu al complexității frecării dintre suprafețele aflate în contact, atunci când se ia în considerare teoria hidrostatică a lubrifierii, este funcțională atât pentru suprafețe convergente cât și divergente, fiecare cu particularitățile aferente. Dacă efectul hidrostatic al lubrifierii este combinat cu efectul mecanic al frecării solide cu contact, problema frecării mixte ce apare în cazul etanșărilor frontale, poate fi rezolvată. După, efectul hidrostatic al lubrifierii poate fi deasemeni, introdus.

Există diverse cauze pentru scurgeri ale etanșărilor frontale. Scurgerile au loc în mod normal, prin spațiul de etanșare radial format de cele două suprafețe de alunecare. Calculele se bazează pe presupunerea că există un film hidrodinamic în etanșările frontale și că scurgerea poate fi calculată în conformitate cu ecuațiile cunoscute de curgere laminară printr-un orificiu inelar radial. Forma suprafețelor pot, cu toate acestea să fie modificate prin încălzire și uzură, de exemplu.

Modelarea pentru rezolvarea soluțiilor este obiectivul inginerie de predicție. Cercetarea se ocupă cu analiza elementului de delimitare sau simularea numerică a comportării unei etanșări frontale. Prezenta analiză cu element de delimitare este una deosebită pentru că ea conține efectul

neliniar datorită modificărilor condițiilor de delimitare care rezultă din contactul inelului static și capul de etanșare a etanșării frontale. Toate acestea au o influență semnificativă asupra comportamentului sistemului. Rezultatele pot fi utilizate pentru optimizarea construcției și calculului, precizie a limitelor sau monitorizarea eșecurilor.

În partea a doua se realizează analiza funcțional-constructivă a unor organe de mașini utilizate în autovehicule rutiere:

Sunt prezentate câteva aspecte interesante cu privire la rezistența roților dințate elicoidale: rezistența miezului și rezistența de suprafață. Un " modul minim " care garantează rezistența la ambele rezistențe, cea de miez și rezistența de contact este propusă ca un " remediu ". Calculatorul este utilizat pentru a se asigura aceste argumente;

Analiza este consacrată în primul rând la proiectarea de roți dințate elicoidale, pentru a rezista la încovoierea dinților și pentru a rezista la pittingul suprafeței dintelui;

evoluția soluțiilor constructive ale lagăerelor care formează îmbinarea cilindrică specifică angrenajelor ce au determinat apariția unor clase specifice ale căror capacitate portantă tind să egaleze performanțele obținute prin cuplarea prin micșorarea cuplajelor;

Datele experimentale privind parametrii operaționali și cei termici ai unei cutii de viteze automate. Date experimentale referitoare la presiunea de funcționare și comanda actuatorilor de tip solenoid este exprimată în procente și este înregistrată pe standul hidraulic de încercare pentru stabilirea și optimizarea cuplajelor și a frânelor unei cutii de viteze automată;

Scopul cercetării este de a indica un model vibrațional controlat automatic focusat pe un sfert de automobil a unui corp uman în poziția așezat pe scaun. Importanța sa este în mare parte datorită impactului accelerațiilor verticale ale corpului uman și să fie capabil să controleze aceste vibrații. Ea marchează aceste accelerații verticale pe baza unui model matematic ținând cont de mase, coeficienți elastici și coeficienți de amortizare. Acest lucru este mai întâi stabilit matematic și apoi simulat în software-ul Matlab, rezultatele clarificând diferențele dintre accelerațiile verticale pe diferite părți ale modelului și amplitudinea lor.

Partea a treia se referă la ergonomie ca proiectare uman-centrată și prezintă contribuțiile candidatei în domeniul sistemelor biologice. Acesta este principalul domeniu în care candidata a efectuat cercetări în ultima perioadă de timp, ca urmare a contractelor la nivel național –director-Contract CNMP/PNCI 2, Nr 91-022/18.09.2007 – 2010: *Ergoingineria locului de muncă- Aplicații în medicina dentară* sau cu parteneri firme-Honeywell, cercetător, expert cheie, în contract AMPOSDRU 1477/24.03.2010, ID 55651- *Ergonomie, prevenție și management performant în medicina dentară prin aliniere la standardele europene*, CNMP/ PNCI 2 nr 41-034/14.09.2007 *MICRODENT-Protocoale clinice pentru optimizarea aplicațiilor microscopice dentare*, CEEEX 116/04.08.2006 cu Academia de Științe medicale București -*Studii privind realizarea de echipamente dentare modulare bazate pe sisteme mecatronice; soluții ergonomice pentru dubla prevenție a afecțiunilor*, CEEEX 88/2006 -*Dezvoltarea și implementarea unor sisteme performante de investigare și recuperare a deformațiilor de coloană vertebrală la populația de vârstă școlară și categorii profesionale cu activități sedentare*, a colaborării fructuoase pe plan național și internațional cu SRED (Societatea Română de Ergonomie Dentară-Romanian Dental Ergonomics Society) –membru fondator și vicepreședinte, ESDE (Societatea Europeană de Ergonomie Dentară- *European Society of Dental Ergonomics*), în special cu Prof. Rotgans Jerome from Medical Faculty, RWTH Aachen University -președintele ESDE Chairman of the Study Group 'Dental Ergonomics' of the German Dental Association, membru fondator și președinte SRE (Societatea Română de Ergonomie-

Ergonomic Romanian Society) și a dezvoltării bazei materiale necesare cercetării prin eforturile proprii ale autoarei.

De asemenea o contribuție hotărâtoare a avut-o implicarea în POSDRU Potențiali viitori conducători de doctorat, Contract AMPOSDRU/21/1,5/G/13798, “*Școala doctorală în sprijinul cercetării în context european*”, în cadrul căruia am tutoriat doi doctoranzi, pe As. Dr. Ing. Kulcsar Raul–Miklos (Cercetări ergonomice asupra comportării coloanei vertebrale a conducătorului auto- *Ergonomic research regarding the spine behaviour during the drive*) și As. Dr. Ing. Borozan Ion-Silviu (Determinarea parametrilor cutiilor de viteze automate în scopul îmbunătățirii caracteristicilor tehnico-funcționale ale acestora -*Automatic gearboxes parametric quality analysis regarding the improvement of the technical and functional characteristics*)- cu teze în domeniul cutiilor de viteze – gears și ergo-autovehicule (Contract AMPOSDRU/21/1,5/G/13798)

I. Scientific achievements

1. Constructive and functional optimization of the mechanical face seals through modeling, simulation and experimental work

1.1. Basic topics of mechanical seals

1.1.1. Introduction

The specific conditions concerning the environment and the durability have a great impact on the construction of the mechanical equipment. The complete adjustment of all the types of mechanical seals implies additional anticorrosive and calorific protection of the elastic pre-tensioned component, the cooling of the surface that is in contact, and recirculation and/or the evacuation of the discharge flow. The study takes into consideration all the factors regarding the selection and disposal of all the elements that are used in the construction of mechanical seals.

The constructive diversification of mechanical seals to a couple of materials according to their destination, depends directly on the allowed speed range, on the pressure inside the sealed space and on the way in which the hydrostatic trimming of the two rings was made, and finally, depends on the operating economic course of activity[3],[5].

The complete adjustment of all the types of mechanical seals implies additional anticorrosive and calorific protection of the elastic pre-tensioned component, the cooling of the surface that are in contact, and re-circularization and/or the evacuation of the discharge flow. All the functional and constructive condition mentioned above have led to the generation of facility thermal seals, which, starting from basic elements like rings, archers, that vary from a wide range that covers various particular requirements.

1.1.2. Construction and operation

a) Construction

A mechanical seals is made, mainly, from the following components (fig 1.1):

- A stationary ring (1) and a sliding one with a relative rotation movement (2), one of these rings allowing the axial movement on the shaft compensation of the wear
- A system of reciprocal pressing system of the two rings – represented in the figure by the cylindrical spring (3) and by the seals represented by the two “o” rings immobile towards the sheaf and the housing.
- The average dimension of the realized clearance h and the axial force verso pressing force F_a , determine a certain pressure behavior inside the clearance that has an influence on lubrication of the contact surfaces, their durability and tightness.

- The compression of the sliding ring by the pressure depends on the h rates between the pressurized surface, A_h , and the sliding surface A , and finally on their mutual position.

$$P_a/p = A_h/A = k \quad (1.1)$$

Taking in consideration the above proportion we can have the following situations (fig 1.2):

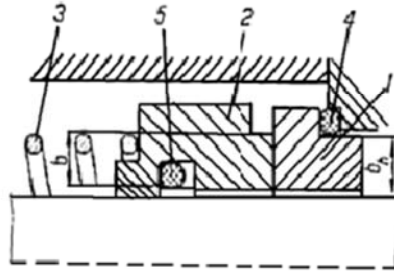


Fig. 1.1. Components of a mechanical seals

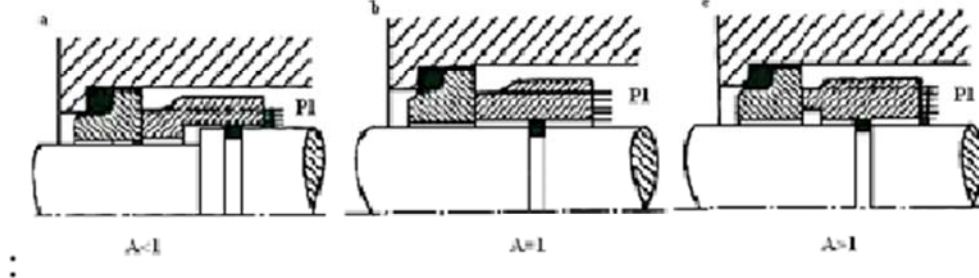


Fig. 1.2. The sliding surface A

b) Operation

- $K > 1$, which means “unsteadily” or “fussy” seals;
- $K \leq 1$, which means “uncharged” or “balanced” seals;
- $K = 0$; we gave this situation when the contact compression is not influenced by the environment pressure, being obtained only through the force of the spring.

The unbalanced seals, having $k > 1$, that is $p_a > p$, have a more pronounced wear of the sliding rings, but in the same time they have a more stable operation, an experimental lower pressure in the clearance. According to the data, the losses through the no seals Q , are in inverse proportion with the square of contact pressure p :

$$Qp^2 = \text{const.} \quad (1.2)$$

c) Energy Consumption

The energy consumption process is taking place because of the following dissipative sources:

- Detention (discharge) of the fluid quantity contained inside of the seal- this loose will be generally speaking, neglected.
- The sliding friction between the mechanical sealed surfaces; it is accepted that these losses can be formulated according to moment M_{fr} [mNm] and the relative angular speed ω [rad/s], with the help of the following ratio:

$$P_{fr} = (\Delta p_{fr} / d_\alpha) \cdot d \cdot \omega / 100 = 10^{-3} \cdot M_{fr} \cdot \omega \quad [w] \quad (1.3)$$

The friction moment that appears at the mechanical seal represents the amount between the moment of friction of the contact surface M_a , and the moment due to the movement of the seal into the fluid M_h .

$$M_a = \pi \cdot D_m^2 / 2 \cdot b \cdot p_a \cdot \mu \quad (1.4)$$

The moment M_a is important; it has a bad influence on the thermic charging of sealing and wear of the rings. The component M_h has a great importance at high speeds having a positive influence, generally having a cooling effect.

$$M_a = \pi \cdot D_m^2 / 2 \cdot b \cdot p_a \cdot \mu \quad (1.5)$$

This last loss will be determined in all the cases. The designer has the opportunity that through the discharge effect to influence the value of p_a and therefore this loss. The contracted ring determines a smaller loss, but is a disadvantage, by representing a greater danger of braking. Estimating the losses through the non-sealing we can have the following situations:

- the conditions of mixed friction in the annular tumble

$$Q_2 = \pi \cdot d \cdot (p_1 - p_2) \cdot h^2 \cdot S / p^2 \quad (1.6)$$

S=interface factor

- mixed friction conditions in the annular thimble

$$Q = c_2 \cdot \pi \cdot d \cdot (p_1 - p_2) \cdot \eta \cdot \sqrt{vb} / p^2 \quad (1.7)$$

- fluid friction conditions in the annular thimble

$$Q = c_3 \cdot \pi \cdot d \cdot (p_1 - p_2) \cdot \sqrt{\eta \cdot bv^3} / p^3 \quad (1.8)$$

The abstraction of the heat is made more often by the sealed medium, excluding the vaporization process in the interstice. The temperature arising inside the interstice is a consequence of the heating produced through the friction, and may produce pronounced detritions, the aerate of the lubricant film that will result in to a that fast growing of friction coefficient and of detritions, in some cases the exceeding of the integration temperature of materials, which can lead as well to a thermic breaking of the rings, reciprocal slider of thermal palling. Taking in consideration all the condition mentioned above, we can say that rings made of materials with a high thermal conductivity, may have a better behavior in connection with the thermic aspects. The seals used for high temperature have to be reared as much as possible, the temperature from interface is being kept under the critical temperature of vaporization, in order to prevent the appearance of dry friction, anticipating, for example (fig.1.3) the construction with double mechanical seals. In case the maximum temperature passes the sensitive point of the elastomeric components of the seal, then we have to use metallic water skins (fig.1.4), having the advantage of a small axial gauge, higher capacities of loading and better flexibility characteristics[1],[2],[4]. Regarding the seals for a higher speed of the shafts of the pumps compressors or turbines, the springs are fixed on the armature or we use seals with an intermediate floating ring (fig1.5). Secondly, it becomes necessary to mix as less as possible the obdurate liquid (a fluid oil with a pressure greater than that of the exploitation

medium) with the exploitation medium, a small energy consumption at obturation (by a small consumption of obturator liquid) as well as by the transference cross section of the obturator liquid in the exploitation liquid. There have been found different solutions like double seals, in whose intermediate space is coursing the obturator liquid (fig1.6).

This answer gives a higher safety against the attrition of inside the fitting. The liquid obturator can be used (2), in the same time (1), for cooling the seal.

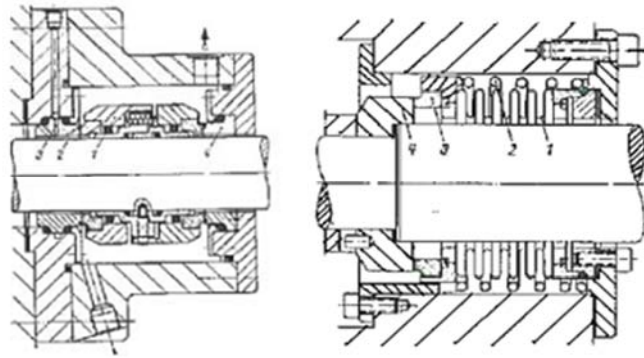


Fig.1.3. The construction with double mechanical seals Fig. 1.4. Metallic water skins

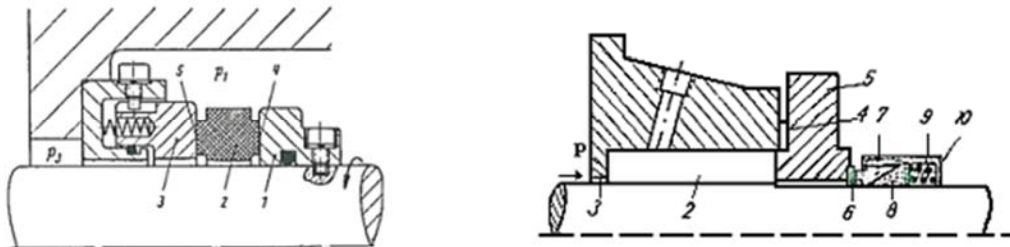


Fig. 1.5 .Seals with an intermediate floating ring Fig. 1.6 .Seals with the obturator liquid

For a better washing result, the washing section has to be as small as possible, in order that a sufficient speed to draw the solid particles. A small opening of the inside can be obtained in various ways: with carbon, bronze or PTFE rings. In the case of working in environments with stringy suspension, the compression springs have to be protected against blockage (fig.1.7)[7],[5].

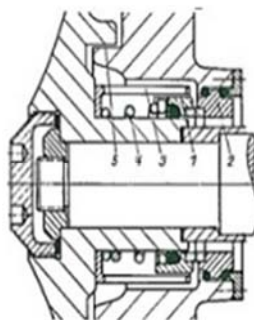


Fig. 1.7. Protection of the compression springs against blockag

1.1.3. Conclusion

In conclusion, the particulars that appear in seal problems, the constructive solutions, the right choosing of materials, as well as the usage of special made accessories lead to the diversification of seals types, taking in consideration the functional aspects as well as those of safety in exploitation.

1.2. Lipseals and mechanical face seals performance criteria

1.2.1. Introduction

A great diversity of contact-seals designs, materials, operating conditions, and factor that affect their performance have not yet allowed the general conclusions on friction and wear of these seals to be drawn. At the same time, the results of studies of particular cases may often lead the design engineer to an erroneous decision if the seal he develops is different in some way from that he has taken as a prototype. To a face seal design, choice of materials and type of seal arrangement, individual requirements such as minimum leakage, maximum life or minimum friction can be met [68],[69].

Labyrinths, stuffing boxes, lip seals, bushings, spiral-groove seals, and mechanical seals made out of a very large number of materials, are the systems that are commonly used for sealing rotating shafts [64]. The behavior of a seal is determined by the complex interaction of a number of factors. Advantages are usually attained at the price of disadvantages in the order directions. For example if the roughness is constant, an increase of the contact pressure reduces leakage, but the wear and frictional heat increase. As against this, increasing leakage losses can reduce the friction and the heat production, but the effectiveness of the unit as a seal is reduced. Again, a high friction may not only lead to increased wear but also, due a thermal distortion, to considerable leakage losses, or it may cause the seal to break down because of a thermal stress cracks [56],[57].

Depending on application, sealing rubber should be strong, heat resistant, cold resistant, or resistant to chemical attack. The characteristics must often be combined; some of them are mutually incompatible. Anyhow, all sealing rubber applications require good friction properties: high wear resistance and low coefficient of friction.

1.2.2. Friction and wear in dynamic contact seals

The performance of seals is characterized by the degree of tightness, service life, power losses, by the extent of damage to the contacting surface in operation, etc. the degree of tightness, wear life t_w , and performance factor I are the most important characteristics of seal performance [9],[65],[79].

In addition to the above factors, temperature, whose level is determined by their joints action, also affects the performance of dynamic seals. Whereas temperature has the major influence

on the frictional effects in the contact area, the leakage is caused by reduction in the contact area pressure and distortions in the geometry of the rubbing surface due to wear (fig.1.8a,b), increased thermal deformations, etc. In some instances, these factors are interdependent [46]. The service conditions of sliding contact seals in machinery, determined by combinations of the above factors, are very diverse. In a face seal (fig1.9), an axial force pressed a rotating floating ring 5 against a fixed counter face 6.



Fig.1.8.a Lipsel Fig.1.8.b PTFE lip seal

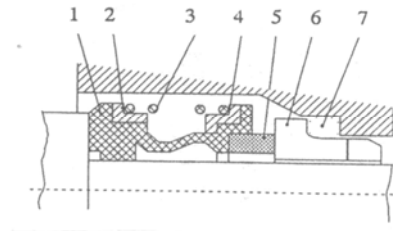


Fig.1.9. Mechanical face seal

The axial leakage path between the floating ring and the shaft is closed by a static seal such as an O-ring 7[5],[37],[53].The static and sliding surface of the traditional stuffing box are effectively interchanged, with the advantage than the geometry if the sliding sealing surface can now be produced more accurately and less expansively and there is no longer any wear on the shaft or shaft sleeve[10],[52]. To compensate for any lack of alignment of the seal faces and for longitudinal thermal expansion of machine and seal, as well as wear of the seal faces, the face seal must contain at least one flexible member such as diaphragm, bellows, elastomeric seal, or springs 1,3.(fig1.9)[9],[72].

In selecting sliding materials, consideration should be given to operating conditions, ease of manufacture and material costs. The chemical activities as well as the physical and mechanical properties have to be considered. By selecting materials with appropriate thermal conductivity coefficients, by additional cooling, lubrication and load “balancing”.

The sealing medium also has a considerable influence on the life of a mechanical seal. Mounting seals on elastomeric rings has a very beneficial effect on wear because of damping actions of the elastomer. Often the durability of a seal is determined not by the wear of the seal alone but by the resistance of ageing of any elastomers used. Intermittent operation as well as increases of contact pressure, friction coefficient, sliding speed and temperature will reduce the life. Since the effects of adhesive wear, abrasive wear, corrosive wear and erosive wear, let alone vibration,

temperature and material effects, can be cumulative. If it defines the intensity of the power lost by friction in the area of contact as the ratio of the power lost by friction and land sliding [51],[38],[10]:

$$\frac{P_{fr}}{A_{al}} = (\mu \cdot p_d \cdot v)_a \quad (1.9)$$

Where: μ - friction coefficient in the contact area;

p_d - pressure in the area of contact;

v - relative speed.

This may give an appreciation of the value limit of operating of the sealing. If we consider for example $\mu=0.1...0.3$ for PTFE lip seal or $\mu=0.005...0.1$ for the elastomer lip seal, the pressures of work of 3MPa sliding speeds of 12m/s: $\frac{P_{fr}}{A_{al}}=3.6 \text{ W/mm}^2$ for PTFE and $\frac{P_{fr}}{A_{al}}=7.2\text{W/mm}^2$ for elastomers.

1.2.3. Performance criteria

A comparative situation between the face seals and lip seals based on technological, operational and cost is presented in tab.1.1. When comparing the values it must be borne in mind that the sealed pressure p_1 for lip seals are lower than the corresponding mechanical seals.

Despite this, it is evident that on account of smaller leakages of the buffer fluid and sealed product, and greater operational safety and reduced maintenance, mechanical seals are much superior to lip seals.

Whereas the initial prices of the lip seals are lower than those of the face seals, the position is reverse upon installation and putting into operation. The labor-intensive maintenance costs are about 20 times higher with lip seals. Despite the more expensive spare parts for mechanical seals their total costs come lower than for lip seals, on account of the long life of the former[39],[12].

It also is taken into account that due to labor savings, smaller leakage losses, greater operational safety, and reduced-down time, face seals are even more economical than would appear.

By means of a metallic support jacket in the carbon ring which is certainly deformed much more than the tungsten carbide seal under high pressure loads, because of its low modulus of elasticity, the previous very good operating characteristics of conventional thermo hydrodynamic seals could be further improved at higher pressure.

In seals, with the stabilized seal gap, the hydrodynamics of the circulations grooves are a better design. Seal gaps are much less sensitive to pressure changes and have even longer service lives.

1.2.4 Conclusion

The behavior of a seal is determined by the complex interaction of a number of factors. Advantages are usually attained at the price of disadvantages in the order directions.

If we compare specific losses through friction: in the usual pressure for lip seals “uncharged” or classical “charged” with

$$\theta = \frac{F_{cr}}{\pi \cdot d} \quad (1.10)$$

Face seals we can notice the net advantage of helip seals, these having as a plus size and lower costs. However, in the field of higher speed and pressure and for hard working environments, the face seals are still irreplaceable. (fig. 1.10)

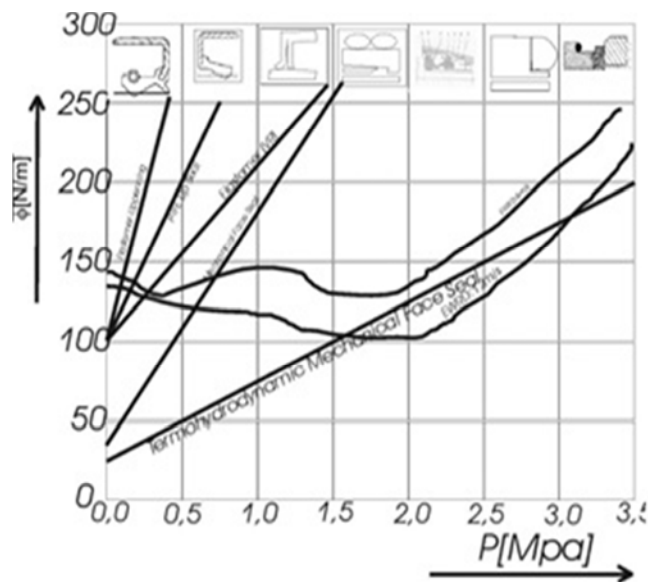


Fig.1.10 Specific friction losses function pressure dependency for different types of seals

Tab.1.1. Performance parameters of seals

Specification parameters / functional conditions	Seal type	
	Face seal	Lip seal
Materials and technology operation	High maintenance, involves polishing the active surfaces of rings	Easy to maintain, for the sealing edge, E class of precision
Space assembly	At $d=idem$	
	maximum	Minimum
Condition processing of axle	correcting with advance	
	radial+axial	Only radial
can compensate for irregularities shape and position of axle	very good	medium/good
Axle wear	zero	existing
Power lost due to friction	reduced	loaded – big
		unloaded - reduced
maintenance expenses	reduced	
Lifetime expenses	comparable	
Initial expenses	high	low
Lubrications and cooling measures	necessary	
Type of fluid	no restrictions	limited – based on compatibility with the lip material

1.3. The flowing-friction dependency at a mechanical face seal

1.3.1. Introduction

It is presented the simple model of the complex friction between the surfaces in contact[43],[44],[45], when taking into account the hydrostatic theory of lubrication, is functional both for convergent surfaces and for divergent ones, with the necessary particularities. If the hydrostatic effect of lubrication is combined with the mechanical effect of the solid contact with friction, the problem of mixed friction that appears at EF can be solved. Afterwards, the hydrodynamic effect of lubrication can also be introduced[50],[14],[58].

From the constructive and functional point of view, the frontal tightening realizes the closing of a premise with a tribologic couple of a fourth class (plane surface couple)[5],[59],[42],[60].

The ring (6) (see Figure 1.11) is immobilized in ratio with the case and constitutes the element of friction. The ring (5) .which is in a forced frontal contact with the first one ,has the role of a pressure element and is rotating with the shaft. We, thus, observe that on the grounds of constructive vicinity, the tightening function in this case is distributed on two levels. The first level is the primary tightening assured through the forced and direct contact between the two rings with relative motion.

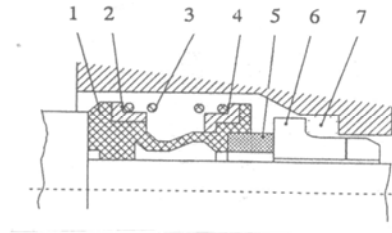


Fig 1.11.

The second level is the secondary tightening, represented in the tightening packing of the two rings over the shaft, and over the case and forbids the escape on the motionless contact areas with the conjugated pieces (the bearing's lid and the shaft).

We observe that, in this way, the solution may give very high performances, suitably influencing every zone. The advantage of separating the functions may consist of:

- the lightening with direct contact becomes prevalent abrasive worn out and thus its' replacement is conditioned by the evolution and the advance of this process. At tightening on cylindrical surfaces, the compensation of wear on radial direction involves the elasticity of the contact, while at frontal contact, a simple axial shift in an interval large enough preserves/rebuilds in natural way (compensates) the tightening function. Secondary tightening acts on cylindrical surfaces but their relative immobility does not lead to significant wear only in cases of electrochemical and contact corrosions or mechano-chemical (tribo-chemical) corrosion, which might be diminished a lot by using additives of extreme pressure and anti-wear protection covers of the surfaces and a suitable choice of the couple of materials.
- the work way of a frontal tightening is based upon the existence of an axial resultant force which has as an effect the pressing of the slipping ring which can shift in axial way on the other ring, and between the ring-shaped contact surfaces a very small clearance is realized, capable of realizing the tightening.

This axial force is the resultant of the following components applied to the ring.

1.3.2. The hydrostatic flowing of the fluid through the clearance of the ring-shaped couple of a mechanical face seal

Theoretically speaking, mechanical face seal may be assimilated with a ring-shaped friction couple with rigid and impermeable active faces having a good smoothness, low roughness. Between the faces there is always a thin and continuous film of hydrostatic Newtonian fluid [40],[41],[35] in rolling flowing.

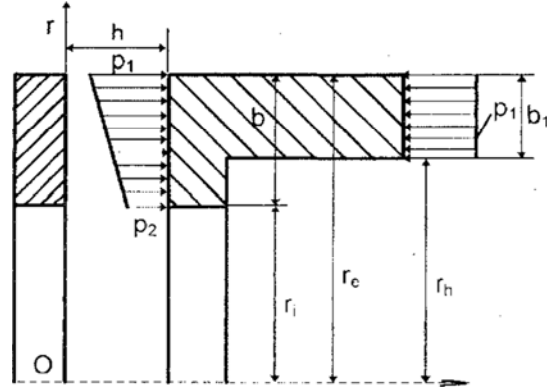


Fig 1.12

With the notations in Figure 1.12. we may write:

The motion equations:

$$\frac{\partial}{\partial x} \left(\eta \frac{\partial v_r}{\partial x} \right) = \frac{\partial p}{\partial r} \quad (1.11)$$

$$\frac{\partial}{\partial x} \left(\eta \frac{\partial v_\varphi}{\partial x} \right) = 0 \quad (1.12)$$

The continuity equation:

$$\frac{\partial v_r}{\partial r} + \frac{v_r}{r} = 0 \quad (1.13)$$

For solving the system of equations, we put the conditions at limit:

The kinematics limit conditions:

$$\begin{aligned} z = 0; v_r = 0; v_\varphi = 0 \\ z = h; v_r = 0; v_\varphi = \omega \cdot r \end{aligned} \quad (1.14)$$

The limit conditions for pressures:

$$\begin{aligned} r = r_e; p = p_1 \\ r = r_1; p = p_2 \end{aligned} \quad (1.15)$$

and, by taking the viscosity constant, the equations become:

The motion equations:

$$\frac{\partial^2 v_r}{\partial x^2} = \frac{1}{\eta} \cdot \frac{\partial p}{\partial r}, \frac{\partial^2 v_\phi}{\partial x^2} = 0 \quad (1.16)$$

The continuity equations:

$$\frac{\partial v_r}{\partial r} + \frac{v_r}{r} = 0 \quad (1.17)$$

This system of equations, allow the analytic determination of the speed and pressure's distribution in the film of fluid, when considering the same limit conditions:

$$v_r = \frac{1}{2\eta} \cdot \frac{d\phi}{dr} \cdot x(x-h) \quad (1.18)$$

$$v_\phi = \frac{\omega r}{h} x \quad (1.19)$$

$$p = p_2 + (p_1 - p_2) \frac{\ln r - \ln r_1}{\ln r_e - \ln r_1} \quad (1.20)$$

In the case of small widths of clearance in ratio with the ray, the pressures' distribution may be considered linear.

The force in the clearance that tries to undo the tightening (in the hypothesis of a Poiseuille flowing):

$$F_{hs} = \pi(p_1 r_e^2 - p_2 r_1^2) + \frac{\pi(r_e^2 - r_1^2)}{2 \ln \frac{r_e}{r_1}} (p_1 - p_2) \quad (1.21)$$

And the flowing that will escape through tightening:

$$Q = \frac{\pi h^3}{6\eta} \cdot \frac{p_1 - p_2}{\ln r_e - \ln r_1} \quad (1.22)$$

The moment of friction in the clearance will be established with the relation:

$$M_{fr} = 2\pi \int_{r_1}^{r_e} \eta \frac{\omega r}{h} r^2 dr = \frac{\pi \eta \omega}{2} \frac{r_e^4 - r_1^4}{h} \quad (1.23)$$

And the coefficient of friction has the value:

$$\mu = \frac{M_{fr}}{F \cdot r_m} \quad (1.24)$$

Where:

$$r_m = \frac{r_i + r_e}{2}$$

The power consumption lost through friction has the value:

$$P_{fr} = M_{fr} \cdot \omega = \frac{\pi}{2} \cdot \frac{\eta \omega^2}{h} \cdot (r_e^4 - r_i^4) \quad (1.25)$$

The simple model of the complex friction between the surfaces in contact, when taking into account the hydrostatic theory of lubrication, is functional both for convergent surfaces and for divergent ones, with the necessary particularities.

1.3.3. Conclusions

Theoretically speaking, mechanical face seal may be assimilated with a ring- shaped friction couple with rigid and impermeable active faces having a good smoothness, low roughness. Between the faces there is always a thin and continuous film of hydrostatic Newtonian fluid in rolling flowing.

If the hydrostatic effect of lubrication is combined with the mechanical effect of the solid contact with friction, the problem of mixed friction that appears at EF can be solved.

Afterwards, the hydrodynamic effect of lubrication can also be introduced.

1.4. The elastohydrodynamic (EHD) lubrication of a mechanical face seal

1.4.1 Introduction

There are various causes for face seal leaks. Leakage normally takes place thru the radial seal gap formed by the two sliding surfaces [86]. Calculations are based on the assumption the a Hydrodynamic film exists in face seals and that the leakage can be calculated in accordance with the known equations for laminar flow thru a radial annular gap. The power consumption can be calculated also from the Newton relation. Normally mechanical seals have radial rigid plain faces and only in special cases do spherical sealing surfaces occur [74]. The form of the surfaces can, however, be altered by heating and wear, for instance.

There are various causes for face seal leaks. Leakage normally takes place through the radial seal gap formed by the two sliding surfaces. Only the primary leakage through the seal gap between the faces of the seals will be considered, since in practice the liquid film thickness h is seldom constant and the actual gap form can considerably deviate from the assumed parallel gap because of temperature differences in the ring[63], deviations Earn the theoretical calculations are to be expected.

In addition to the mechanical forces different temperatures and their gradients also influence the geometry of the seal gap. In the case of elastic distortion the magnitude of the elastic modules and the dimensions of the rings are the determining factors, and in thermal distortions it is

the values of the thermal properties of the materials and the heat transfer factors in conjunction with the construction of the rings which influence the temperature gradients and, in turn, the gap shape. The temperature gradient in both axial and radial directions influences the geometry of the seal gap.

In mechanical seals there are often several heat sources which strongly influence the radial temperature distribution in the rings. In addition to the friction heat from the sliding interface, the medium to be sealed may be a source of heat, as well as a hot shaft or housing [70], and heat from liquid turbulence.

Depending on the direction of the temperature gradient, the temperature distribution in the sealing rings can considerably differ [71]. Those areas of the rings that lie furthest from the heat sink or are nearest to the source of heat show the highest temperatures. They expand to a certain extent then other sectional areas and alter the shape of the original parallel film gap.

In face seals the contact points of the asperities on the two seal surfaces pressed against one another with an average pressure, could distort both plastically and elastically. Thus, the most highly stressed bearing points will be distorted plastically or worn away while the neighboring areas will be elastically distorted. In the usual combinations of materials for face seals, a carbon graphite ring is usually run against a metal, metal oxide, or carbide ring with different elastic modules.

Since the surfaces are always highly finished, the low modulus ring will always take a considerably greater proportion of distortion. For these reasons the sliding surfaces under load will look more like an aerial photograph of a group of lakes than of a group of islands, the hollow spaces between the surfaces are seldom connected to one another. With the rotation of one ring, it is possible to imagine that the liquid is transported from one hollow to another, as in the case of a revolving door, until the liquid particles emerge at the far side of the gap. Thus, in this range there will be no detectable influence of viscosity. As long as liquid inflow and outflow counterbalance each other no pressure builds up in the interface. Where roughness of the sliding surfaces is uniform, the leakage losses with an exchange flow are independent of the seal width, but strongly dependent on the value of the roughness, the closing pressure, the rubbing speed, and the sense and direction of the centrifugal pressure. Furthermore, the inflow and outflow sections of the sliding rings could influence the leakage [61].

On the other hand, non-homogeneous materials can form microscopic ridges and pits due to differing coefficients of heat conduction and expansion and the differing local frictional heating.

Localized contact points expand due to heating and form small oil wedges. The hydrodynamic pressure produced will reduce interface friction by a thermo—hydrodynamic effect.

Hydrodynamic effects can also be observed with slightly porous material such as ceramics, provided that the pores are not intercommunicating, for then no pressure rise is possible. The depressions formed by the pores in turn produce localized grease cups and pressure fields. However, with increasing mean sliding pressure, the carbon, being less elastic is pressed into these pores and displaces the fluid, at greater loads the carbon particles share off with consequent high wear. With carbon against ceramic, deposits of carbon can nearly always be observed on the ceramic rings and, heavy wear is noticeable.

Thermodynamic effects depend on adequate temperature differences. Fluid of good heat transfer coefficients, like water for instance, increase the effect.

1.4.2 The end lubrication

The existence of a film of a lubricant in the seal gap and of a circumferential debit in a Couette flow, will take to the appearance of a EHD sustentation caused in the case of a mechanical face seal to the Irregularities of the sliding surfaces, undulations, pores, thermal deformations, etc., and in case of an special mechanical face Seal by the adequately manufacture on the interface[15],[16],[17].

The high-speed mechanical face seal must work with full film lubrication to ensure an acceptable operation life so that; although there is a sealing system, the functional characteristics are the same as of any friction fluid couple:

- the axial opening force;
- the stiffness of the film;
- the leakage fluid flow thru the seal's interface gaps;
- the friction moment.

The elasto-hydrodynamic lubrication is based in the context of the following working hypothesis: between two rigid sliding surfaces G a stationary, isotherm and incompressible (which viscosity varies only with the temperature $\eta(T)$) Newtonian fluid is laminar flowing.

Since the height of the condoning and stable coating of the lubricant is very reduced in relation with the other dimensions the flow can be considered biaxial.

The elasto-hydrodynamic lubricant regime appears in ordinary friction couples because of the undulations on the sliding sun-faces, or because of pressure/force/temperature defamation: (fig. 1.13)

With the notation from figure 1.13, the differential equations system for the short bearing can be obtained from the Navier-Stokes equations:

$$\theta = -\frac{1}{\rho} \cdot \frac{\partial p}{\partial r} + \nu \cdot \frac{\partial^2 \vartheta_r}{\partial z^2}; \quad (1.26)$$

$$\theta = \frac{\partial^2 \vartheta_\varphi}{\partial z^2}; \theta = \frac{\partial p}{\partial z} \quad (1.27)$$

$$\theta = \frac{\partial \vartheta_r}{\partial r} + \frac{1}{r} \cdot \frac{\partial \vartheta_\varphi}{\partial \varphi} + \frac{v_r}{r} + \frac{\partial v_z}{\partial z} \quad (1.28)$$

The conditions for the limit are:

When $z = 0$, $v_r = 0$; $v_\varphi = \omega \cdot r_\varphi$; $v_z = 0$

when $z = h$; $v_r = 0$; $v_\varphi = 0$; $v_z = 0_z$

$$\text{when } r = r_1, p = p_a \quad (1.29)$$

$$\text{when } r = r_2, p = p_s \text{ and } h = h(\varphi)$$

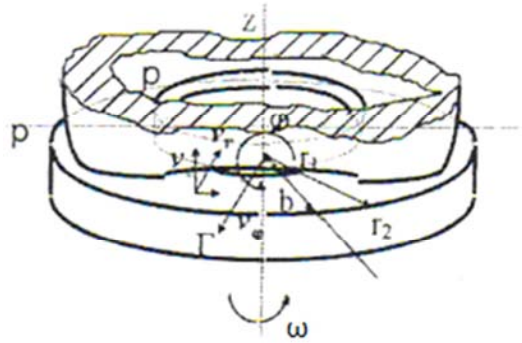


Fig. 1.13. Calculus model for an undulated surface and the other plane [13], [5].

The liquid pressure in the lubricant film is:

$$p = \frac{3}{2} \eta \cdot \omega \cdot \frac{1}{\ln \frac{r_2}{r_1}} \cdot \left(r^2 \cdot \ln \frac{r_2}{r_1} - r_1^2 \cdot \ln \frac{r_2}{r_1} - r_2^2 \cdot \ln \frac{r}{r_1} \right) \cdot \frac{1}{h^3} \cdot \frac{dh}{d\varphi} + \frac{(p_s - p_a) \cdot \ln \frac{r}{r_1}}{\ln \frac{r_2}{r_1}} \quad (1.30)$$

where h is the thickness of the clearance

The radial component of the flowing speed is:

$$v_r = - \left[\frac{3}{4} \cdot \omega \cdot \frac{1}{\ln \frac{r_2}{r_1}} \left(2 \cdot r \cdot \ln \frac{r_2}{r_1} + \frac{r_1^2 - r_2^2}{r} \right) \cdot \frac{1}{h^3} \cdot \frac{dh}{d\varphi} + \frac{(p_s - p_a)}{2 \cdot \eta \cdot \ln \frac{r_2}{r_1}} \cdot \frac{1}{r} \right] \cdot (h_z - z^2) \quad (1.31)$$

Relation (1.30) shows that in the conditions of a continuous film, the total hydrodynamic force of the couple of the friction is zero, if we consider that in some areas of the space between the sliding rings, they appear cavity zones of the air, then for a surface with a big number of undulations, the hydrodynamic force is:

$$F = \frac{3}{16} \cdot \eta \cdot \omega \cdot \left(\frac{1}{h_1^2} - \frac{1}{h_2^2} \right) [r_2^2 - r_1^2 - (r_2^2 + r_1^2) \cdot \ln \frac{r_2}{r_1}] \cdot \frac{r_2^2 - r_1^2}{\ln \frac{r_2}{r_1}} \quad (1.32)$$

where h_1 and h_2 are the minimum and maximum clearance magnitude.

The friction moment calculated in the conditions of the continuity of the lubricant film in the clearance, is:

$$M = \frac{1}{4} \cdot \eta \cdot \omega \cdot (r_2^4 - r_1^4) \cdot \int_0^{2\pi} \frac{d\varphi}{h} \quad (1.33)$$

The leakage flow through the radial annular gap is:

$$Q = \frac{i \cdot (p_s - p_a)}{12 \cdot \eta \cdot r_1 \cdot \ln \frac{r_2}{r_1}} \cdot \int_0^{\varphi_0} h^3 \cdot d \cdot \varphi \quad (1.34)$$

where φ_0 is the angle that contains the parts of the acting where the thickness is reducing.

For all cases, the repartition of the pressure in the interface is important. As a result of the reduced height, the flowing of the liquid can be emaciated as being laminar and inertness. The conditions of a laminar flow on a radial and circumferential direction are

$$Re_r < Re_{rce}; Re_\omega < Re_{\omega cr}$$

where

$$Re_r = \frac{2v_r \cdot h}{\nu} \cdot Re_\omega = \frac{\omega_r \cdot h}{\nu} \quad (1.35)$$

If these conditions are fulfilled, the repartition of the pressure trough the interface is written with the differential equations of Reynolds:

$$\begin{aligned} \frac{\partial}{\partial r} \left(r h^3 \frac{p}{\eta} \cdot \frac{\partial p}{\partial r} \right) + \frac{\partial}{r^2 \partial \varphi} \left(h^3 \frac{p}{\eta} \cdot \frac{\partial p}{\partial \varphi} \right) + 12 f(r, \varphi) p \cdot v_z = \\ = 6 \left(\omega \frac{\partial}{\partial \varphi} + 2 \frac{\partial}{\partial \varphi} \right) (p h) \end{aligned} \quad (1.36)$$

In this equation the first two terms characterize the new trough the interface in a radial and circumferential direction. The third term totalizes the flowing of the liquid in the interface with penetrable portions (the function $f(r, \varphi) = 0$, for penetrable portions).

The term from the right of the equality reflects the EHD and none—stationary adequate processes.

In order to solve the differential equation the limit conditions are introduced:

for

$$\begin{aligned} r = r_e, p = p_1 \\ r = r_1, p = p_2 \end{aligned} \quad (1.37)$$

and also the periodicity conditions:

$$p(r, \varphi) = p(r, \varphi + 2 \cdot \pi) \quad (1.38)$$

When the repartition of the pressure in the interface $p=p(r, \varphi)$ is determined. the opening force of the sealing calculated:

$$F_d = \int_0^{2\pi} \int_{r_1}^{r_e} (p - p_2) r \cdot d\varphi \cdot dr \quad (1.39)$$

This force depends on height of the interface h (fig. 1.14) which magnitude, in the equilibrium conditions of a mechanical face seal, is given by the equality condition of the opening and closing forces.

($F_1 = F_{ar} + F_H$, where: F_{ar} , is the spring force and F_H is the hydraulic force). After that the leakage flow is calculated:

$$Q = \frac{1}{12\eta} \int_0^{2\pi} [rh^3(r, \varphi) \frac{\partial p}{\partial r}]_{r=r_t} d\varphi \quad (1.40)$$

and

$$Q_m = p \cdot Q \quad (1.41)$$

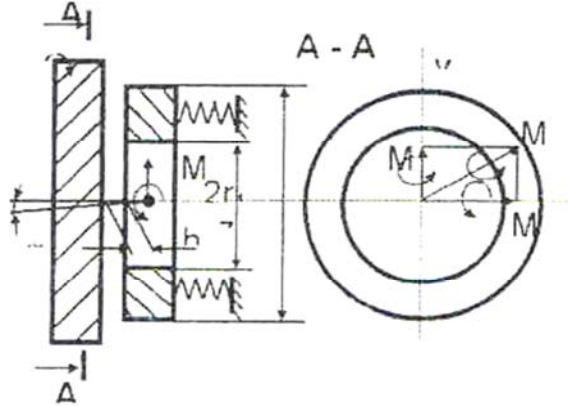


Fig. 1.14.

The moments that oppose the rings angular deformations:

$$\begin{bmatrix} M_x \\ M_y \end{bmatrix} = - \int_0^{2\pi} \int_{r_1}^{r_e} pr^2 \begin{bmatrix} \sin\varphi \\ \cos\varphi \end{bmatrix} d\varphi \cdot dr \quad (1.42)$$

The axial hydromechanics stiffness is:

$$K_{zz} = - \frac{\partial F_d}{\partial h_0} \quad (1.43)$$

The angular stiffness is:

$$K_{LN} = - \frac{\partial M_L}{\partial \alpha_N} \quad (1.44)$$

where L, M are the coordinates of the axes x and y.

The axial and angular liquidation coefficients of the mobile rings:

$$B_{zz} = - \frac{\partial F_d}{\partial h_0}; B_{LN} = - \frac{\partial M_L}{\partial \alpha_N} \quad (1.45)$$

where the point represents the derivation in relation with time.

The power consumption of the annular, radial couple is:

$$P_f = \eta \cdot \omega^2 \int_0^{2\pi} \int_t^{r_e} \frac{r^3}{h(r, \varphi)} d\varphi \cdot dr \quad (1.46)$$

1.4.3 Conclusions

In face seals the contact points of the asperities on the two seal surfaces, pressed against one another with an average pressure p , could distort both plastically and elastically. Thus the most highly stressed bearing points will be distorted plastically or worn away while the neighboring areas will be elastically distorted. In the usual combinations of materials for face seals, a carbon graphite ring is usually run against a metal, metal oxide, or carbide ring. Their elastic modules are normally much different. Since the surfaces are always highly finished the low modulus ring will always take a considerably greater proportion of the distortion in the ratio E_2 / E_1 .

For this reason the sliding surfaces under load will look more like an aerial photograph of a group of lakes than of a group of islands, in the hollow spaces between the spaces are seldom connected to one another. With the rotation of one ring it is possible to imagine that the liquid is transported from one hollow to another as in the case of a revolving door, until the liquid particles emerge at the front side of the gap. Thus in this range there will be no detectable influence of viscosity. As long as liquid inflow and outflow counterbalance each other, no pressure builds up in the interface.

The following requirements for liquid exchange flow and the consequent leakage losses can be summarized as follows: no detectable viscosity influence; no measurable gap pressure; no seal width effect; a strong roughness influence; an approximately quadratic sliding pressure influence; centrifugal force and outlet flow section effects; a sliding speed effect.

1.5. Model and analysis of a mechanical seal by finite element method. Interface tension distribution

1.5.1. Introduction

Modeling to access solutions [13] is the goal of predictive engineering. The research presents boundary element analysis or the numerical simulation of the behavior of a mechanical face seal. The present boundary element analysis is a particularly one for it contains the nonlinear effect due to changes in boundary conditions resulting from the contact of the static ring and the sealing head of the face seal. These all have significant influence on the behavior of the system [88]. The results can be used for optimizing designs, predicting limits or investigating failures.

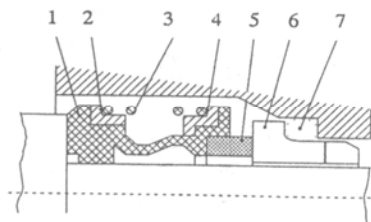


Fig: 1.15

In a face seal (Fig. 1.15) an axial force presses a rotating floating ring 5 against a fixed counter face 6. The axial leakage path between the floating ring and the shaft is closed by a static seal such as an O-ring 7. The static and sliding surfaces of the traditional stuffing box arc effectively interchanged, with the advantage that the geometry of the sliding scaling surfaces can now be produced more accurately and less expansively and there is no longer any wear on the shaft-to-shaft sleeve [85].

To compensate for any lack of alignment of the seal faces and for longitudinal thermal expansion of machine and seal, as well as wear of the seal faces, the face seal must contain at least one flexible member such as a diaphragm, bellows, elastomeric seal, or spring 1, 3 (Fig.1.15).

However, there are various causes for face seal leakage that place through the radial seal gap formed by the two sliding surfaces [84]. Leakage appears in most cases due to the distortions caused by stresses. Therefore, it is of great importance to know the stress distribution along the interface.

1.5.2. Friction contact problems by boundary element analysis

When friction is considered, the tangential displacement in the interface implies energy dissipation. The problem is solved by incremental computation. Portions of the structure can have areas of gaps that can change during a nonlinear analysis

The basic nonlinear solution approach involves a series of incremental solutions is "predicted" using the current state (stiffness and load increment). Depending on the type of nonlinearity, a force imbalance or "residual" is created during an iteration and iterations are required to balance equilibrium (correct) for unbalanced forces [73], [76].

The iterations continue during an increment until the convergence criteria is satisfied. Once convergence is satisfied, a solution is obtained for the increment and the solution progresses to the next increment using this "predictor-corrector" method.

An advancing scheme is used to apply loading in a logical and controlled manner. Advancing schemes are used to apply loading in a logical and an efficient [48],[49],[36], numerically stable solution.

The most common advancing scheme is the application of loads or enforced displacements in equal increments [77],[78]. The magnitude of the load or displacement increment is important, especially when small values of force or displacement cause a large change in response.

1.5.3. Boundary integer formulation [18],[19],[11]

When friction is considered, the dependence between normal tension and tangential ones is defined by the friction coefficient. The slide zone is divided in two parts corresponding with slide state or an adhesion state.

$$t_2 = \pm \mu \cdot t_1(\text{sliding}); |t_2| < \mu \cdot |t_1|(\text{adhesion}); \quad (1.47)$$

The signe in (1) is choose so the energy is dissipated. The friction coefficient depends on the effective total sliding v_e :

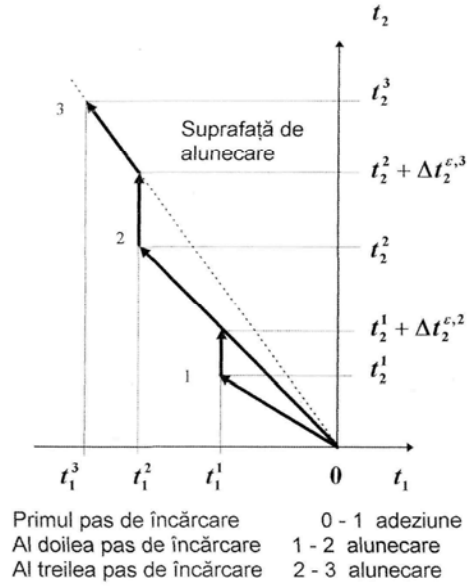


Fig: 1.16

$$\mu(v_e) = \mu_m \left[1 - \left(\frac{\mu_i}{\mu_m} \right) \cdot e^{-h v_e} \right] \quad (1.48)$$

$$v_e = \sum |\Delta v_e| \quad (1.49)$$

-where h is a consolidation coefficient. When the initial friction coefficient μ_i, μ_m -the limit friction coefficient are equals the ideal relationship of Coulomb is available. Therefore, the friction coefficient is continuously changing during the charge.

The new values for the friction coefficient for each charge step. The effect is that, that an element, who is changing the state of contact from adhesion to sliding or from sliding to adhesion, changing the friction coefficient value, presents a residual tangential force

$$\Delta t^{\epsilon, n} = \pm \mu^{n-1} \cdot t_1^{n-1} - t_2^{n-1} \quad (1.50)$$

If there is only sliding to sliding (Fig.1.16):

$$\Delta t^{\epsilon, n} = \pm (\mu^{n-1} - \mu^{n-2}) t_1^{n-1} \quad (1.51)$$

The increment of the tangential force for sliding is:

$$\Delta t_2^n = \pm \mu^{n-1} \cdot \Delta t_1^n + t_2^{\epsilon, n} \quad (1.52)$$

That ensures that after each step of charge the sliding condition $t_2 = \pm \mu \cdot t_1$ (Fig.1.16) is valable. The contact conditions are:

$$\begin{aligned}
 S_c &: \Delta v_1^A + \Delta v_1^B = 0; \Delta t_1^A - \Delta t_1^B = 0; t_1^A < 0; t_1^B < 0; \\
 S_{ca} &: \Delta v_2^A + \Delta v_2^B = 0; \Delta t_2^A - \Delta t_2^B = 0; \\
 S_{cs} &: \Delta t_2^A - \Delta t_2^B = 0; \Delta t_2^k = \pm \mu \cdot \Delta t_1^k + \Delta t_2^{\varepsilon,k}; k = A, B
 \end{aligned}
 \tag{1.53}$$

The contact variables for the fixed ring 6 (Fig.1.15) named "B" are now eliminated using the contact conditions (1, 53). It results:

$$\begin{aligned}
 & \int_{S^A-S_c^A} t_{ij}^{*A} \cdot \Delta u_j^A \cdot dS + \int_{S_{ca}^A} t_{ij}^{*A} \cdot \Delta v_j^A \cdot dS + \int_{S_{cs}^A} (t_{i1}^{*A} \cdot \Delta v_1^A + t_{i2}^{*A} \cdot \Delta v_2^A) \cdot dS = \\
 & = \int_{S^A-S_c^A} u_{ij}^{*A} \cdot \Delta t_j^A \cdot dS + \int_{S_{ca}^A} u_{ij}^{*A} \cdot \Delta t_j^A \cdot dS + \int_{S_{cs}^A} (u_{i1}^{*A} \pm \mu \cdot u_{i2}^{*A}) \Delta t_1^A \cdot dS - \\
 & - \int_{S_c^B} (1-\alpha) \cdot t_{ij}^{*B} \cdot u_1^{0,n} \cdot dS + \int_{S_{cs}^B} u_{i2}^{*B} \cdot \Delta t_2^{\varepsilon,n} \cdot dS
 \end{aligned}
 \tag{1.54}$$

Where "A" -the rotating ring 5 (Fig.1.15).

In (1.54) there is for each contour point the pair of variables:

$$\begin{aligned}
 S^k - S_c^k &: (\Delta u_i^k, \Delta t_i^k); \\
 S_{ca}^k &: (\Delta v_i, \Delta t_i); \\
 S_{cs}^k &: (\Delta v_1, \Delta t_1), (\Delta v_2^k, \pm \mu \cdot \Delta t_1)
 \end{aligned}
 \tag{1.55}$$

Now the problem has solutions, because for each contour point there is for each unknown quantity some relation.

1.5.4. Modeling and analyzing by BEA of a mechanical seal

The face seal has a geometrical axis of symmetry so it was modeled as a structure with axisymmetric elements. The material of static ring and the rotating one is a 40C130 stainless steel, the pressure of the fluid (boiled water) is 1 bar, the motion parameter ($\omega=150s^{-1}$ and the friction coefficient is estimated at 0,15.

With the method described we were obtain the distribution configuration of the equivalent stresses under the form of is surfaces (Fig.1.17) expressed in [MPa], that reveals the most stressed zones of the mechanical face seal. The distribution of the equivalent stresses on radial direction along the interface of the seal is plotted in Fig.1.18.

The configuration of those quantities is an expected one with a maximum to the inner radius of the mechanical seal.

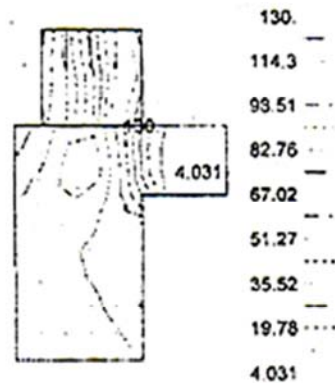


Fig: 1.17

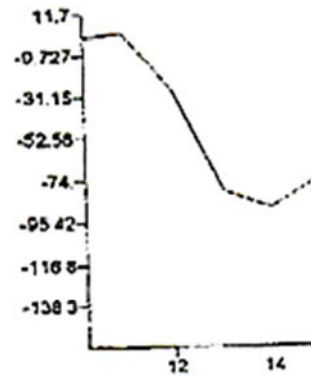


Fig:1.18

The nonlinear analysis makes creating and setting up the proper nonlinear solution strategy.

1.6. Interface contact pressure distribution in dynamic contact face seals; Analyzed by FEM

1.6.1. Introduction

A great diversity of Contact seal designs materials, operating conditions and factors that affect their performance have not yet allowed the general conclusions on friction and wear of this seals to be drawn. At the same time, the results of studies of particular cases may often lead the design engineer to an erroneous decision if the seal develops it different in some way from that he has taken as a prototype. In some instances, these factors are interdependent [67]. The study presents the service conditions of sliding contact seals in machinery, determined by combinations of the above factors analyzed by FEM (finite element method)

The performance of seals is characterized by the degree of tightness, service life, power losses, by the extent of damage to the contacting surfaces in operation; *etc.* the degree of tightness, wear life t_a , and performance factor are the most important characteristics of seal performance. In addition to the above factors, temperature, whose level is determined by their joint action, also effects the performance of dynamic seals [80]. The service conditions of sliding contact seals in machinery, determined by combinations of the above factors, are very diverse. The temperature, pressure, flow rate and properties of the fluid are chosen depending on the seal application.

Dynamic contact seals such as face (axial) seals operate with external continuous friction.

1.6.2. Friction and wear in dynamic contact seals

A great diversity of contact-seal designs, materials, operating conditions, and factors that affect their performance have not yet allowed the general conclusions on friction and wear of these seals to be drawn. At the same time, the results of studies of particular cases may often lead the design engineer to an erroneous decision if the seal he develops is different in some way from that he has taken as a prototype [20],[21],[22],[23].

For the face seals design calculation methods have been devised for the assessment of fluid pressure (with regard to out-of-squareness of the faces and to pressure in the clearance), behavior of the fluid sealed in face clearances, hydrodynamic effect for the sealing rings, deformations of the rings due to pressure and temperature, and also temperature fields in the rings of the rubbing pair.

1.6.3. Design and operation of a mechanic face seal

In a face seal, an axial force presses a rotating floating ring against a fixed counterface or vice versa. The axial leakage path between the floating ring and the shaft is closed by a static seal such as an O-ring, elastomeric sleeve, or U-seal, etc. Figure 1.19 shows a simple form of face seal. The static and sliding sealing surfaces of the traditional stuffing box are effectively interchanged, with the advantage that the geometry of the sliding sealing surfaces can now be produced more accurately and less expensively and there is no longer any wear on the shaft or shaft sleeve. To compensate for any lack of alignment of the seal faces and for longitudinal thermal expansion of machine and seal, as well as wear of the seal faces, the faces seal must contain at least one flexible member such as a diaphragm, bellows, elastomeric seal, or spring. Figure 1.20 shows a very simple design for a face seal.

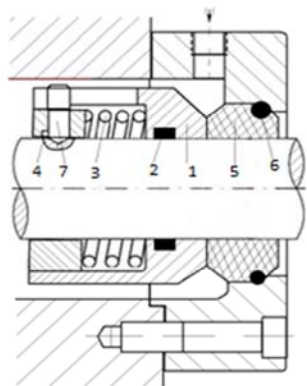


Figure 1.19: Loaded face seal.
(1)floating ringhousing; (2) seal; (3) compression spring; (4) driving ring; (5) counter ring; (6) O-ring; (7) anti-torque drive pin

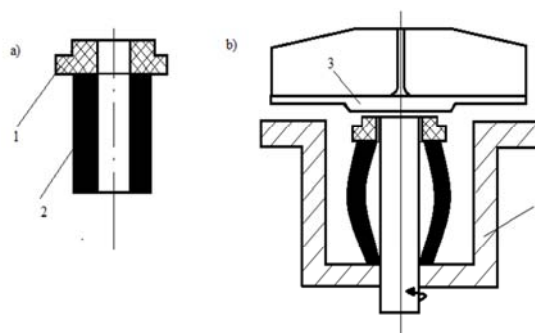


Figure 1.20: Simple face seal design
(a) before fitting; (b) in working position. (1) Synthetic resinring; (2) rubber tube; (3) impeller of pump; (4) pump housing

1.6.4. Tribology/Friction regime of a mechanical seal

In a face seal there are together the functions of a bearing and of a heat exchanger. In order to have an acceptable endurance, the face seals must ensure a complete fluid film of lubricant, so, even if one can talk about a seal, its functional characteristics are the same as of a plane friction fluid joint the opening axial force, the film stiffness, leakage and friction torque. The tribologic behavior of a sliding friction joint is described by the Stribeck relation between the friction coefficient μ and the Gümbelcriteria ($G\ddot{u} = \frac{\eta\omega}{p_m^n} = \frac{\varphi^2}{S_o}$) (Fig: 1.21).

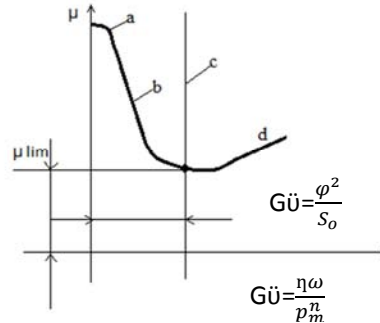


Fig: 1.21

The local contact zone stresses of the face seal appear from the external loading and from the sliding speed. To a precise load (F_m) the contact pressure's distribution (p_{mx}) and its average value as well as the friction torque depend on friction joint's geometry. So the friction force's repartition on different zones of the friction joint is not uniform. The external friction forces are function the stresses condition from the real contact zone. It is necessary to achieve the equilibrium relation :

$$F_{ct0\sin(\theta)} = \int_s^0 p * ds \quad (1.56)$$

that implies that the fluid film pressure distribution is known.

The theory must to consider the: sealed fluid properties; the materials of the two rings of the seal, by their mechanical and thermal properties; the friction joint geometry.

The model of a lace seal must to take into account the interface phenomenon together with the heat transfer, between the seal rings, so the mathematical model consists on: the Reynolds's equation, the interface geometry, the energetic fluid equation, the temperature dependence of the fluid viscosity, the temperature dependence of the fluid density, the interface limit condition film/wall, the Fourier equation, the rings thermal limit conditions, the thermal resilience equations and the supporting conditions of the face seal rings. In all, it is very important that the interface pressure distribution is known. The fluid flow can be considered as laminar and without inertia because the fluid film is very thin.

1.6.5. The friction forces, the friction torque and heat in the sliding friction joint of a face seal

At a given force (F_{ax}), the contact pressure distribution and the friction coefficients depend on the friction joint's geometry. Between two plane, rigid surfaces, with an incident angle $\alpha \neq 0$ and the: Oz breadth infinite ($h = x \cdot \tan \alpha \cong \alpha \cdot x$; $v_z = 0$) (Fig: 1.22), the pressure distribution [90] is:

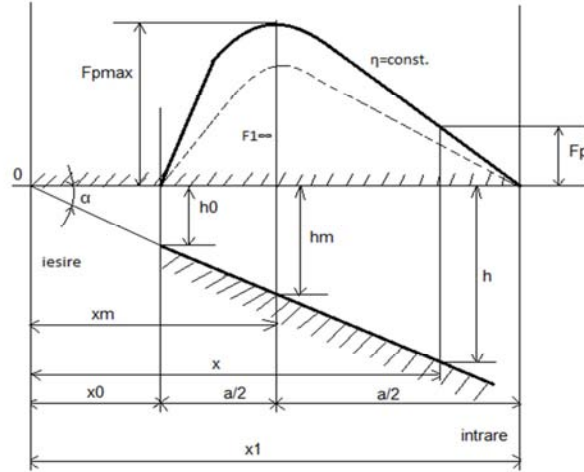


Fig: 1.22.

$$p_x^* = 6\eta v \int_{x_0}^{x_1} \frac{h-h_m}{h^3} dx = \frac{6\eta v}{a \cdot \left(\frac{h_0}{m \cdot a}\right)^2} \Phi_0 \cup \Phi_0 = \frac{(1-\xi) \cdot \xi}{(2m+1)(m+\xi)^2}; \quad (1.57)$$

$$F_{1,\infty} = \int p_x^* dx = \frac{6\eta v}{\left(\frac{h_0}{m \cdot a}\right)^2} \Phi_{1p} \cup \Phi_{1p} = m^2 \left(h \frac{m+1}{m} - \frac{2}{2m+1} \right); \quad (1.58)$$

where:

x_m – the coordinate where the sections average pressure and the height of the lubricant film is:

$$h_m = -\frac{2}{v} v_{1x} \cong a \cdot x_m$$

for $x=x_0$ the minimum thickness of the fluid film is :

$$h_0 = \alpha \cdot x_0 = \alpha \cdot m \cdot \alpha \text{ and } \xi = \frac{x-x_0}{a}; m = \frac{x_0}{a}. \quad (1.59)$$

The friction torque at the interface will be:

$$M_{fr} = 2\pi\mu p_{max}^* \int_r^R r^2 dr = \frac{2}{3}\pi\mu(R^3 - r^3) \cdot p_{max}^* = \mu \cdot F_{ax} \cdot r_m \cup r_m = \frac{2R^3 - r^3}{3R^2 - r^2} \quad (1.60)$$

Together with the Newton and Reynolds equations, the friction force coefficient are:

$$\tau = \eta \frac{dv}{dy} \rightarrow F_{f1,\infty} = \int_0^a \left[\frac{\tau(h)}{\tau(0)} \right] dv = \int \eta v \left(\frac{4}{h} - 3 \frac{h_m}{h^2} \right) dn \quad (1.61)$$

$$\mu = \frac{F_{f1,\infty}}{F_{1,\infty}} = \frac{h_0}{a} \Phi_{1\mu} \cup \Phi_{1\mu} = \frac{1}{3} \left(\frac{2}{m} + \frac{m}{2m+1} + \frac{1}{\Phi_{1p}} \right) \quad (1.62)$$

From the friction power expression:

$$P_{fr} = \mu \cdot F_{ax} \cdot v \quad (1.63)$$

The factor $(p_m^* v_m)$ can be global criteria for the heat control of the friction joint's rings:

$$(p_m^* v_m) = \frac{F_{ax} \cdot \omega}{\pi(D-d)} \leq (p_m^* v_m)_a ; \quad (1.64)$$

Where ω – rotation speed

$$v_m = \omega \cdot r_m \cup r_m = \frac{1}{4}(D+d_0)$$

The fluid friction regime, where the friction coefficient is minimum (Fig: 1.21) appears at the rotation speed (ω) at a limit value of the Sommerfeld invariant (S_0):

$$[S_0] = \frac{p_m \psi^2}{\eta[\omega]} \cup p_m^* \rightarrow [\omega] = \frac{p_m \psi^2}{\eta[S_0]}; [v] = [\omega]r \cdot 10^{-3}; \quad (1.65)$$

$$[\mu] \cong 3 \left(\frac{\eta[\omega]}{p_m^*} \right)^{1/2} \cup p_m^* \quad (1.66)$$

At the boundary friction domain the friction coefficient is:

$$\mu = \frac{\mu_{lim}([\omega] - \omega) + \mu([\omega] - \omega_{lim})}{[\omega] - \omega} \cong \mu_{lim} - \frac{\omega}{[\omega]} ([\mu] - \mu_{lim}) \quad (1.67)$$

From the thermal equilibrium equation results the regime temperature of a boundary friction face seal:

$$P_{fr} = \mu \cdot F_{ax} \cdot v = k \cdot A_T \cdot \Delta t ; t_f = t_0 + \frac{P_{fr}}{k \cdot A_T} \leq t_{max} ; \quad (1.68)$$

where:

k- Thermal coefficient; A_T – the free surface (heat exchanger) of the seal;

The friction regime and the thermal equilibrium are independent. So, the effective friction coefficient (μ) and the regime temperature of the sliding friction joint (t_f) are established by iterations function the temperature lubricant's viscosity variation.

1.6.6. Conclusions

The functional/performance parameters of a mechanical face seal depend on the interface pression and temperature distribution. Therefore, it is very important to know them and the FEM analysis allows the tension distribution, the displacements and the temperature determination. All the other parameters can be then determined.

1.7. Automotive Mechanical Face Seals – Tribological Simulation

1.7.1. Aims and background

The behavior of a face seal is determined by the complex interaction of a number of factors. Advantages are usually attained at the price of disadvantages in other directions. For example if the roughness is constant, an increase of the contact pressure reduces leakage[89], but the wear and frictional heat increase. As against this, increasing leakage losses can reduce the friction and heat production, but the effectiveness of the unit as a seal is reduced. Again, a high friction may not only lead to increased wear but also, due to thermal distortion, to considerable leakage losses, or it may cause the seal to break down because of a thermal stress cracks.

By appropriate seal design, choice of materials and type of seal arrangement, individual requirements such as minimum leakage, maximum life or minimum friction can be met. The research presents the finite element method (FEM) and experimental analysis of the leakage and friction rates of a mechanical face seal for the chemical industry. The behaviour of a mechanical face seal in run can be simulated and illustrated on the computer.

For any of the type dimensions taken into consideration the basic structure consists of primary sealing, formed of:

- the pressure ring/floating ring, elastic and/or in movement of rotation;
- the fixed counter face friction ring.

The ensemble of the sealing shows axial symmetry, both from the point of view of geometry and mechanical loading[54]. Structurally speaking, the pressure ring assembled in elastic way, has 5 degrees of freedom, and some forces act upon it: hydrodynamic force, elastic force, the force of the pressure in the clearance, the centrifugal force and so on.

The simulation on the computer is based upon a solution of the equations of motion of the element assembled in elastic way associated with the interaction of the two rings due to the surface contact with friction[24],[5],[27].

The analysis through FEM allows the detection of instabilities and the determination of the functional parameters of the mechanical face seal[25],[26].

The most important parameter, from the point of view of the performance, is the leakage flow-rate Q proportional with h^3 (the size of the clearance)[28],[29].

Maintaining a pre-established distance between the active surfaces of the rings of the primary seal, which is dependent on the kinematics of the pressure ring[55],[83], the force and moment system to which some forces are opposed, forces like hydrostatic (HS), hydrodynamic (HD), thermo-hydrodynamic (THD) or elastohydrodynamic (EHD) and mechanical through the surface contact with friction, are the key factor in their design[81].

1.7.2. The mechanical face seal-axi-symmetrical problem of modelling

Finite element of symmetrical axial type. The axisymmetrical structures are three-dimensional bodies of revolution[30].

If both the mechanical and thermal loadings are axial symmetrical, the components of displacement in a section that passes through the symmetry axis, completely define the deformation state and the stress state in the structure. Due to this particularity, in the analysis of the stress state, these structures are not treated after the procedures of the three-dimensional analysis, but as a particular case of the bi-dimensional problems in the state of plane deformation.

In many cases, the representation of the behavior of a solid is possible through a bi-dimensional model, exploiting the specific characteristics of the state of tension or deformation or introducing hypothesis.

It is the case of problems of plane deformations, of the plane state of tension, of torsion (the Saint-Venant model), in problems of thin cover and in axisymmetrical problems. In the board in Fig. 1.23 [24],[25],[26],[27],[28] there are mentioned the hypothesis used for obtaining the bi- or one-dimensional models in cartesian or cylindrical coordinates.

The symmetrical analysis is a very powerful modelling technique allowing the reduction of the model size under symmetry without harming the accuracy of the results. This technique asks for symmetrical geometry, symmetrical properties and conditions at limit, but does not involve compulsory symmetry when applying loading. Once the model is created, the conditions at limit and the superposition of the effects may be used for obtaining solutions in the case of asymmetrical loading.

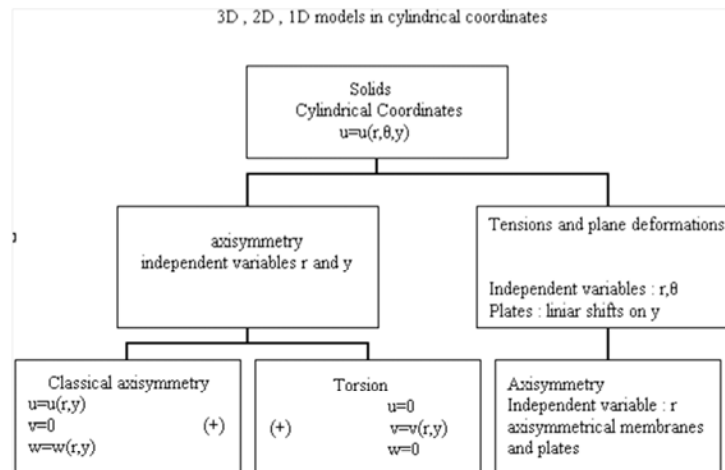


Fig. 1.23. 3D, 2D, 1D models in cylindrical coordinates

By using some components of symmetrical and/or asymmetrical loading, whose effects are superpositioned, the asymmetrical real loading may be achieved. Digitization of a body of revolution of some shape is made in finite elements of a special kind, with the shape of some rings with constant transversal section. These elements called axisymmetrical are bi-dimensional elements

used for representing volumes of revolution. The axisymmetrical elements may be defined in the plane xy or xz of the global coordinates system, and the postprocessing is done for the whole volume of the structure.

For the study of the structure in this case, the study of a section that contains the body axis of revolution is enough and the representation is done in the axis system x, y (Fig. 1.24). For such an element, the knots become nodal circles, with the center on the axis of revolution.

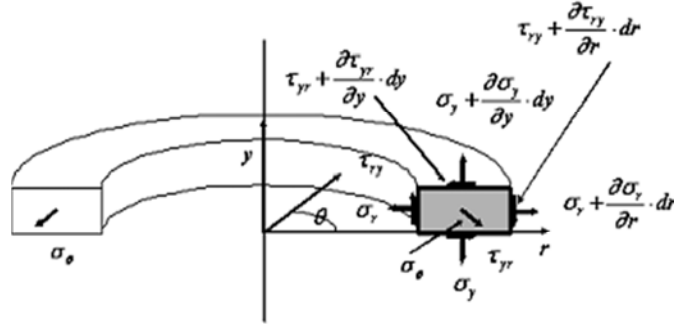


Fig. 1.24. Ring with constant transversal section

The transversal section of the ring-shaped element is defined in a certain transversal section which contains the axis of revolution. Due to symmetry, shifts on circular-lined direction are not produced. The shift vector has, thus, only components on radial direction u and axial direction v . As a result, the degrees of freedom, attached to the element, are the knotted values of these shifts.

The approximation functions express, thus, the variation of these components on the element domain:

$$\begin{Bmatrix} u(r, y) \\ v(r, y) \end{Bmatrix} = [N] \cdot \{\delta\} \tag{1.69}$$

Where $\{\delta\}$ is the vector of knotted shifts.

If natural coordinates s, t are used, the relation becomes:

$$\begin{Bmatrix} u(s, t) \\ v(s, t) \end{Bmatrix} = \begin{bmatrix} N_1 & 0 & N_2 & 0 & \dots & N_n & 0 \\ 0 & N_1 & 0 & N_2 & \dots & 0 & N_n \end{bmatrix} \cdot \begin{Bmatrix} u_1 \\ v_1 \\ \vdots \\ u_n \\ v_n \end{Bmatrix} \tag{1.70}$$

where $n=4$ in the case of four-sided three-dimensional elements

The natural coordinates are normalised coordinates obtained by rating the global coordinates of the entire domain of digitisation to characteristic measures of the finite element.

The axisymmetrical problem differs from the state of plane deformation from the point of view that the normal specific deformation on the plane of work section ϵ_0 is not equal to zero and must be developed in the vector of the specific deformations $\{\epsilon\}$.

Its value is expressed in the following form:

$$\varepsilon_\theta = \frac{u}{r} \quad (1.71)$$

The relation between the specific deformations and shifts has the form:

$$\begin{Bmatrix} \varepsilon_r \\ \varepsilon_y \\ \varepsilon_\theta \\ \gamma_{ry} \end{Bmatrix} = \begin{bmatrix} 1 & 0 & 0 & 0 & 0 \\ 0 & 0 & 0 & 1 & 0 \\ 0 & 0 & 0 & 0 & \frac{1}{r} \\ 0 & 1 & 1 & 0 & 0 \end{bmatrix} \cdot \begin{Bmatrix} \frac{\partial u}{\partial r} \\ \frac{\partial u}{\partial y} \\ \frac{\partial v}{\partial r} \\ \frac{\partial v}{\partial y} \\ u \end{Bmatrix} \quad (1.72)$$

The connection between the tensions and specific deformations is:

$$\begin{Bmatrix} \sigma_r \\ \sigma_y \\ \sigma_\theta \\ \tau_{ry} \end{Bmatrix} = \frac{E}{(1+\nu) \cdot (1-2\nu)} \cdot \begin{bmatrix} 1-\nu & \nu & \nu & 0 \\ \nu & 1-\nu & \nu & 0 \\ \nu & \nu & 1-\nu & 0 \\ 0 & 0 & 0 & \frac{1-2\nu}{2} \end{bmatrix} \begin{Bmatrix} \varepsilon_r \\ \varepsilon_y \\ \varepsilon_\theta \\ \gamma_{ry} \end{Bmatrix} \quad (1.73)$$

where E is the longitudinal coefficient of elasticity; ν – coefficient of Poisson.

If [J] is the Jacobean matrix of conversion and [J] is its reverse, then the derivatives of shifts u, v in relation with global system r, y has the following form:

$$\begin{Bmatrix} \frac{\partial u}{\partial r} \\ \frac{\partial u}{\partial y} \\ \frac{\partial v}{\partial r} \\ \frac{\partial v}{\partial y} \\ u \end{Bmatrix} = \begin{bmatrix} \bar{J}_{11} & \bar{J}_{12} & 0 & 0 & 0 \\ \bar{J}_{21} & \bar{J}_{22} & 0 & 0 & 0 \\ 0 & 0 & \bar{J}_{11} & \bar{J}_{22} & 0 \\ 0 & 0 & \bar{J}_{21} & \bar{J}_{22} & 0 \\ 0 & 0 & 0 & 0 & 1 \end{bmatrix} \cdot \begin{Bmatrix} \frac{\partial u}{\partial s} \\ \frac{\partial u}{\partial t} \\ \frac{\partial v}{\partial s} \\ \frac{\partial v}{\partial t} \\ u \end{Bmatrix} \quad (1.74)$$

where the derivatives vector in relation with the natural system s,t is calculated with relationship (1.70):

$$\begin{Bmatrix} \frac{\partial u}{\partial s} \\ \frac{\partial u}{\partial t} \\ \frac{\partial v}{\partial s} \\ \frac{\partial v}{\partial t} \\ u \end{Bmatrix} = \begin{bmatrix} \frac{\partial N_1}{\partial s} & 0 & \frac{\partial N_2}{\partial s} & 0 & \dots & \frac{\partial N_n}{\partial s} & 0 \\ \frac{\partial N_1}{\partial t} & 0 & \frac{\partial N_2}{\partial t} & 0 & \dots & \frac{\partial N_n}{\partial t} & 0 \\ 0 & \frac{\partial N_1}{\partial s} & 0 & \frac{\partial N_2}{\partial s} & \dots & 0 & \frac{\partial N_n}{\partial s} \\ 0 & \frac{\partial N_1}{\partial t} & 0 & \frac{\partial N_2}{\partial t} & \dots & 0 & \frac{\partial N_n}{\partial t} \\ N_1 & 0 & N_2 & 0 & \dots & N_n & 0 \end{bmatrix} \begin{Bmatrix} u_1 \\ v_1 \\ \vdots \\ u_n \\ v_n \end{Bmatrix} \quad (1.75)$$

Relation (1.75) has a general form, which is valuable both for the linear finite elements and for those of superior order. In the particular case of mechanical face seal model, $n=4$, the element has four knots in r, y plane.

Relations (1.72), (1.74) and (1.75) allow the matrix $[B(s,t)]$ calculus in the relation:

$$\{\epsilon\}=[B]\{\delta\}$$

We notice that matrix $[B]$ contains only four lines in comparison with the plane problem with only three. The matrix of elasticity is at its turn of 4×4 given by relation (1.73). For the calculus of the matrix of stiffness the numeric integration of the expression is also used:

$$[k]=\int_V [B]^T \cdot [E] \cdot [B] \cdot dV \quad (1.76)$$

The *axisymmetrical finite element model of the mechanical face seals*. The knowledge of induced stress configuration of the entire structure is necessary so that we could run some modifications of its configuration in order to satisfy better the conditions imposed by the solicitation, material, reliability, etc.

The basic problem of modelling, having as destination the stress analysis requests the determination of the induced stress in areas where their gradient is high.

The calculus models which use the displacement method – in this category the method of the finite element is also included – uses as basic entity the structure matrix of stiffness, the primary unknowns of the model being the knots shifts of the digitisation array, the tensions are the secondary unknowns. So, for these kinds of models a stiffness analysis of the structure is made.

Geometrically speaking, the mechanical face seals presents rotational symmetry for it is made from revolution bodies (Fig. 1.25).

The study presents two types of chemistry mechanical face seals analysed by FEM that run at $p = 0.1$ MPa, $n = 3000$ rev./min, with fluid at 80°C .

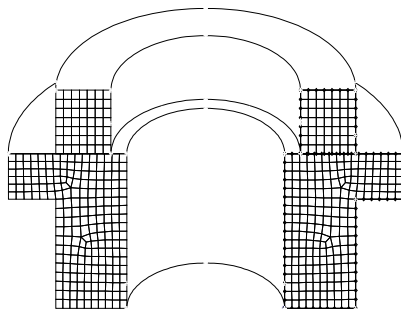


Figure 1.25. Finite elements digitization of the primary seal of a mechanical face seal

Materials combination for primary sealing rings of the mechanical face seal is also known (Table 1.2).

Tab: 1.2 Materials combination for primary sealing rings of the mechanical face seal

<u>Carbo-graphitic material</u>	<u>Cod</u>
Carbo-graphitic materials binded with resin	B1
Rough coal impregnated with resin	B14
Rough coal impregnated with antimony	B17
<u>Plastics</u>	
PTFE + 20% Fiberglass	Y1
PTFE + 25% Graphite powder	Y2
<u>Metallic material</u>	
Ion-nitrate stainless steel	G1
Stainless steel (40C130)	G10
<u>Metallic carbide</u>	
Wolfram Carbide	U1
Silicium carbide	U2
<u>Ceramics</u>	
Al ² O ³ - 89%	V1
Basalt	V2

The models analysis repeats for each two constructive types made by different materials pairs. The contact is described by a new type of 'slide line' elements which includes the stiffness/friction dates, the scale factor and the friction coefficient between the contact surfaces.

The analysis results are shown on sections (Fig. 1.26), and the analysis program system is presented in figure 1.27.

The post-processing concerns geometric digitisation and analysis results in order to control the analysis validation:

- the check up of correct application of the piece, real dimensions, of total volume and of total mass;
- the check up of correct application of loads and of used physical and mechanical proprieties (taking the parts into account the heterogeneous character of the assembly);
- intensity control of deformations and stress (deformations smaller than 0.002 for the steel, for example);
- the check up of global equilibrium conditions using the loads and the calculates reactions;
- the check up of the conformity of the main tensions value with the geometric assembly orientation;
- the displacement amplitude in ratio with the parts dimensions according to the geometrical linearity.

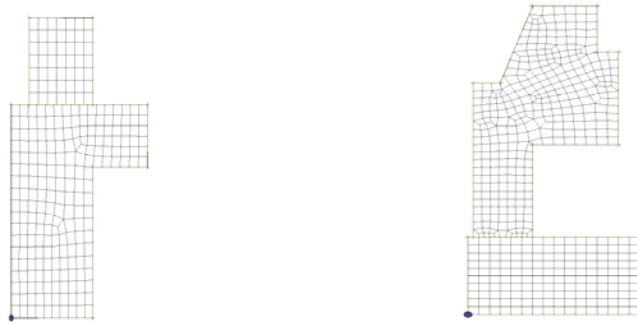


Figure 1.26. Mechanical face seal sections

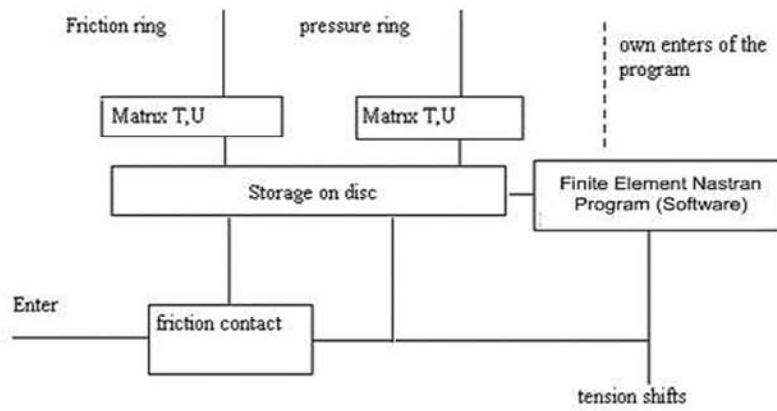


Figure 1.27. Analysis program system

1.7.3. Simulation results

The modelling reproduces the run in behavior of two types of chemistry mechanical face seals. The axial pressure applied to the pressure ring will induce a contact pressure field manifesto in ring friction couple interface. Also this determinates the tension distribution and the displacements. From the thermal point of view the modelling suppose the knowledge of the:

- thermal characteristics of the ring materials;
- sealed fluid temperature;
- temperature which results from the friction in the contact interface.

The size and the distribution of the contact pressures of the axial displacement which determines the size and the shape of the clearance, the theoretical temperature chart, and the thermal flux, result after the FEM analysis (Fig.1.28). The performances parameters of the mechanical face seals depend on pressure distribution and on the interface temperature. FEM applied on mechanical face seals models analysis has given multiples results of the tensions distribution, the displacements, the temperature distribution and of the thermal flux². After post-

processing, we obtain also the interface contact pressure distribution, the displacements and the thermal loads of the rings (Fig. 1.27).

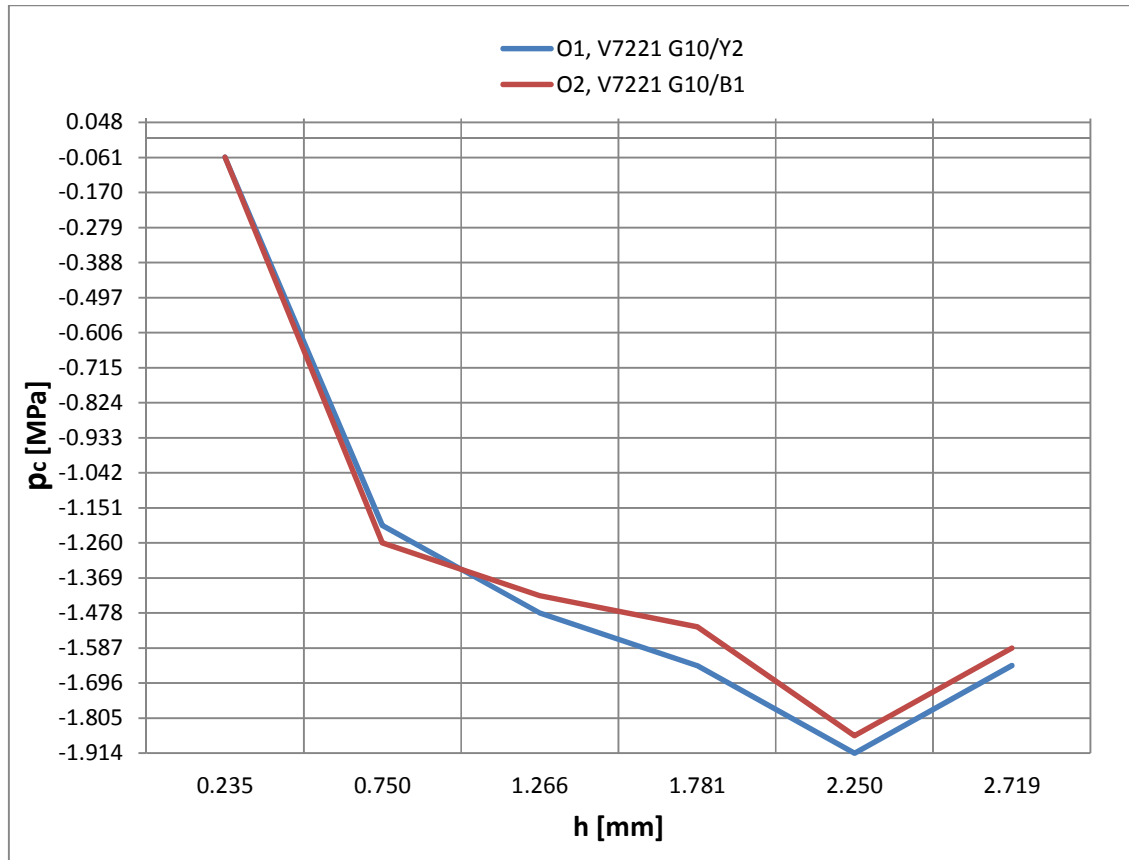


Fig. 1.28. The contact pressure distribution along the interface of a face seal by FEM

1.7.4. Leakage flow-rate evaluation

In unisothermal flow case of a incompressible fluid for an axial symmetry configuration, the Reynolds equation has the following form[31]:

$$\frac{d}{dr} \left(\frac{h^3}{\eta} \frac{dp}{dr} \right) = 0 \quad (1.77)$$

where η is dynamic viscosity of work fluid.

Keeping in mind the following:

- in the limit below of the mentioned case, the float rate of leakage in the clearance is given by:

$$Q = \frac{\pi d_m \Delta p h^3}{12 \eta b} \quad (1.78)$$

where $d_m = 0.5(d+D)$; $b = 0.5(D-d)$; $h = 0.5(Rz1+Rz2)$;

Δp – the tension drop from the interface.

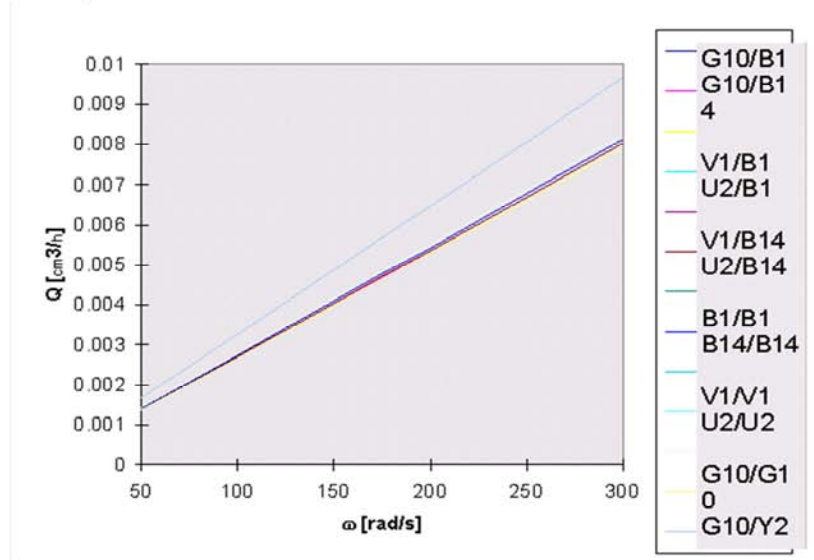


Fig. 1.29. Flow losses variation through outflows to a frontal tightening angular speed functional for different material

- the dynamic viscosity varies due to the temperature (T) of the fluid on a Slotte dependence (polynomial):

$$\eta = \frac{\eta_f}{1 + (T - T_f)} \quad (1.79)$$

where η_f is dynamic viscosity of working fluid at the reference temperature T_f ;

- power lost due to the friction in the interface is:

$$P_{fr} = \mu \cdot p_a A_T r_m \omega \quad (1.80)$$

where: μ -friction coefficient in the interface. $A_T = \pi(D^2 - d^2)/4$

ω -angular speed of the pressure ring (it transforms into heat).

$$P_{fr} = k_T A_T (T - T_f) \quad (1.81)$$

where: $k_T = \frac{\lambda_1}{l_1} + \frac{\lambda_2}{l_2}$

$\lambda_{1,2}$ - thermal conductivity of the ring materials.

$l_{1,2}$ - axial dimension of the rings.

The new flow relation:

$$Q = \frac{A_T h^3}{12b^2} \frac{\Delta p}{\eta_f} \left(1 + \frac{\mu p_a A_T \omega}{2\pi b k_T} \right) \quad (1.82)$$

or:

$$Q = \frac{A_T h^3}{12b^2} \cdot \frac{\Delta p}{\eta_f} \cdot \left[1 + \frac{\mu}{k_r} \cdot (pv) \right] \quad (1.83)$$

The flow losses variation through outflow to a frontal tightening are presented in figure 1.29

1.7.5. Conclusion

FEM analysis has taken into consideration the two physic aspects with fundamental influences on mechanical face seals function like: thermal and mechanical.

From mechanical point of view, the safe function of mechanical face seals involves the existence of stable cover of fluid in the clearance couple. It must carry the contact pressure created on the interface through the elastic elements and also the pressure of the tightening fluid. The stable functioning can be perturbed when the thermal and mechanical displacement of the assembly are combined with the nonlinearity induced through an unfit assemblage. From the analysis of the friction contact surfaces results that:

- the film thickness is of a micrometer size, order of the same size as the geometrical precision of the plane combined with the form and position deviations, which is also dependent on the relative position (nonalignment) of the activesurfaces of the primary sealing rings
- the transversal sections of the sealing surface must be as uniform as possible in order to prevent distortions;
- the contact pressure in the clearance shows an allure that confirms the theory of the hydrodynamic lubrication;
- the variation of the contact pressure with friction in the clearance, on radial direction is quasi-identical for all the pairs of analysed materials with some exception (the antifriction superior properties of PTFE (Y2));
- the maximum value of the contact pressure for any of the analysed alternatives is bigger than the pressure of the sealed fluid which ensures the fulfill of the sealing function;
- by knowing the real distribution of the calculated pressures in the clearance one can evaluate with precision the most disadvantageous level of the flow rate;
- the axial displacements of the pressure ring resulted through calculus are of the same sense with those of the friction ring, overcoming them with values that do not lead to the installation of dry friction (at limit – adherence) but keeping the sealing function;
- the axial displacements of the two rings of the primary sealing with values between (0.012, 0.1) μm are situated below the level of the measure of the microgeometric active surfaces, having an insensible influence over the clearance measure;
- for materials couple PTFE/PTFE (Y2/Y2) the level of axial displacements overcomes the microgeometric measure of the active surfaces, not being recommended to be used.

NOMENCLATURE

h – the size of the clearance
 kT – heat transfer factor
 n – rotational speed
 p – sealed fluid pressure
 r – radius
 s, t – natural coordinates
 u – radial direction shift vector
 v – axial direction shift vector
 x, y, z – global coordinates
 E – longitudinal coefficient of elasticity
 Q – leakage flow-rate

ω – angular speed
 ϵ_0 – normal specific deformation on plane of works section
 η – dynamic viscosity of working fluid
 ν – coefficient of Poisson
 σ – tension
 $\{\delta\}$ – vector of knotted shifts
 $[J]$ – the Jacobian matrix.

1.8. Calculation by Finite Element Method (FEM) of Temperature Distribution in the Components of a Mechanical Face Seal

1.8.1 Aims and background

The temperature in the seal interface due to frictional heat has a considerable influence on the behavior of a face seal, affecting wear and thermal distortion. If the temperature is too high vaporization of the lubricant film occurs, causing increased friction and wear [1],[82]. The safe working temperature of the face materials can also be exceeded and the seal will then fail due to welding or thermal stress cracks. The friction heat produced in the seal interface can be removed by conduction, convection and radiation processes. The heat produced in the seal interface is transported away by conduction in the seal rings and from the seal rings it is passed on to surrounding fluids by convection. Some also is lost to the surroundings by radiation. The maximum temperature in the interface is of particular interest[66].

Face seals are used over a temperature range from -200°C to $+1000^{\circ}\text{C}$. The properties of many materials are only known at room temperatures so that exact calculation of the maximum permissible temperature difference and thermal resistance factors at the working temperatures is not possible[87].

1.8.2. Fundamentals

Different temperatures and their gradients influence the geometry of the seal gap. In the case of elastic distortion the magnitude of the elastic modulus and the dimensions of the rings are the determining factors and in thermal distortions it is the values of the thermal properties of the materials[62], such as thermal conductivity λ , thermal expansion coefficient α , and heat factors in conjunction with the construction of the rings which influence the temperature gradients and, in turn, the gap shape[29].

The temperature gradient in both axial and radial directions influences the geometry of the seal gap.

A. Axial temperature gradients

The axial temperature gradient leads to distortion of the sealing rings. Newman and Forray[5] derived formula for the thermal distortion of the face of a ring, elastically clamped on the internal or external diameter. With the notation of figure 1.30 (where: d – inner diameter of the ring; D – external diameter of the ring) and assuming that there is a linear axial temperature gradient,

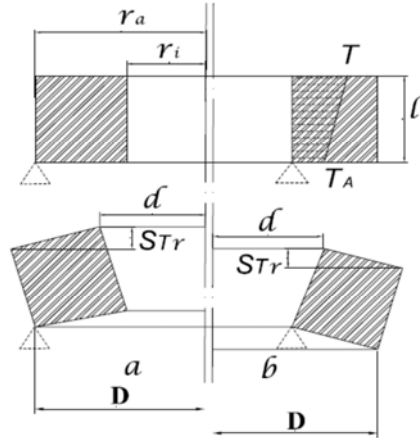


Fig: 1.30. Thermal distortion due to axial temperature gradients. (a) light clamping on the external edge; (b) light clamping on the internal edge.

$$S_{Tr} = \frac{\alpha C_a (r_a^2 - r_i^2) C_F}{2} \quad (1.84)$$

Where:

$$C_a = \frac{T - T_A}{l}$$

and C_F is a shape factor.

With face seals, the heat loss is mainly at d or D . In the case of distortion due to the influence of the axial temperature gradient, heat loss at D has the effect of producing a negative distortion S_{Tr} , i.e. contact results at d . If the heat loss is at d then the outermost regions of the ring are hotter and contact occurs at D , making S_{Tr} positive¹.

B. Radial temperature gradients

In mechanical seals there are often several heat sources which strongly influence the radial temperature distribution in the rings.

In addition to the friction heat from the sliding interface, the medium to be sealed may be a source of heat, as well as a hot shaft or housing, and heat from liquid turbulence. Depending on the direction of the temperature gradient (the heat loss can be at d or D) the temperature distribution in the sealing rings can differ considerably. Those areas of the rings which lie furthest from the heat sink or are nearest to the source of heat show the highest temperatures. They expand to a greater extent than other sectional areas and alter the shape of the original parallel film gap. Assuming a constant source of heat and constant operating conditions, with a linear temperature gradient in axial direction, we have:

$$C_r = \frac{T-T_A}{e} \text{ in } ^\circ\text{C/mm}, \quad (1.85)$$

$$e = r_a - r_i$$

for the axial ring distortion, and the approximate formula:

$$S_{T_a} = \alpha l C_r \quad (1.86)$$

results where α is the thermal expansion coefficient for temperature range $(T+T_A)/2$ and l the axial length of the ring which is expanding. The radial temperature gradient C_r depends upon the heat source, the thermal conductivity and the heat transfer coefficient, which in turn is influenced by the liquid, the viscosity and the speed. Exact values for constant operating conditions can only be established by tests. If the heat sink lies at D , then S_{T_a} becomes negative and the contact of the rings is at the internal periphery. For a heat reduction at d , S_{T_a} is positive and contact takes place near the external periphery [5].

C. Temperature gradients

The axial and radial temperature gradient distributions in mechanical seals can differ considerably. Above all, the seal design, construction of materials, location of heat sink, quantity of heat to be dissipated, the heat transfer coefficients and the cooling method all have a considerable influence. Exact values can only be attained by measurement under operating conditions.

Qualitatively, however, it can be said that a low conductivity is associated with a large temperature gradient and high face temperature and vice versa. Furthermore, for the same conductivity, the temperature gradient in the rotating ring is higher than in the stationary ring, if both rings are in contact with the coolant. Also, the better the heat transfer coefficient from ring to medium, the higher the temperature gradient in the ring [5].

D. The heat transfer coefficient

Seal rings have to be at a higher temperature than the sealed medium (coolant) in order for heat to be transferred from ring to medium. In most face seals the frictional heat flows axially in the ring since the heat sinks are normally at d and D . If equal areas are assumed and the seal width b is taken for the heat flow path length, and a constant coolant temperature t is assumed:

$$\frac{PfV}{C_4} = \frac{\lambda(T-t)}{b} \quad (1.87)$$

where:

P – net closing force per unit area of interface;

f – friction coefficient;

V – relative sliding speed of interface;

C_4 – conversion factor depending on units used;

t – temperature of sealant or coolant.

In fact, however, the heat transfer process is considerably more complicated. The heating effect can be limited or increased by the design and layout of the rings, the insulating effect of elastomeric mountings and static seals, compression seating and surface coatings and by

indentations in the seal surfaces or ring parts. The transfer from seal ring to coolant involves various temperature differentials. The heat transfer coefficient is a function of the Reynolds Number Re , laminar flow assists the heat transfer process. Viscosity, flow rate and entry turbulence of the coolant in the seal space, or additional agitation of the coolant liquid, open springs and indentations of the seal also have a strong influence on the heat transfer. If all these factors are combined in one dimensionless heat dissipation factor C_w for a constant operating condition and one type of seal, then the temperature T in the seal gap is:

$$T = \frac{PfVb}{C_w C_4 \lambda} + t \quad (1.88)$$

Depending upon the nature of the coolant and the operating conditions, the values of C_w lie in the range 0.2 – 0.9, the actual temperatures in the seal gap can be considerably greater than those calculated by equation (1.87). Thus the heat dissipation factor C_w can be defined as the relationship of the seal interface temperature to the actual temperature T_w :

$$C_w = \frac{T_R}{T_w} \quad (1.89)$$

The temperature dependence of thermal conductivity λ must also be considered in equation (1.88). A linear variation of the temperature coefficient β for the temperature range in question can be assumed and the average value set at:

$$\lambda_m = \frac{\lambda_T + \lambda_{T_1}}{2} \quad (1.90)$$

E. Heat crazing

One of the greatest dangers in mechanical seals is the formation of thermal stress cracks on the sliding faces. These can be caused by a momentary overload due to dry running, as a result of failure of the coolant or by a large load or speed variation. The cracks lead to increased wear and with balance of seals can cause the seal face to part.

Thermal stress cracks can be largely avoided if the physical and mechanical properties of the face and the operating conditions are considered carefully enough when the seal is designed.

A surface cracks when differential thermal expansion causes the surface stress to exceed the material strength. Using Hooke's law [27],

$$E\varepsilon = \sigma_1 - \nu\sigma_2 \quad (1.91)$$

and the thermal expansion equation

$$\varepsilon = \Delta T \alpha \quad (1.92)$$

Kingery calculated the greatest permissible temperature difference ΔT which the material can just bear without being damaged by thermal stress [27]:

$$\Delta T = \frac{\sigma_z(1-\nu)C_1}{E\alpha} \quad (1.93)$$

where:

ν – Poisson's ratio;

E – elastic modulus;

σ_z – tensile strength.

The form factor C_1 takes into account the shape of the ring. The calculation of the highest permissible temperature difference ΔT in the surface depends on the thermal conductivity of the material. The greater the thermal conductivity the smaller is the results breakdown. Many years of practical experience and test results confirm that to assess the resistance of an individual material to heat crazing, a factor $B_1 = \Delta T \lambda$ can be used. This is the thermal stress resistance factor.

The values of the maximum permissible temperature difference are not by themselves sufficient to determine the thermal stress effect, and the resistance factor B_1 is therefore introduced.

Carbon and graphite, in particular, are notable and with good dry running characteristics, high chemical stability and great stiffness, are particularly suitable as seal materials¹.

1.8.3. Axial symmetrical modeling of heat transfer in primary seal of a mechanical face seal

Equation expressing mathematically a body temperature field, is :

$$\Theta = f(x, y, z, t) \quad (1.94)$$

and the temperature gradient:

$$\text{grad}\Theta = \vec{n}_0 \frac{\partial \Theta}{\partial \vec{n}} \quad (1.95)$$

If q represents the unitary thermal flux, the Fourier law expression becomes:

$$q = -\lambda \frac{\partial \Theta}{\partial \vec{n}} = -\lambda \cdot \text{grad}\Theta \quad (1.96)$$

The heat conductivity coefficient λ is a material constant and varies with the temperature linearly, in most cases. The temperature variation in space and time in a body interior or a field, is expressed by the differential equation of conduction (Fourier) [1.91, 1.92]:

$$\frac{\partial}{\partial t}(\gamma c t) = \frac{\partial}{\partial x} \left(\lambda_x \frac{\partial \Theta}{\partial x} \right) + \frac{\partial}{\partial y} \left(\lambda_y \frac{\partial \Theta}{\partial y} \right) + \frac{\partial}{\partial z} \left(\lambda_z \frac{\partial \Theta}{\partial z} \right) + M \quad (1.97)$$

where:

Θ – temperature;

t – time;

c – specific heat;

γ – specific weight;

$\lambda_{x,y,z}$ – coefficients of thermal conductivity after x,y,z directions;

M - the flow of internal heat sources.

In the variational approach of the method, the integration of the equation (1.87) in time and space limit conditions, is equivalent to minimizing:

$$J = \int_V \left\{ \frac{1}{2} \left[\lambda_x \left(\frac{\partial \theta}{\partial x} \right)^2 + \lambda_y \left(\frac{\partial \theta}{\partial y} \right)^2 + \lambda_z \left(\frac{\partial \theta}{\partial z} \right)^2 \right] - \left(M - c\gamma \frac{\partial \theta}{\partial t} \right) \theta \right\} dV - \int_{S_2} q \theta dS + \int_{S_2} \alpha \theta \left(\frac{1}{2} \theta - \theta_E \right) dS \quad (1.98)$$

where:

α – heat transfer coefficient by convection from surface S to the surrounding environment or reverse;

θ_E – exterior environment temperature.

The problem can be treated as an bidimensional case, if the structure's geometrical form and thermal load, shows axial symmetry. In the seal form Fig.1.30 the temperature varies only by x and y axes, and the finite element is a tor with quadrilateral section. In equation (1.95) radius x is variable on finite element's surface as so for the toroidal finite element the expression becomes [6]:

$$J = 2\pi \bar{r} \int_{V_e} \frac{1}{2} \left[\lambda_x \left(\frac{\partial \theta}{\partial x} \right)^2 + \lambda_y \left(\frac{\partial \theta}{\partial y} \right)^2 \right] dV - \int_{V_e} M \theta_e dV - \int_{S_2e} q \theta_e dS + \int_{S_3e} \alpha \theta_e \left(\frac{1}{2} \theta_e - \theta_E \right) dS$$

(1.99)

Minimizing J results:

$$\left(2\pi \bar{r} \int_{V_e} [B]^T [D] [B] dV + \int_{S_1e} [N]^T [N] dS \right) \{ \theta \}_e - \int_{V_e} M [N]^T dV - \int_{S_2e} q [N]^T dS - \int_{S_3e} \alpha \theta_E [N]^T dS = 0$$

(1.100)

If we consider the radius in the center of gravity of the finite element, the differential element of volume will be $dV = 2\pi \bar{r} dA$ [27],[29],[30]. For the finite elements with heat exchange by thermal flux on the contour, the differential element of surface is: $dS = 2\pi r' dl$, where $r' = \frac{(x_k + x_i)}{2}$ is the radius measured at the half side which has heat exchange by thermal flux.

For finite elements with heat exchange by convection, $dS = 2\pi r'' dl$, where $r'' = \frac{(x_i + x_k)}{2}$ is the radius measured at the half side which has heat exchange by convection. Assuming in this case too, that M is constant on the surface of the finite element and that: q, α , θ_E are constant on the finite element's side with heat exchange on the contour, the equation (1.100) becomes:

$$\left(2\pi\bar{r}^2 \int_{A_e} [B]^T [D] [B] dA + \alpha r'' \int_{l_3 e} [N]^T [N] dl \right) \{\Theta\}_e - 2\pi\bar{r}M \int_{A_e} M [N]^T dA - 2\pi r' q \int_{l_2 e} [N]^T dl - 2\pi r'' \alpha \Theta_E \int_{l_1 e} [N]^T dl = 0 \quad (1.101)$$

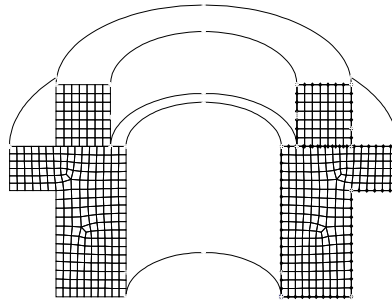


Fig:1.31. Meshing in axisymmetric elements of the EFS103 – S mechanical face seal.

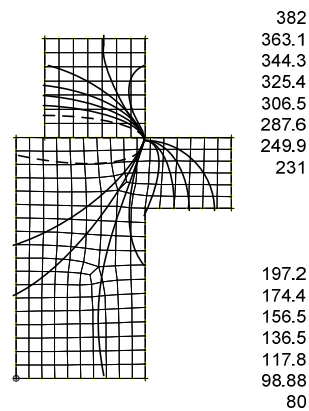


Fig: 1.32. Isotherms distribution in primary seal rings of the EFS103 – S mechanical face seal for sealed environment of water with detergent at 80°C.

The analysis of the thermal state with FEM [2] of the sealing rings depends on the temperature of the sealing zone and the heat produced by the interface between the rings due to relative motion with friction ($n=3000$ rot/min) [27],[29],[30]. The mechanical face seals present rotational symmetry for it is made from revolution bodies (Fig. 1.31). The results of the calculations with FEM are given in figure 1.32.

1.8.4. Conclusions

Instabilities of any nature are the main causes for removal from use of the mechanical face seals. Effects of temperature distribution are the key elements in the study of mechanical face seal's instabilities.

As a result, it is important to have a detailed knowledge about the thermal state of the primary seal rings.

2. Constructive and functional analysis of machine parts used in road vehicles

2.1 Rectangular section circlips / retaining rings axial load - carrying capacity considerations

2.1.1 Introduction. Fundamentals

The axial load-carrying capacity of the circlips. / retaining rings analyses wasn't found by the authors in literature. Some technical design necessities such as small axial dimensions in industrial robots pretension devices constructions lead the authors to take into account the research by means of FEM (finite element method) of this aspect. The conclusions of the study can be directly applied in technical design and in the future if experimental research results are added, the reconsideration of the present standards regarding shape, dimensions, and materials can be made [91].

Circlips / retaining rings are designed to position and secure component in bores and houses, simultaneously provide rigid end - play take - up in the assembly to compensate for manufacturing tolerances or wear in the retained parts.

The fundamental shaping of the circlip is of curved bars of same firmness. The ring must possess an exactly determined eccentricity z , so that it deforms approximately under tension. Following the computation method for the dimensioning of the rings is to be pointed out in this section. It concerns particularly the determination of the relations of the bending stress whether, the radial width b and the deformation D , -- d_3 (fig. 2.1).

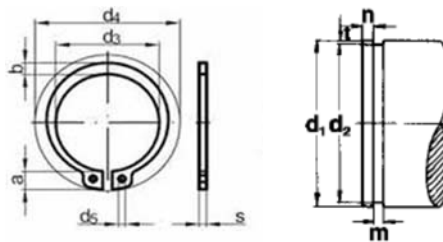


Fig. 2.1

For the technical designer, who uses standardized and/or in a list manufactured rings on shafts or in housings with nominal diameter, a computation is not necessary. It is of crucial importance however with special applications of the normal rings and particularly with the construction of special rings. The main requirement of the technical designer to the circlip is the transmission of greatest possible axial forces of the machine part which can be specified on the groove of the shaft or the housing. The circlip must exhibit as large a thickness as possible s and width b and the groove a large depth t for the fulfillment of this demand (fig. 2.1).

Since the ring with pre-loading must sit in the groove d_2 . The diameter d_3 of the ring is smaller in the relaxed condition than the g become groove diameter d_2 . For the assembly the inside diameter of the ring d_3 must be become so far increased, be pushed to it over the shaft with diameter D , can. The deformation of the ring should be as far as possible flexible thereby. The

bending stress resulting from the diameter change off is to be computed. To the circular deformation of a straight bar with the cross-sectional height b on a neutral radius of curvature r the well-known relationship applies

$$\frac{1}{r} = \frac{M_b}{EI} \quad (2.1)$$

where:

$$I = \frac{W \cdot b}{2}, \text{ for } \frac{M_b}{W} = \sigma_b, \text{ and for } 2 \cdot r = D \quad (2.2)$$

$$\sigma_b = \frac{E \cdot b}{D}$$

If a bar with a neutral radius of curvature r , already curved, is deformed on a radius ρ , the equation is: $\frac{1}{r} - \frac{1}{\rho} = \pm \frac{M_b}{EI}$ (2.3)

Using the names for the neutral diameters, usual with circlips

$$r = \frac{1}{2} \cdot D_3; \rho = \frac{1}{2} \cdot D_1; \frac{2}{D_3} - \frac{2}{D_1} = \pm \frac{M_b}{EI} \quad (2.4)$$

The further derivative takes place left for the shaft rings and right for the housing rings. Figure 2.2 shows circlips for shafts and housings with the main dimensions.

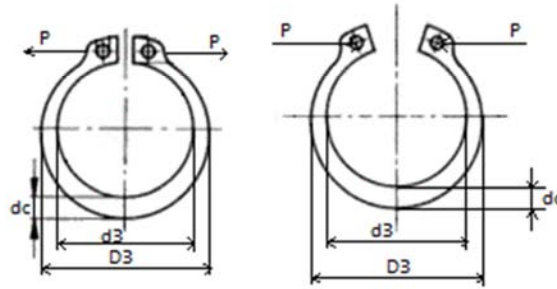


Fig. 2.2.

$$\frac{2}{D_3} - \frac{2}{D_1} = - \frac{M_b}{EI} \quad (2.5)$$

where $I = \frac{W \cdot b}{2}, \quad \frac{M_b}{W} = \sigma_b$

$$\frac{1}{D_1} - \frac{1}{D_3} = - \frac{\sigma_b}{E \cdot b} \quad \frac{1}{D_3} - \frac{1}{D_1} = - \frac{\sigma_b}{E \cdot b} \quad (2.6)$$

$$\sigma_b = \frac{(D_1 - D_3) \cdot E \cdot b}{D_1 \cdot D_3} \quad \sigma_b = \frac{(D_3 - D_1) \cdot E \cdot b}{D_1 \cdot D_3} \quad (2.7)$$

The size of the neutral diameter depends on the eccentricity z . Their correct choice is a condition for the application of the formulas. It is not possible to indicate for all kinds of ring and large fixed value for z . As average value can be set however.

$$\begin{aligned}
 D_3 &= d_3 + \frac{2}{b} + \frac{b-2z}{2} & D_3 &= d_3 - \frac{2}{b} - \frac{b-2z}{2} \\
 D_3 &= d_3 + 0,75 \cdot b & D_3 &= d_3 - 0,70 \cdot b \\
 D_1 &= d_1 + 0,75 \cdot b & D_1 &= d_1 - 0,70 \cdot b \\
 \sigma_b &= \frac{(d_1 - d_3) \cdot E \cdot b}{(d_1 + 0,75 \cdot b)(d_3 + 0,75 \cdot b)} & \sigma_b &= \frac{(d_3 - d_1) \cdot E \cdot b}{(d_1 - 0,70 \cdot b)(d_3 - 0,70 \cdot b)} \quad (2.8)
 \end{aligned}$$

Before one dissolves the equations 2.8 at given values of D . and d_3 for the computation the width after b , it is simpler to estimate the width first and calculate the tension. After the first result a correction is according to the relation:

$$\sigma_b \approx (d_1 - d_3) \cdot b$$

The then still existing deviations from the circle are seized in the equation 2.9. by the factor 1.15. The neutral diameters D . and D_3 amount to with circlips $D, = D, \pm b$ and/or. $d_3 \pm b$. it results then:

$$\sigma_b = \frac{1,15(d_1 - d_3) \cdot E \cdot b}{(d_1 + b)(d_3 + b)} \quad \sigma_b = \frac{1,15(d_3 - d_1) \cdot E \cdot b}{(d_1 - b)(d_3 - b)} \quad (2.9)$$

For the dimensioning of special pliers and for special applications of circlips it is often important in particular to know the forces which are necessary for the flexible deformation. This applies particularly with the utilization of the favorable feather/spring characteristics of the circlips firmness same as curved bars with the employment as foreign suspensions in electrical contacts.

$$\sigma_b = \frac{M_b}{W} = \frac{P \cdot l \cdot 6}{b^2 \cdot s}$$

Becomes:

$$P = \frac{\sigma_b \cdot b^2 \cdot s}{6 \cdot l} \quad (2.10)$$

The bending stress is computed after the equations 2.8 or 2.9. If it lies over the yield strength of the material, then only this may be used.

The crucial question with the application of the circlips is those the axial load-carrying capacity. It cannot be answered by denomination of a number. The maximum stress of the circlip connection depends on different always dunging factors.

The most important are the firmness of the work material, into which the groove is in-stung, the groove surface and the form of the pressing in slightly machine part (sharp edged, rounded, selvedge distance chamfers). There is thus computation methods necessarily, which consider these changing factor.

2.1.2 Computation of the circlip

Before today for the computation of the circlip used procedures were used, tried one frequently to compute the ring on cutting. With a ring in accordance with figure 2.3, sitting in a close deep groove, the possibility is given, against which a sharp edged machine part presses, that the ring in the cross section F is cut.

A condition is with the fact however that the materials of the pressing in slightly and the fixed part possess at least one firmness, which lies over that of the hardened spring steel of the circlip.

Since this condition is hardly ever given, and which selected relationship from groove depth to groove width is according to figure 2.4, are practically no cases admits become, with which a circlip was destroyed by cutting.

If the ring thickness is larger s than the groove depth t , before cutting the ring at the contact surface with the groove wall is stressed so highly on pressure that the material of the ring stretches itself, and up and the housing ring goes to the shaft ring together, i.e. they jump out of the groove[92]

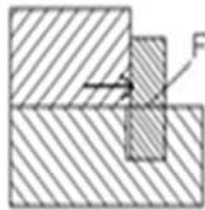


Fig. 2.3

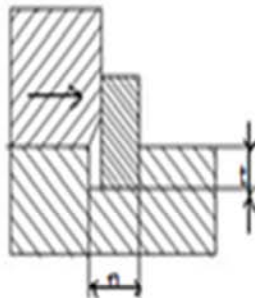


Fig. 2.4

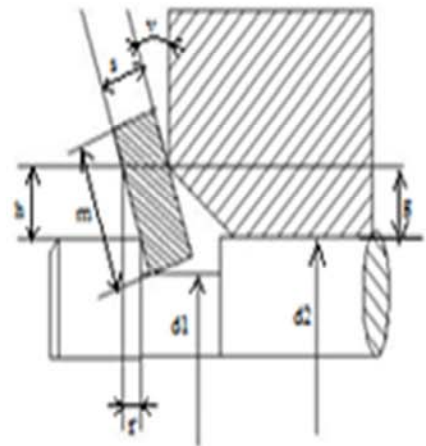


Fig. 2.5

And already for a long time the computation method for the ring, applied introduced by Seeger, with success, proceeds from the assumption that the ring deforms conical with the pressure of a machine part due to a bending moment or inverts, as one also says.

Figure 2.5 shows one in the cross section the better comprehensibility because of exaggerated strongly inverted represented circlip (inverting angle IP), which sits in the groove d_2 of a shaft D . Against the ring a machine part with the strength P , presses by chamfers g and the flexible deformation of the edge of groove i arises an effective lever arm h . due to inverting shifts itself the machine part axially the amount f .

If the machine part possesses a roundness, chamfers or a seldge distance, then the presence of the lever arm h is apparent.

In the case of sharp edged plant the lever arm arises if necessary as a result of flexible and also plastic deformation i of the groove and the pressing in slightly machine part by inverting tensions in the circlip, which with a too large inverting angle to lasting conical deformations and to break of the ring to lead, develop.

If one regards the circlip as an axially fitting with springs element, applies:

$$P_R = C \cdot f \quad (2.11)$$

The spring rate C of the circlip with one middle width b_m is calculated to:

$$C = \frac{\pi \cdot E \cdot s^3}{6 \cdot h^2} \ln \left(1 + \frac{2 \cdot b_m}{d_2} \right) \quad (2.12)$$

One sets the value constant for the individual ring

$$\frac{\pi \cdot E \cdot s^3}{6} \ln \left(1 + \frac{2 \cdot b_m}{d_2} \right) = K \quad (2.13)$$

$$\text{thus applies: } C = \frac{K}{h^2} \quad (2.14)$$

The lever arm h is independent of the ring and can vary with each application.

To small inverting angles Ψ applies according to figure 2.5:

$$\Psi = \frac{f}{h^2} \quad (2.15)$$

The equations 2.13, 2.14, 2.15 result in under introduction of security S :

$$P_R = \frac{\Psi \cdot K}{h \cdot S} \quad (2.16)$$

The invoice amount K is indicated for each circlip from the material spring steel. With the use of rings from materials with other modulus of elasticity E' the invoice amount K is to be corrected.

$$K' = K \cdot \frac{E'}{21000} \quad (2.17)$$

Equation 2.16 calculates the service life under the condition that the ring transfers the forces in a direction. This condition is nearly always fulfilled. If the ring should be stressed however changing in both directions, the load-bearing capacity is reduced by 30% [93].

2.1.3 Computation of the axial shift

Inverting a circlip under the pressure of a machine part conditionally in accordance with figure 2.5 an axial shift f . the shift is often small and without functional meaning.

In addition, there are constructions, with which the size of the shift of interest, occurring under the load, is. In the case of to large shift measures must be met if necessary for reduction the same. The computation of the shift f takes place also assistance of the equations 2.13 and 2.14.

From both equations results:

$$f = \frac{P \cdot h^2}{K} \quad (2.18)$$

To this purely theoretical shift, which does not consider any deformation of the groove edge and the pressing in slightly machine part, a so-called initial shift A is added as empirical value.

Them amount to 0.03 to 0.07 mm and consider the shift, which results, until all basic surfaces come fully to the request. For the overcoming of the initial shift, which more or less arises with all under pre-loading not standing connections, only small forces are necessary. It applies thus:

$$f = \frac{P \cdot h^2}{K} + A(\text{mm}) \quad (2.19)$$

The computational collection of the deformation of the groove edge and the pressing in slightly part is hardly possible.

With small lever arms, with which the theoretical shift is small and must on inaccuracies concerning the inverting angle be counted the results of the computation are unreliable.

With large lever arms against it the deformation of groove and machine part hardly affects itself and the calculation agrees good with the attempt due to the only small axial force.

If it is shown that with given strength P the shift is too high, either the squarely affecting lever arm h must by arrangement of a supporting disk made smaller or the invoice amount K by application of a strengthened circlip to be increased.

With the application of the axially fitting with springs Seeger rings it is to be known for the constructor from interest to, with which strength the play take-up takes place.

2.1.4 FEM results

The analysis was made for a DIN 471 Seeger ring of 8 mm. The applied load was scaled in 10 steps from 100 to 10000 N. Figures 2.6, 2.7, present the displacement state for a 400 and a 2500 N load. At the load of 2500 N. the deformation was of 10^{-2} mm when the assembly lost stability (the circlips inverts) [94].

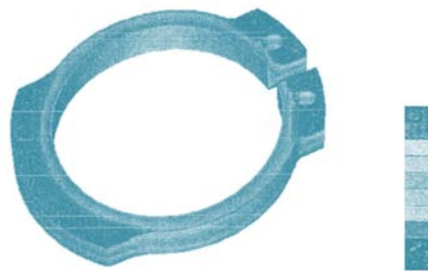


Fig 2.6



Fig 2.7

2.1.5 Conclusion

For the reaching of high load-carrying capacities it is to be thus always aimed at that the effective lever arm is as small as possible h . Even if already in the preceding sections one referred to occasionally on that, was to be made attentive again here in detail on it. Because if this influence of the lever arm on the load-carrying capacity of the circlips is also apparent, it must be particularly pointed out that this fact is frequently not considered sufficient. Serious damage is often the result.

In The FEM analyse, sharp edges were considered for the machine parts. In principle to differentiate between machine parts, those, usually is manufactured, sharp edged be can and such, which referred frequently as standard parts, one chamfers, rounding or a selvedge distance to exhibit. In the first case the danger always according to experience exists that the machine part, which could be kept sharp edged pressing in slightly to the circlip, chamfers one nevertheless in accordance with design receives, since all other sharp edges are broken and the technical designer ignores the influence the same on the load-carrying capacity of the circlip. Some technical design necessities such as small axial dimensions in industrial robots prehensile devices constructions lead the authors to take into account the research by means of FEM (finite element method) of this aspect.

The conclusions of the study can be directly applied in technical design and in the future if experimental research results are added, the reconsideration of the present standards regarding shape, dimensions, materials can be made. The authors aim to analyse in the future the influence of chamfers and rounding of machine parts on the lever arm of the axial load that affects the load - carrying capacity of the circlip. Also they plan to analyse circular section circlips.

2.2 Considerations upon the circular section of the circlips/retaining rings axial load-carrying capacity

2.2.1 Introduction

The reference standards as well as the specialty literature offer very many useful data to the designer. But, in specific applications, requiring small axial limits, they are insufficient to provide a satisfying safety without additional calculation. By means of FEM (finite element method), the authors are trying to point out the real behaviour of the assembly in such cases

Circlips / retaining rings are designed to position and secure component in bores and houses. Simultaneously they provide rigid end – play take – up in the assembly to compensate for manufacturing tolerances or wear in the retained parts. For the technical designer, who uses standardized and/or in a list manufactured rings on shafts or in housings with nominal diameter, a computation is not necessary. It is of crucial importance however with special applications of the normal rings and particularly with the construction of special rings.

The reasoning for the fundamentals of the bending calculus is presented in detail for circlips with rectangular section, and FEM analysis has been done.

The authors propose to analyze circular section circlips. The conclusions of the research can be directly applied in technical design. In the future, if experimental research results are added, also the reconsideration of the present standards regarding shape, dimensions, and materials can be made

2.2.2 Fundamentals

The strength calculation is based on the consideration that a circlip -for the shaft or for the housing– is a curved bended bar.[91, 95]. The ideal solution is a curved bar of same firmness.

The circular section is particularized in fig.2.8 and the following equations:

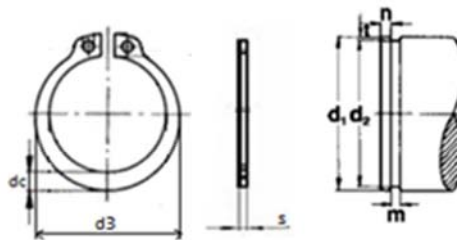


Fig. 2.8

$$\frac{1}{r} = \frac{M_b}{EI} \quad (2.20)$$

If a bar with a neutral radius of curvature r , already curved, is deformed on a radius ρ , the equation is:

$$\frac{1}{r} - \frac{1}{\rho} = \pm \frac{M_b}{EI} \quad (2.21)$$

Using the names for the neutral diameters, usual with circlips

$$r = \frac{1}{2} \cdot D_3; \quad \rho = \frac{1}{2} \cdot D_1; \quad \frac{2}{D_3} - \frac{2}{D_1} = \pm \frac{M_b}{EI} \quad (2.22)$$

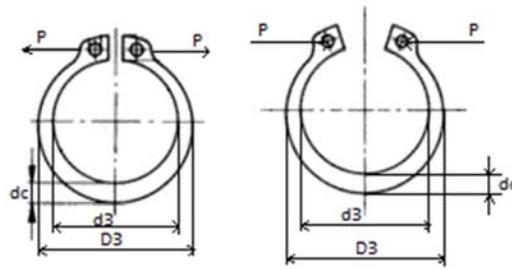


Fig. 2.9

$$\frac{1}{D_1} - \frac{1}{D_3} = - \frac{\sigma_b}{E \cdot d_c} \quad \frac{1}{D_3} - \frac{1}{D_1} = - \frac{\sigma_b}{E \cdot d_c} \quad (2.23)$$

$$\sigma_b = \frac{(D_1 - D_3) \cdot E \cdot d_c}{D_1 \cdot D_3} \quad \sigma_b = \frac{(D_3 - D_1) \cdot E \cdot d_c}{D_1 \cdot D_3} \quad (2.24)$$

$$\sigma_b = \frac{1,15(d_1 - d_3) \cdot E \cdot d_c}{(d_1 + d_c)(d_3 + d_c)} \quad \sigma_b = \frac{1,15(d_3 - d_1) \cdot E \cdot d_c}{(d_1 - d_c)(d_3 - d_c)} \quad (2.25)$$

$$\sigma_b = \frac{M_b}{W} = \frac{P \cdot I \cdot 6}{d_c^2 \cdot s} \text{ becomes } P = \frac{\sigma_b \cdot d_c^2 \cdot s}{6 \cdot I} \quad (2.26)$$

2.2.3 Computation of the circlip

For the special cases mentioned above it is of interest the axial loading behaviour (and axial load-carrying capacity) of the ring as well as its stability in the reserved groove (in the shift or housing)

Fig. 2.9 presents the situation in which a machine part presses a circlip with an axial force. At first sight, shearing seems to condition for the drawing out of use of the ring, so that, at the beginning of the use of these machine elements it was very much insisted on this kind of calculation. It was observed that, because of the relationship between the depth of the groove and the thickness of the

ring, the shear never takes place because at loadings under the maximum stress there takes place a loss of stability by deformation (as in fig. 2.10,a, b, c)

It is said that the ring is "inverted" The deformation is determined by the occurrence of a lever arm that modifies by a bending moment the shape of the ring that becomes conical. For a better understanding of the situation, the deformation (the characteristic angle ψ) is exaggeratedly enlarged. As to be seen, between the chamfer g and the level of the elastic deformation i of the groove edge, there appear the lever arm. It results in a displacement of the machine element adjacent on the distance f . Similarly, the phenomenon appears in the case of rounded edges at adjacent machine elements. For sharp edges, plastic deformation of the groove edge (together with elastic deformation) contributes also to the apparition of the lever arm. For loads that determine a too high value of the angle ψ there appear permanent conical deformations or even the failure of the ring.

If the ring is considered an axial elastically element, the formula (2.27) is applied

$$P_R = C \cdot f \quad (2.27)$$

$$\frac{\pi \cdot E \cdot d_c^3}{6} \ln \left(1 + \frac{2 \cdot d_{mc}}{d_2} \right) = K \quad (2.28)$$

$$C = \frac{K}{h^2} \quad (2.29)$$

$$\psi = \frac{f}{h^2} \quad (2.30)$$

$$P_R = \frac{\psi \cdot K}{h \cdot S} \quad (2.31)$$

$$K^I = K \cdot \frac{E^I}{21000} \quad (2.32)$$

2.2.4 FEM results

The analysis was made for a .STAS 8436-69 ring of 3.4mm.

The applied load was scaled in 10 steps from 15 to 1500 N.

In figures 2.11, 2.12 and 2.13, is presented the displacement of the ring for 150 and 300 N

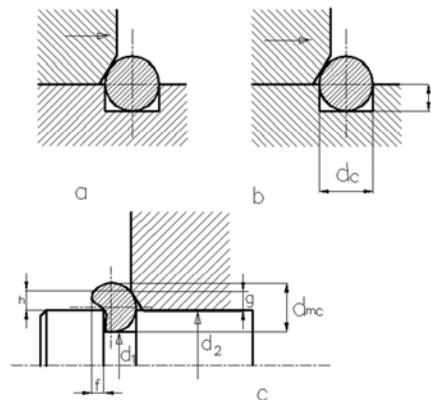


Fig. 2.10

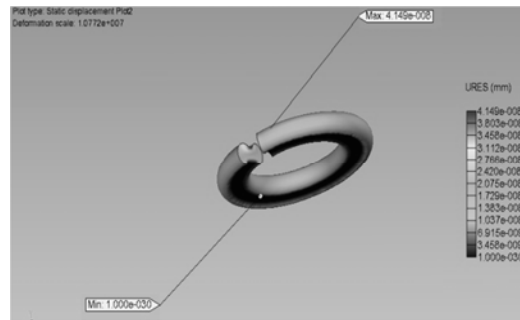


Fig. 2.11

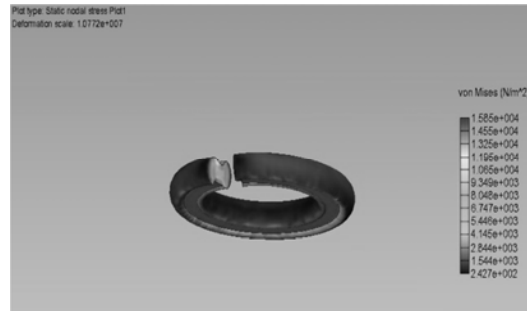


Fig. 2.12

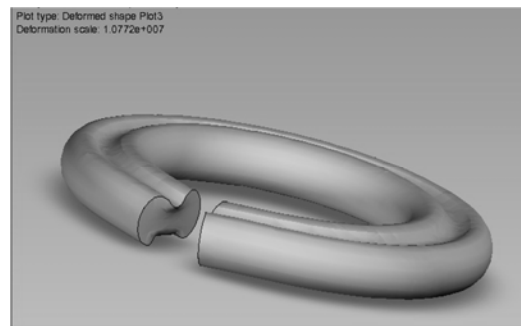


Fig. 2.13

2.2.4 Conclusions

For the reaching of high load-carrying capacities it is to be thus always aimed at that the effective lever arm is as small as possible h .

The conclusions of the study can be directly applied in technical design and in the future if experimental research results are added, the reconsideration of the present standards regarding shape, dimensions, and materials can be made.

2.3 On the priority of the modulus versus the center distance predimensioning of the evolventical gear calculus

2.3.1 Introduction

The study presents some interesting aspects about the strength of helical gears: the beam strength and the surface strength. A “minimum modulus” that guarantees the resistance of the gear at both strength, the beam strength and the contact strength as a “remedy” is proposed. The PC is utilized in order to ensure the arguments.

The research is devoted primarily to the analysis and design of helical gears to resist bending failure of the teeth and to resist pitting of failure of the tooth surface.

2.3.2 Teeth failure

Failure by bending will occur when the significant tooth stress equals or exceeds either the yield strength or the endurance limit. A surface failure occurs when the significant contact stress equals or exceeds the surface endurance strength.

The known (2.1), (2.2), (2.3), (2.4), (2.5), formula for computing the bending stress in gear teeth in which the tooth form (fig. 2.14) entered into the equation is:

$$\sigma_F = \prod Y_F \frac{K_F F_t}{b m_n} \leq \sigma_{FP} \quad (2.33)$$

$$i \in (F, \varepsilon S, \beta) \quad (2.34)$$

Relation (2.33) takes into account that the maximum stress probably occurs while a single pair of teeth is carrying the full load, at a point where another pair of teeth is just on the verge of coming into contact. The contact ratio should be somewhat greater than unity, say about 1.5, to achieve a quality gear set, so for the gears cut with sufficient accuracy, the top-load condition is not the worst, because another pair of teeth will be in contact when this condition occurs. Examination of run-in teeth will show that the heaviest loads occur near the middle of the tooth.

On the other hand pitting is a surface failure due to many repetitions of high contact stresses.

To obtain the expression for the surface contact stress the Hertz theory is employed. For gears pure rolling exists only at the pitch point (fig. 2.15). Elsewhere the motion is a mixture of rolling and sliding.

Equation(2.35) does not account for any sliding action in the evaluation of stress. The first evidence of wear occurs near the pitch line.

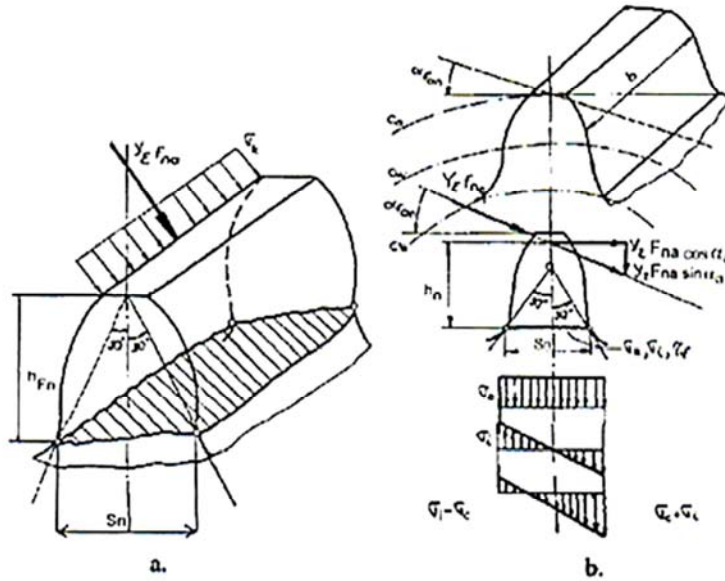


Fig. 2.14

$$\sigma_H = Z_E Z_\epsilon Z_H Z_\beta \left(\frac{K_H F_\beta u \pm 1}{d_{w1} b u} \right)^{1/2} \leq \sigma_{HP} \quad (2.35)$$

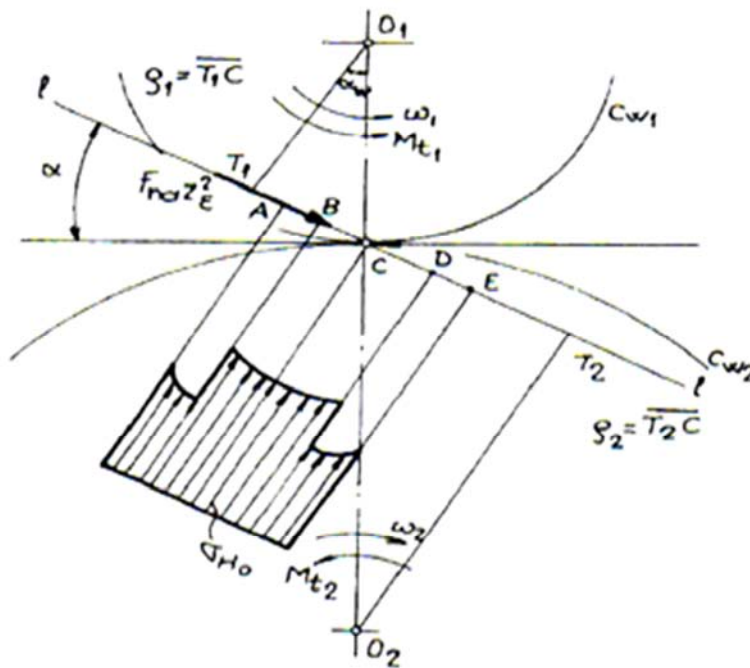


Fig. 2.15

2.3.3 Numerical application

For an imposed center distance of $a=200$ mm and a speed ratio $i=2$, the case taken into account in order to establish the variation of contact stress σ_H and of the bending stress σ_F for a helical gear is presented in table 2.1.

Table 2.1

Nr.	Item	Symbol	Unit	Pinion	Gear
1	Normal pressure angle	α_n	degree	20	
2	Helix angle	β	degree	8	
3	Coefficient of shifted profile	χ		+0,1079	-0,485
4	Dedendum	h_t		1,25 m_n	
5	Addendum	h_{an}		1,00 m_n	
6	Pitch circle diameter	d	mm	44,1	157,2806
7	Working pitch circle diameter	d_b	mm	41,4677	147,6250
8	Tooth width	b	mm	25	
9	Precision			8	
10	Surface roughness	R_a		0,8; 1,6	
11	Number of rotations	n	rpm	1850	925
12	Power	P	Kw	2,9	
13	Direction of load			Single direction	
14	Meshing number		repetition	Over 10^7 repetitions	
15	Material			41M ₀ C _r 11	40C _r 10
16	Surface hardness	HB	MPa	3000	2700
17	Lubricant			TIN 125EP STAS 10588-76 with 125-140 $mm^2/s(C_{st})$	
18	Strength Tolerable on dedendum	σ_{Ftim}	MPa	580	
19	Factor of profile	y_F		2,53	2,4
20	Factor of load distribution	y_ϵ		0,672	
21	Factor of helix angle	y_β		0,842	0,958
22	Factor of life	k_t		1	
23	Dimension factor of root stress	y_{sa}		1,63	
24	Dynamic load factor	k_v		1,053	
25	Over load factor	k_A		1	
26	Safety factor	S_F		1,25	
27	Allowable Hertz stress	σ_{Hlim}	MPa	760	

Table 2.1

Nr.	Item	Symbol	Unit	Pinion	Gear
28	Regional factor	Z_H			2,537
29	Material constant factor	Z_F	MPa ^{1/2}		189,8
30	Contact ratio factor	Z_ϵ			0,802
31	Factor of helix angle	Z_β			0,995
32	Factor of life	Z_N			1
33	Factor of lubricant	Z_L			1,05
34	Surface roughness factor	Z_R			1,02
35	Sliding speed Factor	Z_V			1,053
36	Hardness ratio factor	Z_W			1
37	Dimension factor of root stress	$K_{H\alpha}$			1,554
38	Factor of load distribution	$K_{H\beta}$			1,03
39	Dynamic load factor	K_V			1,053
40	Safety factor	S_H			1,15

For several values of the modulus and teeth number (Tab.2.2) the σ_H -contact stress and σ_F -bending stress were calculated with M-Design program.

Table 2.2

Modulus[mm]	1	1,25	1,5	2	2,5	3	4	5	6	8	10
Teeth number											
Z_1	130	107	89	67	53	44	33	27	22	16	13
Z_2	270	213	178	133	107	89	67	53	45	34	27

The results are presented in figure 2.16.

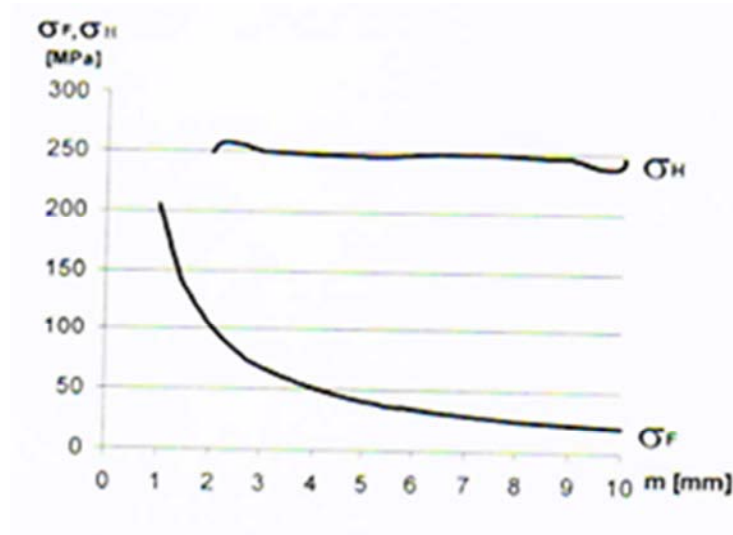


Fig. 2.16

2.3.4 Conclusions

From figure 2.16 results that the magnitude of the modulus influence essentially the bending strength of the helical gear (as the modulus increase, as the bending strength decrease considerably) and doesn't influence the contact strength.

So, for a certain chosen material it is convenient to pre dimension the minimum modulus that guarantees the bending resistance of the helical gear.

2.4 Determination of the optimum variant of shaft-hub joint for gears

2.4.1 Introduction

The evolution of the constructive solutions of the joint that form the cylindrical fitting specific to the gears determined the occurrence of some typified families whose carrying capacity tend to equal the performances obtained by the joint by shrinking joints. From figure 19 can be observed the advantage shown by the shrink joints with the double conics intermediate elements fig. 2.17 c, which allows the obtaining of high performance solutions.

The choice of one of the joint solution (fig. 2.17) according to the analyzed parameters (G/M_t) ; $(G/M_t)/(G/M_t)$ and $(G/M_t)/(G/M_t)_e = |(G/M_t)/(G/M_t)_e|/d$ - (fig.19)- give the best accomplishment of the formulated requirements.

Key words: shaft-hub, gears, key joints, elastic hub-hydropath

The principle of relatively immobilization (joint) of some parts that form the specific cylindrical fits for gears may be of the type: with or without intermediate elements [103], [100], [104].

From the category of the ones with intermediate elements are mentioned:

-Shrink joints with cylindrical smooth surfaces with intermediate conic elements -rings- annular keys (fig. 2.17.a);

-Shrink joints with cylindrical smooth surfaces with intermediate elements elastic hub-hydrograph (fig. 2.17.b);

-Shrink joints with double conic intermediate elements (fig. 2.17.c);

-Key joints (fig. 2.17.d).

Of the category of those without intermediate elements are mentioned:

-Shrink joints pushed or fretted (fig. 2.17.e).

According to the figure 2.17 it is observed the existence of a large number of modalities of relatively fixing the shaft and the hub, but the main request of choice of one of the alternatives is constituted by the ratio between the weight and the transmissible torque, that is that of a maximum carrying capacity.

In the choice of the fixing solution of the gear on the shaft, it always must be made a compromise between the economic requirement for a compact construction, of some low costs of fabrication and the technical condition of a great carrying capacity [100] (

The best accomplishment of some requirement like: high reliability, safety in exploitation, the minimum of tension concentrations, high qualities of the fabrication of joint surfaces etc., depends on the consideration of the following conditions:

a) The choice of a solution that best accomplishes the working requirements.

b) The compact construction and the right dimensioning of all the joint elements.

c) The use of proper materials.

d) Mechanical working and thermal treatments as cheap as possible.

e) The easy assembling and disassembling.

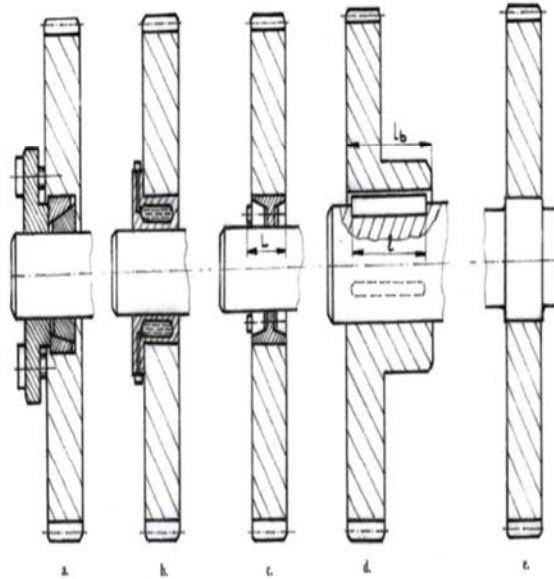


Fig. 2.17

f) Optimum servicing and working conditions for on all the load steps.

Each condition in part has a more or less influence on the carrying capacity, so at the question regarding “THE MOST FAVORABLE” choice of the joint it cannot be found an universal right/valid answer without a comparative analysis.[103].

2.4.2 Comparative analysis

Among the options of fixing the gear on the shaft (fig. 2.17) are analyzed the alternatives c) and d) which are considered to be the most used in the machine construction.

The choice derives also by the fact that at an inadequate process of the joint surfaces, but also a inadequate thermal treatment or a defective assembling drives at unfavorable displacement of the contact spot which determine the occurrence of some extremely high normal forces (fig. 2.18).

The consequences can be failures of the surface, bending breaking or displacements.

In such of these cases, errors of execution and assembling determine a real carrying capacity, which can be really different from the calculated one.[100, 101].

The calculations were made for:

- $d \in (25;400)$ mm- the shaft diameter;
- σ_{BG} - the fatigue coefficient of concentration [100];
- $\sigma\sigma$ - dimensional coefficient [100];
- $\sigma\sigma$ - the surface quality coefficient [100];

- Shaft material OL 50 STAS 500/2-80;
 - The torsion of the shaft is after a pulsate cycle;
 - $c=1,5$ the safety coefficient at the fatigue resistance;
- It was determined: the weight of shaft included in hub (G);

- transmissible torques of joint (M_t);
- the ratio between the weight and the transmissible torque (G/M_t);
- $(G/M_t)/(G/M_t)_{\text{standard}}$.

The values of the mentioned parameters are shown in the table 2.3.

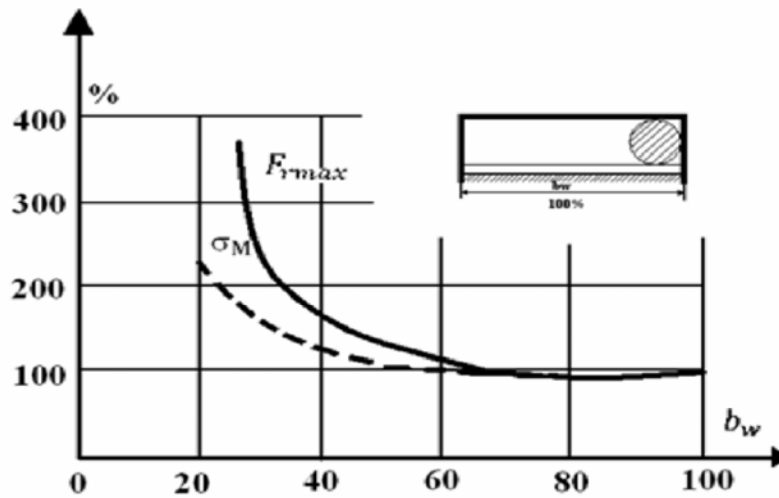


Fig. 2.18.

Tab. 2.3 The values of the mentioned parameters

No.	d [mm]	One key joint		Two key joints		DOBIKON(standard)	
		$(10^{-3}G)/M_t$		$(10^{-3}G)/M_t$	$\frac{G/M_t}{(G/M_t)_e}$	$(10^{-3}G)/M_t$	$\frac{(G/M_t)}{(G/M_t)_e}$
0	1	2	3	4	5	6	7
1	25	1.52	7.23	0.93	4.42	0.210	1
2	28	1.216	5.15	0.93	3.94	0.236	1
3	30	1.099	4.30	1.02	4.00	0.255	1
4	35	1.176	3.37	0.66	2.47	0.348	1
5	40	1.297	5.19	0.886	4.19	0.211	1
6	50	1.327	4.97	0.928	3.74	0.267	1
7	60	1.338	5.17	0.924	3.59	0.257	1
8	70	1.419	6.14	0.956	4.13	0.231	1
9	80	1.381	5.67	0.884	3.66	0.244	1
10	100	1.234	5.66	0.951	4.36	0.218	1
11	130	1.447	5.52	0.975	3.72	0.262	1
12	160	1.353	6.66	0.884	4.35	0.203	1
13	190	1.630	6.12	1.021	3.83	0.266	1
14	220	1.675	6.54	1.033	4.03	0.265	1
15	240	1.674	6.36	0.975	3.70	0.263	1
16	280	1.9	7.19	1.055	3.99	0.264	1
17	300	1.86	7.29	1.065	4.17	0.255	1
18	360	1.94	7.26	1.098	4.11	0.267	1
19	400	1.92	7.41	1.086	4.20	0.259	1

According to the obtained values the dependence $[G/M_t]/[G/M_t]_{\text{etalon}}$ (d) that reflects the maximum carrying capacity of the joint, is represented graphically (fig. 2.19).

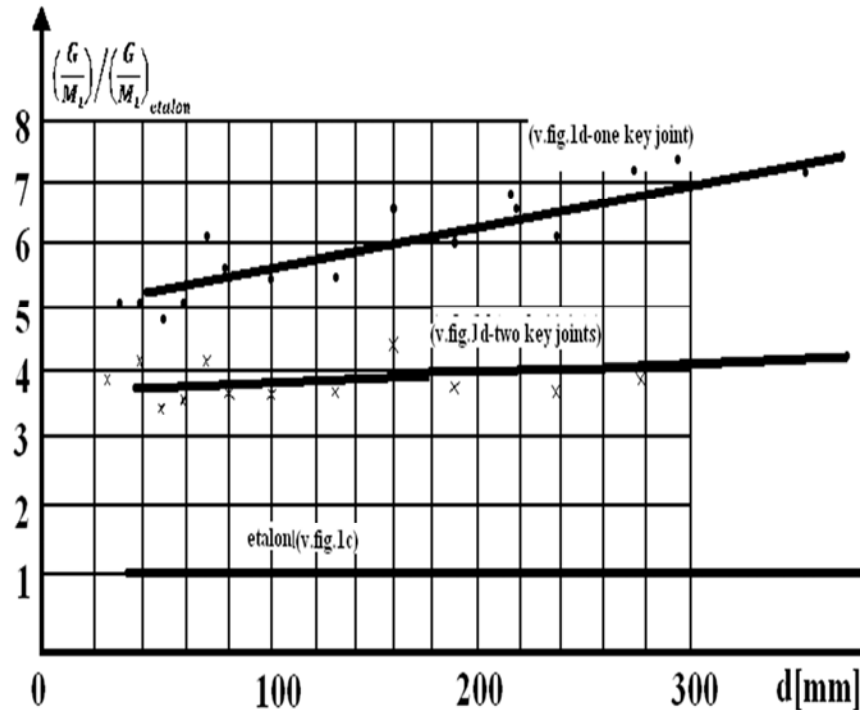


Fig. 2.19.

2.4.3 Conclusion

The evolution of the constructive solutions of the joint that form the cylindrical fitting specific to the gears determined the occurrence of some typified families whose carrying capacity tend to equal the performances obtained by the joint by shrinking joints.

From figure 2.19 can be observed the advantage shown by the shrink joints with the double conics intermediate elements fig. 2.17c, which allows the obtaining of high performance solutions.

The choice of one of the joint solution (fig. 2.17) according to the analyzed parameters (G/M_t) ; $(G/M_t)/(G/M_t)$ and $(G/M_t)/(G/M_t)_e = |(G/M_t)/(G/M_t)_e| / (d)$ - (fig. 2.19)- give the best accomplishment of the formulated requirements.

2.5 Hydraulic and termographical test rig for automatic gearboxes

2.5.1 Introduction

This document contains experimental data regarding operational stats and thermal stats of an automatic gearbox. Experimental data regarding the operating pressure and the command of the solenoid actuators is being expressed in percentage and current and is being recorded on the hydraulic test rig for establishment and optimization of the clutches and brakes operations from an automatic gearbox.

This test rig is made for testing the automatic gearboxes under different speeds and with varying torque through all the gears.

On this test rig is mounted only the hydraulic control block of the tested gearbox. The test rig is presented in figure 2.20 and figure 2.21.



Fig. 2.20. The test rig of the control block for determining the functional parameters of the clutches and brakes with the visualization of the register data.

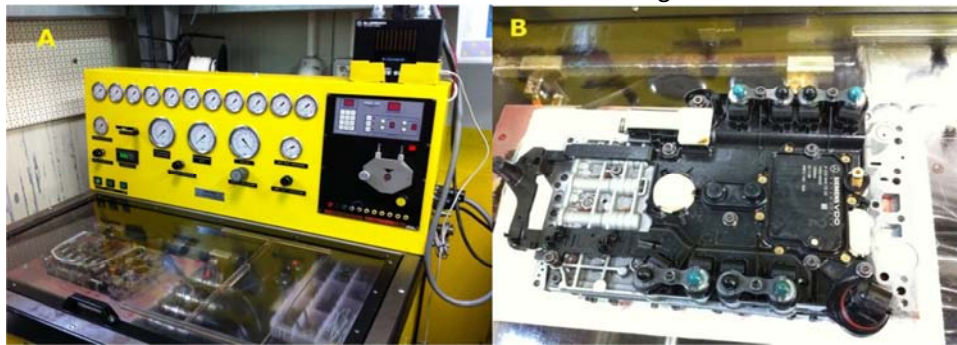


Fig. 2.21. A) Detail of the control pannel of the test rig and its hydraulic control module; B) Hydraulic block of the 7G TRONIC gearbox.

Figure 2.22 represents the change of pressure influenced by the gear and the clutch or brake of the 7G TRONIC, as follows: K1 clutch „1”, acts on “Ravigneaux” planetary gear set responsible for the gears 3, 4, 5; K2 clutch „2” responsible for the gears 4, 5, 6, 7; K3 clutch „3” responsible for the gears 1, 2, 3, 5, 6, 7, R; B1 brake „1” responsible for coupling the gears 2, 6, R; B2 brake „2” responsible for coupling the gears 1, 2, 3, 4; B3 brake „3” responsible for coupling the gears 1, 7, R; BR brake for reverse, responsible for coupling the reverse gears R1 and R2.[109,110 ,111 ,113]

Details regarding the hydraulic pressure for each clutch and break, correlated with the opening or closing of the pressure valves can also be found in tabular form. Values extracted from the hydraulic control module.

In figure 2.22 is represented the pressures when changing through all the gears in ascending order, then the engine torque is transferred to the gearbox through the lock-up torque converter (Lock-up, LU), then it simulates a descending gearchange. [107, 108]

Another part of the analysis on the test rig consists of a percentage analysis of valve opening under the action of the solenoids and electric current charged to the solenoid during the opening and closing time of the valves, according to the gear changing.

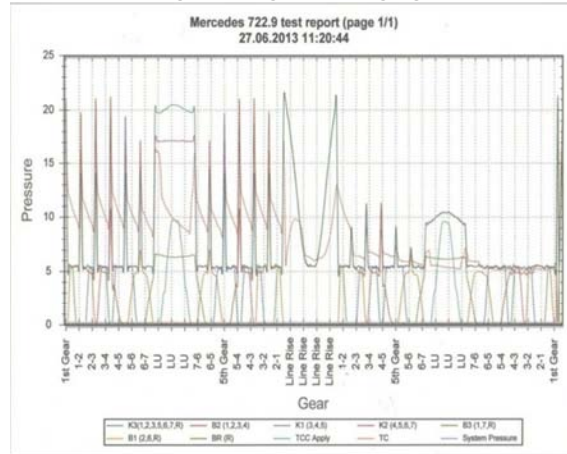


Fig. 2.22. Pressure analysis [bar] in 7G Tronic gearbox during the opening/closing of command valves of the clutches and brakes.

2.5.2 Thermographic registrations test rig

The dynamic test rig for automatic gearboxes allows recording of thermal phenomena with thermographic means. The test rig is shown in figures 2.23 and 2.24 where: A- 7G Tronic automatic gearbox; B-driving electric motor; C-brake; D-control panel.

On this test rig are recorded the temperature variations using a B200 Thermograph and temperature sensors (thermocouples) mounted on the gearbox housing.



Fig. 2.23. Dynamic test rig for automatic gearbox at variable speeds.

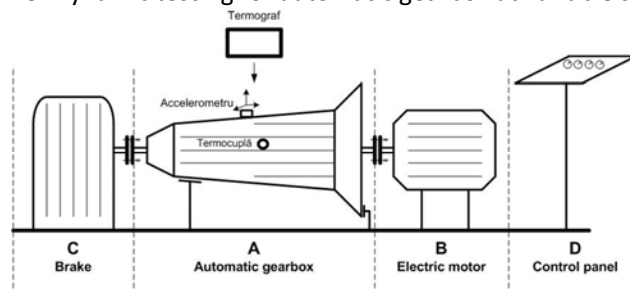


Fig. 2.24. Diagram of dynamic test rig.



Fig. 2.25. Detail "D" – Control panel.

During the thermographic experiment are recorded the temperatures released through the 7G Tronic gearbox housing, operating under idle and load, analyzing the distribution of the temperature in each gear.

The principle of thermographic method is based on measuring the surface temperature of the object using different methods: direct contact or telemetry. Direct contact measuring is the main method, using liquid crystal that changes its color depending on the local temperature. Telemetry calculates the temperature in a point, basing on the infrared energy emitted by the point.

Currently the infrared cameras have been greatly improved by allowing analysis of captured images, both static and dynamic.

For this purpose were taken a series of digital images with an infrared camera. The thermographic examination is used to measure the temperature of an object (in this case the automatic gearbox), using infrared detection devices based on self-releasing infrared radiation.

The thermograph analyzes the gearbox temperature, and measures the temperature change.

Very useful in this regard is the temperature gradient, represented by the temperature difference.

Infrared waves are electromagnetic waves in continuation of the visible light range from red spectrum. They are located in the wave length range 700 nm to 1000 μm . The thermograph captures a huge amount of information, as a consequence we need specialized software that captures analyses and processes the information transforming it in a color map that can later be interpreted by a thermography specialist.

The thermographic device is a FLIR B200 and presents a technique that detects and records the hot and cold areas of automatic gearboxes by detecting the infrared radiation emitted by the hot oil from the gearbox. [112] The main technical characteristics of this device are: resolution 200X150 pixels; 2X digital zoom; integrated digital camera; ability to make annotations; touchscreen; interchangeable lens 25 ° and optional 15 ° and 45 °.

The device's (figure 2.26) temperature measurement ranges from -20 °C to +120°C. The integrated digital camera (1.3 megapixels) allows observing and inspecting faster and easier, in addition it presents the "picture in picture" that allows overlapping of infrared film over digital image. [109]



Fig. 2.26. – The FLIR B200 device used in thermographic studying. A - the back of the device with the display and its setting. B - the underside of the device with the connecting hubs. C - normal photographic image in the display. D - Thermographic image of the same object in detail C. [112]

Also, on the test rig were mounted the thermocouples NI USB TC01 (figure 2.27) that have their own communication interface, without the need of a dedicated acquisition card.



Fig. 2.27. Thermocouple NI USB TC01, brand National Instruments.

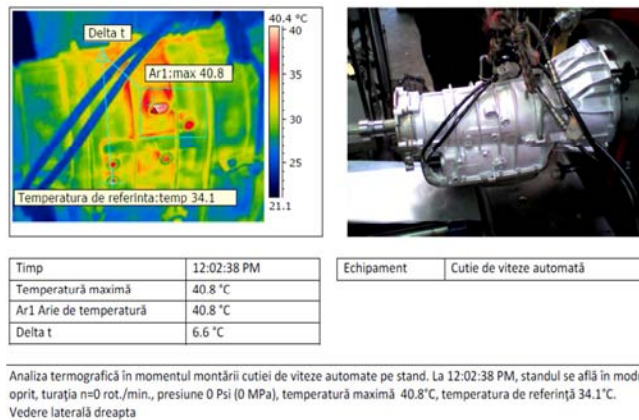


Fig. 2.28. Thermographic analysis at the beginning of the experiment.

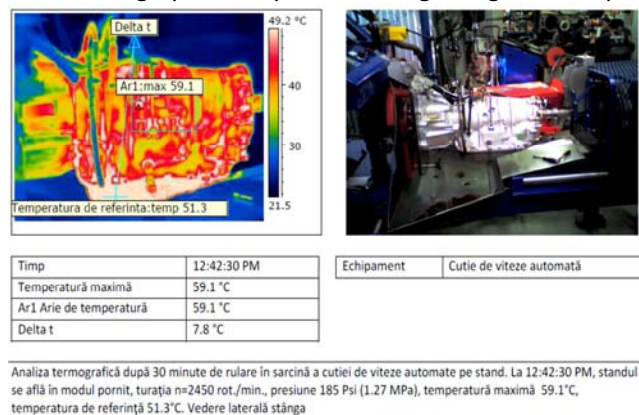


Fig. 2.29. Thermographic analysis at the end of the experiment.

Figure 2.28 shows the initial state of the thermographic experiment. This time, the automatic gearbox is fixed on test rig with special mount that also ensures the motion transfer from the engine-gearbox-brake.

Figure 2.29 represents the final moment of the experiment when the gearbox reaches the maximum temperature during entrainment on the bench.

The thermographic reports have four distinct elements for temperature reception:

- point called "Maximum temperature" [° C] is the point showing the maximum temperature of all recorded thermographic ;
- "Temperature area" represents the area that includes the point of maximum temperature;;
- point called "Reference temperature" [° C] is the medium temperature of the object studied thermographicly;
- point "delta t" is the unreferenced capture in the thermographic, it represents the difference between the "maximum temperature" and "reference temperature".

It can also be generated a full thermographic report, using the FLIR B200 and the NI USB TC01 thermocouple, regarding the evolution of the thermographic experiment of the automatic gearbox.

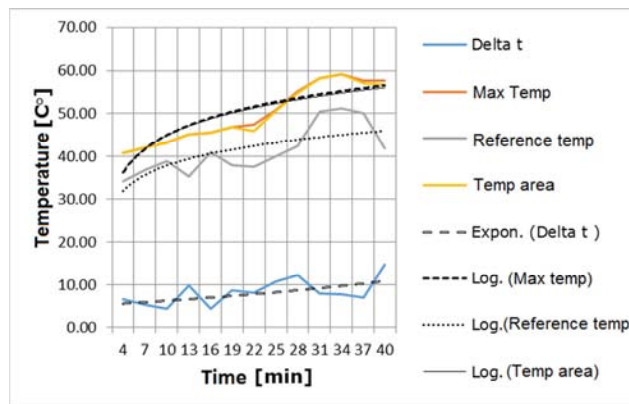


Fig. 2.30. Summary of thermography in time with each curve characteristic temperature trends.

In figure 2.30 was made a summary of the entire thermographic report of the automatic gearbox, observing the points of maximum temperature and temperature reference points. Also, for each of these curves were drawn trend lines using statistical regression method, thereby forecasts and estimates of possible temperatures.

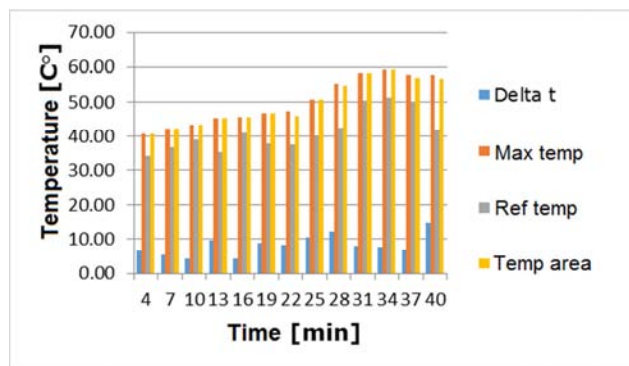


Fig. 2.31. Representing the entire thermographic report analyzed by bar chart.

Figure 2.31 shows the synthesis report of the automatic gearbox thermographic method highlighting the characteristic differences in temperature with respect of time, using the bar chart.

2.5.3 Conclusion

This correlation between the thermographic survey and the detail functioning of the automatic gearbox is highlighting emerging digital and thermal imaging of warmest areas in the automatic gearbox, especially the multi-couplings and planetary gears. These results will form the basis and reference to determine which areas will generate more heat therefore which areas will have more usage.

2.6 The energetic balance of the friction clutches used in automotive

2.6.1 Introduction

The energetic transfer through the friction clutch is accompanied by dissipative processes. The causes that produce these processes are the friction from the plate package. The dissipative restrictions that are independent of the temperature gradient or the direction of the heat flux present in the clutch's mass are imposed by the maximum temperatures admitted by the friction materials, by the electrically insulating materials and the lubricant (if it takes place in a wet environment).

A clutch is a device which transfers energy for one rotating shaft to another in order to perform some useful work.

In the simplest terms, a clutch can be thought of as a starting device because that is what happens when a clutch is engaged. But, more importantly, while engaged it is transferring energy. The clutch takes energy from a power source such as an engine and transfers it to where it is required.

A clutch consists on two halves: a driving half and a driven half. The driving half is attached to the power source and rotates with it. The driven half is attached to the shaft requiring the energy and is started with each engagement. In addition, the clutch must have some means of engaging and disengaging the two halves.

Friction couples rely upon a frictional force occurring between two surfaces to develop the required torque. The torque is called dynamic torque when slippage occurs between the surfaces and static torque when no slippage occurs. Usually the two surfaces are of dissimilar materials. The combination of the two materials used is referred to as friction couple and their contacting surfaces as interfaces.

When the friction couples operate within a fluid, it is referred to as wet operation. Dry operation does not depend upon the presence of fluid. Also within the wet clutch oil additives, especially the extreme pressure/anti-wear additive has beneficial effects on the frictional characteristics and the wear of the friction material.

The torque transmitted is related to the actuating force, the coefficient of friction, and the geometry of the clutch or brake. This is a problem in statics which will have to be studied separately for each geometric configuration. However, temperature rise is related to energy loss and can be studied without regard to the type of brake or clutch, because the geometry of interest is that of the heat-dissipating surfaces.

The centrifugal clutch is used mostly for automatic operation. If no spring is used, the torque transmitted is proportional to the square of speed. This is particularly useful for electric-motor drives where, during starting, the driven machine comes up to speed without shock. Springs can also be

used to prevent engagement until a certain motor speed has been reached, but some shock may occur.

Magnetic clutches are particularly useful for automatic and remote-control systems. Such clutches are also useful in drives subject to complex load cycles.

Hydraulic and pneumatic clutches are also useful in drives having complex loading cycles and in automatic machinery, or in robots. Here the fluid flow can be controlled remotely using solenoid valves. These clutches are also available as disk, cone, and multiple-plate clutches.

Problem formulation

The thermal process caused by the relative slip of the friction surfaces (in direct contact or by the use of the lubricant) is the most intense and meaningful process. Its importance in the energetic balance of engaging and disengaging can be shown through a simple artifice applied to the motion equations.

The motion equations can be written in the differential form:

$$\begin{aligned} (M_1 - M_{a1}) \cdot \omega_1(t) dt &= (M_2 + M_{a2}) \cdot \omega_2(t) + \\ M_c(t) \cdot (\omega_1(t) - \omega_2(t)) dt \end{aligned} \quad (2.36)$$

Or in the integral form:

$$W_1 = W_u + W_a + W_d \quad (2.37)$$

Where:

$$M_{a1,2} = J_{1,2} \cdot \frac{d\omega_{1,2}}{dt} \text{ ,dynamic friction clutch (of acceleration) ;}$$

W_1 - the total energy ; W_u – the useful energy; W_a – the energy needed to accelerate the reduced masses at the secondary shaft ; W_d –dissipated energy through friction.

The evaluation of the dissipation percentage when engaging on both states loaded and unloaded is accomplished by the dimensionless loss coefficient:

$$\alpha_W = \frac{W_d}{W_u + W_a + W_d} ; \alpha_{W0} = \frac{W_d}{W_a + W_d} \quad (2.38)$$

This relation proves that the less favorable situation under the energetic balance aspect belong to the no load status (with some simplified hypothesis [114],[218, 219, 220] for $\omega_{1,2}$ (t) and

$M_c(t)$ $\alpha_{W0} \cong 0.5$, because $W_d \cong W_a = \frac{1}{2} \cdot J_2 \cdot \omega_2^2$.

When engaging with load, the most common case found, there are two phases:

$$a) \forall t \in t_m; t_{a1} \cup M_c(t) \leq M_2 \exists \omega_r(t) = \omega_1(t) \cup \omega_2 = 0$$

When the entire energy taken over by the clutch is transformed into the thermic energy and dislocation energy (usage energy):

$$W_1 \Big|_{t_m}^{t_{a1}} = W_d \Big|_{t_m}^{t_{a1}} = \int_{t_m}^{t_{a1}} M_c(t) \cdot \omega_r(t) dt \quad (2.39)$$

$$b) \forall t \in t_m; t_a \cup M_c(t) > M_2 \exists \omega_r(t) < \omega_1(t) \cup \omega_2(t) > 0$$

that correspond to the acceleration of the secondary shaft , when from the total energy taken over by the shaft with the separation of the effects, you can distinguish the components for :

-Defeating the exterior resistances (M_2)

$$W_u \Big|_{t_{a1}}^{t_a} = \int_{t_{a1}}^{t_a} M_2 \cdot \omega_2(t) dt \quad (2.40)$$

-The acceleration of the reduce masses at the secondary shaft

$$W_a \Big|_{t_{a1}}^{t_a} = \int_{t_{a1}}^{t_a} M_{a2} \cdot \omega_2(t) dt = J_2 \cdot \frac{\omega_2^2}{2} \quad (2.41)$$

-Dissipative processes caused by friction

$$W_d \Big|_{t_{a1}}^{t_a} = \int_{t_{a1}}^{t_a} M_2 \cdot \omega_2(t) dt + \int_{t_{a1}}^{t_a} M_{a2} \cdot \omega_2(t) dt \quad (2.42)$$

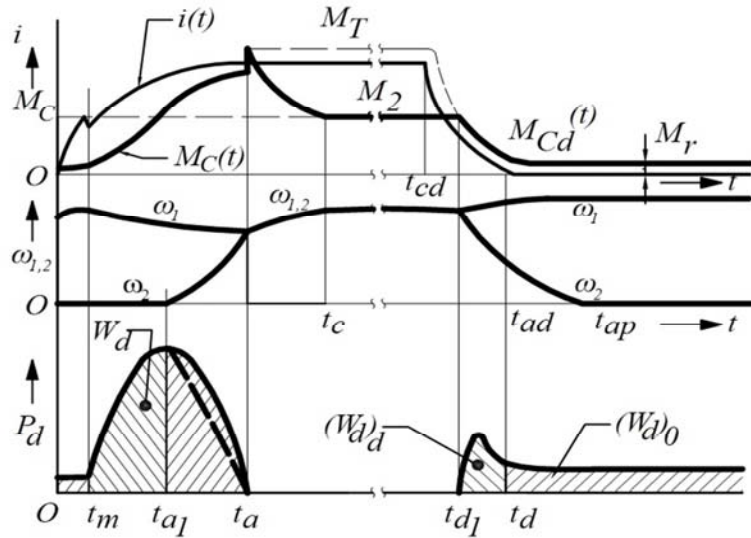


Fig. 2.32. Energy balance

For the whole loaded engaged process, the dissipative energy has a value (fig. 32.):

$$W_d = W_d \Big|_{t_m}^{t_{a1}} + W_d \Big|_{t_{a1}}^{t_a} = \int_{t_m}^{t_{a1}} M_C(t) \cdot \omega_r(t) dt + \int_{t_{a1}}^{t_a} M_2 \cdot \omega_r(t) dt + \int_{t_{a1}}^{t_a} M_{a2} \cdot \omega_r(t) dt = \alpha^2 \cdot M_{0\max} \cdot \int_0^{t_a} \left[1 - \exp\left[-\frac{t-t_m(\tau, S)}{\beta \cdot K \cdot \eta \cdot \tau} \right] \right]^2 \cdot \omega_r(t) dt \quad (2.43)$$

Dealing in a similar way, it can be determine the expression for the dissipated energy at disengaged status.

$$(W_d)_d = W_d \Big|_{t_d}^{t_a} = \int_{t_d}^{t_a} M_{Cd}(t) \cdot \omega_r(t) dt = M_{C\max} \cdot \int_{t_{d1}}^{t_d} \left[\exp\left(-\frac{t}{\tau \cdot do} \right) \right]^2 \cdot \omega_r(t) dt \quad (2.44)$$

Because of the particularities in the process of engage and disengaged, you will always have :

$$W_d > (W_d)_d$$

If functioning for a long period of time in the disengaged status, there can appear an important plate package heating, due to the remaining torque.

The dissipated energy for this date can be expressed in quantity with the expression:

$$(W_d)_0 = W_d \Big|_0^{t_{ad}} = \int_0^{t_{ad}} M_r(\omega_r) \cdot \omega_r(t) dt \cong M_r \cdot \omega_r \cdot t_{ad} \quad (2.45)$$

The variation of the measurements that determine the energetic balance in possible and functional regimes are shown in figure .

The hatched surfaces show the dissipated energy when $\omega_r > 0$.

From the analysis of the last three equations (2.43), (2.44) and (2.45) , it can be seen that the heating of the clutch is intense the longer slip regime .

In the case of a wrong dimensioning, the friction surfaces can get worn prematurely and even be destroyed through overheating. If the frequency of the switching between regimes is more often, the conditions become harder.

2.6.2 Problem Solution

Although the dissipative phenomenon caused by the remaining torque is less intense than the one from engage or disengaged states, in a prolonged period of time, the amount of heat developed can be higher than the one produced in acceleration and braking.

Thus, this functioning regime must be accorded a special attention, because ignoring it could lead to major deficiencies.

For the quantity determination of the dissipative processes you must know: the engaging kinematics ($\omega_{1,2}(t)$, so $\omega_r(t)$), the tribological and electromagnetic behavior of the clutch $M_c(t)$, $M_{cd}(t)$ and $M_r(\omega_r)$.

Because the possibilities for thermal charging depend o the cooling conditions, when verifying the heat calculus you must consider the work regime of the clutch.

Thus in hard coupling conditions the total dissipated energy at a single use must be compared to the admitted energy for dissipating through this inequality:

$$W_{d1} \leq (W_{d1})_{adm} \quad (2.46)$$

In the easy and moderate coupling conditions, the maximum dissipated energy in one hour will be compared with the admitted value :

$$W_{dh} = Z \cdot W_{d1} \leq (W_{dh})_{adm} \quad (2.47)$$

$$(W_d)_{oh} \leq (W_{dh})_{adm} \quad (2.48)$$

Where:

Z – rate of activations per hour .

The rate of activations per hour can be seen in Fig. 3 where it is shown its dependence on the mix load work of friction (in loaded and unloaded states) and the clutch dimension.

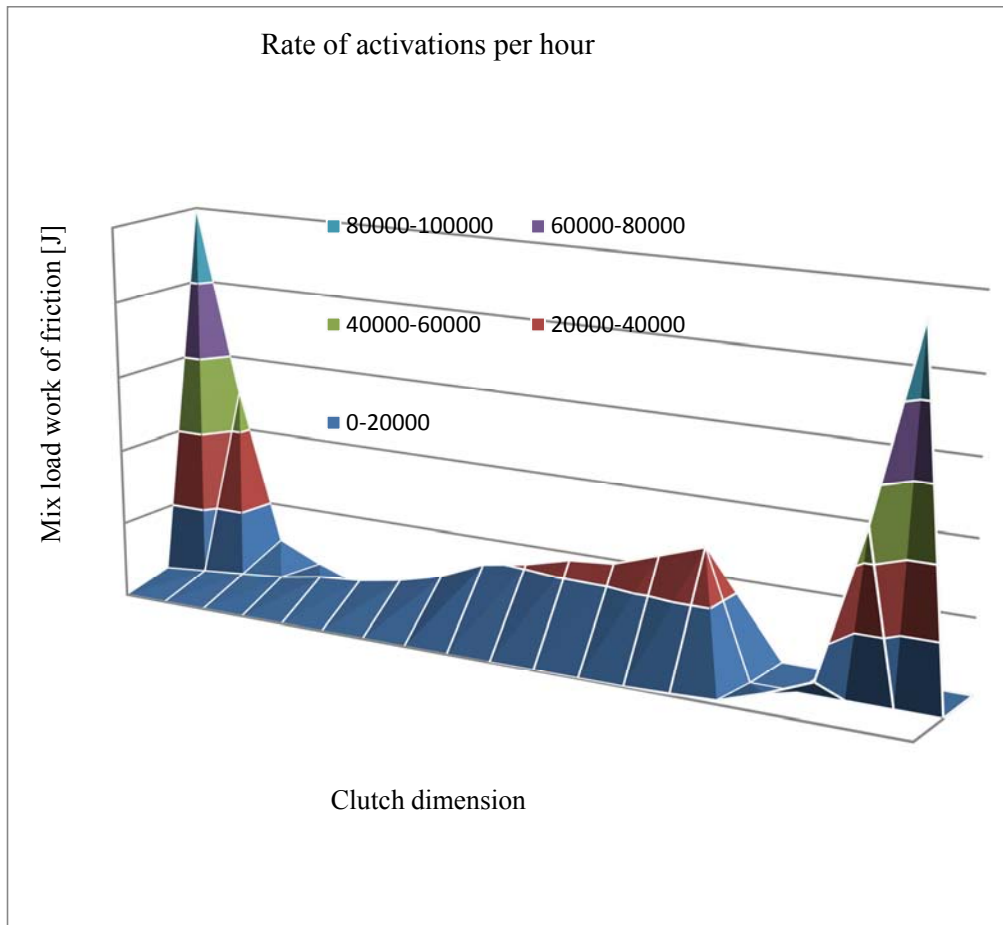


Fig. 2.33. Rate of activations per hour.

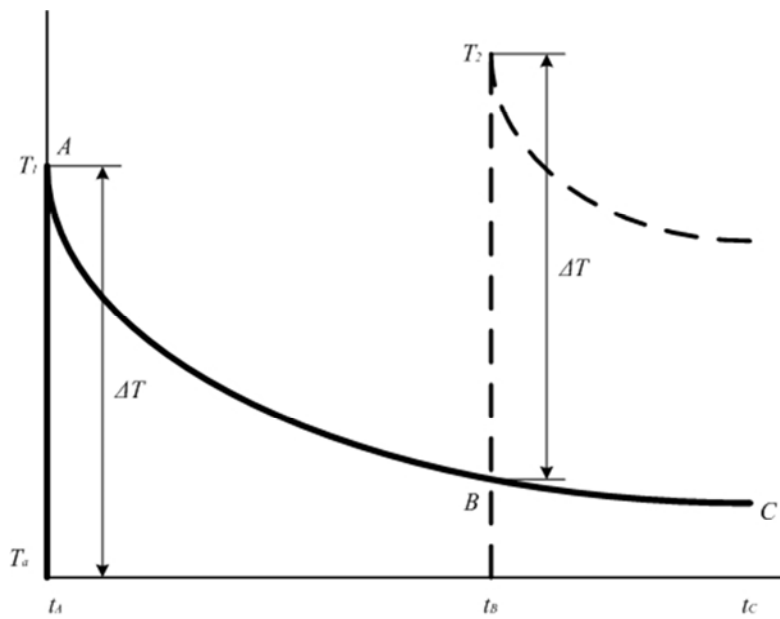


Fig. 2.34. The effect of clutching operations on temperature.

Figure 2.34 shows the effect of clutching operations on temperature. T_a is the ambient temperature. Note that the temperature rise ΔT may be different for each operation.

At time t_a a clutching or braking operation causes the temperature to rise to T_1 at A. Though the rise occurs in a finite time interval, it is assumed to occur instantaneously.

The temperature then drops along the decay line ABC unless interrupted by another clutching operation. If a second operation occurs at time t_b , the temperature will rise along the dashed line to T_2 and then begin an exponential drop as before.

2.6.3 Conclusion

Depending upon application, it may be desirable to have a large or small differential between the static and the dynamic torques.

For instance, when engagement is made at rest (no slippage between interfaces), as would occur for a clutch-coupling or a holding brake, the static torque should be more dominant.

If the clutch or brake is required to slip continuously, as in a tensioning application, very little differential is desirable to avoid a stick-slip condition.

The experimental program has a vital importance because of the big influence of the cooling way of the clutch and the environmental fluid used for this purpose.

The results reveal some phenomenological particularities, offering thus useful data for the practical applications. Even smaller quantities produced in mechanical transmissions that have a large number of clutches and brakes in their build, or that have the cooling conditions difficult, must not be neglected.

2.7 Active suspension LQ control for improving riding comfort

2.7.1 Introduction

The purpose of this research is to point out a controlled vibration quarter car model of a human body in seated position. Its importance is mostly due to the vertical accelerations impact of the human body and be able to control these vibrations. This study marks these vertical accelerations based on a concentrated mass mathematical damped model. This is first established mathematically and then simulated in Matlab software, its results clarifying the differences between accelerations at different parts of the model and their range. Then the study focuses on the controller built in Simulink. The first part of the study describes the quarter car model with concentrated masses depicting also mass, stiffness, damping and forces repartition.

A vehicle's suspension system typically consists of springs and shock absorbers that help to isolate the vehicle chassis and occupants from sudden vertical displacements of the wheel assemblies during driving. A well-tuned suspension system is important for the comfort and safety of the vehicle occupants as well as the long-term durability of the vehicle's electronic and mechanical components.

In this case, to simulate the active suspension control, a quarter car model coupled with a two DOF human body model well analysed and described in literature have been used [115], [117], [118].

In this scenario, several conceptual human body models are available in literature, specifically designed for capturing the main vibrational behaviour of the driver while in the seated position.

While adding complexity, active suspensions have shown an ability to minimize vehicle accelerations, rattle space utilization, or improve road holding to various degrees over certain frequency ranges. One common control technique that is based on full state feedback is the optimal Linear Quadratic Regulator (LQR) technique. There have been various optimal LQR controls solutions developed for quarter, half, and full car models.

A quarter car model represents a corner (1/4) of a vehicle. The sprung mass of the car body is connected by a spring and damper to the unsprung mass of the suspension components by the suspension spring and the damper. It is generally assumed that the tire damping is negligible [116], [121].

Adding a two DOFs human body model with a standard two DOFs quarter car model it is obtained a four DOFs driver-car system on which the linear quadratic optimal control design was performed to obtain the optimally controlled behaviour. It was used the human body model described by Griffin, et al., 2003 from which it has been extracted the necessary values and mean values of their human body models.

The first part of the study describes the quarter car model with concentrated masses depicting also mass, stiffness, damping and forces repartition [119]. Later on, it is revealed the Matlab sequel which simulates based on modal analysis the behaviour of the model. Graphic solutions are also given as results.

Of high importance is the difference between human head vibrations (vertical accelerations) and the vehicle body vibrations, pointing the need of optimization the car suspension and/or the seat suspension in order to reduce head vibration. Thus the study focuses later on, on controlling the suspension in order to reduce vibrations.

Having this entire behaviour simulated, the difference between human head vibrations (vertical accelerations) and the vehicle body vibrations is highlighted, thus the controller then reduces the head of the driver's vibrations while driving over the speed bumper.

2.7.2 Driver-car lumped mass model

Until now, several approaches of modelling the human body from a perspective lumped model were made. Authors like Patil, Palachinamy [120], Griffin [118], [123], Abas, Abouelatta [115], have developed lumped human models starting from a basic type, 1 degree of freedom (DOF) to seven and even 9 DOF lumped human model. There have been studied all of these models and

extracted the type of human model that had also a background of analysis and real human models monitoring comparison.

Beside this approach, some authors like: Gillespie [116], Gündoğdu [117], Wakeham, Rideout [122] also created quarter-car, half-car and even full car models. From their discoveries it was collected a quarter-car model that suited better the approach.

By mixing up the human body models created with the quarter-car model and adding human head vibrations as a distinction from the rest of the body it has been created an original model based on the support of existing types and also data compared with real humans adding novelty and originality of the discovery.

Considering the four DOFs driver-car system, it has been determined the system that lead to calculate the vibrational matrixes.

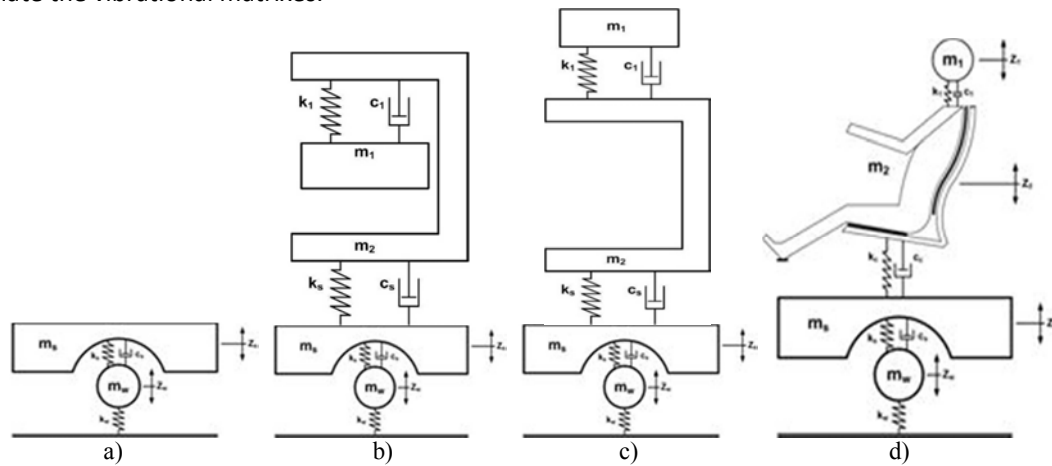


Figure 2.35. a) Gillespie quarter car model [116], b) Gillespie model [116] coupled with model 1b Griffin [123] human model, c) Coupled models with derivation of the second mass as the human head, d) Coupled models with respect to a real behaviour of the seated human model

Where, $m_1, m_2, k_1, k_c, c_1, c_c$ – masses, stiffness and damping of upper and lower body based on the Griffin human body model [122] and $m_s, m_w, k_s, k_w, c_s, c_w$ – masses, stiffness and damping according to Gillespie quarter car model [116].

2.7.3 Linear-quadratic controller design

For the design of the regulator gains, the approach was extended suggested by Wakeham and Rideout [122]., by adopting the extended four DOFs quarter car model (as described in the previous section). The corresponding general linear system expressed in the state-space form is described as follows:

$$\dot{\mathbf{x}} = \mathbf{A}\mathbf{x} + \mathbf{B}\mathbf{u} + \mathbf{C}\mathbf{d} \quad (2.49)$$

where the system states vector,

$$\mathbf{x} = [v_1 \quad v_2 \quad v_s \quad v_w \quad z_{12} \quad z_{2s} \quad z_{sw} \quad z_{wr}]^T \quad (2.50)$$

is defined considering the head, body, sprung and unsprung velocities, followed by neck, cushion, suspensions and tire deflections. Moreover, vectors u and d represent the control action (force actuation) and the external disturbance (time derivative of the road profile variations) respectively.

Given the state variables, the state transition matrix A , as well as the control matrix, B , and the disturbance matrix C , are derived as follows:

$$A = \begin{bmatrix} -\frac{c_1}{m_1} & \frac{c_1}{m_1} & 0 & 0 & -\frac{k_1}{m_1} & 0 & 0 & 0 \\ \frac{c_1}{m_2} & -\frac{c_1+c_c}{m_2} & \frac{c_c}{m_2} & 0 & \frac{k_1}{m_2} & -\frac{k_c}{m_2} & 0 & 0 \\ 0 & \frac{c_c}{m_s} & -\frac{c_c+c_s}{m_s} & \frac{c_s}{m_s} & 0 & \frac{k_s}{m_s} & -\frac{k_s}{m_s} & 0 \\ 0 & 0 & \frac{c_s}{m_u} & -\frac{c_s+c_w}{m_u} & 0 & 0 & \frac{k_s}{m_u} & -\frac{k_w}{m_u} \\ 1 & -1 & 0 & 0 & 0 & 0 & 0 & 0 \\ 0 & 1 & -1 & 0 & 0 & 0 & 0 & 0 \\ 0 & 0 & 1 & -1 & 0 & 0 & 0 & 0 \\ 0 & 0 & 0 & 1 & 0 & 0 & 0 & 0 \end{bmatrix} \quad (2.51)$$

$$B = \begin{bmatrix} 0 & 0 & \frac{1}{m_s} & -\frac{1}{m_u} & 0 & 0 & 0 & 0 \end{bmatrix}^T \quad (2.52)$$

$$C = [0 \ 0 \ 0 \ 0 \ 0 \ 0 \ 0 \ -1]^T \quad (5.53)$$

According to the LQR method, a parametric performance index needs to be defined, in order to retrieve the corresponding optimal gains. The proposed performance index is derived as an extension of [122].:

$$J = \int_0^{\infty} \ddot{z}_s^2 + \rho_1 z_{sw}^2 + \rho_2 \dot{z}_s^2 + \rho_3 z_{wr}^2 + \rho_4 \dot{z}_w^2 + \rho_5 \ddot{z}_1^2 + \rho_6 \ddot{z}_2^2 dt \quad (2.54)$$

where two extra terms (last two terms in eq. 2.54) were added in order to reduce human body vibrations. It is worth nothing that putting the two gains ρ_5 and ρ_6 to zero, the performance index reduces to the one proposed by [122].

After deriving the LQ control gain vector, K , eq. 1 can be elaborated as:

$$\dot{x} = [A + B K] x + C d \quad (2.55)$$

2.7.4 Test case

In this particular approach, it has been defined a case study where just vertical vibrations are considered. In this scenario, it has been extracted both car data and passenger data from several conceptual human body and car models available in literature, specifically designed for capturing the main vibrational behavior of the driver while in the seated position. The four DOFs driver-car system

on which the linear quadratic optimal control design was performed is used in order to obtain the optimally controlled behavior for the human body while driving.

Head vibrations and upper body (vertical accelerations, displacements), vehicle body vibrations (vertical accelerations, displacements), suspension travel (vertical accelerations, displacements), and tire deflection (displacements) have been determined using numerical simulations, where integration of equation (2.55) was computed exploiting an exponential integration scheme.

Numerical results demonstrate that the proposed controller is able to reduce the driver head’s vibrations in both situations more than the standard approach, leading this way to an improvement of comfort.

For the vehicle data it was chosen a medium sized car for with a total mass of approximately 1200 kg and each of the four *unsprung* mass of 36 kg. Typical values for stiffness and damping of suspension ($C_s = 980 \text{ Nm/s}$, $K_s=16 \text{ KN/m}$) and tire ($C_w=0.4 *C_s$, $K_w=10*K_s$) were assumed according to [116]. The passenger data for the human model is extracted from the L. Wei, M.J. Griffin 1998 [123] model:

Table 2.4: Passenger data table.

Stiffness (N/m)		Damping (Nm/s)		Mass (kg)	
k_1	k_c	c_1	c_c	m_1	m_2
25760	30000	310.4	2416	36.8	39.04

A discrete bump scenario was selected for the test. Its corresponding input disturbance (i.e. road profile height, as showed in Figure 2.35) was defined according to the following continuous function:

$$Z_r(t) = \begin{cases} \frac{a}{2} \left(1 - \cos\left(2\pi \frac{v}{L} t\right) \right), & t_0 \leq t \leq t_0 + \frac{L}{v} \\ 0 & \text{otherwise} \end{cases} \quad (2.56)$$

The input disturbance series, d_k , for simulating the scenario was then computed by differentiating the given formula for a speed, V , of 50 km/h; a bump height, a , of 0.1 m; and a bump length, L of 2 m, .a sinusoidal road profile was modelled:

2.7.4 Results

The results of the investigations for are shown in the following figures (Fig. 2.36, Fig. 2.37):

In these figures it can be noticed that all the vertical accelerations belonging to the human body are less than the limit supported by average humans, which is 10m/s^2 . By using the controller these vertical vibrations related to the lower and upper body are in the range of human body comfort domain which is approximately 5-6 m/s^2 .

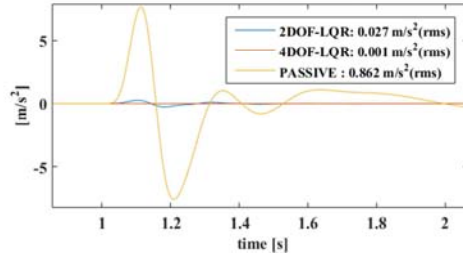


Fig. 2.36 Head accelerations

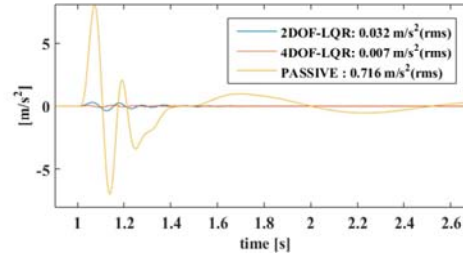


Fig. 2.37 Human body accelerations

2.7.5 Conclusions

The novelty in this approach lies in the designing of LQR optimal control of an active suspension system, whose particularity is that it uses the basic quarter car model by adding the also the inertia, stiffness and damping to capture human being vibrational behavior. A second particularity consists in the mathematical background of the used models, and the derivation of a suitable performance index, the LQR is applied to derive the controlled suspension. Numerical results demonstrate that the proposed controller is able to reduce the driver head's vibrations in both situations more than the standard approach, leading this way to a deep improvement of comfort.

3. Modeling, simulation and experimental work on biological systems

3.1 Car seats ergonomic evaluation

3.1.1. Introduction

The purpose of this research is to observe the ergonomic advantages of different car seats and how the driver is constrained to them during the drive. The study was conducted by taking in to consideration the dynamical characteristics of a standard vehicle and subjecting the human body model provided by the AnyBody Modelling System, to inertia and centrifugal forces, in three different driving posture cases. The simulation using the AnyBody Modelling System, is validated with the results of a real case thermographical experiment. The model proved to be viable and offered an image of different car seats advantages from ergonomic point of view.

The influence of different forces and vibrations transmitted to the human body through the car seat during the drive shows a distinctive importance because they inflict a state of tiredness, especially to the driver who makes an additional effort in comparison the other passengers [169, 206, 207, 208].

The main effort results from centrifugal and inertia forces creating a postural stress, the effort made during the operation of different commands and the steering wheel, effort made for maintaining the balance in the seat while driving on uphill or downhill or following the road where the vehicle is driven [170, 209, 214, 215].

Vehicle designers all around the world are trying to create functional seats that provide adequate physiological driving conditions. The creation of ideal driving condition implies a determination of the drivers efforts, their measuring and the response of the human body to each of these efforts, their comparison to normal physiological limits and as a result of this, the interventions on the driver's seat for setting the driver's demand to his physiological possibilities [129, 130, 131, 132, 133, 171].

Due to the presence of soft tissues, of bones, of internal organs and also because of the configurationally particularities, the human body is a complex mechanical system. External forces can be transmitted to the human body in vertical, horizontal, sitting positions or through the hands while driving. The ways of transmitting these forces (Fig. 3.1) through the human body and the influence that they have on internal organs and tissues are of particular importance [128, 134, 135, 172, 173].



Figure 3.1. Different ways of transmitting the external forces to and trough the human body.

3.1.2 The vehicle dynamics and track characteristics

To determine the forces that act on the driver or on the passengers, during the drive, it is necessary first to determine the vehicle dynamic characteristics. Therefore, in this study it is considered a passenger car with the next characteristics, extracted from the vehicle's technical book:

The cylinder capacity	$V_c = 1995 \text{ [cm}^3\text{]}$
Maximum power	$P_{\max} = 105 \text{ [kW]}$
Maximum torque	$M_{\max} = 190 \text{ [Nm]}$
Revolutions at maximum power	$n_p = 6000 \text{ [rev/min]}$
Revolutions at maximum torque	$n_M = 4250 \text{ [rev/min]}$
Gearbox type	5 speed manual
Central transmission ratio	$i_0 = 4.5$
	$i_1 = 4.32$
	$i_2 = 2.46$
Transmission ratios of the gearbox	$i_3 = 1.66$
	$i_4 = 1.03$
	$i_5 = 0.85$
	$L = 4.25 \text{ [m]}$
Gauge dimensions	$B = 2.013 \text{ [m]}$
	$H = 1.421 \text{ [m]}$
Wheelbase	$A_m = 2.76 \text{ [m]}$
Axle track	$E_c = 1.5 \text{ [m]}$
Tire type	255/55 R16 H
Own mass	$G_a = 1435 \text{ [kg]}$
Maximum speed	$V_{a_{\max}} = 210 \text{ [km/h]}$
Payload	$Q_u = 475 \text{ [kg]}$
Average consumption	$C_{\text{med}} = 5.9 \text{ [l/100km]}$

Using these characteristics combined in the formulas from [129], the vehicle's engine external characteristics, traction forces [Fig. 3.2], speed and acceleration [Fig. 3.3] were determined for each speed gear.

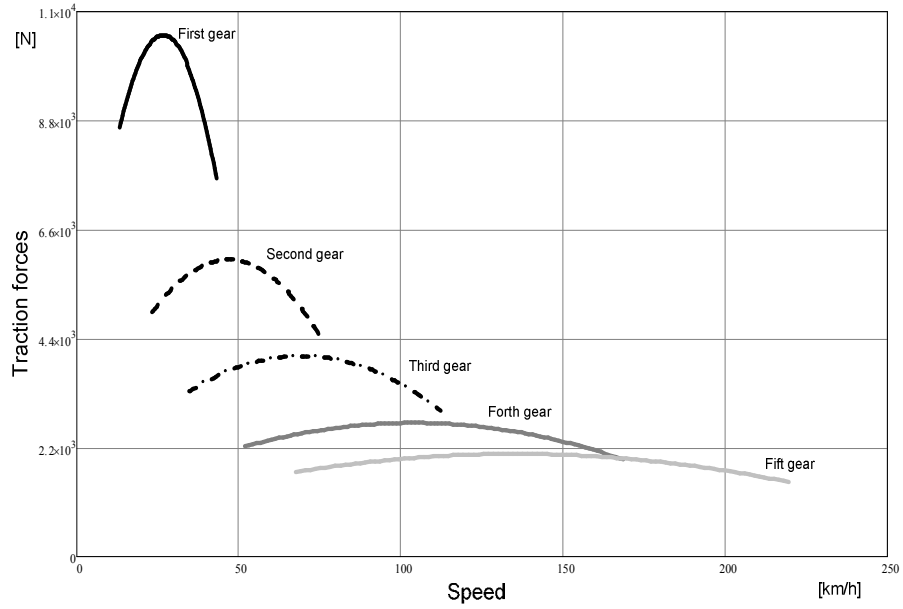


Figure 3.2. The traction forces for each gear depending on the vehicle speed.

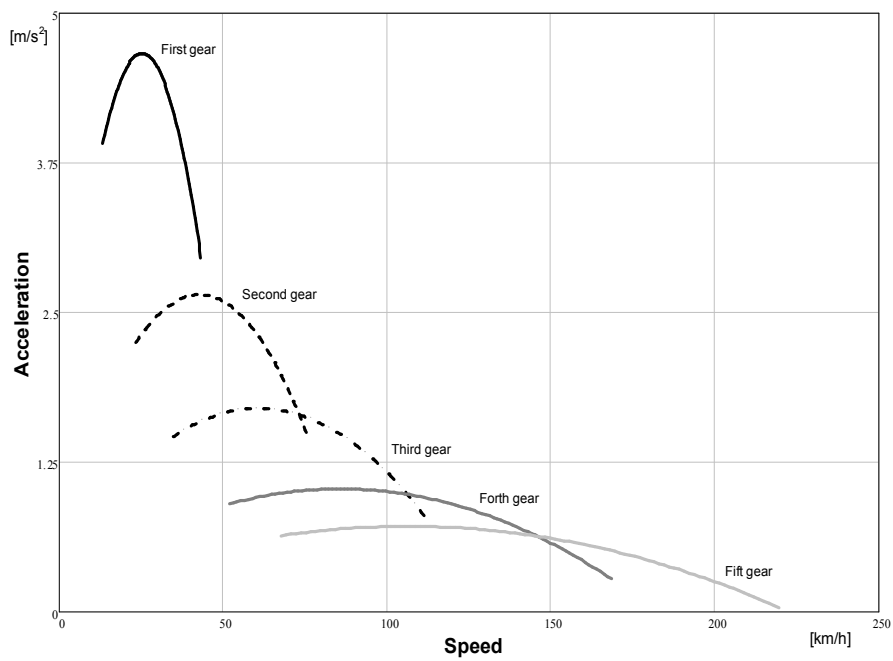


Figure 3.3. The acceleration for each gear depending on the vehicle speed.

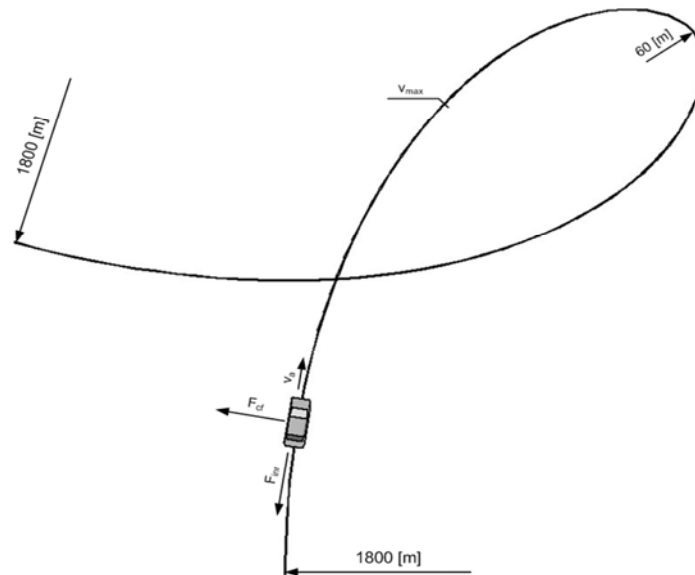


Figure 3.4. The curvilinear trajectory.

The next step in this study was to determine the inertia and centrifugal forces that act on the driver. Therefore, it is considered a human model with its own mass of 80 kg. Because the influence of these external forces is more pronounced on the upper part of the body, in the driving position, the study is focused on the reactions of this upper body.

When a person's upper body stands upright, the mass of the trunk, head and arms presses vertically on the lower lumbar spine with a force of approximately 55% of bodyweight, which in this case is 44 kg [128, 134, 174, 217].

As resulted in figure 3.2 and 3.3, it is also well-known that the vehicle's traction forces and acceleration have higher values in the first gear, and they decrease as the gear number and vehicle's speed increases. Thereby the inertia forces that act on the upper body have a range of high values at the vehicle start off, and they decrease as the speed gear number and vehicle's speed increases until the speed is constant.

In figure 3.5 and 3.6 are represented the inertia force and the centrifugal force, that act on the upper body part of the human model while the vehicle is driven along a curvilinear trajectory (Fig. 3.4) starting with a radius of 1800 m, 60 m radius in the middle, and exiting the curve with a radius of 1920 m.

Because in the second part of this study it is used the AnyBody Modelling System software to simulate the three cases of driving, is important to mention that the simulation of each body movements is based on time steps [135, 216]. Therefore the drive along the curvilinear trajectory is divided in 100 time steps.

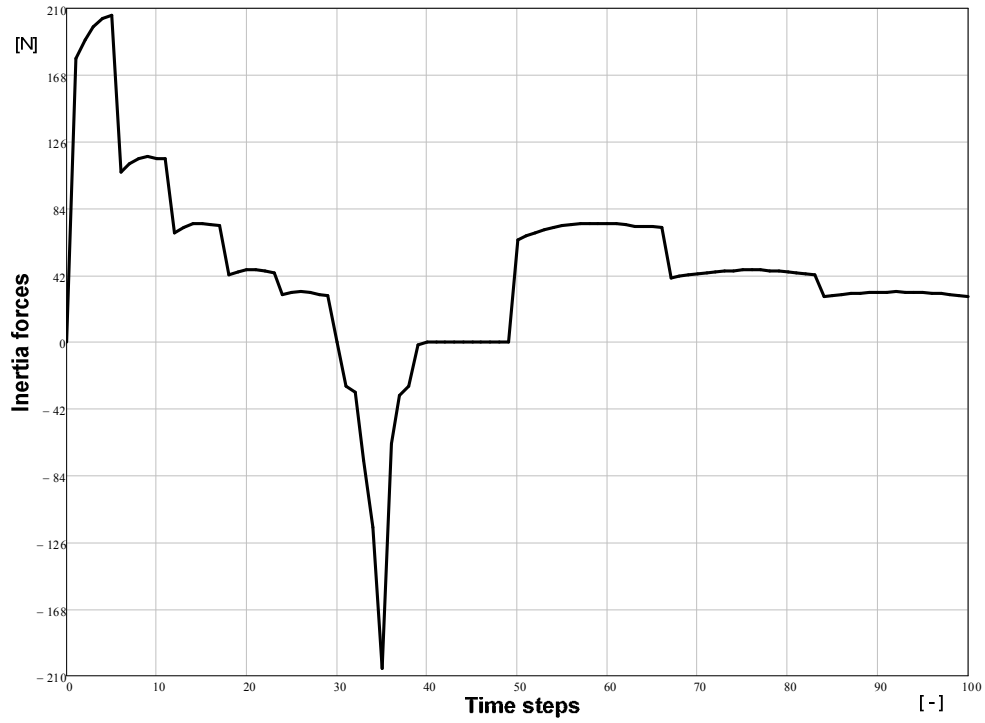


Figure 3.5. The inertia force that act on the upper body part.

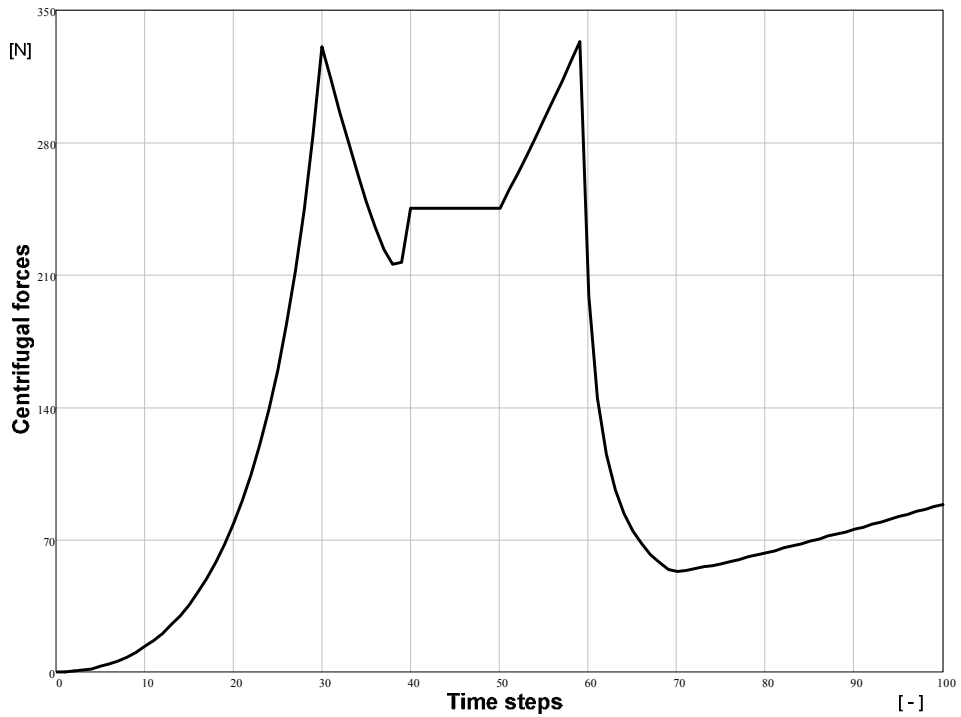


Figure 3.6. The centrifugal force that act on the upper body part.

3.1.3 Simulation using AnyBody Modeling System software

The AnyBody Modelling System is a software system for simulating the mechanics of the live human body working in concert with its environment.

The body models are available in the standard demo package that can be used in conjunction with the AnyBody human body simulation software. Starting from a standing human model, using pre-defined muscles and bone attachments, and building the seated driving postures scenarios, have been developed.

For the seated position, the car seat was added virtually through a node that offers a stable platform for the pelvis region. The angles for the legs were obtained from an ideal theoretical position for the purpose of minimizing their involvement in the general muscle activity of the body system.

All activities include certain tensions in the hands given by the steering wheel load. Because of this factor, the model has forces attached to the nodes belonging to each of the hands. This ensures that the data output is similar to that which would be obtained from a real life model and further adds to the accuracy of the model [134].

All movement patterns were carefully studied for muscle collision and kinematical correctness; after all data was considered viable, the next phase of the study – using inverse dynamics, was conducted. The data was then extracted from the output of the program for the various muscle groups that were of interest (trunk muscles and abdominal muscle activity). The most relevant data was considered the trunk muscle fatigue. Muscle fatigue (Activity) is defined by the AnyBody solver as muscle force divided by strength.

The simulation was made for three different cases each representing a car seat type and the way the human body is constrained to it.

The first case represents a standard car seat with the upper body of the human model poorly constrained to the backrest. On the upper body are acting the inertia force and the centrifugal force. Because the upper body it is poorly constrained to the backrest, results a movement on the resultant force direction, effort made to keep the balance in the car seat. The second case represents a car seat with lumbar support and the upper body constrained to the backrest. In this case the upper body moves only on the centrifugal force direction, with less effort made to keep the balance in the car seat. The third case represents a car seat with lateral trunk and lumbar supports. The upper body is constrained to the backrest and to the lateral trunk supports, and it is subjected to inertia and centrifugal forces. Because it is constrained on both force directions, results no movements and almost no effort made to maintain the balance in the car seat.

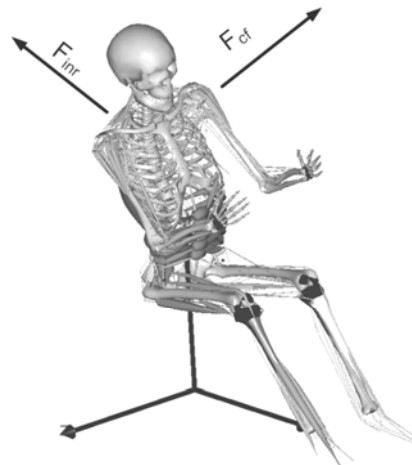


Figure 3.7. The AnyBody human model subjected to inertia and centrifugal forces during the drive.

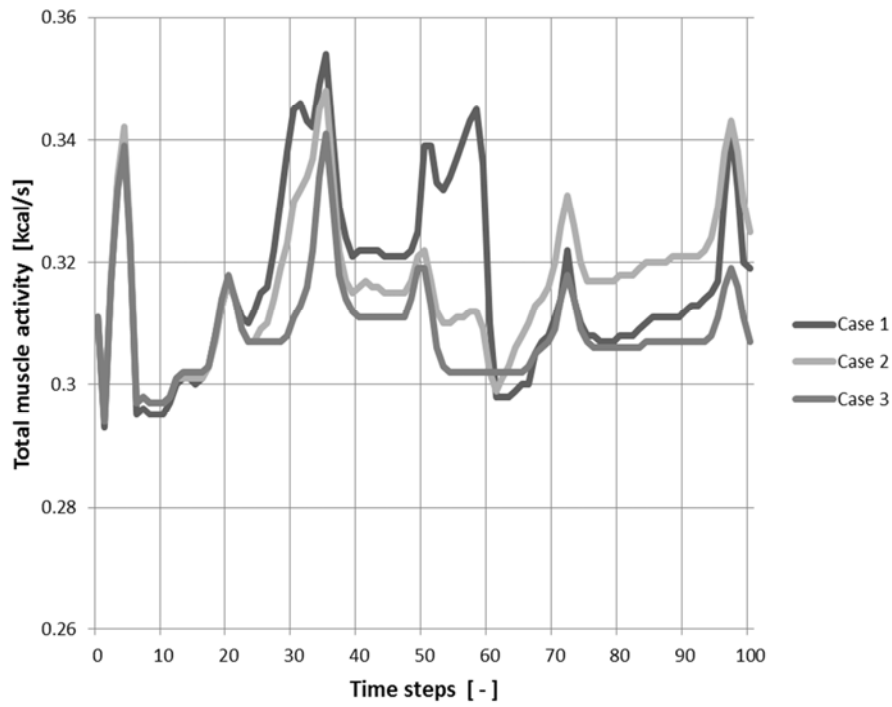


Figure 3.8. The total muscle activity for each case.

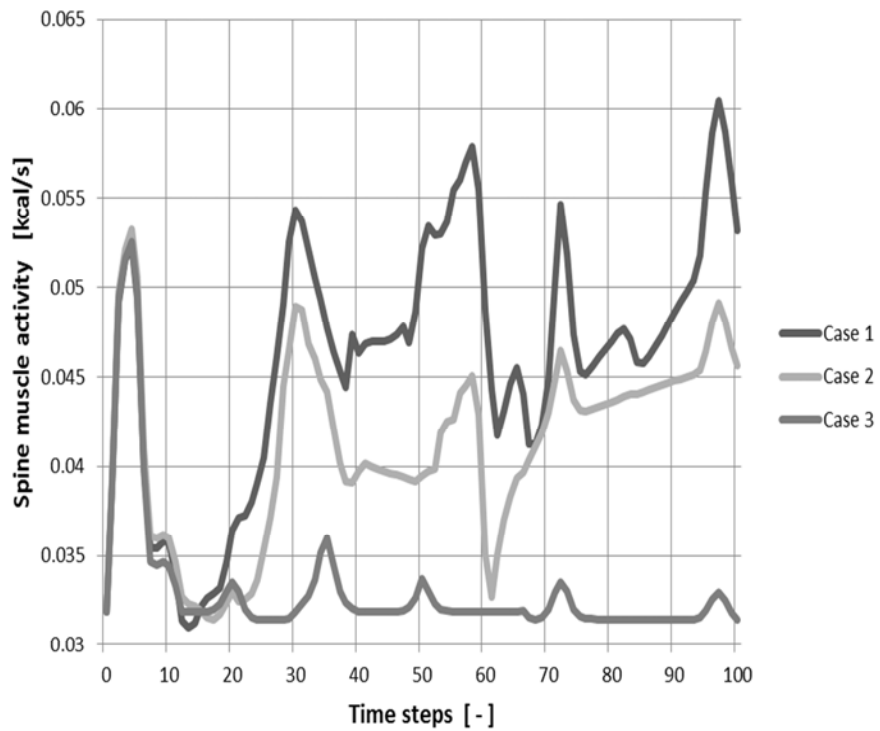


Figure 3.9. The spine muscles activity.

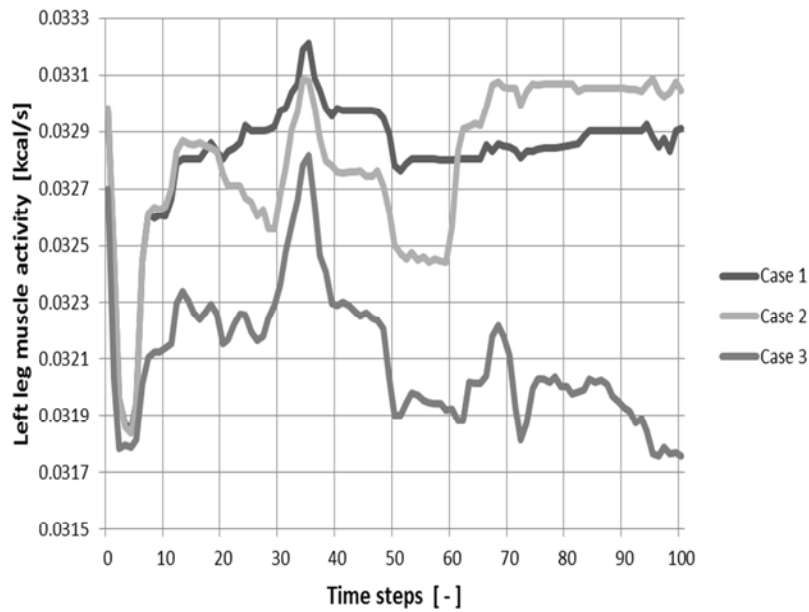


Figure 3.10. The left leg muscles activity.

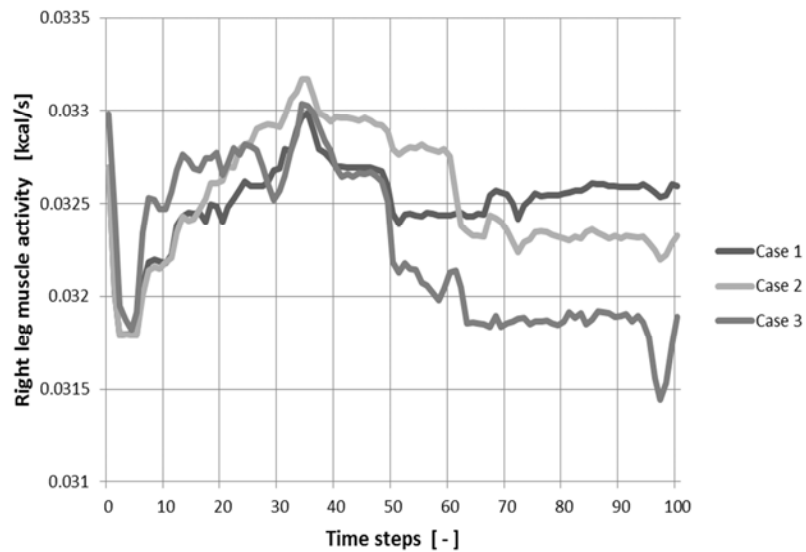


Figure 3.11. The right leg muscles activity.

In figure 3.8 is represented the total muscle activity, for each case of driving and car seat type. It is clearly revealed that overall in the first case that the energy consumption has higher values and that in the third case the effort made to keep the balance in the car seat is minimal.

In figure 3.9 is represented the spine muscles activity, for each case of driving and car seat type, and in figure 3.10 and 3.11, the left and right legs muscles activity. It is clearly revealed that overall in the first case that the energy consumption has higher values and that in the third case the effort made to keep the balance in the car seat is minimal.

To highlight the importance of the lateral trunk and lumbar supports presence in the car seat design, in the driving simulation were added low frequency and high amplitude vibrations

reproducing the passing over road irregularities. This type of vibrations amplify the effort made to maintain the balance in the car seat, and for a prolonged time they can cause severe musculoskeletal affections, especially to the lumbar spine where they can cause intervertebral disc side compactions leading to back pain.

3.1.4 Thermographical experiment

The temperature recorder (thermograph) is an important tool for medical diagnosis because science has managed to prove that all diseases cause temperature changes in a suffering organ. Some types of disorders lower the temperature in that particular organ, others raise it.

The infrared camera we used was FLIR B200 which is based on settings that sense and record on tape the cold and warm areas of the human body by detecting infrared radiations which react to blood flow [136, 211].

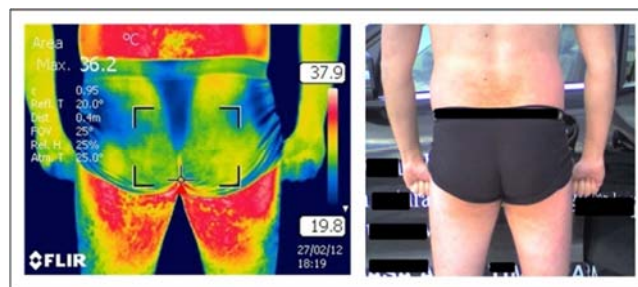
With the help of the infrared camera there were taken a set of pictures which give the possibility to analyse the body temperature distribution and at the same time the increase of muscle contraction.

The conditions that had to be fulfilled to assure the accuracy of the study were the following: low surrounding temperature, to avoid errors in measuring the real body temperature; the driver's position was maintained for a longer period of time; the driver posed shirtless so that the body temperature could be most accurate; the vehicle had the same dynamical characteristics with the one in the simulation; the car seat design included variable geometry offering the possibility to reproduce the three simulation cases.

The study underwent by reproducing the driving on a similar track to the one used in the simulation.



a)

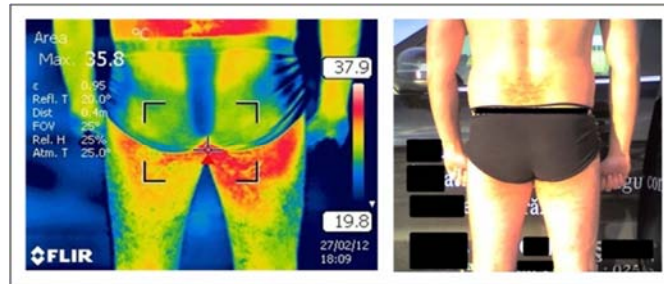


b)

Figure 3.12. The first case scenario: a) the spine muscle contractions; b) the legs muscle contractions.



a)

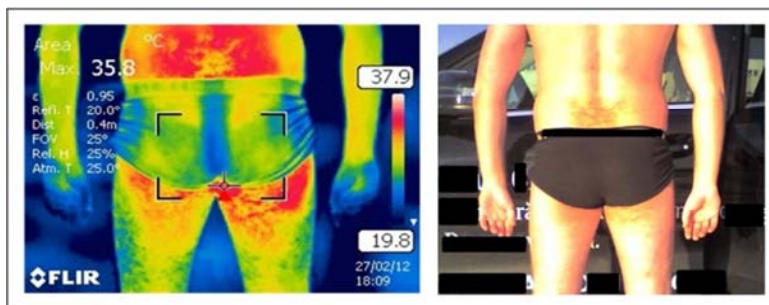


b)

Figure 3.13. The second case scenario: a) the spine muscle contractions; b) the legs muscle contractions.



a)



b)

Figure 3.14. The third case scenario: a) the spine muscle contractions; b) the legs muscle contractions.

In processing the thermographic recordings, Sp1 and Sp2 points are denoted. These points are located on the spine muscle groups. In these points, the spine muscle temperature was recorded. Figure 3.76 presents graphically the temperature variation of the Sp1 and Sp2 points.

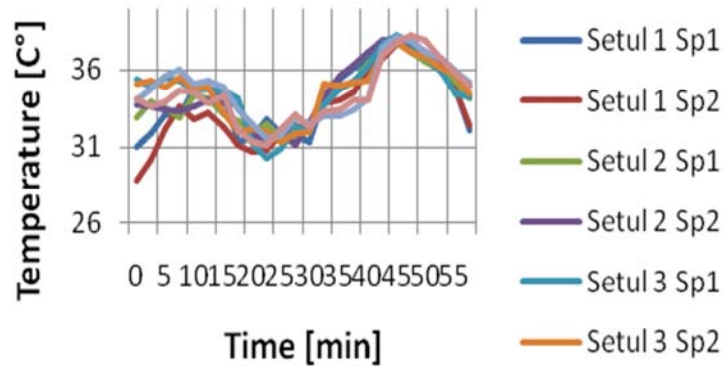


Figure 3.15. Sets points record temperatures Sp1 and Sp2.

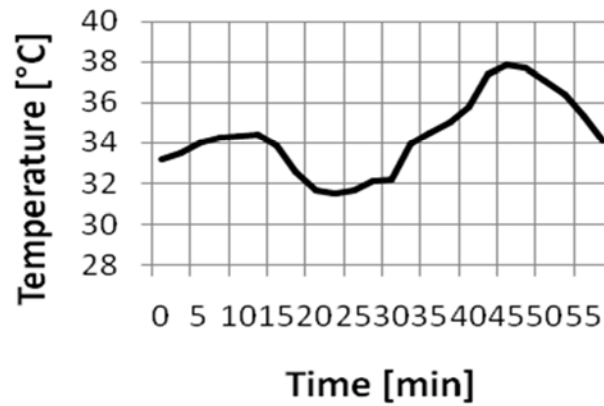


Figure 3.16. Average points Sp1 and Sp2 temperatures.

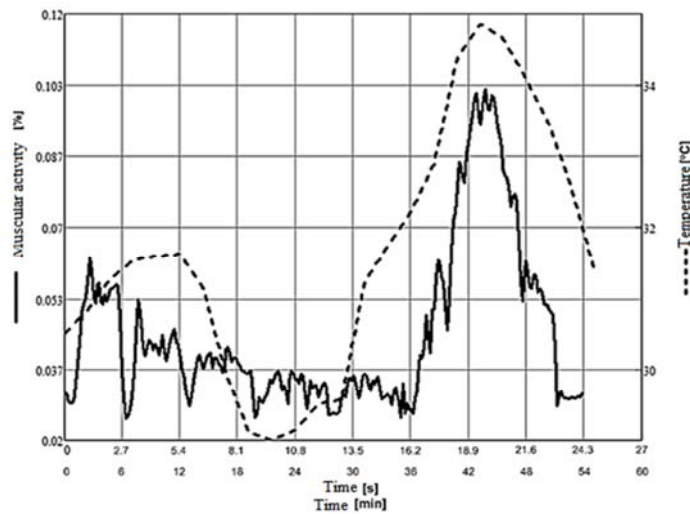


Figure 3.17. Comparison of variation work muscle groups of the spine through software simulation anybody, and temperature variation of the same muscle groups as determined by thermographic analysis.

3.1.5 Conclusions

Back pain is one particularly crucial problem that is in a driver's best interest to avoid. A good driving position and correct posture is vital for the efficient practice driving and to avoid chronic back pain. After a careful examination of the data and statistical analysis, a clear distinction between the energy consumption for the three driving postures became apparent. According to the results the ergonomic optimal posture is the 3th one representing a car seat with lateral trunk and lumbar supports. This result is validated also by the thermo graphic experiment by highlighting the temperature distribution. This shows that the posture with the smallest energy consumption and muscle activity is the 3th one. These results are highlighting the importance of the car seat designed with trunk lateral and lumbar support that has to be comfortable; it should fit to lumbar curvature, and contact should be maintained with it while driving. Another aspect of the study is the possibility of pointing out the individual muscle strain for the various trunk muscles.

This sort of data obtained from driving posture simulations and compared with thermo graphic results, is very useful in ergonomic design of the car seats, and also in improving the prevention of the musculoskeletal disorders by using ergonomics.

3.2 The drivers spine analytical model

3.2.1 Introduction

The study presents the determination of the analytical expression in the coronal plane of the drivers spine while driving along curved roads. Further on the analytical expression is used to determine ergonomic parameters for the car seat design. The analytical expression is determined by developing an experiment to monitor the position variation in time of the vertebrae in the sagittal and coronal plane. The results lead to three sinusoidal equations of which amplitude values describing the variation in time of angles between the vertebrae gives an image regarding the deformation degree of the intervertebral discs.

THE possibility to drive in complete healthy and safety conditions not only for the professional drivers but also for the rest of the population which uses vehicles as frequent transportation means leads to efficiency by improving the quality of life [180, 182].

In this context it is noted the following objectives and research directions: the development of modern mathematical models and principles to be included in a design or control algorithm.

The ergonomic optimal body posture of the driver sitting in the car seat, is influenced by the structural and design characteristics of the seat. The seat has to constrain the body so that the spine form takes the anatomical ideal or the ergonomic optimal shape [183, 184].

Therefore to design an ergonomic car seat it is proposed to start from the ideal anatomical shape of the spine in the sagittal and coronal plane.

The present study is based on the ergonomics research regarding the spine's behavior while driving along curved roads.

3.2.2 Analytical expression of the spine in the sagittal plane

In order to determine the design parameters of the car seat it is necessary to know the analytical shape of the spine in sagittal plane and coronal plane.

The analytical expression of the spine in sagittal plane in standing position is:

$$y = \frac{1}{L} \left(\frac{m}{6} - \frac{A}{3} \right) \cdot x^3 + A \cdot x^2 - L \cdot \left(\frac{m}{6} - \frac{2 \cdot A}{3} \right) \cdot x + \frac{R}{L} \cdot x + \left(\frac{m}{6} - \frac{2 \cdot A}{3} \right) \cdot \frac{L^2}{\pi} \cdot \sin \frac{\pi \cdot x}{L} - \frac{R}{L} \cdot \sin \frac{\pi \cdot x}{L} \quad (3.1)$$

L and R are x, y coordinates of the point L5-S1 from figure 3.18.

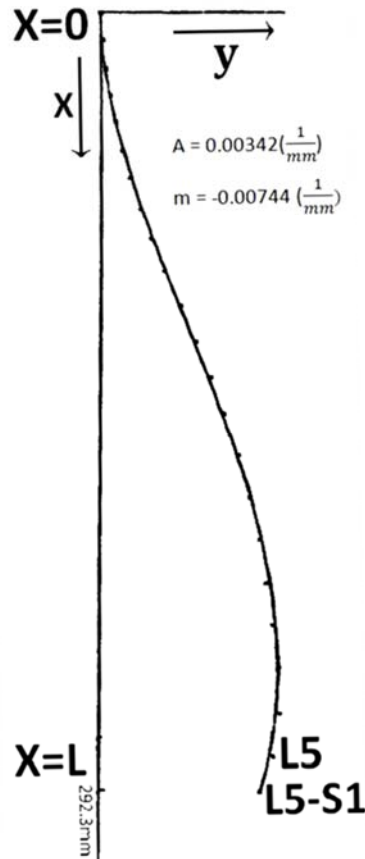


Figure 3.18. The spine analytical shape in the sagittal plane in standing position.

From the analysis of 30 X-Rays have been obtained values for A parameter between $0.00003mm^{-1}$ and $0.00005mm^{-1}$ and for the m parameter values between $0.00005mm^{-1}$ and $0.0015mm^{-1}$. These values are for the erect position of the spine.

According to international standards, the correct posture while driving is achieved by placing the trunk in such a way that the angle between it and the thigh reach $110^\circ - 120^\circ$ (Fig. 3.19).

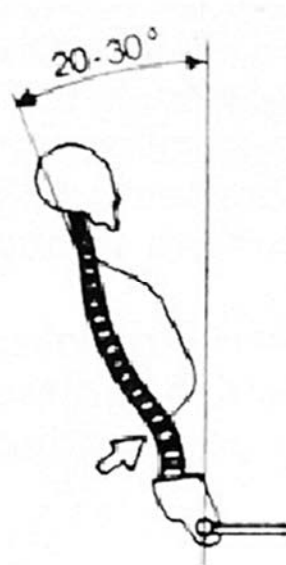


Figure 3.19. The correct seated position while driving.

Using the MathCAD software the spine form in seated position was determined based on the HP (hip point) point coordinates and the line that contains the HP point and represents the spine inclination according to International Standard ISO 3958-1977.

The line equation in the xOy coordinate system presented in figure 3.18, is:

$$\text{incl}(x) = \text{tg}(\beta) \cdot (x - x_{\text{HP}}) + y_{\text{HP}} \quad (3.2)$$

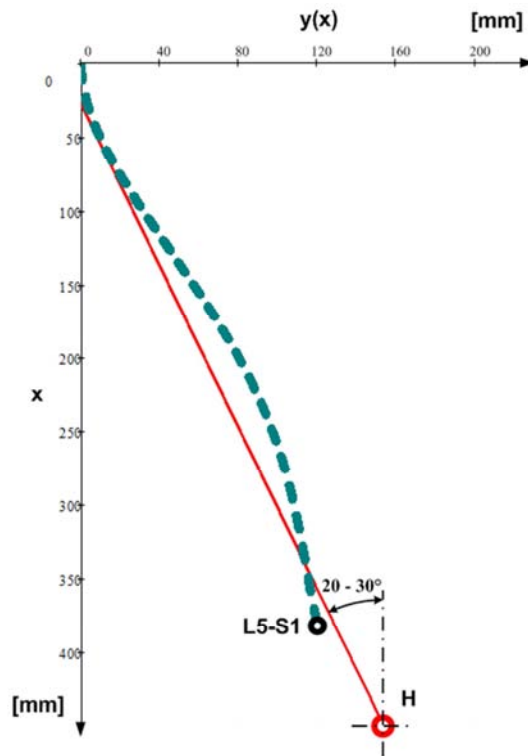


Figure 3.20. The spine analytical shape in the sagittal plane in seated position.

For the seated position the values are: $A=0.00004\text{mm}^{-1}$ and $m=0.0016\text{mm}^{-1}$.

3.2.3 Analytical expression of the spine in the coronal plane

The optimal ergonomic body posture of the driver sitting in the car seat is influenced by the structural characteristics of the seat. The body has to be constrained to the seat such way so that the spine's form is an ideal anatomical or ergonomic optimal shape. Therefore to design and construct the car seat, it is proposed to start from the ideal anatomical shape of the spine in the coronal plane (Fig. 3.21). [137, 138]

To determine the design parameters of the car seat is necessary to know the analytical form of the spine's shape in the coronal plane. In the coronal plane, the shape of the spine can be expressed mathematically by the equation of a straight vertical line. Vertebrae centers are collinear. Considering a reference system as in figure 16, the vertical line's equation containing vertebrae centers is considered to be $x = 0$.

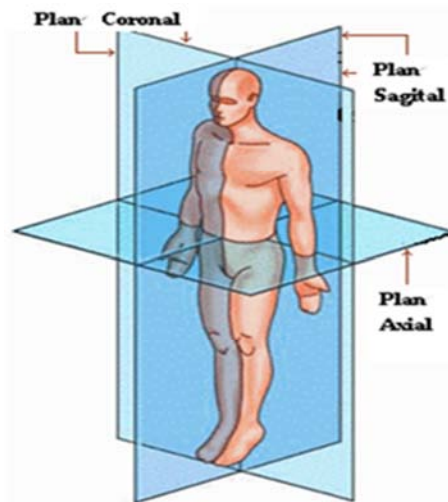


Figure 3.21. Anatomical planes.

Point O, the origin of the coordinate system coincides with the lowest point of the coccyx.

The analytical expression $x = 0$ of the spine's shape in the coronal plane is only valid if the vehicle is at rest, or the vehicle travels on a rectilinear continuous road (unreal case).

Due to the centrifugal force acting on the human body while the vehicle is traveling along a, the human body changes its posture in the coronal plane in the opposite direction of the centrifugal force, to maintain the balance in the car seat.

Thus the spine's shape changes depending on the vehicle's traveling speed and the curved path's radius, causing the spine shape mathematical expression in the coronal plane to be a motion law.

The spine shape is the line containing the centers of the vertebrae. Anatomically, the shape and movement of the spinal column are shown by the relative rotational movement between the vertebrae.

According to anatomy and kinematic studies of the human spine, it is concluded that the center of rotation between two vertebrae is the center of the intervertebral disc that connects the two vertebrae.

Thus intervertebral disc can be considered a ball joint with three degrees of freedom corresponding to rotation after three axes.

In figure 3.20 are shown as an example, L3 and L4 vertebrae centers as CL3 and CL4 points, and the rotation centers of the L2, L3, L4 and L5 vertebrae, as CrL2-L3-L4 and CrL4 CrL3-L5.



Figure 3.22. The spine in the coronal plane related to the coordinate system xOy.

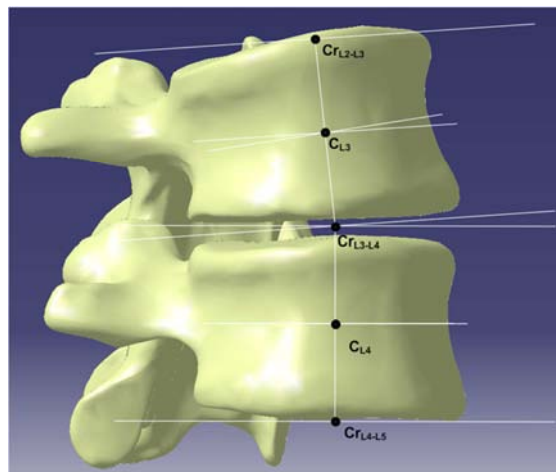


Figure 3.23. L3 and L4 vertebra centers (CL3 and CL4), and the rotation centers of the L2, L3, L4 and L5 vertebrae (CrL2-L3-L4 and CrL4 CrL3-L5).

Considering the vertebrae in the coronal plane as represented by segments connecting the rotation centers, the shape of the spine may be given by the angles α_i of these segments.

Figure 3.21 represents the lumbar segment in the coronal plane. The L1, L2 ... L5 vertebrae are the CrT12-L1CrL2-L3-L3 CrL1-L2CrL2, CrL2-L3CrL3-L4-S1 ... CrL4-L5CrL5 segments. The relative rotation between two vertebrae is given by the angle α_i between the segments representing the two vertebrae.

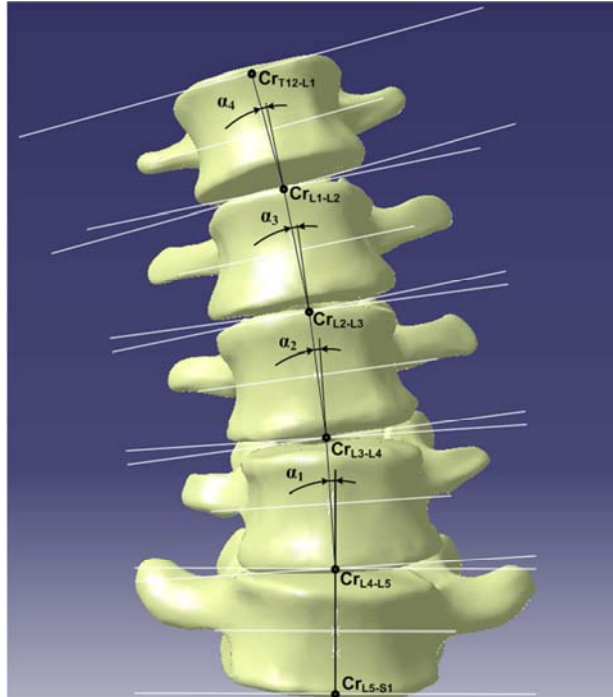


Figure 3.24. The lumbar spine with the segments representing L1, L2 ... L5 vertebrae.

The motion law of the spine in the coronal plane can be expressed as a function of the vehicle speed (v_a), the curved trajectory radius (r_{tr}) and the upper body mass (m_{cs}), function that returns the values of the α_i angles.

$$f(v_a, r_{tr}, m_{cs}) \rightarrow \alpha_i \quad (3.3)$$

To determine the function given by relation (3.3), we created an experiment that for a given route and a constant driving speed, the upper body movements in the coronal plane were monitored.

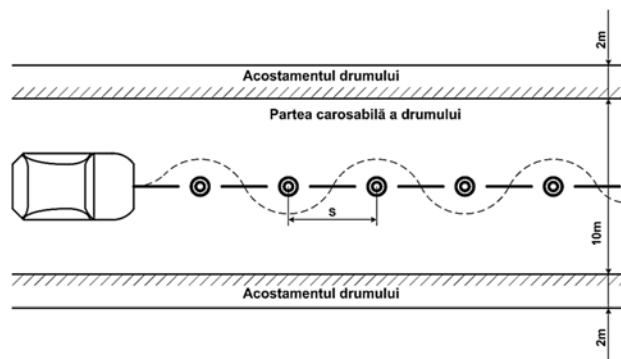


Figure 3.25. The route used in the experiment.

The track used in the experiment is the same track used to determine the dynamic cornering ability of the vehicles (fig. 3.25).[140]

In the experiment we used the motion sensor manufactured by *PASCO scientific* and the PASCO CI-6400 Science Workshop 500 Interface (fig. 3.27).

The motion sensor MotionSensor II (fig. 3.26) operates on the sonar principle. The sensor can measure distances between 0.15m and 8m, between it and the object of interest (fig. 3.26).

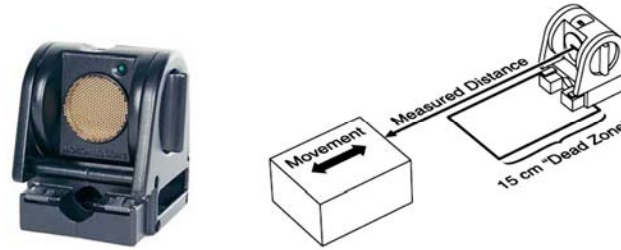


Figure 3.26. Motion Sensor II.



Figure 3.27. PASCO CI-6400 Science Workshop 500 Interface.

Before measurements, the motion sensor must be calibrated.

In this experiment the driver's upper body sideway movements in the coronal plane were monitored. To monitor the movements in the coronal plane the motion sensor was used to determine the positions in time of three points on the driver's body right side. In figure 3.28 is shown the positioning of the sensor. The first point is on the right side of the C1 vertebra, located at a distance of $d_C = 0.477\text{m}$ from the sensor. The second point is placed on the right shoulder on the T4 vertebra's right side, located at a distance of $d_T = 0.39\text{m}$ from the sensor. The third point is located next to the L1 vertebra located at a distance of $d_L = 0.419\text{m}$ from the sensor.

In figure 3.28 is shown the sensor in the first position for determining the C1 vertebra movements. The r_C , r_T and r_L distances from the seat surface, were determined by anthropometric measurements of the driver's body in seated position. Thus $r_C = 0.8\text{m}$, $r_T = 0.585\text{m}$ and $r_L = 0.4\text{m}$.

The experiment was carried out in three stages. In each stage the position in time of one of the three points is determined. In each stage the vehicle is traveling with a constant speed of 15km/h according to the vehicle dynamic steering ability tests. [140]

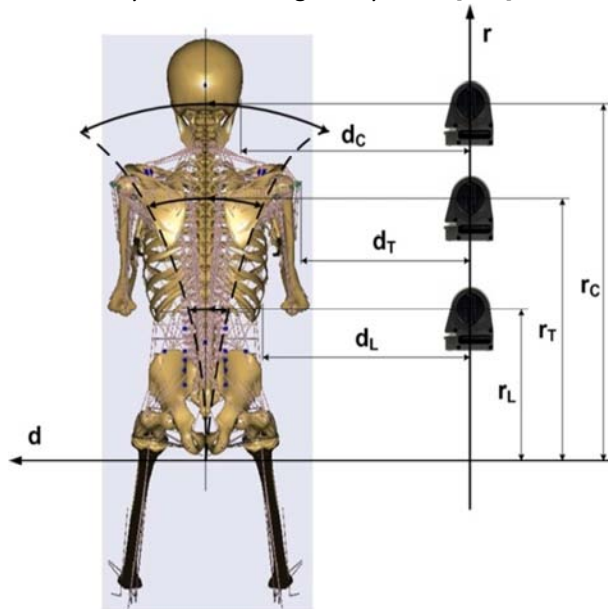


Figure 3.28. Points of interest for sensor positioning.



Figure 3.30. The sensor in the first position for determining the C1 vertebra movements.

3.2.4 The experimental results and data processing

The traveling time in one direction and performing a series of measurements, is about 15s.

Figures 3.30, 3.31 and 3.32 are presented graphically the results of series of measurements for the three points. At each step corresponding to a point were performed seven series of measurements.

For each point were averaged seven sets of measurements. Thus the results of processing experimental data are presented graphically in figure 3.31.

As a first analysis of the results obtained, it can be seen that the variation in time of the position of the three points can be expressed as a sinusoidal function with the same frequency but different amplitudes.

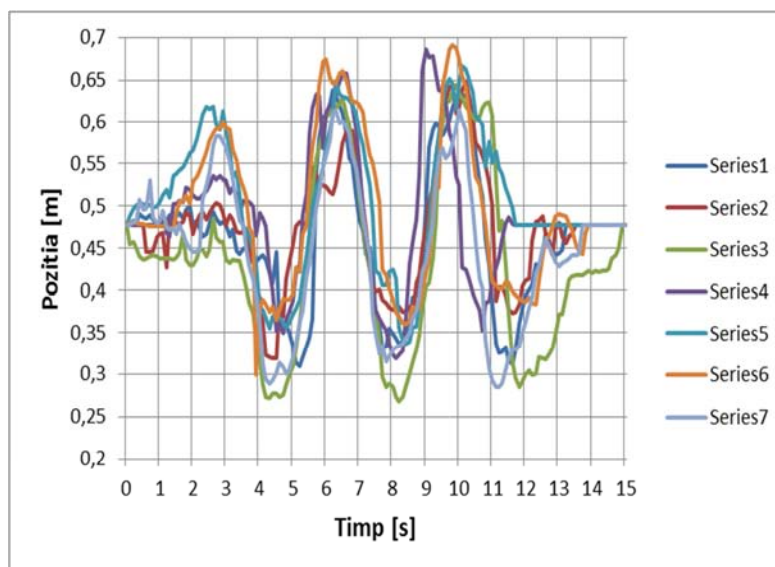


Figure 3.30 - The series of measurements for the C1 vertebra.

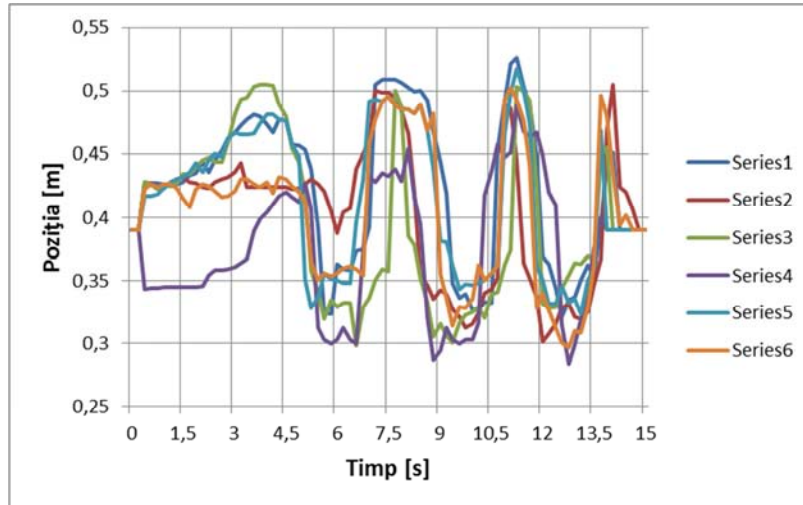


Figure 3.31 - The series of measurements the T4 vertebra.

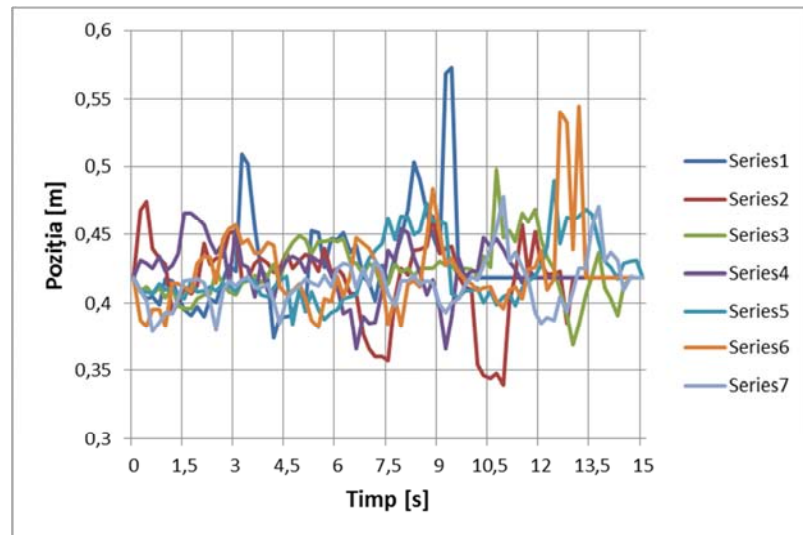


Figure 3.32 - The series of measurements for the L1 vertebra.

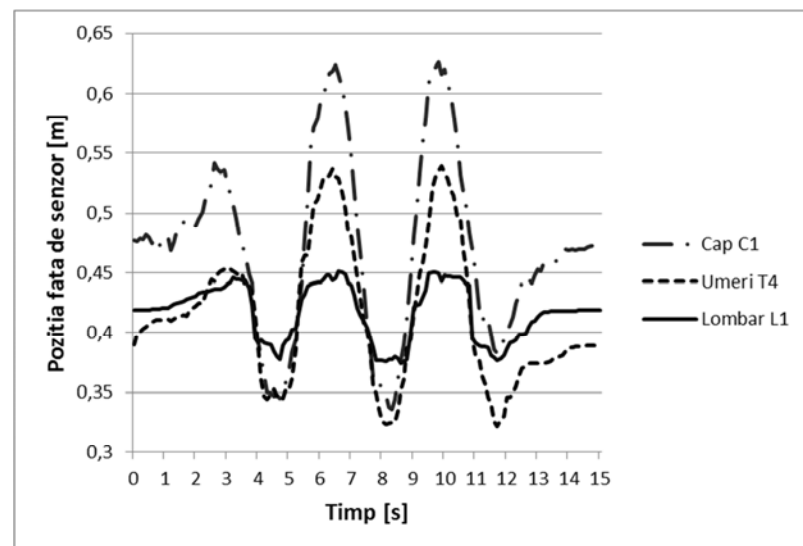


Figure 3.33 – Graphical representation of the positions in time of the three points.

3.2.5 Determination of the sinusoidal functions describing the variation in time of the C1, T4 and L1 vertebra positions

Using the Mathcad software the position in time values for the three points were introduced as the following strings:

cp :=		um :=		lb :=	
	0		0		0
0	0.477	0	0.39	0	0.418
1	0.476	1	0.399	1	0.418
2	0.479	2	0.401	2	0.418
3	0.478	3	0.403	3	0.419
4	0.482	4	0.405	4	0.419
5	0.479	5	0.407	5	0.419
6	0.474	6	0.409	6	0.419
7	0.48	7	0.411	7	0.42
8	0.473	8	0.411	8	0.42
9	0.473	9	0.411	9	0.42
10	0.475	10	0.411	10	0.42
11	0.48	11	0.411	11	0.421
12	0.469	12	0.41	12	0.422
13	0.476	13	0.412	13	0.424
14	0.485	14	0.413	14	0.425
15	...	15	...	15	...

The *cp* string corresponds to the C1 point, *um* string corresponds to the T4 point and *lb* string corresponds to the L1 point.

The next step is to determine the frequency of each string.

$$tcpmax_i := \begin{cases} i & \text{if } \max(cp) = cp_i \\ 0 & \text{otherwise} \end{cases}$$

$$\max(tcpmax) = 98$$

$$tcpmin_i := \begin{cases} i & \text{if } \min(cp) = cp_i \\ 0 & \text{otherwise} \end{cases}$$

$$\max(tcpmin) = 83$$

$$tummax_i := \begin{cases} i & \text{if } \max(um) = um_i \\ 0 & \text{otherwise} \end{cases}$$

$$\max(tummax) = 99$$

$$\text{tummin}_i := \begin{cases} i & \text{if } \min(\text{um}) = \text{um}_i \\ 0 & \text{otherwise} \end{cases}$$

$$\max(\text{tummin}) = 117$$

$$\text{tlbmax}_i := \begin{cases} i & \text{if } \max(\text{lb}) = \text{lb}_i \\ 0 & \text{otherwise} \end{cases}$$

$$\max(\text{tlbmax}) = 70$$

$$\text{tlbmin}_i := \begin{cases} i & \text{if } \min(\text{lb}) = \text{lb}_i \\ 0 & \text{otherwise} \end{cases}$$

$$\max(\text{tlbmin}) = 86$$

The time interval between the maximum and minimum for each string is determined:

$$\Delta\text{tcp} = \frac{|\max(\text{tcpmax}) - \max(\text{tcpmin})|}{10} = 1.5\text{s} \quad (3.4)$$

$$\Delta\text{tum} = \frac{|\max(\text{tummax}) - \max(\text{tummin})|}{10} = 1.8\text{s} \quad (3.5)$$

$$\Delta\text{tlb} = \frac{|\max(\text{tlbmax}) - \max(\text{tlbmin})|}{10} = 1.6\text{s} \quad (3.6)$$

In order to determine the single frequency in all three strings, the average of the three time periods is determined:

$$\Delta t = \frac{\Delta\text{tcp} + \Delta\text{tum} + \Delta\text{tlb}}{3} = 1.6333\text{s} \quad (3.7)$$

Thus, the frequency will be:

$$f_{\Delta t} = \frac{1}{\Delta t} \quad (3.8)$$

The amplitude of each string is determined as follows:

$$\text{acp} = \frac{\max(\text{cp}) + \min(\text{cp})}{2} \quad (3.9)$$

$$\text{aum} = \frac{\max(\text{um}) + \min(\text{um})}{2} \quad (3.10)$$

$$\text{alb} = \frac{\max(\text{lb}) + \min(\text{lb})}{2} \quad (3.11)$$

The *cp* string amplitude is noted *acp*, the *um* string amplitude is noted with *aum*, and the amplitude of the *lb* string is noted *alb*.

The sinusoidal functions describing the position variation in time of the C1, T4 and L1 vertebrae points are the following:

$$y_{cp_i} = cp_0 + a_{cp} \cdot \cos(f_{\Delta t} \cdot i \cdot \pi) \quad (3.12)$$

$$y_{um_i} = um_0 + a_{um} \cdot \cos(f_{\Delta t} \cdot i \cdot \pi) \quad (3.13)$$

$$y_{lb_i} = lb_0 + a_{lb} \cdot \cos(f_{\Delta t} \cdot i \cdot \pi) \quad (3.14)$$

In the figures 3.34, 3.35 and 3.36 the sinusoidal functions are represented in comparison to the cp , um and lb strings graphic form. For each case can be seen that the sinusoidal functions all are very close to the allure of the strings measured values.

In conclusion it can be considered that these sinusoidal functions can describe the position variation in time of the C1, T4 and L1 vertebra's points, while driving on a sinusoidal trajectory.

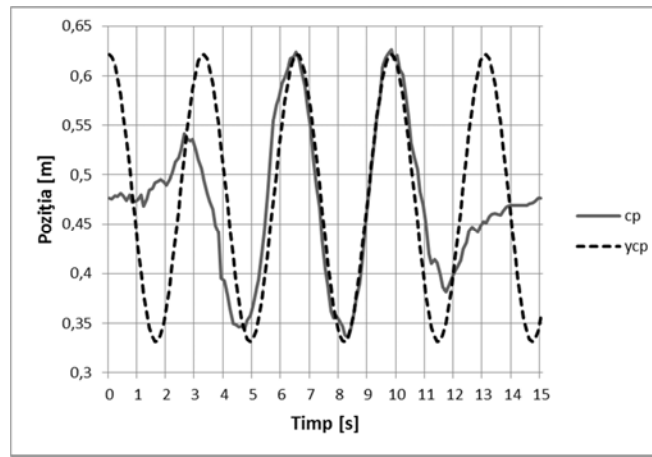


Figure 3.34 - Graphical representation of the y_{cp} sinusoidal function compared with the cp string.

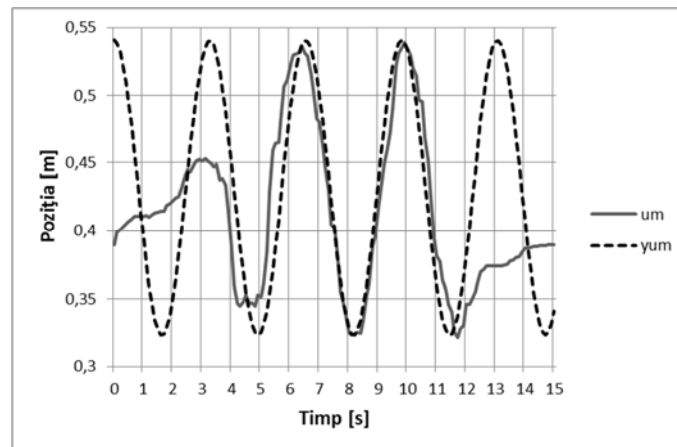


Figure 3.35 - Graphical representation of the y_{um} sinusoidal function compared with the um string.

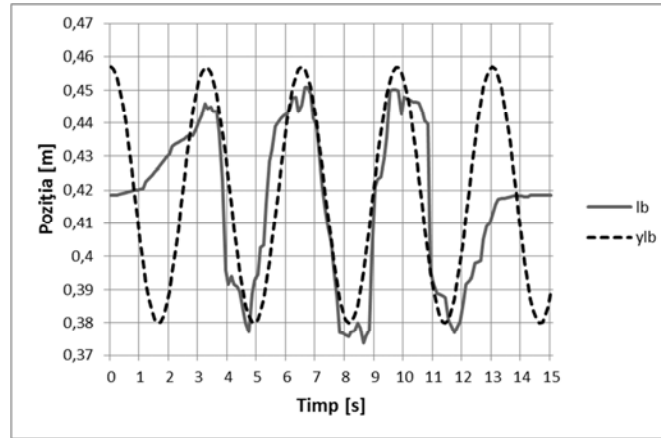


Figure 3.36 - Graphical representation of the y/lb sinusoidal function compared with the lb string.

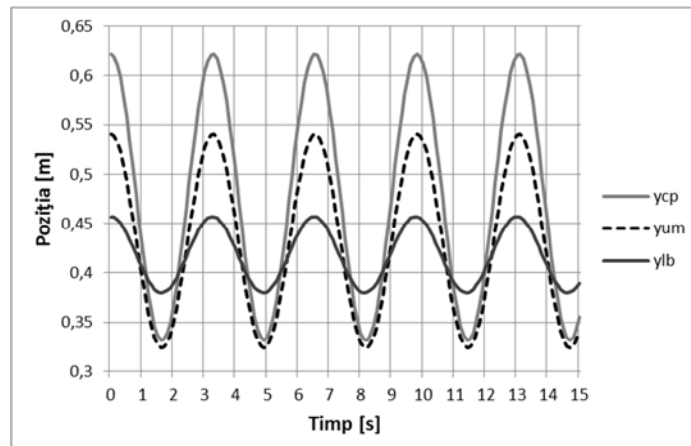


Figure 3.37 – The sinusoidal functions describing the position variation in time of the C1, T4 and L1 vertebrae points.

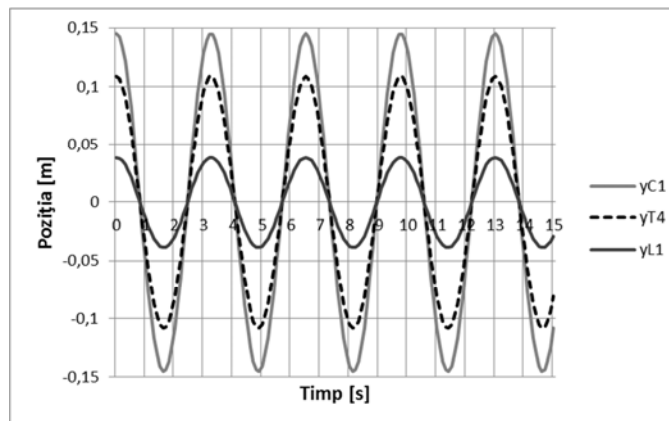


Figure 3.38 – The sinusoidal functions describing the position variation in time of the C1, T4 and L1 vertebrae.

The sinusoidal functions describing the position variation in time of the C1, T4 and L1 vertebrae in the coronal plane are:

$$yC1_i = acp \cdot \cos(f_{\Delta t} \cdot i \cdot \pi) \quad (3.15)$$

$$yT4_i = aum \cdot \cos(f_{\Delta t} \cdot i \cdot \pi) \quad (3.16)$$

$$yL1_i = alb \cdot \cos(f_{\Delta t} \cdot i \cdot \pi) \quad (3.17)$$

3.2.6 Conclusions

The amplitude values of the sinusoidal functions describing the variation in time of angles between the vertebrae gives an image regarding the deformation degree of the intervertebral discs.

An ergonomic posture of the driver's body seated in the vehicle's seat implies the spine to be in a shape that subjects the intervertebral discs to uneven tensions causing deformations that in some cases can exceed the limits at which the musculoskeletal affections of the spine can be avoided or treated by physiotherapy.

3.3 The drivers spine movement equation in the coronal plane

3.3.1 Introduction

The research presents the determination of the movement equation of the drivers spine in the coronal plane, during the drive. Using the movement equation, the spines movements in the coronal plane were simulate by using the MathCAD and CATIA software.

On this line was proposed a methodology to approach the interaction between driver and the vehicle to allow accurate conclusions for the driving activity.

Recent years have brought the current general trend in the design, construction and operation of motor vehicles (research centers of companies producing curricula of universities / departments field, masters that include ergonomics and comfort of road vehicles, European legislation, etc.), namely the transformation of the interior components of passive elements with uncontrolled reaction to changing human factor elements able to adapt continuously [176].

In the current scientific and technological conditions is required reconsideration of the research, analysis and design optics of the working places by applying outstanding results obtained recently in some new areas of human activity such as systems theory, cybernetics, information theory, operational research , computer science and ergonomics [177, 178, 179].

It should be noted that if the configuration of the safety, ventilation, lighting, heating, etc..., interior equipment is analyzed and properly carried out, in terms of scientific evidence (evidence based) on the behavior of the driver's body, especially the spine with associated muscles, still requires further study which continually preoccupied car manufacturing companies [181, 186, 187].

3.3.2 Determining the movement equation of the spinal column in the coronal plane

Using the coordinate system shown in figure 3.39 it is considered that the center of each vertebra is moving along the arch of circle with center the origin of the coordinate sistem, and radius equal to the height above the x-axis, the seat surface. The length of each arc of circle is depending on the vehicle traveling speed and the radius of the trajectory.

In the coordinate system shown in figure 3.39, the sinusoidal functions are variations on the x-axis:

$$XC1_i = acp \cdot \cos(f_{\Delta t} \cdot i \cdot \pi) \quad (3.18)$$

$$XT4_i = aum \cdot \cos(f_{\Delta t} \cdot i \cdot \pi) \quad (3.19)$$

$$XL1_i = alb \cdot \cos(f_{\Delta t} \cdot i \cdot \pi) \quad (3.20)$$



Figure 3.39. – The spine in the coronal plane related to the coordinate system xOy.

The equations of the arch on what the C1, T4 and L1 vertebrae are moving are given by the relations:

$$YC1_i = \sqrt{r_C^2 - XC1_i^2} \quad (3.21)$$

$$YT4_i = \sqrt{r_T^2 - XT4_i^2} \quad (3.22)$$

$$YL1_i = \sqrt{r_L^2 - XL1_i^2} \quad (3.23)$$

In the coronal plane and the coordinate system (fig. 3.39), the spine shape is a curved line given by the following equation:

$$y(x) = a_i \cdot x^3 + b_i \cdot x^2 + c_i \cdot x + d_i \quad (3.24)$$

In this equation the unknowns are: a_i , b_i , c_i , and d_i . Knowing the coordinates of four points, the unknowns a_i , b_i , c_i , and d_i are determined with the *Cramer* method:

$$\begin{cases} YC1_i = a_i \cdot XC1_i^3 + b_i \cdot XC1_i^2 + c_i \cdot XC1_i + d_i \\ YT4_i = a_i \cdot XT4_i^3 + b_i \cdot XT4_i^2 + c_i \cdot XT4_i + d_i \\ YL1_i = a_i \cdot XL1_i^3 + b_i \cdot XL1_i^2 + c_i \cdot XL1_i + d_i \\ d_i = 0 \end{cases} \quad (3.25)$$

Due to the fact that the origin is one of the four points results that d_i is equal to 0. So the system of equations (3.25) is transformed into a system of three equations with three unknowns:

$$\begin{cases} YC1_i = a_i \cdot XC1_i^3 + b_i \cdot XC1_i^2 + c_i \cdot XC1_i \\ YT4_i = a_i \cdot XT4_i^3 + b_i \cdot XT4_i^2 + c_i \cdot XT4_i \\ YL1_i = a_i \cdot XL1_i^3 + b_i \cdot XL1_i^2 + c_i \cdot XL1_i \end{cases} \quad (3.26)$$

$$\Delta_i = \begin{bmatrix} XC1_i^3 & XC1_i^2 & XC1_i \\ XT4_i^3 & XT4_i^2 & XT4_i \\ XL1_i^3 & XL1_i^2 & XL1_i \end{bmatrix}$$

$$\Delta a_i = \begin{bmatrix} YC1_i & XC1_i^2 & XC1_i \\ YT4_i & XT4_i^2 & XT4_i \\ YL1_i & XL1_i^2 & XL1_i \end{bmatrix}$$

$$\Delta b_i = \begin{bmatrix} XC1_i^3 & YC1_i & XC1_i \\ XT4_i^3 & YT4_i & XT4_i \\ XL1_i^3 & YL1_i & XL1_i \end{bmatrix}$$

$$\Delta c_i = \begin{bmatrix} XC1_i^3 & XC1_i^2 & YC1_i \\ XT4_i^3 & XT4_i^2 & YT4_i \\ XL1_i^3 & XL1_i^2 & YL1_i \end{bmatrix}$$

$$a_i = \frac{\Delta_i}{\Delta a_i}; b_i = \frac{\Delta_i}{\Delta b_i}; c_i = \frac{\Delta_i}{\Delta c_i}$$

Using the Mathcad software has created a program sequence that limits the curve given by the equation (3.24) that describes the shape of the spine in the coronal plane, between the origin and the center of C1 vertebra. The program sequence is:

$$(x) = \begin{cases} (a_i \cdot x^3 + b_i \cdot x^2 + c_i \cdot x + d_i) & \text{if } 0 \leq \\ \leq (a_i \cdot x^3 + b_i \cdot x^2 + c_i \cdot x + d_i) \leq YC1_i & \\ (break) & \text{otherwise} \end{cases}$$

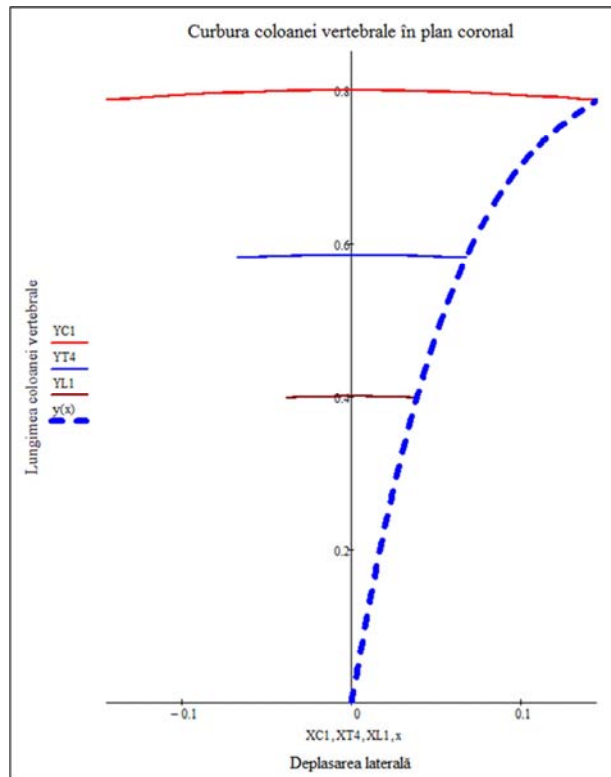


Figure 3.40– The shape of spinal colum in coronal plane at the maximum right lateral tilt.

In figure 3.40 is shown the graph obtained with the Mathcad software in which is represented the shape of the spinal column in coronal plane at the maximum right lateral tilt, given by the equation (3.24). Also in this graph are the corresponding trajectory arch centers of the C1, T4, and L1 vertebrae.

3.3.3 Spine motion simulation using Mathcad software

Through Animation function, Mathcad software allows changes to a graphic animation using software integrated FRAME variable.

Starting from the equation (3.24), which describes the shape of the spine in the coronal plane between the origin and the center of C1 vertebra, was created the following sequence of program that animates the graph in figure 3.40.

$$y(x) = \begin{cases} (a_{FRAME} \cdot x^3 + b_{FRAME} \cdot x^2 + c_{FRAME} \cdot x + d_{FRAME}) & \text{if } 0 \leq \\ \leq (a_{FRAME} \cdot x^3 + b_{FRAME} \cdot x^2 + c_{FRAME} \cdot x + d_{FRAME}) \leq YC1_{FRAME} & \\ (break) & \text{otherwise} \end{cases}$$

In figure 3.38 are shown some frames from the created animation in Mathcad software.

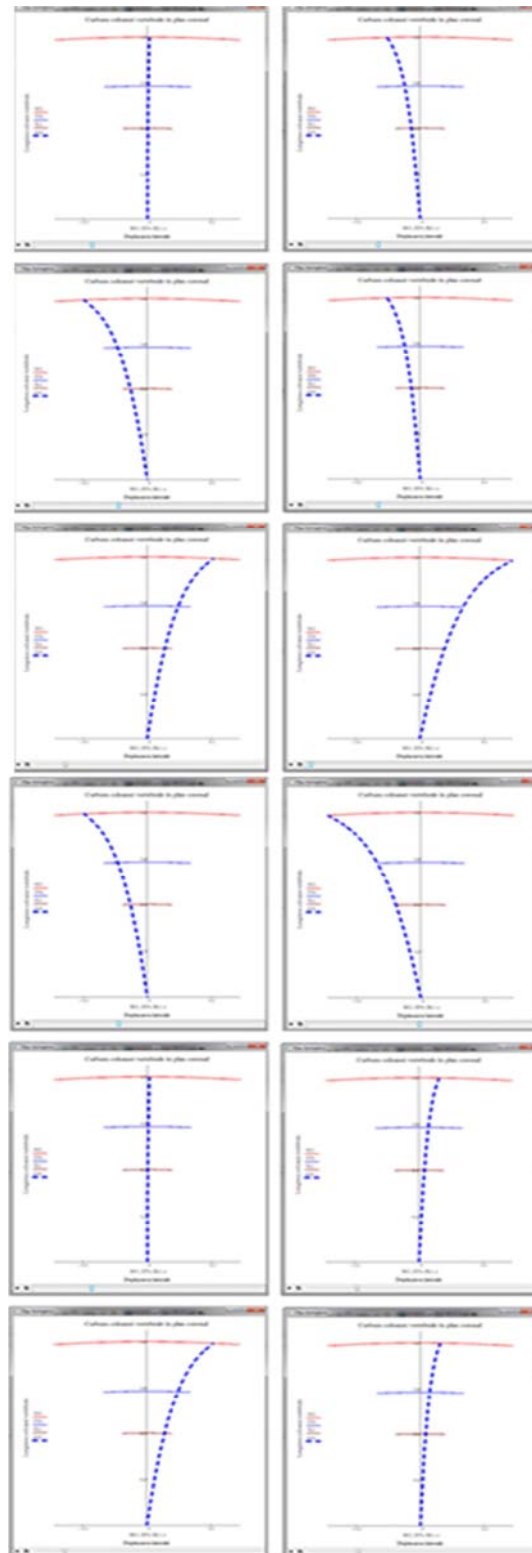


Figure 3.41 – Extracted frames from Mathcad simulation.

3.3.4. Spine motion simulation using CAD software CATIA

Vertebrae 3D model was realized using the ATOS IIe optical high-end 3D Digitizer by 3D scanning the vertebrae from a human corpse. The digitizer uses the spatial triangulation and generates a cloud of points on the object surface. It has been obtained a cloud of points with the shape of the vertebra 3D model. The 3D model was generated by transforming the cloud in NURBS surfaces using the Geomagic Studio 3D software. Final design of the vertebrae was realized by importing these surfaces in CAD software CATIA V5 [175, 185, 189, 199].

The steps of the 3D design of vertebrae are shown in figures 3.42, 3.43 and 3.44.

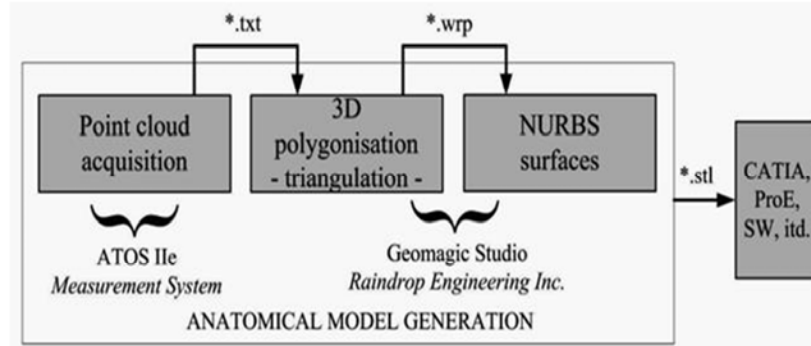


Figure 3.42 – Generating anatomical model.

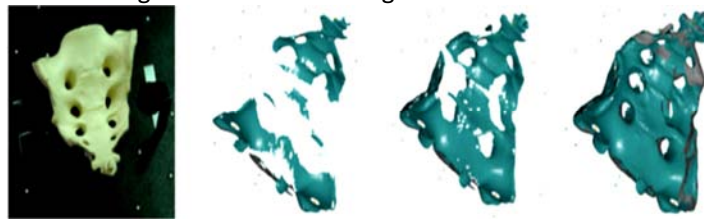


Figure 3.43 – The vertebra scanning.

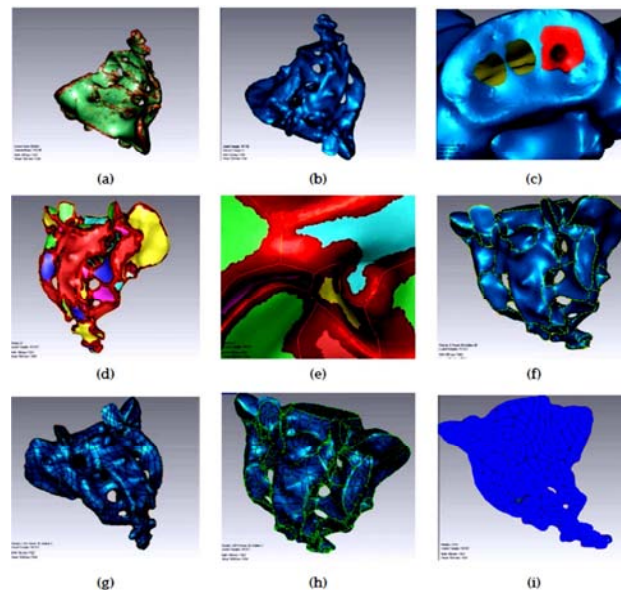


Figure 3.44 – The vertebra reconstruction.



Figure 3.45 – The 3D model of the spine by using CATIA.

To achieve spine motion simulation with CAD software CATIA, the DMU Kinematics module is selected. Because the simulation of the spine movement is only in the coronal plane, spine assembly is such that the motion of each vertebra is restricted in the rotation joint at the center of rotation [210, 212, 213].

Using DMU Kinematics module, the simulation is done with the function Simulation with Laws. The laws of motion are given by the time variation of angle α_i .

The angle α_i is determined by the difference between the two slopes to the curve given by equation (3.24) in the centers of two consecutive vertebrae. To determine the slope in the center of the vertebrae we should know that center of coordinates must be reported to the reference system. From the 3D model of the whole spine created in CAD software CATIA V5, we extract the values of the distances between the centers of the vertebrae. The values of the distances between the centers of the vertebrae are given in Table 3.1.

These values will be introduced in Mathcad software under the string of numbers with the note dv . Knowing the center of each vertebra is moving in an arc of a circle with its center at the origin of the coordinate system, we determine the radius of these arcs with the relationship:

$$r_u = r_c - \left(\sum_{j=0}^u dv_j \right) \cdot 10^{-3}$$

Where u is a counter for determining the number of orders according to Table 3.1.

Each of the vertebrae is moving under a center of an arc of a circle with a time variation given by the sinusoidal function similar to those given by the relations (3.18), (3.19) and (3.20). The amplitude of movement is determined by the intersection of the arc corresponding to each center of the vertebrae, and the curve that describes the shape of the spine extreme point side slope.

Table. 3.1 – Distances between the centers of the vertebrae.

Nr. crt.	Vertebra s	Distance [mm]
1.	C2 – C3	15,7
2.	C3 – C4	14

3.	C4 – C5	14,9
4.	C5 – C6	14,5
5.	C6 – C7	15
6.	C7 – T1	16
7.	T1 – T2	18,48
8.	T2 – T3	21
9.	T3 – T4	21,5
10.	T4 – T5	21,5
11.	T5 – T6	22,46
12.	T6 – T7	23,46
13.	T7 – T8	24,47
14.	T8 – T9	25,49
15.	T9 – T10	27
16.	T10 – T11	28
17.	T11 – T12	29,5
18.	T12 – L1	30,98
19.	L1 – L2	31,49
20.	L2 – L3	31,92
21.	L3 – L4	32,45
22.	L4 – L5	32,47

To determine the coordinates of these points, the following sequence was created using the software program Mathcad:

$$xiv_{u,k} = \begin{cases} h_k & \text{if } trunc \left[\left(\sqrt{r_u^2 - h_k^2} \right) \cdot 10^4 \right] = \\ = trunc \left[(a_0 h_k^3 + b_0 h_k^2 + c_0 h_k) \cdot 10^4 \right] \\ 0 & \text{otherwise} \end{cases}$$

$$xv_u = \max(xiv_{u,k})$$

Where $k = 0 \dots 145 \cdot 10^6$, $h_k = k \cdot 10^{-6}$.

$$yv_u = \sqrt{r_u^2 - xv_u^2}$$

Knowing the coordinates of the center vertebrae in the coronal plane, the shape of the spine side slope extreme point, can be determined from the slopes of the curve (3.24) in these points with the following relationship:

$$\gamma_u = \arctg \left(\frac{y(xv_u + 10^{-6}) - y(xv_u - 10^{-6})}{(xv_u + 10^{-6}) - y(xv_u - 10^{-6})} \right)$$

Thus the angle α will be:

$$\alpha amp_u = (\gamma_{u+1} - \gamma_u)$$

The values of the angles αamp and γ are returned in radians by the Mathcad calculation software. The values of the angle αamp represent the amplitude of the sinusoidal function given by the following relationship (3.27). The functions describing the variation in time of the angle between the vertebrae.

$$\alpha_u = [\alpha amp_u \cdot \sin(f_{\Delta t} \cdot i \cdot \pi)] \cdot \frac{180}{\pi} \quad (3.27)$$

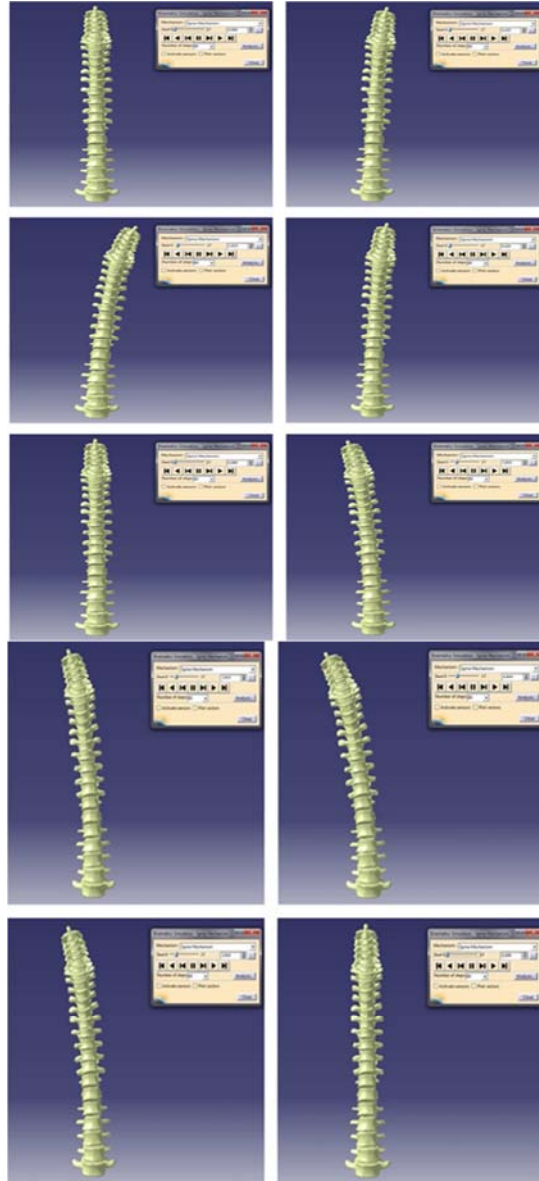


Figure 3.46 – Extracted frames realized with CAD software CATIA V5.

3.3.5 Conclusion

The amplitude values of the sinusoidal functions describing the variation in time of angles between vertebrae gives an insight into the degree of deformation of intervertebral discs.

According to the literature the maximum tilt in the coronal plane of the lumbar vertebrae are 5° for L1-L2; 5° for L2-L3; 4.5° for L3-L4; 2.2° for L4-L5; 1 degrees for L1-S1.

This sort of ergonomic analysis over the driver spine involves a study of the effects of vibration on the human body.

As reported above it is evident that we have a maximum interest for understanding the pathogenesis of diseases caused by vibration, to determine the hygienic conditions of operation of vehicles. Such research should focus on framing all operation of machinery, especially motor vehicles, in parameters corresponding to operator health insurance, in this analysis of driver and passengers.

On this line was proposed a methodology to approach the interaction between driver and the vehicle to allow accurate conclusions for the driving activity.

3.4. Experimental determination of the intervertebral stress

3.4.1. Introduction

The aim of this study is to determine the intervertebral stress that leads to spine musculoskeletal affections. To determine the intervertebral stress, the L4 and L5 vertebrae were made by using rapid prototyping. Between the vertebrae the intervertebral disc was made by using silicon material. In the intervertebral disc five force sensors were inserted. A STEWART platform was used to remake the vertebra's relative movements during that time with the aid of the five force sensor, the intervertebral stress was recorded. It was clearly shown at what load and movements during the drive, spine musculoskeletal affections can appear.

To determine the musculoskeletal affections it is necessary to perform a stress and deformation analysis of the spinal column by modelling, simulation and experimental validation.

The continuous contraction of the muscles from the spinal column determines a supplemental load on vertical direction increasing the equivalent stress from the vertebrae and especially in the intervertebral discs determining deformations which in some cases cross over the point that musculoskeletal disease can be treated or recovered by physiotherapy. [151, 152, 153, 188]

The form of the spinal column in sagittal plane and the amplitudes of the inclination in the coronal plane are determined directly from the driver body reactions to the forces that occur from the car running on different routes. In the case of a non-ergonomic position of the spine in sagittal plane, the amplitudes of the inclination in the coronal plane lead to deformation of the intervertebral discs, which exceed the aforementioned anatomical limits. [128, 149, 190, 201]

The driver's body optimal ergonomic posture while seated on the car seat is influenced by construction characteristics of the seat in order to constrain the body as its spine shape to follow the ideal anatomic spine shape or ergonomic optimal. As this is known, in order to design and manufacture of auto vehicles car seats, it is proposed to start from the ideal anatomical shape of the human spine. [129, 138, 150, 202, 203, 204, 205]

The analysis aims to determine the equivalent stresses of the two vertebrae and intervertebral disc special deformations.

In order to determine the design parameters of the car seat it is necessary to know the analytical shape of the spine in sagittal plane and coronal plane [192, 193].

The analytical expression of the spine in sagittal plane:

$$y = \frac{1}{L} \left(\frac{m}{6} - \frac{A}{3} \right) \cdot x^3 + A \cdot x^2 - L \cdot \left(\frac{m}{6} - \frac{2 \cdot A}{3} \right) \cdot x + \frac{R}{L} \cdot x + \left(\frac{m}{6} - \frac{2 \cdot A}{3} \right) \cdot \frac{L^2}{\pi} \cdot \sin \frac{\pi \cdot x}{L} - \frac{R}{L} \cdot \sin \frac{\pi \cdot x}{L}$$

(3.28)

L and R are x, y coordinates of the point L5-S1 from figure 3.46.

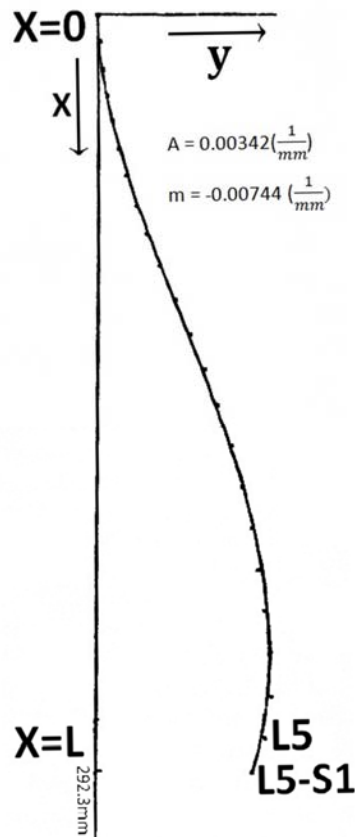


Figure 3.47. The spine analytical shape in the sagittal plane.

From the analysis of 30 X-Rays have been obtained values for A parameter between 0.00003mm^{-1} and 0.00005mm^{-1} and for the m parameter values between 0.00005mm^{-1} and 0.0015mm^{-1} . These values are for the erect position of the spine.

For the seated position the values are: $A=0.00004\text{mm}^{-1}$ and $m=0.0016\text{mm}^{-1}$. [141, 151, 152, 191]

3.4.2. Methodes

A. Experimental Analysis of the intervertebral strains

For the experimental analysis a mechatronic device was designed to determine the intervertebral stress. The device is designed to implement to a spine segment flexion-extension and lateral bending movements under a constant or variable load.

To obtain the vertebrae specific movements, the STEWART platform was used.

B. The STEWART platform

The initial position of the platform is characterized by the points O_M and O'_M with the upper platform parallel to the base.

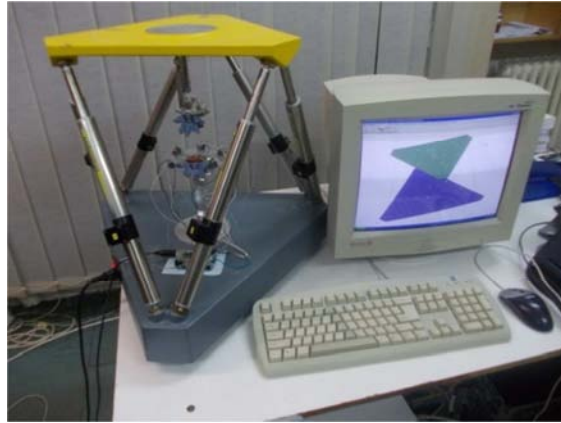


Figure 3.48. The STEWART Platform.

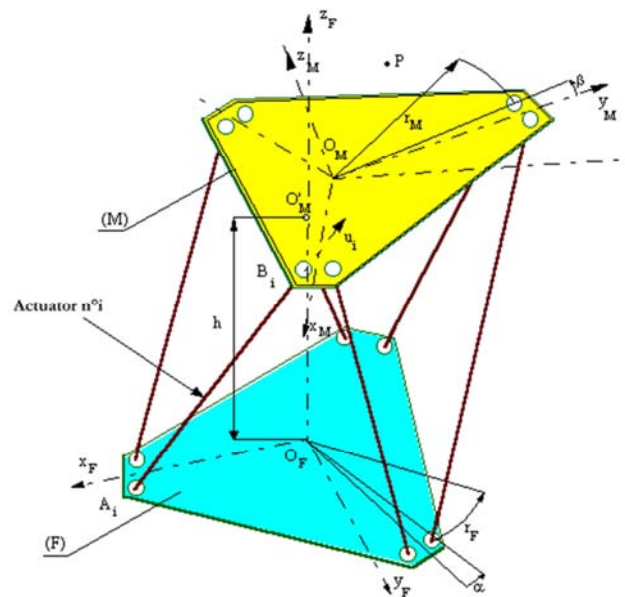


Figure 3.49. - The geometrical characteristics of the platform STEWART.

The upper platform has six degrees of freedom referring to the base:

- 3 translation degrees of freedom characterized by point O_M , the origin of the mobile frame R_M in the fixed frame R_F and respecting the positioning vector:

$$\overrightarrow{O'_M O_M} = x_M \overrightarrow{x_F} + y_M \overrightarrow{y_F} + z_M \overrightarrow{z_F} \quad (3.29)$$

- 3 rotation degrees of freedom, characterized by the frame orientation R_M by respecting the fixed frame R_F .

C. The vertebrae prototyping

Vertebrae 3D model was realized using the ATOS IIe optical high-end 3D Digitizer by 3D scanning the vertebrae from a human corpse. The digitizer uses the spatial triangulation and generates a cloud of points on the object surface. It has been obtained a cloud of points with the shape of the vertebra 3D model. The 3D model was generated by transforming the cloud in NURBS

surfaces using the Geomagic Studio 3D software. Final design of the vertebrae was realized by importing these surfaces in CAD software CATIA V5, as shown in chapter 3.3.

The L4 and L5 vertebrae from CAD designs, CATIA V5 by were made by rapid prototyping (fig. 3.50).



Figure 3.50. The final shape of the vertebrae.

The material used to make the vertebrae is Objet VeroBlue Fullcure 840. The mechanical characteristics are showed in table 3.2.

It can be seen that the Objet VeroBlue FullCure 840 material used for vertebrae prototyping, has approximately the same mechanical properties of bone tissue of the vertebrae (Table. 3.2).

The intervertebral disc was made of two pieces each having a thickness of 5mm. The material used in making the intervertebral discs is a silicone material that has mechanical characteristics close to those of the intervertebral disc (Table.3.2). Both, the inferior and upper surfaces of the vertebrae L4 and L5, vertebrae resulted from prototyping were classified moulded to a height of 5 mm. The reason why the silicone material was poured directly on the surfaces of the vertebral disc is that to be identical.

Table 3.2. The mechanical characteristics of the material Objet VeroBlue FullCure 840

Objet VeroBlue FullCure840					
	ASTM	Units	Metric	Units	Imperial
Tensile strength	D-638-03	MPa	50-60	psi	7250-8700
Elongation at break	D-638-05	%	15-25	%	15-25
Modulus of elasticity	D-638-04	MPa	2000-3000	psi	290,000-435,000
Flexural Strength	D-790-03	MPa	60-70	psi	8700-10200
Flexural Modulus	D-790-04	MPa	1900-2500	psi	265,000-365,000
HDT, °C @ 0.45MPa	D-648-06	°C	45-50	°F	113-122
HDT, °C @ 1.82MPa	D-648-07	°C	45-50	°F	113-122
Izod Notched Impact	D-256-06	J/m	20-30	ft lb/inch	0.375-0.562
Water Absorption	D-570-98 24hr	%	1.5-2.2	%	1.5-2.2
Tg	DMA, E _s	°C	48-50	°F	118-122
Shore Hardness (D)	Scale D	Scale D	83-86	Scale D	83-86
Rockwell Hardness	Scale M	Scale M	73-76	Scale M	73-76
Polymerized density	ASTM D792	g/cm ³	1.18-1.19		
Ash content Vblack	USP281	%	0.21-0.22	%	0.21-0.22

D. Device for fixing and positioning the vertebrae

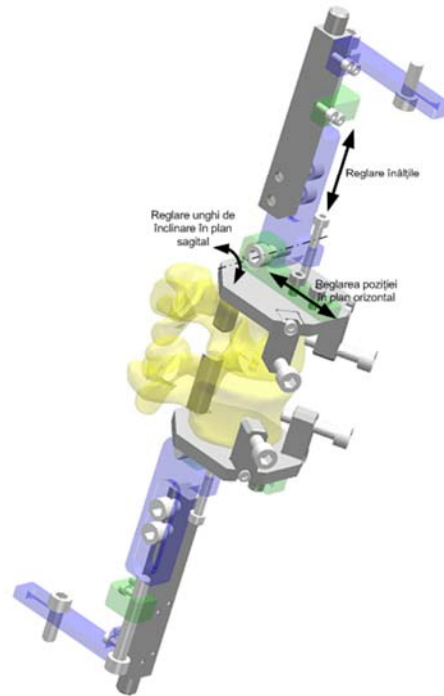


Figure 3.51. The device for fixing vertebrae and its adjustments.

The device shown in Fig. 3.51 was designed for fixing and adjusting the position of the vertebrae. The design was realized using CAD software Solid Edge V20.

The device's clamping mode in the Stewart platform is presented in figure 3.52.



Figure 3.52. The device's clamping mode on the Stewart platform.

E. Determining the loads in the intervertebral disc



Figure 3.53. Circular pressure sensor $\Phi 7,6\text{mm}$.

In order to determine the tensions in the intervertebral disc five circular force sensors were used. These are presented in figure 3.53.

According to technical specifications, the pressure sensor changes its resistance depending on the force exerted on it. When no force is applied its resistance is equal to 1M Ω . When the maximum force is applied the resistance will drop to 2,5 k Ω .

The sensors were arranged on half intervertebral disc corresponding to L5. The arrangement and numbering of sensors is given in figure 3.54.

To record the data the Arduino UNO open-source platform was used. The software and hardware-base is flexible and easy to use. Consists of a small platform shown in figure 3.55 (6.8 cm / 5.3 cm - the most common variant) built around a signal processor.

Since the electrical resistance value returns from the sensor, it was necessary to determine a function for determining the force value.

The force is given by equation (3.30), where X is the electrical resistance of the sensor.

$$F = e^{\frac{x+152.83}{127.77}} \cdot 10^{-3} \cdot 9.81 \quad (3.30)$$

In figure 3.56 is shown the final assembly of the mechatronic device for determining the intervertebral loads.

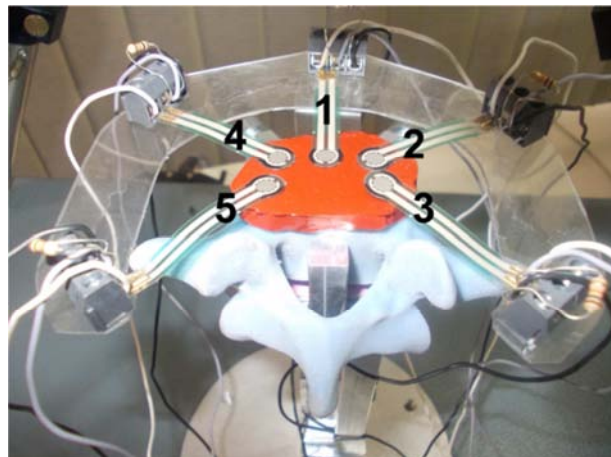


Figure 3.54. The arrangement and numbering of the force sensors on half of the L5 intervertebral disc.



Figure 3.55. Open-source Arduino UNO processing platform. [12]

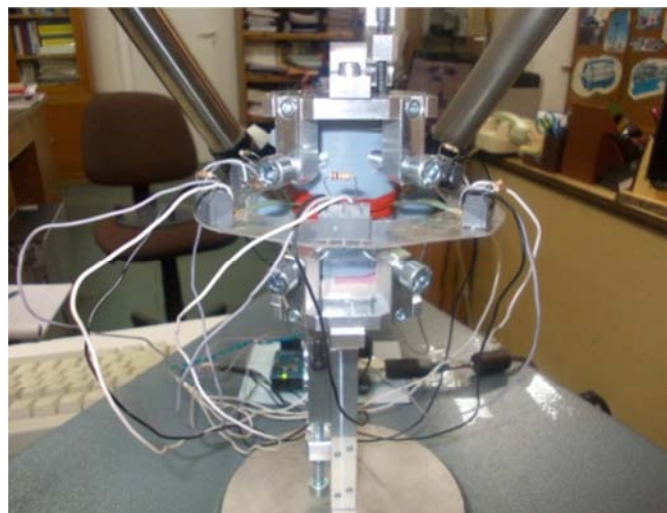


Figure 3.56. Final Assembly of mechatronic device for determining the intervertebral loads.

3.4.3. The experiment and results

In the platform STEWART software was introduced a sinusoidal equation of motion for the vertebra L4 related to the L5 vertebra equation. The acceleration of gravity multiplied by the upper body mass of the driver. As result of the experiment, the graph from figure 3.57 was obtained, which represents the forces variation in time, recorded by each sensor.

In this graph it can be seen that the opposite sensors (sensor 2 and sensor 5) recorded the highest values of loading the test sample.

Knowing the forces on the sensor and the sensor surface using the calculation software Mathcad were determined, the pressures of the zones on the circumference of the intervertebral disc, where the pressure sensors have been placed.

The pressure variation in time is shown in figure 3.58.

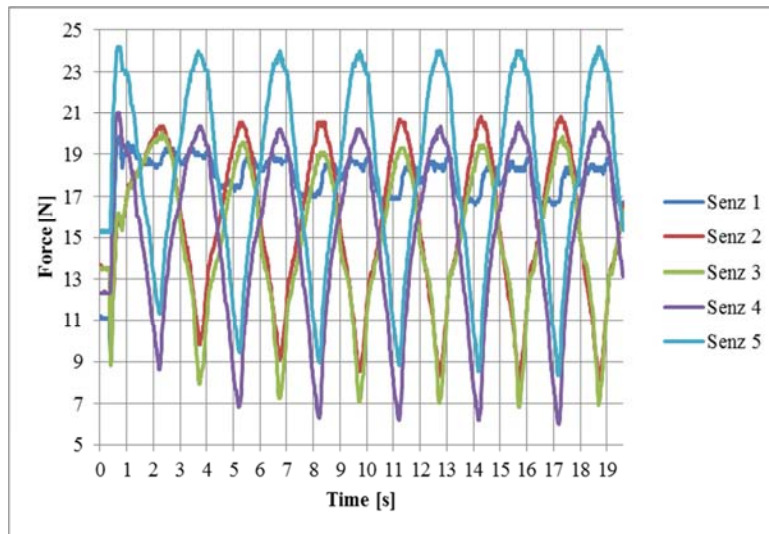


Figure 3.57. The force variation in time recorded on each sensor.

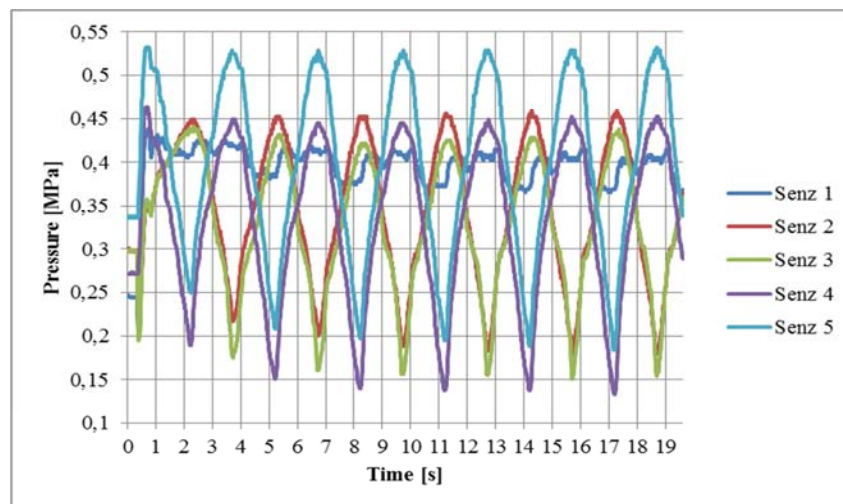


Figure 3.58. The pressure variation in time recorded on each sensor.

3.4.4. Conclusions

It can be observed that the maximum pressure distribution in both vertebrae and the intervertebral disc are concentrated on the exterior circumference in all analysed situations.

In comparison with the empirical data from the specialized literature, the equivalent pressure in the intervertebral disc with limit values of 3 MPa on the circumference on a thickness of 6 mm, from this study analysis this value is also recorded on the left circumference in the sagittal plane of the intervertebral disc.

From the experimental data it can be observed that the highest values recorded were captured by the sensor number 5 placed in the left side of the sagittal plane of the intervertebral disc.

The apparition of muscular-skeletal disorders in report with the mentioned values can be determined by medicine specialists.

Muscular and skeletal disorders, deformations of the intervertebral discs and vibrations that stress the human body while driving are very complex.

Many empirical models based on real phenomenon but there is not yet a single model to capture all of these influences and to conduct to an ergonomic approach of the behavior of the human spine while driving.

The complexity of the theoretical approach can be enhanced by the fact that at the smallest variation of the parameters can appear diverse reactions upon the human body.

The realization of a design of the human spine by 3D scanning of the vertebrae extracted from a human corpse and the modelling surfaces with the CAD software CATIA V5 was the starting point of the real model from what there can be determined analytical equations that describe the spine movement, angles, and their amplitudes.

Amplitude values of the sinusoidal functions that describe the time variation of intervertebral angles offer a complex image of the intervertebral discs deformation.

A non-ergonomic posture of the driver while seated implies a shape of the human spine both in coronal and sagittal planes that stress the intervertebral discs at non-uniform on the whole shape of these discs provoking deformations which in many cases surpass the limit values at a level where muscular-skeletal disorders can be avoided or treated with physiotherapy.

3.5. Modeling, simulation and experimental determination of the spine muscles activities of the driver

3.5.1. Introduction

The aim of this study is to determine the driver's spine muscles' activities and to simulate the human body movements during the drive by using the AnyBody software. To validate the simulation result, a temographical experiment was made that registered the back muscles' activities. The simulation and the termographical experiment proved to be useful tools to determine spine musculoskeletal affections among drivers, and can also be used in the human-based ergonomic design of the vehicle's interior.

Main body movements while driving are the coronal plane opposition due to centrifugal forces that occur when running the vehicle on curved trajectories and the movements in the sagittal plane due to inertial forces at the start or brake of the car [194, 195, 196].

To determine the driver's body movements while driving and especially muscular activity to keep the body in balance on the vehicle seat it is necessary to know the centrifugal and inertial forces acting on the body [197, 198, 200].

3.5.2. Experimental determination of lateral and longitudinal vehicle acceleration.

In order to determine the inertial and centrifugal forces acting on the body of the driver we designed an experiment to measure the vehicle's accelerations in the lateral plane due to running on a curvilinear path and longitudinal acceleration due to starting and braking of the vehicle.

a. Determination of accelerations in the lateral plan.

In the experiment, during the vehicle's running on a sinusoidal path the accelerations in the lateral plan were recorded by using accelerometer PASCO Acceleration Sensor. The accelerometer was placed on the front passenger seat in a vertical plane coinciding with the coronal plane of the spine. Figure 3.59 presents the layout of the accelerometer.



Figure 3.59. Layout accelerometer for acceleration registration in lateral plan.

In this experiment, three sets of tests were conducted (as shown in figure 3.60).

In figure 3.61 it is presented graphically the average of the three sets of measured accelerations.

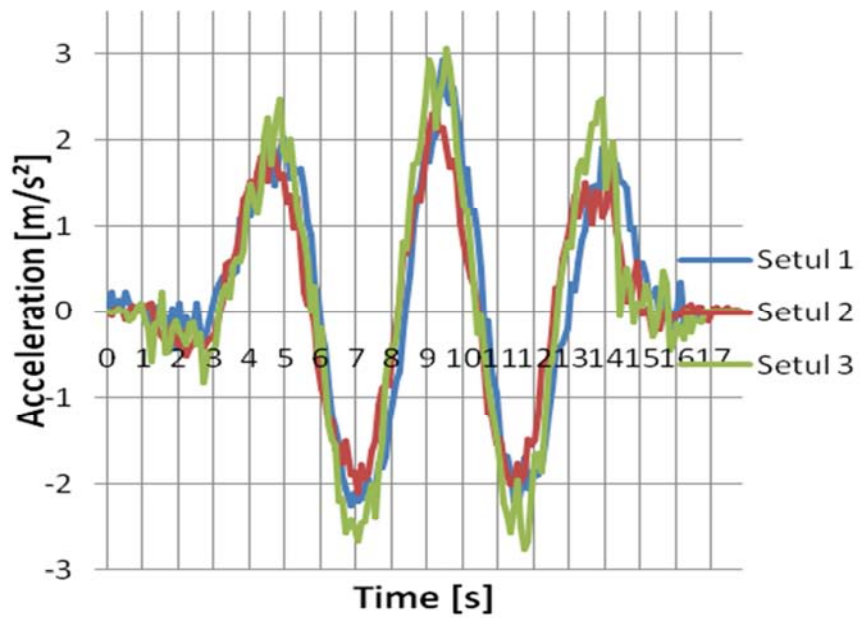


Figure 3.60. Accelerations in the lateral plane.

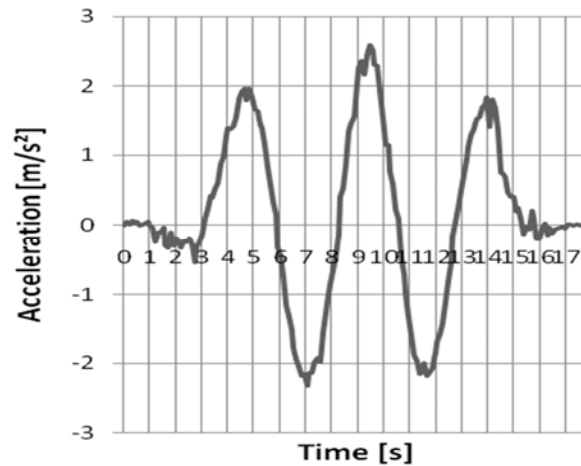


Figure 3.61. Average lateral acceleration

b. Determination of accelerations in the longitudinal plan

To determine the accelerations in the longitudinal plan, the car ran straightly by accelerating from 0 km/h to 80 km/h, after which it decelerated until stopping without locking the wheels.

Longitudinal accelerations were recorded by placing the accelerometer PASCO Acceleration Sensor in a vertical plane which coincides with the sagittal plane of the spinal column.

From starting off and up to 80 km/h, the gear change from first gear to fifth gear was made at the engine speed of 3000 rot/min.

In this experiment, there were four sets of tests carried out as shown in figure 3.62. Each test had a duration of about 27s. In figure 3.63 it is shown graphically the average of the accelerations in longitudinal plan.

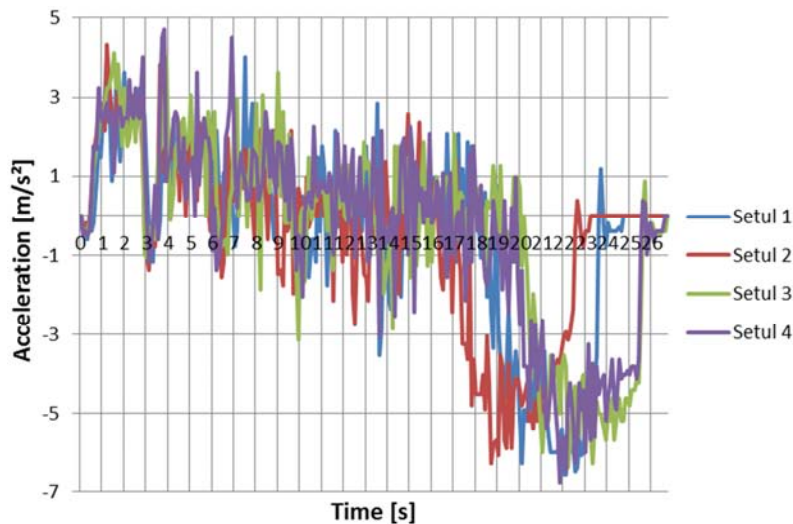


Figure 3.64. Accelerations in the longitudinal plan.

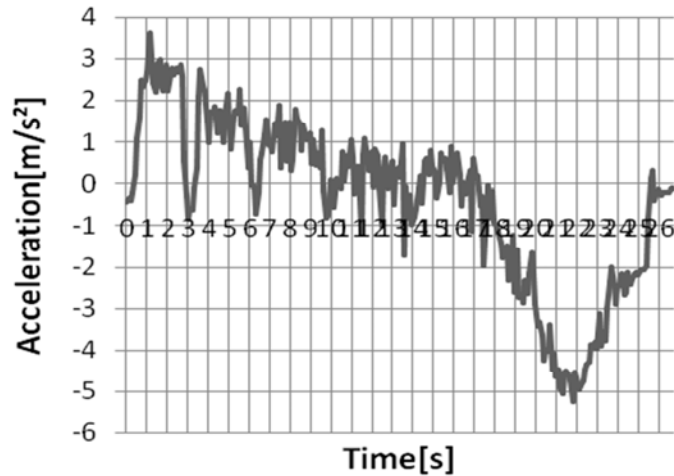


Figure 3.65. Average acceleration in longitudinal plan.

In the graph in figure 3.65 it can be distinguished the gear change moments.

3.5.3. Determination of muscles' activity for movements in the coronal plane

Knowing the accelerations in the lateral plane, the centrifugal force that presses on the top side of the driver's body result from the product of mass of the upper body and acceleration.

According to the literature, the mass of the human upper body is considered 55% of the total body mass. The human body model used in the simulation is considered with a total mass of 80kg, equal to the driver's body mass, thus resulting upper body weight as 44kg. The point of application of the centrifugal force on the human body model in the AnyBody software is the C1 vertebra center (fig. 3.64).

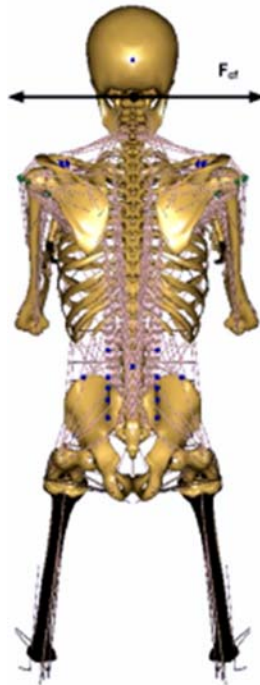


Figure 3.64. Point of application of centrifugal force.

Due to the fact that the registration of the lateral acceleration level for each set, has a time duration of about 17.7 and the sampling rate is 10Hz, simulating movements in the coronal plane was done in 177 steps [128, 138, 151].

In order to reveal the activity of each muscle group, muscle fibers activities were averaged for each muscle group. The results thus obtained are shown in figures 3.65 – 3.68, in which the muscle groups are designated as follows: ESR - Erector spinae right; ESL - Erector spinae left; MR - right multifidus; ML - left multifidus; PMR - Right Major psoas; PML - Major psoas left; QLR - Quadratus Lumborum right; QLL - Quadratus Lumborum left.

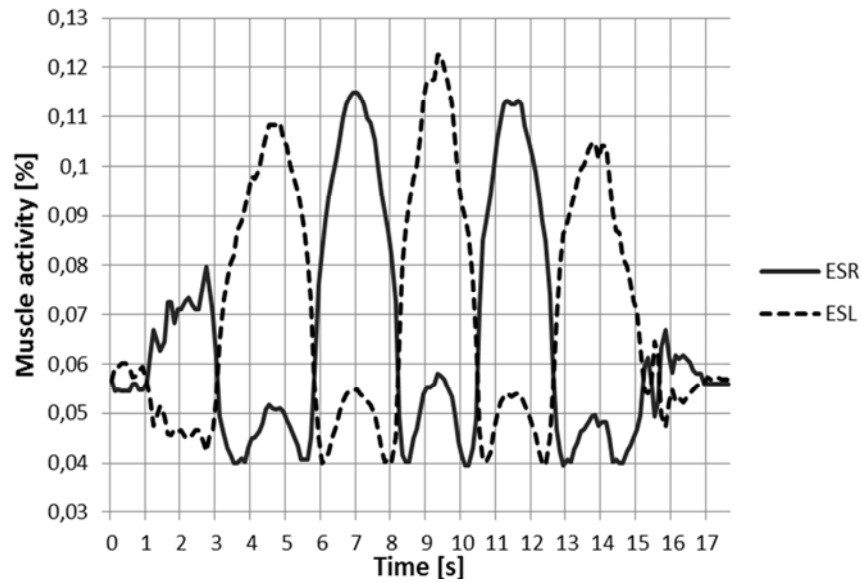


Figure 3.65. Averages muscle activities of groups Erecto Spinae.

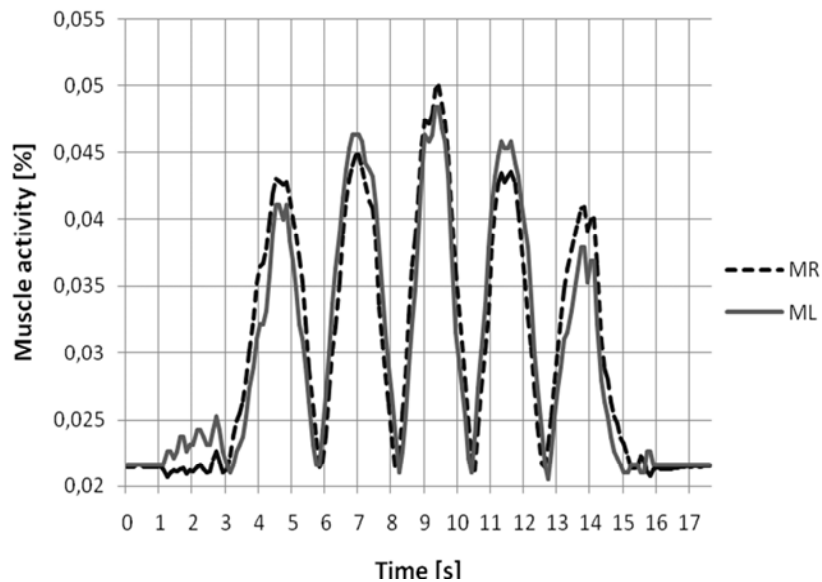


Figure 3.66. Averages muscle activities of groups Multifidus.

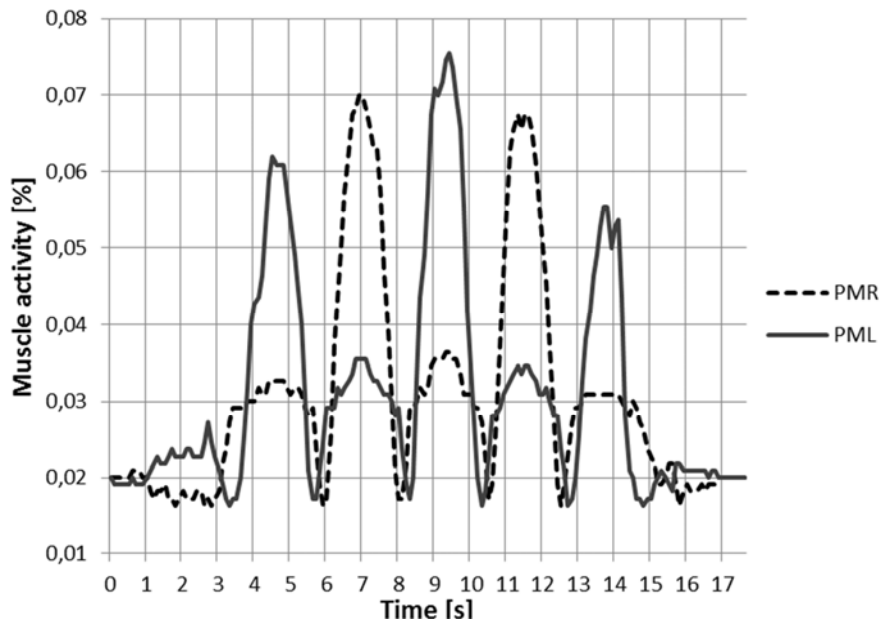


Figure 3.67. Averages muscle activities of groups Psoas Major.

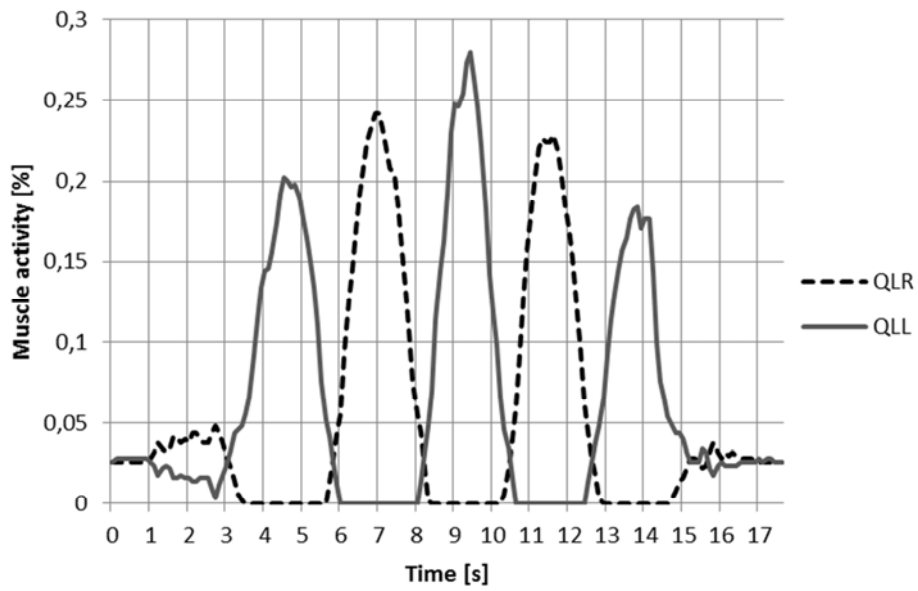


Figure 3.68. Averages muscle activities of groups Quadratus Lumborum.

Figure 3.68 presents the final results of each muscle activities, denoted as: ES – Erector Spinae; M – Multifidus; PM – Psoas Major; QL – Quadratus Lumborum. Figure 3.70 graphically presents the total activity of the four muscles.

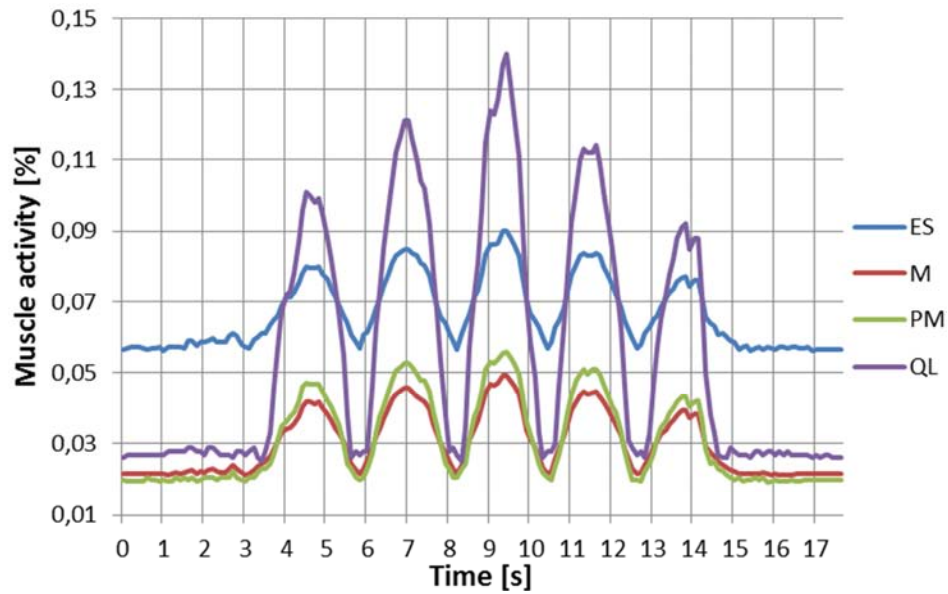


Figure 3.69. Muscle activity of muscle groups.

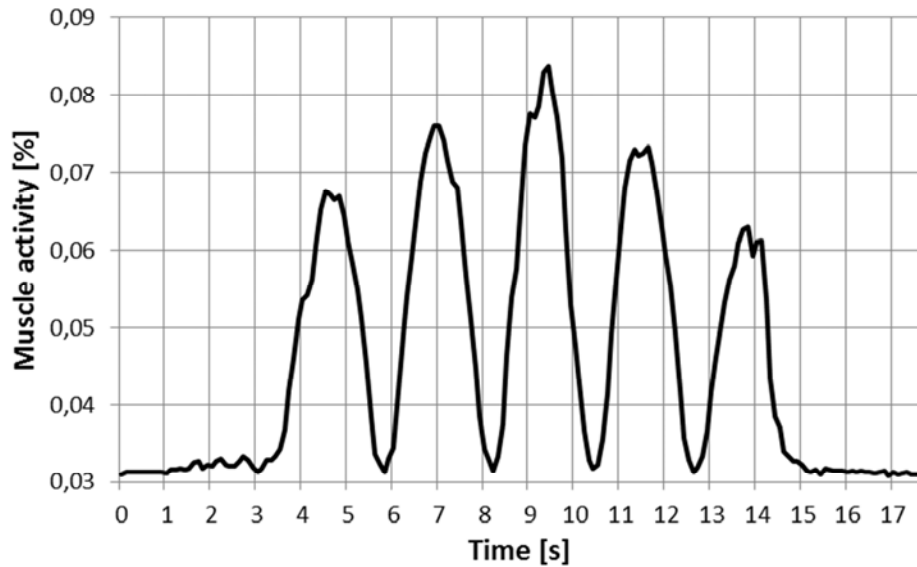


Figure 3.70. Total muscle activity of the four muscles.

Knowing the accelerations in the longitudinal plane, the centrifugal force that presses on the top side of the driver's body result from the product of mass of the upper body and acceleration.

The point of application of the centrifugal force on the human body model in the AnyBody software is the C1 vertebra center (Fig. 3.71). Because the acceleration in the longitudinal record for each set had a term for about 26.8 s and a sampling frequency of 10 Hz, simulating movements in the sagittal plane was done in 269 steps. As the muscle groups in the simulation right / left acting synchronized, muscle activities on both sides of the column are equal. Therefore, the results were extracted only for the muscle activity on the right side of the spine.

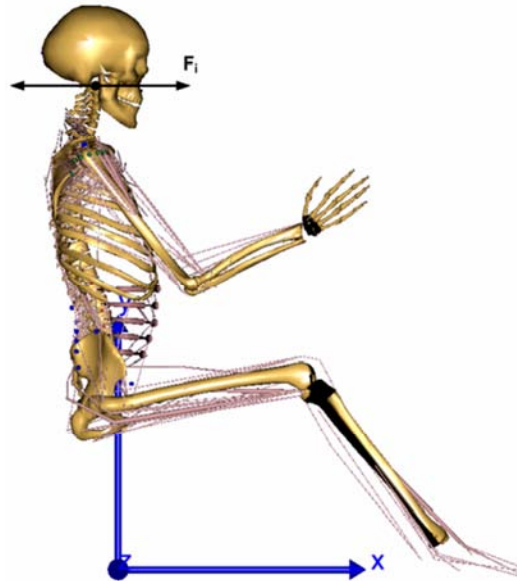


Figure 3.71. The point of application of the force of inertia.

In order to reveal the activity of each muscle group, muscle fibers activities were averaged for each muscle group. The results obtained are shown in figure 3.72, the muscle groups are designated as follows: ES – Erector Spinae; M – Multifidus; PM – Psoas Major; QL – Quadratus Lumborum.

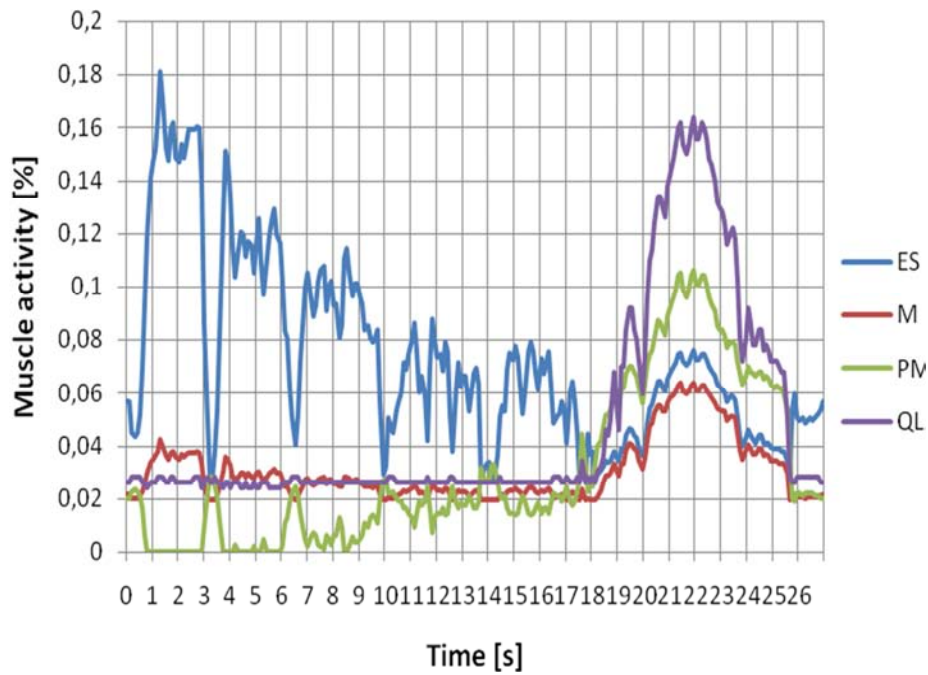


Figure 3.72. Averages muscle activities of ES muscle groups, M, PM and QL.

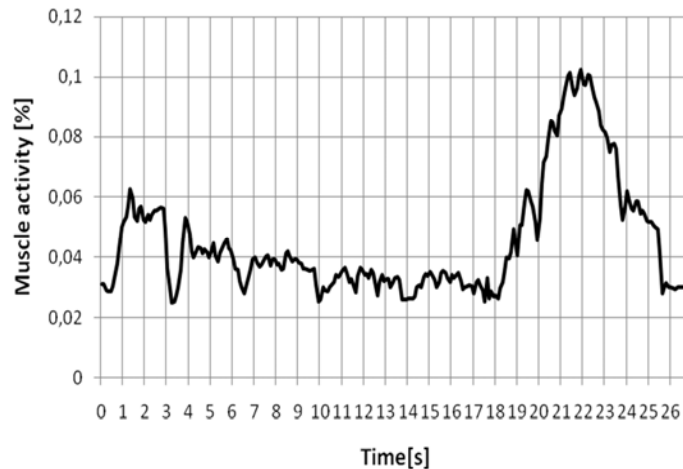


Figure 3.73. Total muscle activity of the four muscles groups.

3.6. Human body posture before and after maxillofacial surgery

3.6.1. Introduction

The aim of this study is to observe how the posture is affected by maxillofacial fractures and how it is improved after maxillofacial surgery. The procedure for all tests is non-invasive and it's formed by a Multi Sensor Electronic Baropodometric Platform, a PodoScanalyzer (2D), the D.B.I.S Software witch calculates the values of the B.P.I. Index, Body Analysis Kaptur System and Dynamic Image System. Using the Baropodometer we evaluate the balance of the human body, oscillations of the pressure centre, visual information of poor posture. a group of 10 patients with different maxilla fractures were investigated before surgery and after. For each patient there were made two analyses. A dynamic analysis which determined how the maxilla fracture affects the walking, and how it is improved after the surgery, and a stabilometry analysis which determined how the maxilla fracture affects the standing posture of the body, and how it is improved after the surgery. As conclusions, the body posture is affected by the maxillofacial fractures and improves after the surgery.

The posture is the human body behavior in relation with the environment in which he lives, and in relation with the laws that governs these environment, first of all the force of gravity. To do this, man has developed a specialized structure to overcome gravity, called the tonic postural system of vertical stability. [128, 162, 163, 164]

Posture is the relative alignment of the various body segments with one another. The stress applied to the body segments is minimal when the person has a good posture and therefore the body alignment is balanced. When a person has a poor posture, the body's alignment is out of balance causing exaggerated stresses to various body segments. [165, 166]

Over time this continual stress, even at low levels produce musculoskeletal disorders and create anatomical adaptations. The body's efficiency will be affected and the accumulation of the trauma causes psychic and physical stress. [166, 167]

3.6.2. Aim

The aim of this study is to observe how the body posture is affected by maxillofacial fractures, and how improves after maxillofacial surgery.

3.6.3. Methods

For this study it is used a modular electronic baropodometric detection platform (with a length of 160 cm, Multi Sensor with 25,600 sensors on 40cm width and 2 walkways of 80cm each), an optoelectronic system composed from an infrared video camera, a PodoScanalyzer for recording the patient's foot under pressure by determining the length, circumference and geometry with length, angles and width. The software used to analyse and interpret the data was the Milletrix Software. It recorded the static, dynamic and stabilometry analysis. The D.B.I.S. software (Digitalized Biometry Images System) calculates the B.P.I. index which indicates the numerical values of the entire investigation. The entire system is non-invasive.

Using the above described baropodometer a group of 10 patients with different maxilla fractures were investigated before surgery and after. For each patient there were made two analyses. A dynamic analysis which determined how the maxilla fracture affects the walking, and how it is improved after the surgery, and a stabilometry analysis which determined how the maxilla fracture affects the standing posture of the body, and how it is improved after the surgery.

For the dynamic analysis the patient is asked to walk on the pressure plate (baropodometer) a few times before the data recording, to calibrate the baropodometer. In this analysis the gravity centre point's trajectory, speed and the pressure distribution on the footprint are recorded.

The stabilometry analysis consists in requiring the patient to stand on the pressure plate and remain in an orthostatic, natural and relaxed position for 2 minutes. In this analysis the patient's oscillations, radar balance and pressure distribution are recorded. [168]

3.6.4. Results

In figure 3.74 and 3.75 are presented the dynamic analyses of a patient. In these figures are presented the gravity center trajectory and the pressure distribution on the footprint.

In figure 3.76 and 3.77 are the stabilometry analyses of a patient. In these figures are presented the pressure distribution on the footprint and the radar balance.

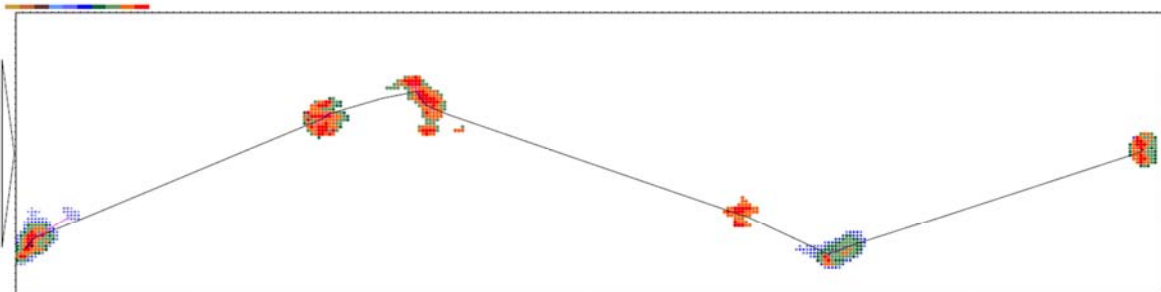


Figure 3.74. Dynamic analysis of a patient before maxillofacial surgery.

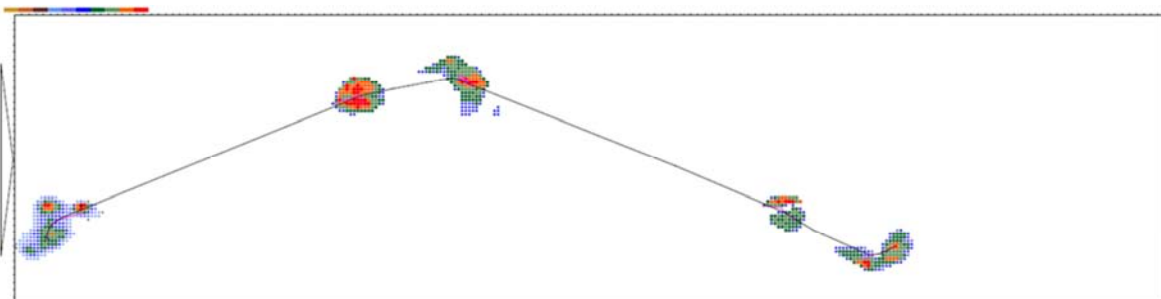


Figure 3.75 Dynamic analysis of a patient after maxillofacial surgery.

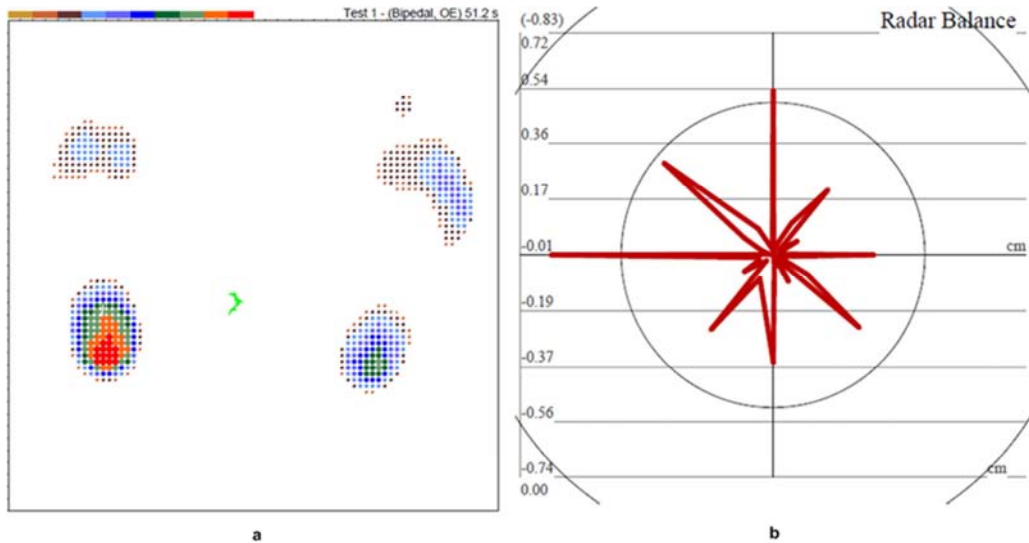


Figure 3.76. Stabilometry analysis of a patient before maxillofacial surgery.

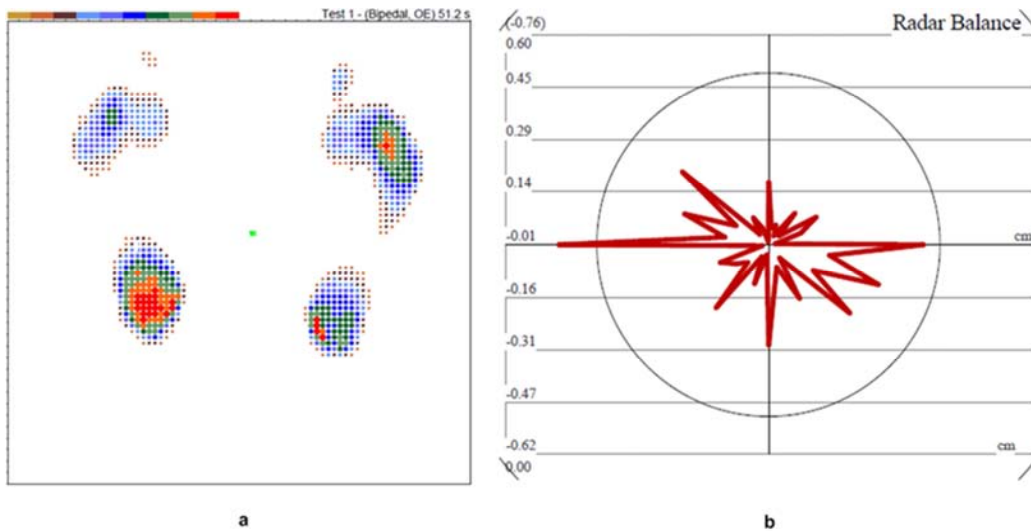


Figure 3.77. Stabilometry analysis of a patient after maxillofacial surgery.

3.6.5. Conclusion

After a careful examination of the data and statistical analysis, a clear distinction between the results of the analyses before the maxillofacial surgery and after it, became apparent. The body posture is affected by the maxillofacial fractures and improves after the surgery.

The use of the baropodometer is recent technology and there are very few studies about its use as it is normally used for clinical purposes, which explains the little existence of academic articles on this matter. However, recent research has proven it to be an excellent methodology for assessing balance by means of the dislocation of the pressure center.

II. Academic and professional achievements

This section of the habilitation thesis mentions the main achievements of the candidate within the last 18 years after defending the PhD thesis. The Ministry of Education with the order 3460/15.03.1999 confirmed the Romanian PhD diploma. In year 2000 I was employed as Associate Professor at the University Politehnica Timisoara at the actual Department of Mechatronics.

The teaching activities at the University Politehnica Timisoara comprised:

- “Calculul și construcția echipamentelor electronice”, “Elemente de inginerie mecanică” at ETC Faculty;
- “Ergonomia echipamentelor medicale”, “Organe de mașini”, “Calculul și construcția autovehiculelor rutiere” at Mechanical Faculty (at Medical Engineering, Mechanical Engineering and Road Vehicles Specializations) – bachelor degree;
- “Advanced ergonomics and human factors in machine design” – master degree.

I published several books addressed to students, specialists and researchers:

1. Veronica Argeșanu, V. Vacarescu – Ergoinginerie. Aplicatii in medicina dentara, Ed. Eurostampa, 2010, ISBN 978-606-569-158-2.
2. Veronica Argesanu - Organe de masini. Transmisii mecanice, Ed. Politehnica, 2008, ISBN 978-973-625-764-3.
3. Veronica Argesanu - Organe de masini. Transmisii mecanice. Completare versiune CD, Ed. Politehnica, 2008 ISBN 621.81; 621.85.
4. Veronica Argesanu - Fundamente de inginerie mecanica, Editura Politehnica, 2006, ISBN 973-625-360-0.
5. Veronica Argesanu, M. Luchin, A. Radu - Organe de masini. Arbori, lagare, cuplaje, Ed. Politehnica, 2006, ISBN 973-625-390-2, 978-973-625-390-4.
6. Veronica Argesanu - Elemente de inginerie mecanica in constructia echipamentelor electronice, Ed. Eurostampa, Timisoara, 2005, ISBN 973-687-256-4.
7. Veronica Argesanu, L.MADARAS - DESIGN. ARBORI. LAGARE. CUPLAJE, Editura POLITEHNICA Timisoara, 2003, ISBN: 973-661-024-1.
8. L. Madaras, Veronica Argesanu - Organe de masini Vol.III, Ed. Eurostampa, 2007, ISBN 973-687-307-2, 973-687-588-5.
9. L. Madaras, Veronica Argesanu - Organe de masini Vol.II, Ed. Eurostampa, 2006, ISBN 973-687-307-2, 973-687-410-9.
10. L. Madaras, Veronica Argesanu - Organe de masini Vol.I, Ed. Eurostampa, 2005, ISBN 973-687-307-2, 973-687-308-0.
11. Veronica Argesanu - Ergonomia echipamentelor si departamentelor medicale, Editura Eurostampa, 2004 ISBN 973-687-200-9.
12. Veronica Argesanu - Constructia mecanica a echipamentelor electronice, Editura „Politehnica” Timisoara 2002, ISBN 973-8247-75-6.
13. Veronica Argesanu, G.E. MOCUȚA - MODELAREA PROBLEMEI NELINIARE CU AJUTORUL METODEI ELEMENTULUI FINIT. Aplicații la îmbinări neconvenționale prin strângere cu elemente intermediare conice și etanșări frontale, Editura MIRTON Timișoara, 1999, ISBN 973-578-889-6.
14. Veronica Argesanu, V. DOLGA, G.E. MOCUTA - ELEMENTE DE INGINERIE MECANICĂ ÎN CONSTRUCȚIA ECHIPAMENTELOR ELECTRONICE, Editura EUROSTAMPA, Timisoara, 1999, ISBN 973-8027-13-6.
15. V. ATIȚOAI EI, Veronica Argesanu, I. NICOARĂ, ș.a. – Optoelectronica. Materiale. Componente. Aplicații, Editura EUROSTAMPA, Timișoara, 1999, ISBN 973-8027-19-5.
16. V. ATIȚOAI EI, GE. MOCUȚA, Veronica Argesanu - ECHIPAMENTE PENTRU ILUMINARE SCENICĂ, Editura EUROSTAMPA, Timișoara, 2000, ISBN 973-8027-26-8.

17. Veronica Argesanu, L.MADARAS - DESIGN. TRANSMISII MECANICE, Editura POLITEHNICA Timisoara, 2002, ISBN: 973-625-031-8.
18. L.MADARAS, Veronica Argesanu - DESIGN. IMBINARI. ARCURI, Editura POLITEHNICA Timisoara, 2002, ISBN: 973-8247-95-0.
19. L. MĂDĂRAS, Veronica Argesanu, G.E. MOCUȚA – IMBINĂRI. ELMENTE ELASTICE.COMPENDIU, Editura MIRTON, TIMISOARA, 2000, ISBN 973-585-148-2.
20. L. MĂDĂRAS, G.E.MOCUȚA, Veronica Argesanu - ARBORI LAGĂRE CUPLAJE COMPENDIU, Editura MIRTON, Timișoara,1999, ISBN: 973-578-850-0.
21. N. GHEORGHIU, L.MĂDĂRAS, I.NICOARĂ, V. ARGEȘANU ș.a - TEHNICI EXPERIMENTALE PENTRU ORGANE DE MASINI, Editura MIRTON, Timisoara, 1999, ISBN 973-578-812-8.
22. V. Argesanu - FUNDAMENTE DE INGINERIE MECANICA, Curs pentru invatamant la distanta, Centru de multiplicare.Universitatea Politehnica Timisoara 2006.

I am involved in many professional organizations:

- Societatea Romana de Ergonomie (SRE) – founder, president.
- European Society of Dental Ergonomics (ESDE)2003.
- Societatea Romana de Ergonomie Dentara RO (SRED) 2006- founder, vice-president,.
- Societatea Romana de Mecatronica RO(Membru fondator) 2000 - founder.
- Association for Multidisciplinary Research – Vest Zone INT (ACM-V) 2003.
- Asociatia Romana de Robotica (ARR) 1989.
- Asociatia Romana de Tribologie (ART) 1990.
- Romanian Association of Mechanical Transmissions (ROAMET) 1991- founder and responsible for Timisoara branch.
- Asociatia Romana de Teoria Mecanismelor si Masinilor (ARoTMM) 1985.

As member or president of the above-mentioned professional organizations, I participated in many conferences, workshops and congresses as plenary speaker, chairman or trainer:

- Congres International de Ergonomia Dentala – Cursuri de perfectionare, iunie 2006, Porto, Portugalia;
- Certificate of Attendance Seria Nr.492, DCC Constanta countys “CMEREGISTRY, the 5th Congress of Oro-dental Health and Dental Management in the Black Sea Region, Albena – Constanta 2007;
- Certificate – Hands – On Introduction And Exercises about Ergonomic Principles in Practice, 2007 Constanta Romania;
- Certificate for sustaining the conference “Dental ergonomics mirrored in mechatronics”, the 20th ESDE annual meeting, 2007, Dental Ergonomics – Health for the Dental Team, iunie 2007;
- Curs perfectionare/workshop “Dental Equipament innovation What are the principles? How to apply them? Annual meeting of ESDE/june, Bensheim, Germania.
- Conference/workshop: Requirements for dental equipment to assure a healthy way of working; Basic ergonomics rules to treat patients, ESDE Congresso Anual, 2006 Porto, Portugal.
- Certificat workshop – Dental microscope, Certificat participare curs The meaning of Ergonomical awareness for risk factors minimalization at Dentist’s, Inauguration of the Polish association of Dental Ergonomics unde patronage of Polish Academy of Science Wroclaw, Polonia, 2007.
- Biometrica posturale e biometria digitalizata, 12-15.03.2008, Seconda Universita degli studi di Napoli, Facolta di Medicina e Chirurgia;
- Chairman/Scientific Commite Black Sea VII-Important aspect for the application of ergonomics, The V-th international congress of oro-dental health and managent in the Black

- Sea region and the 20th Congress of ESDE, Albena, Mamaia, mai 2007, respective conferinte internationale MTM Cluj Napoca;
- Value Based Management (VBM) UPT – Takata, Timisoara 2014 – 2015, “Vehicle safety systems”;
 - Al XV-lea Conmgres international al Zilelor medicale banatene, Medicina mileniului III, Timisoara, 20 – 22 mai 2010;
 - The Forth International Conference Social Work Perspective on Quasi-Coercive Treatment of Offenders “Social control and vulnerable groups”, Timisoara, 24th – 25th April 2013;
 - Exchange of ideas focusing on the opportunity for an international project – 3D modelling, Mechatronics, Center for computing and communication, RWTH Aachen University, Medical Faculty, University Hospital, Aachen 2008;
 - Ergo Management Preventiv la Faculty of General Dental Practice (UK), The Royal College of Surgeons of England, 2013;
 - Simpozionul “Parteneriate in domeniul prioritare – Elemente de monitorizare a proiectelor finantate”, 07 – 10 mai 2008, Sinaia.

I also have specializations and qualifications in:

- Ergonomic Principles for Patient Treatment, Absolvent cu certificat seria C nr. 7352/mai 2004, UMFVB Timisoara (Prof. Oene Hokverda, Olanda, Prof. Dr. Jerome Rotgans, Germania);
- Congres International de Ergonomie Dentala – Cursuri de perfectionare, iunie 2006, Porto Portugalia;
- Certificate of Attendance Seria Nr. 492, DCC Constanta countys ‘CMEREGISTRY, the 5th Congress of Oro-dental Health and Dental Management in the Black Sea Region, Albena – Constanta 2007;
- Certificate – Hands – On Introduction And Exercises about Ergonomic Principles in Practice, 2007 Constanta Romania;
- Certificate for sustaining the conference “Dental ergonomics mirrored in mechatronics”, the 20th ESDE annual meeting, 2007, Dental Ergonomics – Health for the Dental Team, Iunie 2007;
- Certificat de absolvire- IX Corso Teorico e Pratico Biomedica Posturale e Biometria Digitalizzata, Direttore del corso prof. R. Gimigliano, prof. C. Villani, 12-18 marzo, 2008,seconda Universita degli Studi di Napoli Italia;
- Certificat de participare Congres international “Interdisciplinaritate in Medicina Dentara actuala”, 25/28 iulie, 2008, Timisoara;
- Diploma participare la Annual Meeting ESDE (European Society of Dental Ergonomics) 2008, Desenzano del garga , 30-31 mai, 2008, Italia;
- Program perfectionare /training”La coreratta Postura secondo gli innovativi sistemi posturali ed antidecubito VICAIR e presentazione nuovi ausili OFFCARR”; “Workshop sull” industria toscana dei medical device”; “3rd telemedicine workshop”; “L’ausilio come sintesi di innovazione, ricerca tehnologica e di esigenze riabilitative” 25-30 mai, 2008, Exposanita, 16th international healthcare exhipision (products, tehnologies, meetings, seminars, training courses), Bologna, Italia;

Based on the above activities I developed partnerships and research activities with: Politechnic Universities from Bucharest, Iasi, Galati, Cluj, etc, Medical Universities from Timisoara, Bucharest, Iasi, Constanta, Oral Health Institute Groningen Olanda (Prof. Dr. Jerome Rotgans), Rwth Aachen Center for computing and communication (Torsten Khulen), Wroclaw, Polonia (ass.prof.Ph.D.Dr. Anna Symanska), Universitatea de Studii Napoli (prof. R.Gimigliano), Universita degli Studi Sapienza from Roma (prof. C.Villani), Universitatea de Studii din Roma (Dr. Eng. Piero Galasso) Facultatea de Tehnologie Biomedicala, Universitatea de Studii Palermo (Dr.Cuccia Antonio Marco, Dr.Domenico

Caradona), German Universities (Sohr Steffen, Dierks Uwe, Groner Horst, Hansel Michael), and others.

As result of my teaching activities, specializations, qualifications, member or president of professional organizations, and participant in many conferences, workshops and congresses, I coordinated or I was scientific researcher/key expert in the following research grants:

1. FP7 250485/2010, Think Motion, Senior Researcher;
2. Contract nr.603/2007, Consulting privind aplicarea principiilor ergonomice in proiectare, NOVAR ELECTRIC /HONEYWELL, Project director;
3. Contract AMPOSDRU/21/1,5/G/13798, "Scoala doctorala in sprijinul cercetarii in context european", Collaborator;
4. Contract AMPOSDRU 1477/24.03.2010 ID 55651, "Ergonomie, preventie si management performant in medicina dentara prin aliniere la standardele europene", ANCS, Key expert SRED;
5. Contract CNMP/PNCIDI 2, Nr 91-022/18.09.2007 – 2010, "Ergoingineria locului de munca-aplicatii in medicina dentara", CNMP, Project director;
6. CNMP-PNCIDI 2 nr.41-05 /20.09.2007, "Impactul factorilor de mediu in dinamica formarii si comportamentului structurilor dintilor temporali", CNMP, Scientific researcher;
7. CNMP/ PNCIDI 2 nr 41-034/14.09.2007, "MICRODENT-protocoale clinice pentru optimizarea aplicatiilor microscopice dentare", CNMP, Scientific researcher;
8. CEEEX 116/04.08.2006 cu Academia de stiinte medicale Bucuresti, ETAPA I,II/2006, "Studii privind realizarea de echipamente dentare modulare bazate pe sisteme mecatronice; solutii ergonomice pentru dubla preventie a afectiunilor", CEEEX, Scientific researcher;
9. CEEEX 116/04.08.2006 cu Academia de stiinte medicale Bucuresti, ETAPA III,IV/2007, "Studii privind realizarea de echipamente dentare modulare bazate pe sisteme mecatronice;solutii ergonomice pentru dubla preventie a afectiunilor", CEEEX, Scientific researcher;
10. CEEEX 88/2006 2006 – 2008, "Dezvoltarea si implementarea unor sisteme performante de investigare si recuperare a deformatiilor de coloana vertebrala la populatia de varsta scolara si categorii profesionale cu activitati sedentare", CEEEX, Scientific researcher;
11. CEEEX 21 I 03/07.10.2005, "Cercetari privind posibilitatile de utilizare ale sistemelor robotice in scopul cresterii competitivitatii tehnico-economice a industriei romanesti", CEEEX, Scientific researcher;
12. 36/1999 cod CNCSU 204/1999, "Metode si mijloace pentru incercarea transmisiilor mecanice si a componentelor acestora. Etapa: „Implementarea rezultatelor cercetarii in unitati de invatamant si unitati economice cu profil industrial”", Consiliul National al Cercetarii Stiintifice Universitare, Scientific researcher;
13. 36/1998 cod CNCSU 280/1998, "Metode si mijloace pentru incercarea transmisiilor mecanice si a componentelor acestora. Etapa: „Cercetari experimentale”", Consiliul National al Cercetarii Stiintifice Universitare, Scientific researcher;
14. 198/16.07.1997 – 1999, "Cercetari Experimentale privind optimizarea functional constructiva a etansarilor frontale", S.C. ROSEAL S.A., Contract Responsible;
15. BC 34/24.03.2015, 2016, "Descopera CONTITECH", Student competition and summer school, Expert in Ergonomics.

As result of my research activity I registered in 2010 2 Trademark to OSIM, as follows:

1. Argesanu Veronica , Kulcsar Raul Miklos, Anghel Mirella, Jula Mihaela, Borozan Ion Silviu, Jula Mihaela – "Dispozitiv mecatronic de determinare a solicitariilor intervertebrale", Nr. Patent: RO127454-A1 Inregistrat OSIM nr. A/01101 in data de 12.11.2010;
2. Argesanu Veronica, Diaconu Aurel, Farkas Imre Albert, Anghel Mirella, Borozan Ion Silviu, Talpos-Niculescu Cristina – "Sistem ergo-mecatronic de urmarire a miscarilor capului uman", Nr. Patent: RO127446-A2, Inregistrat OSIM nr. A/01102 in data de 12.11.2010.

The publishing activity during this period as result of the research and development activities was very extensive, so I published 6 papers in ISI Journals, 16 papers in Scopus, Elsevier Science Direct and Inspec indexed Journals, 16 papers indexed ISI Conference, 39 Scopus, IEEE and Springer indexed conferences and other 54 papers without indexing in different national and international conferences. The ISI Journal indexed papers are the following:

1. Veronica Argeşanu, R. Kulcsar, I. Borozan - Automotive mechanical face seal – Tribological Simulation, Journal of the Balkan Tribological Association, 2011, pp 1-12, Vol. 17, No. 1, ISSN 1310-4772;
2. Veronica Argeşanu, R. Kulcsar, I. Farkas - Calculation by Finite Element Method (FEM) of Temperature Distribution in the Components of a Mechanical Seal, Journal of the Balkan Tribological Association, 2011, pp 13-20, Vol.17, No. 1, ISSN 1310-4772;
3. Penta,S.; Penta,V.; Lucianu,B.; Anghel,M.; Argesanu,V. - Thermographic Investigation of Ergonomic Medical Posture in Dentistry, Revista de Chimie 2015, ISSN 0034-7752;
4. Popescu, M. , Argeşanu, V. - Optimization model for heated tool butt welding hydro-carbon chemistry transporting pipelines, Materiale Plastice 2006, ISSN 0025-5289;
5. Popescu, M., Argeşanu, V., Jula, M. - Aspects of hot stability of high density polyethylene, Materiale Plastice 2010;
6. Mocuța, D., Comes, C.,Argeşanu, V., Dimitriu, B., Burlibaşa, M. - The Transition Impact on Life Quality in Romania, Metarlugia International, 2009, ISSN 1582-2214.

I also was member in international conferences organizational committees:

- Conferinta Internationala de Mecanisme si Transmisii Mecanice, 2008, "Politehnica" University from Timisoara, Ed. Politehnica Timisoara, 1224-6077, CNCSIS B+, Host: section tribology organizer member, reviewer;
- The 9th International conference of mechanisms and mechanical transmissions MTM 2004, Technical University of Cluj-Napoca, Ed. Acta Tehnica Napocensis, reviewer;
- Mecanisme si Transmisii Mecanice, ARoTMM, ROAMET/ Univ. Politehnica Timisoara, Ed. Politehnica Timisoara - Bul. St., CNCSIS B+, reviewer.

I was oral speaker in the following important conferences:

- Ergonomic design of the dental workplace based on the human-centered concept, Quintessence International Romania, Bucuresti, 02 aprilie 2008 ;
- Ergonomic design of the dental workplace based on the human-centered concept, Medicina dentara a secolului 21-aportul ergonomiei in optimizarea practicii, Bucuresti 17 mai 2008 ;
- Ergonomic Importance of the physical and mental aspects/Significance of the technical equipment design, A 20-a intrunire anuala ESDE 2007, Aplicatii ale ergonomiei de catre industrie, profesori si dentisti-organizata in cadrul celui de 'Al V-lea Congres International de Sanatate Oro-dentara si Management in Euroregiunea Marea Neagra ;
- Dental Ergonomics mirrored in mechatronics, The 20th ESDE annual meeting, 2007, Dental Ergonomics-Health for the Dental Team, iunie 2007 ;
- Current antropometric data as starting point for the adaption of working technology. A statistic study, 22st ESDE Annual Meeting 2009 « When work is an art », Krakow, Poland ;
- Mechatronics, Virtual Reality Workshop, RWRH Aachen University 2008 ;
- Ergonomic design of the dental workplace based on the human-centered concept, Congres International « Medicina dentara a secolului 21. Aportul ergonomiei in optimizarea practicii » Bucuresti, Hotel Ibis Parlament 2008;
- Thermographic Methods used in Dentistry Ergonomics, 22st ESDE Annual Meeting 2009 « When work is an art », Krakow, Poland ;
- Current Methods of Investigation of the Postural Status in Dental Medicine, Milenium III Medicine, The International Congress of Medical Days in Banat, 15th Edition 2010.

I am permanently a member of the bachelor committees for the Road Vehicles and Mechanical Engineering Specializations from UPT; also, I conducted bachelor and dissertation theses in

collaboration with Continental Automotive, Takata and Johnson Controls, member in the board of Road Vehicles, Thermal Systems and Equipment.

In addition, I was referent in many doctoral committees at UPT and UMFVBT, scientific referent of scientific books (ex. Ph.D.Dr. Mirella Anghel, Notiuni generale de ergonomie dentara, Ed. Orizonturi Univeritare, Timisoara, 2005), member of the editorial board of Oral Health and Dental Management, and CNCSIS expert reviewer since 2004.

I founded and accredited the master of Ergoengineering in Mechatronics in 2009.

As result of the CNMP/PNCDI 2, Nr 91-022/18.09.2007 – 2010 Contract I developed and equipped (peak performance and noninvasive equipment and specialized software) the Ergoengineering Laboratory that is unique in our country.

I added also organizational activities: member in the department council (2008 – 2012) and member of the UPT senate – the scientific research commission (2012 – 2016).

III Career evolution and development plans

The methodology of rapid machine design attempts to shorten design – to – manufacture time of production equipment by using advanced engineering tools such as Computer Aided Design systems (CAD) and Finite Element Analysis (FEA) during the conceptual design phase. It is hypothesised that by identifying the best of all available design concepts overall development time can be shortened. Further timesaving results from building machine components out of fabricated structures instead of casts. This provides a high degree of flexibility in terms of changing the design and/or making modification to design specifications. Special FEA modelling techniques and principles allow designers to create models that are optimized for fast computing time at reasonable accuracy.

The role and importance of the transmission have increased in the last years. In addition to the original function of torque and speed conversion, transmissions have become a central part of the powertrain with drivability-defining characteristics due to individual launch and shift logic, high dynamics and optimized shift comfort. In fact, active transmissions with fully integrated electric drives are responsible for traction generation and management. As a result, transmissions will definitely remain a focus topic in automotive engineering. In some concepts, they even will adopt a leading role and become the key to efficient drives.

Developments and issues dealing with automotive transmissions and drives are focused on the following topics:

- What improvements to customer-relevant vehicle characteristics can be achieved using new or improved concepts for drives, transmissions and components?
- What are the challenges and opportunities of conventional and electrified drives?
- What are the tools for efficient transmission and power train development?

Automobile manufacturers are reacting to changing customer needs with a growing range of electrically powered and hybrid vehicles. However, to operate at maximum efficiency, these cars need transmission systems designed to meet new and challenging requirements. Research must supply innovative gear and drive concepts that will help manufacturers position themselves successfully in electro mobility, the market of the future.

Today's economies are dramatically changing, triggered by development in emerging markets, the accelerated rise of new technologies, sustainability policies, and changing consumer preferences around ownership. Digitization, increasing automation, and new business models have revolutionized other industries, and automotive will be no exception. These forces are giving rise to four disruptive technology-driven trends in the automotive sector: diverse mobility, autonomous driving, electrification, and connectivity.

Most industry players and experts agree that the four trends will reinforce and accelerate one another, and that the automotive industry is ripe for disruption. Given the widespread understanding that game-changing disruption is already on the horizon, there is still no integrated perspective on how the industry will look in 10 to 15 years as a result of these trends.

Ergo-engineering - trans disciplinary applied science that studies the possibilities to optimize the design of the man-machine system and the organization of workflow efficiency - currently acquires increasing importance in the field of road transport. Application of ergo-engineering principles plays an important role in preventing chronic disease and provides professional business solutions to optimize the prevention, correction and management of musculoskeletal disorders (MSDs) and risks, generating superior results in the quality of employment in health and safety at work and thus quality of life.

Solutions that will be used in transport aimed at health. Their development requires partnership-type physiotherapy practice engineering, plus component impact on the economy concerned and assigned the main role of partner in public road transport. Follow competitiveness to two successive levels: contribution to the competitiveness of the Romanian economy by increasing the competitiveness of research and development.

Ergo-engineering presents at the moment, the following priorities:

- Prevention of musculoskeletal and psychosocial disorders of the driver and associated risk factors;
- Improving the safety and quality of transport.

These priorities of the domain are consistent with the direction developed by the European Community, evidenced by the "Health and safety in the organization of the work environment" mentioned in Section V, Chapter I of the Agreement on the European Economic Area (EEA), which is an important aspect of social policy, eliminating occupational diseases is an integral part of creating an Economic Areas European homogeneous. Similarly, on 24 February 2005 the European Parliament adopted a report (Promoting health and safety at work - "Promoting Health and Safety at the Workplace") that meet the requirements of the Commission for application in national laws and regulations on occupational diseases possibilities for prevention.

Ergo-engineering of the workplace of public road transport is increasing practical purpose: competitiveness-enhancing technologies, products, services and appropriate individualized Ergonomic intrinsic quality of the workplace by preventing occupational diseases (MSD) health, safety and welfare at work.

The research aims to provide imaging activity monitoring, and legislation, biometrics subjects, systematic technical - functional related equipment, developing strategies and flexible development models achieved by designing the system, the composition of algorithms, programs, modelling 3D and experimental testing, optimization by introducing flexible modular mechatronic systems, observing tire functional movements driver, pilot research center developing advanced ergonomic in the public road transport.

The priorities of ergonomics concords with the directions domain developed by the European Community, evidenced by:

- The "Health and safety in organizing working environment" mentioned in Section V, Chapter I of the Agreement on the European Economic Area (EEA), which is an important aspect of social policy - elimination of professional diseases. Likewise, on 24 February 2005 the European Parliament adopted a report: "Promoting Health and Safety at the Workplace" that addresses the application within the national laws and regulations on occupational diseases and possibilities for prevention.

The bibliographical references (selection) known in the field are:

1. Belenky M. Human-centered ergonomics: Proprioceptive pathway to occupational health and peak performance in dental practice. In: Murphy DC, ed. Ergonomics and the dental care worker. Washington DC: Am Pub Health Assoc, 1998: 275-99
2. Dougherty M. Feel-based design: A reason to endorse ergonomic standards. J Colo Dental Assoc 1999; 78(4):22-25
3. OSHA: Occupational Safety & Health Administration, U.S. Dept. of Labor. Ergonomics Program, final rule, Federal Register 65:68261-68870 (2000).

The mentioned research fields are important issues in many areas of the EU Framework Programme for Research and Innovation HORIZON 2020, because they focus on quality of life and the product-

oriented research projects. All the author's mentioned scientific achievements are in the mentioned fields and will form the basis of the further career development plan.

The own career evolution and development plans will be shown in the following sections: key research directions, objectives, planned activities and financial and human resources.

Key research directions

1. Constructive and functional research in the field of mechanical machines.
2. Constructive and functional research in the field of road vehicles.
3. Human centered design/Ergonomics.

In order to achieve the previous research activities the author aims to:

- continuously developing of the devices and equipment in the Lab and own development of the prototypes for the considered applications;
- founding of research rooms with the necessary infrastructure for the PhD and interested master students;
- permanent connection and research exchanges with the researchers from both Romania and abroad;
- maintaining of an important role and giving a great contribution to the professional associations;
- participation of PhD students at several Summer Schools and internships;
- preparing and applying in several consortiums for proposals for EU HORIZONT 2020 projects, bilateral collaborations and national research or structural grants;
- publishing of scientific papers and new books in the area;
- developing the research group in field of Mechanical Design and Ergonomics together with other PhD advisors inside of the Doctoral School of UPT – IOSUD;
- attracting as PhD students of the best students and developing the topic of the PhD study according with the running projects and grants;
- founding of a research network with the researcher groups from companies.

IV. References

1. Aithani D.; Lockhart H.; Auras R. & Tanprasert K. (2006). "Predicting the Strongest Peelable Seal for 'Easy-Open' Packaging Applications", Journal of Plastic Film and Sheeting
2. Basu P. & Butler J. (2008). "Studies on the operation of loop-seal in circulating fluidized bed boilers", Mechanical Engineering Department, Dalhousie University, P.O. Box 1000, Halifax, Nova Scotia, Canada
3. Cristea, V. s.a. (1973). Etanșări ET, București 1973
4. Kharitonov V. (1977). "Mechanical seals for vessels with agitators", Chemical and Petroleum Engineering
5. Mayer, E. (1961). Leakage and Friction of Mechanical Seals
6. Paper E3, England
7. Nagaralli R.; Ramakrishna A. & VaradaRajulu A. (1997).
8. "Physico-Mechanical Properties of Filled Polyethylene Films", Journal of Plastic Film and Sheeting
9. Argesanu, V; Madaras, L, (2003). *Leakage, wear and friction in the mechanical face analyzed by FEM, ROTRIP* Galati, Romania
10. Gheorghiu, N; Argesanu, V, (1996). *Compararea performantelor etansarilor tip manseta de rotatie cu cele frontale*, Arad
11. Knothe, K.; Welles, H, (1992). *Finite Elemente, einEinführung für Ingenieure*, Springer-Verlag, Berlin, Heidelberg, New York, London, Paris, Tokyo, Hong Kong, Barcelona, Budapest
12. Mayer, E, (1987). *Mechanical Seals*, Hewnes – Butterworth, London, Boston Muller, H-K; Waschle, P, (1990). *EWDR – eineneuedruckbelastbare Wellen-dichtung*, Anbetriebstechnik 29 Nr.10
13. V. Argesanu - Asigurarea functional constructive a durabilității optime pentru etansarile frontale cu contact direct. Teza de Doctorat. Timisoara, 1998
14. Kragelsky and Mikhin. N.M. - Friction. Wear. Lubrification. Tribology Handbook vol.1, 2,3, Mir Publishers. Moscova. 1981.
15. Argesanu V., Mocuta G.E. 1998, Evaluarea debitului de pierderi prin neeranseitati, functie de parametrii functionali, ai unei etansari frontale ,EFS 103- S, Revista Romana de Mecanica Fina si Optica-Supliment, Nr.2/1998.
16. Argesanu V. et al., 1992, Cupla Inelara de frecare-elementul vital pentru etansari axiale, Analele Universitatii din Oradea.
17. Carius G. et al., 1984, Controlling the Friction and Wear Behavior Pneumatic Seals by Influencing the Friction Energy Density by Way or Surface Modification, 10th international Conference on Fluid Sealing, Innsbruck.
18. R. Bausinger, R. Schnaidt. R. Boiler, -Finite elemente auf PC. 7M4 Erbringen bei Böblingen. Gcrmany. 1992

19. M Gafitanu, V. F. Poterșu, N. Mihalachc, -Elemente finite și de frontieră cu aplicații la calculul organelor de mașini. Editura Tehnică. București, 1987
20. Arauz, G.L.m San Andres, L.A. - Experimental Pressures and Film Forces in a Squeeze Film Damper, Trans. ASME, j. of Tribology, Vol. 115, No. 1, p. 134-140, 1993.
21. Barnard, P.C. and Weir R.S.L. - A theory for mechanical seal face thermodynamics -8th International Conference on Fluid Sealing, Sept. 11-13th, 1978.
22. Batoz, J.L., Dhatt, G. - Modelation des structures par elements finis, volume 1,2,3, Hermes, Paris, 1990.
- Praktische Einführung mit Zahlreichen Beispielen, Edition Exportsoft, Böblingen, 1992.
23. Bill, C.R. - Wear of Seals Materials Used in Aircraft propulsion Systems. Wear 59 (1980), p. 165 / 189.
24. A. TUDOR: Friction and Wear of Materials. Bucharest, 2002.
25. D. GARBEA: Finite Element Analysis. Bucharest, 1990.
26. F. BOUCHUT: Nonlinear Stability of Finite Volume Methods for Hyperbolic Conservation Laws. Birkhauser Verlag, Basel, Switzerland, 2000.
27. R. FLITNEY: Seals and Sealing Handbook. Elsevier, Oxford, 2007.
28. V. Argesanu, A. Popa: Interface Contact Pressure Distribution In Dynamic Contact Face Seals, Analyzed By Fem . In: 3rd International Conference With International Scientific Comitee Research And Development In Mechanical Industry, Radmi, 2003, Institute Imk '14 October' Krusevac, Institute Of Faculty Of Mechanical Engineering Podgorica, 14-18 September 2003, Session Code E-4, P. 1168, Serbia And Montenegro.
29. V. ARGESANU, G. E. MOCUSA: Nonlinear Modelling by Finite Element Methods. Timisoara, 1999.
30. V. ARGESANU, L. MaDa RAS: Model and Analysis of a mechanical seal by finite element method. Interface tension distribution, UDC 539.3+519.6, Facta Universitatis, Series Mechanics, Automatic Control and Robotics, **3** (15) (2003), University of Nis, Serbia.
31. F. BOUCHUT : Nonlinear Stability of Finite Volume Methods for Hyperbolic Conservation Laws, Birkhäuser Verlag, Basel, Switzerland, 2000.
32. Argesanu. V.. Mocuta. G.F.. - Evaluarea debitului de pierderi prin nctanseitati. funcție de parametri funcționali, ai unei ctansari frontale. EFS 103 - S. Revista Romana de Mecanica Fina si Optica - Supliment. Nr. 2/1998.
33. V. Argesanu, A. Popa, "Intrface contact pressure distribution in dynamic contact face seals analyzed by FEM", 3rd International Conference, "Research and development in mechanical Industry", RaDMI 2003, 14-18 September 2003, Krusevac-Podgorica, Session E, pag. 1168-1172
34. ***Catalog de firma S.C. ROSEAL S.A. RO-Odorheiul Secuiesc, 1997.

-
35. Noël Brunetiere, The Lubrication Regimes of Mechanical Face Seals, Bearings and Seals ,September 2014
- 36 Long Wei, Peng Gao Zhang, Gui Fang Fang, Simulation Calculation of Friction Factor of the End Face for Mechanical Seals Based on Fractal Theory, Researching and Designing in Mechanical Engineering, Mechatronics, Automation and Control November 2014,
37. Alisa Filofteia Oprea, Nicolae Popa, Constantin Onescu, Considerations Regarding the Pumps Vibration Monitoring Using Proactive and Predictive Maintenance Programs, Strength, Mechanical Vibrations and Reliability, Materials and Technology, September 2014
38. Alisa Filofteia Oprea, Nicolae Popa, Constantin Onescu, Considerations Regarding the Pumps Vibration Monitoring Using Proactive and Predictive Maintenance Programs, Strength, Mechanical Vibrations and Reliability, Materials and Technology, September 2014
39. Chuan Jun Liao, Shuang Fu Suo, Wei Feng Huang, Research on Feature Extraction Method Based on Rub-Impact Acoustic Emission Signals of Mechanical Seal End Faces, October 2010
40. Jian Jun Sun, Bo Qin Gu, Effect of Spring Pressure on Basic Performance of Contacting Mechanical Seals, September 2007
41. Wei Zheng Zhang, Shu Rong Yu, Yan Wang, Xue Xing Ding, Liquid Film Features Analysis on Mechanical Seals with Micro-Pore Face by CFD, Fluid Machinery and Engineering, October 2011
42. Ze Pei Huang, Zhi Zhang, Jun Kai Zhang, Kan Chen, Pan Fu, Zhi Bin Lin, Research on the Micro Scope Condition of End Face of Liquid-Lubricated Mechanical Seals, Robotics, Control and Measurement Technology, February 2014
43. Hui Qin Hao, Xin Qi Yu, Qing Gang Liu, Jia Hui Yu, Numerical Analysis on Sealing Properties of Mechanical Seals with a Laser-Textured Face, Computer Aided Design, Modeling and Analysis, July 2012
- 44 Xin Qi Yu, Pei Ying Peng, Hui Qin Gao, Jia Hui Yu, Numerical Analysis on Tribological Properties of Mechanical Seals with a Laser-Textured Face, October 2010
- 45 Gui Fang Fang, Peng Gao Zhang, Long Wei, Effect of Surface Topography on Contact Property of the End Face for Mechanical Seal, Mechanical Engineering and Manufacturing Technology, October 2013
- 46 Long Wei, Peng Gao Zhang, Gui Fang Fang, Effect of Surface Topography on Average Film Thickness between the End Faces for Mechanical Seal, Applied and Computational Mechanics in Designing and Research, October 2014
47. Xin Qi Yu, Mei Hong Liu, Zhen Hui Wang, Pei Ying Peng, Ren Liang Cai, Experimental Investigation on Friction Performance of Mechanical Seals with a Laser-Textured Seal Face, December 2006
48. Yi Xie, Shuang Fu Suo, Yong Jian Li, Fang Jun Ge, Yu Ming Wang, Mechanical Seal Face Texturing by the Acousto-Optic Q-Switched Pulsed Nd:YAG Laser, Processing Technology, August 2011

-
49. Fang Bo Ma, Peng Yun Song, Jie Gao Numerical Analysis of Radial Groove Gas-Lubricated Face Seals at Slow Speed Condition Mechanical Control and Information Processing Technology, February 2012
50. Peng Gao Zhang, Bo Qin Gu, Long Wei, Qi He Liu Numerical Simulation of Lubricant Liquid Film of the Laser Surface Textured Micro-Pore Face Mechanical Seal, Mechanical Engineering and Engineering Design September 2013
- 51 Applied Mechanics and Mechanical Technologies, An Analysis of the Lubrication Characteristics of Mechanical Seals with Parallel Sealing Faces Using an Average Flow Model, Applied Mechanics and Mechanical Technologies, July 2015
52. Min Zhou, Hua Bin Wen, Wen Hui Wang, Yong Hu, Yan Shi, Liang Li, An Analysis of Mechanical Seal Failure of HTM Pump and its Improvement, Industrial Equipment and Engineering, November 2014
53. Jian Ke Li, Rong Mo, Hai Cheng Yang, Zeng Qiang Wang, Research on Conjugate Heat Transfer in Mechanical Seals of the Aircraft Engine December 2012
- 54 Xin Qi Yu, Qing Gang Liu, Hui Qin Gao, Jia Hui Yu Liquid Film Performance Analysis of the Mechanical Seals with a Laser-Textured Micro-Pore Face, October 2010
55. Min Zhou, Wei Hui Wang, Yan Shi, Hua Bin Wen, Analysis of Sealing Device Failure of HTM Pump and its Countermeasure, Research and Design Solutions in Machinery Industry, February 2014
56. Long Wei, Peng Gao Zhang, Gui Fang Fang, Effect of Surface Topography on Average Film Thickness between the End Faces for Mechanical Seal, : Applied and Computational Mechanics in Designing and Research, October 2014
- 57 Xin Qi Yu, Mei Hong Liu, Zhen Hui Wang, Pei Ying Peng, Ren Liang Cai, Experimental Investigation on Friction Performance of Mechanical Seals with a Laser-Textured Seal Face, December 2006
58. Yi Xie, Shuang Fu Suo, Yong Jian Li, Fang Jun Ge, Yu Ming Wang, Mechanical Seal Face Texturing by the Acousto-Optic Q-Switched Pulsed Nd:YAG Laser August 2011
59. Fang Bo Ma, Peng Yun Song, Jie Gao, Numerical Analysis of Radial Groove Gas-Lubricated Face Seals at Slow Speed Condition, Mechanical Control and Information Processing Technology, February 2012
60. Peng Gao Zhang, Bo Qin Gu, Long Wei, Qi He Liu, Numerical Simulation of Lubricant Liquid Film of the Laser Surface Textured Micro-Pore Face Mechanical Seal, Mechanical Engineering and Engineering Design, September 2013
61. Mikiko Oyabu, Jun Tomioka, An Analysis of the Lubrication Characteristics of Mechanical Seals with Parallel Sealing Faces Using an Average Flow Model Applied Mechanics and Mechanical Technologies, July 2015
62. Min Zhou, Hua Bin Wen, Wen Hui Wang, Yong Hu, Yan Shi, Liang Li An Analysis of Mechanical Seal Failure of HTM Pump and its Improvement, Industrial Equipment and Engineering, November 2012

63. Jian Ke Li, Rong Mo, Hai Cheng Yang, Zeng Qiang Wang, Research on Conjugate Heat Transfer in Mechanical Seals of the Aircraft Engine, November 2012
63. Jian Ke Li, Rong Mo, Hai Cheng Yang, Zeng Qiang Wang, Research on Conjugate Heat Transfer in Mechanical Seals of the Aircraft Engine, December 2012
64. Xin Qi Yu, Qing Gang Liu, Hui Qin Gao, Jia Hui Yu, Liquid Film Performance Analysis of the Mechanical Seals with a Laser-Textured Micro-Pore Face October 2010
65. Min Zhou, Wei Hui Wang, Yan Shi, Hua Bin Wen, Analysis of Sealing Device Failure of HTM Pump and its Countermeasure, Research and Design Solutions in Machinery Industry, February 2014
66. Jian Feng Zhou, Bo Qin Gu, Chun Lei Shao, Optimum Design of Flat End Face Mechanical Seal Based on Coupling Analysis, November 2010
67. Zhei Wei Liu, Lin Dong, Ke Li, Mechanical Design, June 2014
68. Peng Gao Zhang, Long Wei, Xiu Feng, Numerical Simulation of Deformations of Rotary and Stationary Rings of Contact Mechanical Seal Based on ANSYS Workbench, Mechanics and Dynamics, Applied Mechanics, Advanced Development in Manufacturing and Industry Engineering, August 2014
69. Wen Ji Hu, Yu Yu, Ji Xiang Zhou, Xue Bin Tang, Implementation of the Dynamic Tension Load of Cell Membrane and its Stress Analysis, Measurement, Testing, Monitoring, Detection: Technologies, Analysis and Methodology March 2014
70. Bhagwana Ram Manda, K.V. Sreedharan, S. Athmalingam, V. Balasubramaniyan, P. Chellapandi, Experience with Mechanical Seal of Prototype Fast Breeder Reactor's Secondary Sodium Pump during Testing, Thermodynamics and Thermal Engineering, Fuel and Diesel, July 2014
71. Asiye Shavkat, Mutellip Ahmat, Kaysar Ismayil, Mamtimin Ghenni., Contact Analysis of Sealing Rings for Welding Bellows Mechanical Seal, Material Science and Technology in Manufacturing October 2011
72. Jie Gao, Peng Yun Song, Xiao Yun Hu, Fang Bo Ma, Calculation Method of Mechanical Face Seal Temperature Based on Heat Conduction Angle, Material Section, February 2012
73. Jiang Ping Zhao, Fu Sheng Shi, The Analysis of Twin-Screw Compressor New Liquid Film Seal Structure, Modeling, Analysis and Simulation, June 2012
74. Yu Cai, He Juan Chen, Numerical Simulation of Cavity Flow within the Flow Field, Mechanical Engineering: Research, Development and Solutions, June 2013
75. Jun Kai Zhang, Er Qing Zhang, Zhen Di Ge, Pan Fu, Mechanical Seal End Faces Friction Condition Monitoring Based on Particle Filter, Mechanical Engineering: Research, Development and Solutions, June 2013

-
76. Jun Kai Zhang, Er Qing Zhang, Zhen Di Ge, Pan Fu, Mechanical Seal End Faces Friction Condition Monitoring Based on Particle Filter, Measurement and Instrumentation, Monitoring, Testing and Detection Technologies, January 2015
77. Yong Hong Fu, Jing Hu Ji, Xi Jun Hua, Qin Sheng Bi, e of a Laser Surface Textured Mechanical Seal
78. Jian Yu Cai, He Juan Chen, Numerical Simulation of Cavity Flow within the Flow Field, Mechanical Engineering: Research, Development and Solutions
79. Peng Gao Zhang, Long Wei, Xiu Feng, Numerical Simulation of Deformations of Rotary and Stationary Rings of Contact Mechanical Seal Based on ANSYS Workbench, Mechanics and Dynamics, Applied Mechanics, Advanced Development in Manufacturing and Industry Engineering
- 80 Peng Gao Zhang, Bo Qin Gu, Long Wei, Qi He Liu, Numerical Simulation of Lubricant Liquid Film of the Laser Surface Textured Micro-Pore Face Mechanical Seal, Mechanical Engineering and Engineering Design
81. Jian Feng Zhou, Bo Qin Gu, Chun Lei Shao, Optimum Design of Flat End Face Mechanical Seal Based on Coupling Analysis
82. Jia Sheng Li, Bao Cheng Lu, PID Algorithm Application in the Mechanical Sealing Based on BP Neural Network, Computation Methods and Algorithms for Modeling, Simulation and Optimization, Data Mining and Data Processing
83. Jie Ren, Shi Lin Yan, Mei Liu, Preparation of Foam Ni/Carbon Nanotubes Material for Enhanced Stationary Seal Ring
84. Jian Ke Li, Rong Mo, Hai Cheng Yang, Zeng Qiang Wang, Research on Conjugate Heat Transfer in Mechanical Seals of the Aircraft Engine, Research on Conjugate Heat Transfer in Mechanical Seals of the Aircraft Engine
85. Chuan Jun Liao, Shuang Fu Suo, Wei Feng Huang, Research on Feature Extraction Method Based on Rub-Impact Acoustic Emission Signals of Mechanical Seal End Faces
86. Peng Liu, Zheng Lin Liu, Sheng Dong Zhang, Bo Qin, Liang Zhao, Research on Performance of Stern Shaft Mechanical Seal Based on FLUENT, Manufacturing and Mechanical Engineering, Equipment, Design and Simulation, Analysis of Dynamic Systems
87. Halida Musha, Mamtimin Gheni, Buhalqam, Shape Optimization and Strength Evaluation of Metal Welded Bellows Wave of Mechanical Seal
88. Hai Yang Zhang, Wei Bing Zhu, Gang Zhou, Xu Hao, Study on the Thermal Stress Couple Field of Nuclear Power Pump Mechanical Seal Based on ADINA, Applied Mechanics, Monitoring and Control. Mechanical and Industrial Engineering.
89. Ze Gang Sun, Chang Niu Yang, Lei Chen, The Study of Mechanical Seal Leakage Detection System, Mechanical Engineering, Control and Automation Technologies, Equipment
90. Vogelpohl G. –Betriebsichere Gleitlager, Berlin, Springer, 1962.
91. Argesanu. V., s.a., Elemente de inginerie mecanica, editura: Eurostampa. Timișoara, 1999

92. Madaras, L., Argesanu, V., Design. îmbinări. Arcuri., editura: Politehnica. Timișoara, 2002
93. Voinea. R., s.a., Introducere in mecanica solidului cu aplicații in inginerie, editura: Academiei Romane, 1989
94. *** Seeger Ringe. Handbuch
95. Manualul inginerului mecanic. Materiale, Rezistenta materialelor. Stabilitate elastica si vibrații, editura: Tehnica. București, 1973
96. *** DIN 471 Seeger ring
97. Jula, A., s.a. Proiectarea angrenajelor evolventice, Editura Scrisul Romanesc, Craiova, 1989.
Madaras, L., Argesanu, V., Organe de masini, vol. 1, Editura Eurostampa, Timisoara, 2005.
Radulescu, Gh., s.a., Indrumator de proiectare in constructia de masini, vol. III, Editura Tehnica, BUCURESTI, 1986
98. *** Metoda generala pentru calculul geometric si de rezistenta a angrenajelor paralele cilindrice exterioare si interioare cu dantura dreapta si inclinata, TS40, ICTCM-Bucuresti, 1979.
99. *** STAS 12.268-84. Angrenaje. Calculul de rezistenta.
100. Gheorghiu N. & Madaras L. (1986). *Considerations regarding the evolution of joint by shrinking of the conic surfaces*, The fifth National Symposium of Mechanic Machineries and Transmissions, MTM'88, pg.361, Cluj Napoca
101. Guang M. & Wen-Ming Z. & Hai H. & Hong-Guang L. & Di C. (2007). *“Micro-rotor dynamics for micro-electromechanical systems (MEMS)”*, State Key Laboratory of Mechanical System and Vibration, Shanghai Jiao Tong University, 800 Dongchuan Road, Shanghai 200240, China
102. Korakianitis T. & Boruta M. & Jerovsek J. & Meitner P. (2008). *“Performance of a single nutating disk engine in the 2 to 500 kW power range”*, School of Engineering and Materials Science, Queen Mary, University of London, London, UK
103. Manea Gh. – *Organe de masini*, Ed. Tehnica, 1970. Zografos A. & Dini D. & Olver A. (2008). *“Fretting fatigue and wear in bolted connections: A multi-level formulation for the computation of local contact stresses”*, Department of Mechanical Engineering, Imperial College London, South Kensington Campus, Exhibition Road, London SW7 2AZ, UK
104. Sheng X. (2008). *“Model identification and order response prediction for bladed wheels”*, Applied Mechanics, Technical Centre, Cummins Turbo Technologies Co. Ltd., St Andrew's Road, Huddersfield, West Yorkshire HD1 6RA, UK
105. *** BIKON TECHNDK GmbH company prospects
106. *** OERLIKON company prospects
107. Argeșanu V., Kulcsar R., Borozan I., „Automotive mechanical face seal – Tribological Simulation”, Journal of the Balkan Tribological Association 2011, pp 1-12, Vol. 17, No. 1, ISSN 1310-4772, Indexată ISI Thompson Scientific, Factor de impact= 1.104.

108. Borozan I., Argeşanu V., Maniu I., Kulcsar R., „The energetic balance of the friction clutches used in automotive”, Recent Researches in Automatic Control, 13th WSEAS International Conference on Automatic, Control, Modelling & Simulation (ACMOS'11), Lanzarote, Canary Islands, Spain, May 27 – 29.2011, ISBN: 978-1-61804-004-6, pp.: 252-256.
109. Maniu I., Varga S., „Les Trains Cycloïdaux Qui Equipent Les Boites De Vitesses Automatiques” Tenth World Congress On The Theory Of Machine And Mechanisms, Oulu, Finland, June 20-24, 1999
110. Maniu I., Varga S., „Cinematica, acţiunea şi comanda unei cutii de viteză automată cu 3+1 trepte de rulare”, 6th Conference on fine mechanic and Mechatronic COMEFIM'6, 2002, Braşov, Romania, 10-12 October, 2002.
111. Maniu I., Varga S., „Structura, cinematica şi comanda unei cutii de viteză automată pentru autovehicule”, Simpozionul national cu participare internationala Proiectarea asistată de calculator, PRASIC'02, Vol. III, Design de produs, 7-8 Noiembrie 2002, Braşov, România, ISBN 973-635-076-2.
112. *** www.flir.com
113. *** <http://techcenter.mercedes-benz.com>
114. Berkov Yu. P., Naumov E. D., Petrov V. V. and Shantyr S. V., Diagnostic method and device for friction couples, 1993
115. W. Abbas, O. B. Abouelatta, M. El-Azab, M. Elsaydy, A. A. Megahed, *Optimization of biodynamic seated human models using genetic algorithms*, Engineering (2010), 2, 710-719.
116. T. Gillespie, Fundamentals of Vehicle Dynamics, Society of Automotive Engineers, Warrendale, 1992
117. Ö. Gündoğdu, Optimal seat and suspension design for a quarter car with driver model using genetic algorithms, International Journal of Industrial Ergonomics 37 (2007), 327-332
118. Y. Matsumoto, M.J. Griffin, Mathematical models for the apparent masses of standing subjects exposed to vertical whole-body vibration, Journal of Sound and Vibration 260 (2003) 431–451.
119. Z. Nawawi, N. Ismail, A. R. Yusoff, " , Applied Mechanics and Materials, Vol. 471, pp. 14-19, Dec. 2013
120. Z. Patil, M. Palachinamy, D. Ghista, Man-tractor system dynamics: Towards a better suspension system for human ride comfort, Journal of Biomechanics, Vol. 11(1978) 397-406.
121. M.F. Soong, Rahizar Ramli, Wan Nor Liza Wan Mahadi, Ride Evaluation of Vehicle Suspension Employing Non-Linear Inerter, Applied Mechanics and Materials, Vol. 471, pp. 9-13, 2013
122. K. J., Wakeham, and D. Geoff Rideout. Model complexity requirements in design of half car active suspension controllers ASME 2011 Dynamic Systems and Control Conference and Bath, 2011.
123. L. Wei, M.J. Griffin, Mathematical models for the apparent mass of the seated human body exposed to vertical vibration, Journal of Sound and Vibration 212 (1998) 855–874.
124. G. Allen. *A critical look at biomechanical modeling in relation to specifications for human tolerance of vibration and shock*. AGARD Conference Proceedings No. 253, Paper A25-5, Paris, France, pp. 6–10, 1978
125. M. Patil, M. Palachinamy, D. Ghista, *Man-tractor system dynamics: Towards a better suspension system for human ride comfort*, Journal of Biomechanics, Vol. 11(1978) 397-406.
126. K. J., Wakeham, and D. Geoff Rideout. *Model complexity requirements in design of half car active suspension controllers* ASME 2011 Dynamic Systems and Control Conference. American Society of Mechanical Engineers, 2011.

127. J.Y. Wong. *Theory of Ground Vehicles*, Wiley; 4 edition, 2008
128. Adams M. ; Bogduk N. ; Burton K. ; Dolan P. "*The Biomechanics of Back Pain Second Edition*", Churchill Livingstone Elsevier, 2006. J. Clerk Maxwell, *A Treatise on Electricity and Magnetism*, 3rd ed., vol. 2. Oxford: Clarendon, 1892, pp.68–73.
129. Brîndeu L., Popa C., Ștefan C., Hegedus A. "*Identification of Human Body Model, Sitting on a Vehicle Chair*", 3th. Mini. Conf. on VSDIA, Budapest, Nov. 6-8, 2000.
130. Brîndeu L., Popa C., Szeidert I. "*A mathematical model of the human body in the case of standing position*", Simp. Șt. Internațional "Universitaria ROPET 2000", secț. Ing. Mec., Petroșani, 2000.
131. Brîndeu L., Silaș Gh., Toader M., Popa C., Ștefan C. „*Methods for identifying the mechanical characteristics of human body seated in the car*”, Analele Univ. Oradea, Fasc. Mec. Sec. Mec. Vibr. Rez. Mat, vol. II, 2000.
132. Grecu V., Dumitru N., Grecu L. "*Modeling dynamic behavior of human upper limb kinematic chain*", ICOME, 2010.
133. Steven M. K., Avram A. E. "*SPINE Technology Handbook*", Elsevier, 2006.
134. *** (2007) [www.anybodytech.com /index.php?id=691](http://www.anybodytech.com/index.php?id=691) - ANYBODY technology tutorials, inverse dynamics analysis, *Accesed on: 2011-01-20*.
135. *** Biomechanics Of Vertebral Manipulations In Chronic Low Back Pain, http://www.plasma.uaic.ro/COMB/analele%20stintifice/2005/22_ailoai_b_iomechanics.pdf, *Accesed on: 2011-02-02*.
136. *** www.flirb200.com/ FLIR B200 Infrared Camera Users's Manual and Tutorials, *Accesed: 2010-06-03*.
137. Borozan I. S.; Maniu I.; Kulcsar R. M.; „Ergonomic analysis on driving an Automatic Gearbox equipped vehicle”, SACI 2012 IEEE 7th International Symposium on Applied Computational Intelligence and Informatics, May 24-26, 2012, Timisoara, Romania.
138. Borozan I. S.; Kulcsar R. M.; “Vertebral column bioengineering analysis at bending and torsion”, International Conference on Human-Machine Systems, Cyborgs and Enhancing Devices HUMASCEND, Iasi, Romania, June 14-17, 2012.
139. Goran Devedžić, Saša Ćuković, Vanja Luković, Danijela Milošević, K. Subburaj, Tanja Luković, "ScolioMedIS: web-oriented information system for idiopathic scoliosis visualization and monitoring", *Journal of Computer Methods and Programs in Biomedicine*, Vol.108, No.-, pp. 736-749, ISSN -, Doi 10.1016/j.cmpb.2012.04.008, 2012.
140. Hilohi C., Untaru M., Soare I., Druța Gh., „*Metode si mijloace de incercare a automobilelor*”, Editura Tehnică București, 1982.
141. Hinza B., Seidel H., „*The Significance Of Using Anthropometric Parameters And Postures Of European Drivers As A Database For Finite-Element Models When Calculating Spinal Forces During Whole-Body Vibration Exposure*”, *International Journal Of Industrial Ergonomics*, Elsevier, 2008.
142. Kolich M., „*A conceptual framework proposed to formalize the scientific investigation of automobile seat comfort*”, *Applied Ergonomics*, Elsevier, 2008.

143. Kulcsar R. M.; Madaras L.; "Ergonomical study regarding the effects of the inertia and centrifugal forces on the driver", MTM & Robotics 2012, The Joint International Conference of the XI International Conference on Mechanisms and Mechanical Transmissions (MTM) and the International Conference on Robotics (Robotics'12), Clermont-Ferrand, France, June 6-8, 2012 Applied Mechanics and Materials, Vol. 162, Mechanisms, Mechanical Transmissions and Robotics, ISBN-13:978-3-03785-395-5, pp. 84-91.
144. Muksian R., Nash C.D.Jr. "A Model For The Response Of Seated Humans To Sinusoidal Displacements Of The Seat", J. Biomechanics, Vol.7, Pp 209-215, Pergamon Press, 1974.
145. Tae-Yun Koo¹, Kee-Jun Park, „A Study On Driver’s Workload Of Telematics Using A Driving Simulator: A Comparison Among Information Modalities”, International Journal Of Precision Engineering And Manufacturing Vol. 10, No. 3, Pp. 59-63, 2009.
146. Tanasoiu Aurelia, Copaci Ion, "On The Reduction Of Accelerations Transmitted To Transported Freight For The 4-Axle Platform Car With Mobile Cover", Wseas Transactions On Applied And Theoretical Mechanics, Volume 5, 2010, Issn: 1991-8747, E-Issn: 2224-3429.
147. Witoldpawlus, Hamid Reza Karimi, Kjell G. Robbersmyr, "Ahead Prediction Of Kinematics Of Vehicles Under Various Collision Circumstances By Application Of 149. Armax Autoregressive Model", Wseas Transactions On Applied And Theoretical Mechanics, Volume 6, 2011, Issn: 1991-8747, E-Issn: 2224-3429.
148. Witoldpawlus, Jan Eivind Nielsen, Hamid Reza Karimi, Kjell Gunnar Robbersmyr, "Development Of Mathematical Models For Analysis Of A Vehicle Crash", Wseas Transactions On Applied And Theoretical Mechanics, Volume 5, 2010, Issn: 1991-8747, E-Issn: 2224-3429.
149. Argeşanu Veronica, "Ergonomia echipamentelor și departamentelor medicale" Editura Eurostampa, Timișoara 2004.
150. Diana E. De Carvalho, Jack P. Callaghan, „Influence of automobile seat lumbar support prominence on spine and pelvic postures: A radiological investigation”, Applied Ergonomics, Elsevier, 2012.
151. Seokhee Naa, Sunghyun Limb, Hwa-Soon Choia, Min K. Chung, „Evaluation of driver’s discomfort and postural change using dynamic body pressure distribution”, International Journal of Industrial Ergonomics, Elsevier, 2005.
152. VerveraM., R. de Langea, J. van Hoofa, J.S.H.M. Wismans, „Aspects of seat modelling for seating comfort analysis”, Applied Ergonomics, Elsevier, 2005.
153. Zenk R., Franz M., Bubb H., Vink P., "Technical note: Spine loading in automotive seating", Applied Ergonomics, Elsevier, 2012.
154. *** <https://learn.adafruit.com/force-sensitive-resistor-fsr/>
155. Argesanu, V. , Kulcsar R. M. , Borozan I. S. , Jula M. , Cukovic S. , Bota E. , "The drivers spine analytical model" Intelligent Systems and Informatics (SISY), 2014 IEEE 12th International Symposium 11-13 Sept. 2014 Subotica;
156. Cacciabue P. C., Carsten O., „A simple model of driver behaviour to sustain design and safety assessment of automated systems in automotive environments”, Applied Ergonomics, Elsevier, 2010.
157. Galasso, A. "Experiences in modelling vibroacoustics for the automotive prototyping", Proceedings of the vibro-acoustic users conference, Belgium, january 29 –30, 2003.

158. Goran Devedžić, Saša Ćuković, Vanja Luković, Danijela Milošević, K. Subburaj, Tanja Luković, "ScolioMedIS: Web-oriented information system for idiopathic scoliosis visualization and monitoring", *Journal of Computer Methods and Programs in Biomedicine*, Vol.108, No.-, pp. 736-749, ISSN -, Doi 10.1016/j.cmpb.2012.04.008, 2012.
159. Grujicic M., Pandurangan B., ş.a. "Seat-cushion and soft-tissue material modeling and a finite element investigation of the seating comfort for passenger-vehicle occupants", *Materials and Design*, Elsevier, 2009.
160. Grujicic M., Pandurangan B., ş.a. "Musculoskeletal computational analysis of the influence of car-seat design/ adjustments on long-distance driving fatigue", *International Journal of Industrial Ergonomics*, Elsevier, 2010.
161. Gyouhyung K., Maury A., „Driver sitting comfort and discomfort (part II): Relationships with and prediction from interface pressure", *International Journal of Industrial Ergonomics*, Elsevier, 2008.
162. Alexopoulos E.C.; Stathi I.C.; Charizani F. (2004). *Prevalence of musculoskeletal disorders in dentists*, *BMC Musculoskelet Disord*; 5: 16.
163. Baladowski M.; Kotowicz-Gears A.; Jaworski P., (2/2007). *Lighting and its role in the Ergonomics of Dental Team Work*, *Ace of Dentistry*, pp. XII-XIV.
164. Ergonomics and Disability Support Advisory Committee (EDSAC) to the Council on Dental Practice (CDP). *An introduction to ergonomics: risk factors, MSDs, approaches and interventions*. American Dental Association;2004.
165. Houglum P.A.; Perrin D.H. (2005). *Therapeutic exercise for musculoskeletal injuries Second Edition*, *Human Kinetics*, pp 325.
166. Podariu A.C., Jumanca D, Găluşcan A., Văcaru R., Muntean R.(2003). *Treaty of preventive dentistry*, Editor Waldpress, Timișoara.
167. Sbenghe T. (2002). *Movement science*, Ed. Medicală, Bucuresti.
168. ***<http://www.diasu.com/home.html>, Accesed: 03.2013.
169. Fu Xing Li ,The Applied Research of Ergonomics in Lying Plate of Repair, *Industrial Engineering, Product Design, Numerical Modelling and Simulation*, August 2014
170. Chun Lei Sang, Jin Dong Ren, Yong Qing Liu, Meng Dong Mi, Shi Hai Li, Xiao Xian Gao , *Development of an Adjustable Physical Mockup Used for Design Validation of Passenger Car Ergonomics and Interiors*, *Product Design and Engineering Management*, January 2013
171. J.S. Mohamed Ali, F. Fatin Bazilah , *Mirrorless Car: A Feasibility Study, Crash and Safety*, *Transportation and Ergonomics*, October 2014
172. Pu Wang, Tao Huang , *Construction of China Railway Freight Car Color Coating Genealogy*, *Advanced Design, Modelling, Analysis Science in Manufacturing Technologies*, December 2012
173. Xiao Ming Du, Jin Dong Ren, Yong Qing Liu, Zhong Xian Chen, Shi Hai Li, Chun Lei Sang, *Cab Conceptual Design for the Equipment System Used for Passenger Car Ergonomic Design and Evaluation*, *Product Design and Development*, November 2012
174. Raul Miklos Kulcsar, Lucian Madaras, Inocentiu Maniu, Ion Borozan, Veronica Argesanu, *Ergonomic Study Regarding the Effects of the Inertia and Centrifugal Forces on the Driver*, *Mechanical Transmissions*, March 2012
175. Darliana Mohamad, Baba Md Deros, Dzuraidah Abdul Wahab, *Development of 2D Image Capture Method Software for Recognizing Drivers' Postural Angles*, April 2012

176. P. Gokila, P. Suresh, Parameters Influenced in Car Seat Design from Ergonomic Perspectives - A Review, Labour Safety, Ergonomics, Reliability and Safety of Machines and Mechanisms, July 2014
177. Nan Ding, Yue Tong Chen, Can Huan Li, Jia Ning Lei, Jin He Qian, Bo Yang, Driving Position Comfortability Design of a Low Aerodynamic Drag Energy Saving Car, Mechanics and Dynamics, Applied Mechanics, Advanced Development in Manufacturing and Industry Engineering, August 2014
178. M.S.S. Mohamed, B.M.T Shamsul, R. Rahman, Nawal Aswan Abdul Jalil, Issues Surrounding Car Center Stack Designs in Malaysia: An Exploratory Study, Ergonomics in Design, May 2015
179. Yu Zhong Chen, Yong Qin Feng, Yan Yin, Xiao Rui Zhang, Improvement in Design and Manufacture of Automobile Based on Ergonomics Theory, Vehicle Engineering and Carrier Operation Engineering, January 2014
180. Ahmad Rasdan Ismail, Siti Nuratikah Abdullah, Ezrin Hani Sukadarin, Baba Md Deros , Ergonomics Assessment of Seat Design Based on Buttock Pressure and Anthropometrics Data, Transport Ergonomics , December 2013
181. D.D.I Daruis, B.M. Deros, M.J.M. Nor, M. Hosseini Fouladi , Relationship between Objective and Subjective Methods in Evaluating Static Discomfort of Car Driver Seat, Computer-Aided Design, Manufacturing and Engineering, January 2012
182. Li Jia Li, Li Li Zhao, Yu Yang Dai , Analysis and Research on Driver's Comfort in the Process of Getting on and off the Car, Materials Engineering, Modeling and Others, September 2012
183. K. Syakirah, A.A. Faieza, M. Rosnah Yusuff , Development of an Ergonomic Infant Seat with Restraint System for Use in an Aircraft , Vehicles Engineering, June 2014
184. Duan Shu Song , Application and Research of Chinese Cultural Elements on Concept Car Design, Advanced Technologies in Mechanical and Manufacturing Engineering, January 2013
185. E.S. Esakki Raj, Tamil Selvan, S. Thanabalan, Joseph Mervin, S. Anish, Design and Analysis of SUPRA AISI 1018 Carbon Steel Car Frame Using ANSYS, Developments in Automobile, July 2014
186. Li Jia Li, Li Li Zhao , Simulation and Research on Man-Machine Engineering of Trunk Lid, Modeling, Analysis and Simulation, June 2012
187. Ahmad Rasdan Ismail, Mohd Zaki Nuawi, Nur Farhana Kamaruddin, Mohd Nizam Ab Rahman, Whole Body Vibrations Exposure to Malaysian Driver Using Novel IKaz Method, April 2012
188. Zhen Wang, Fang Bian, Ping Li , Designing of Vehicle Operation and Control Based on Semiotics, Applied Mechanics, Mechanical Engineering, Mechatronics, Automation and Control, September 2014
189. Katarína Senderská, Albert Mareš, Jozef Kováč , Application of Virtual Reality Means in Dashboard Function and Dashboard Assembly Fixture Ergonomic Analysis, Researching and Designing of Industrial and Manufacturing Systems, December 2014
190. Qiu Lei Du, Li Ai Pan, Design Research of Novel Self-Propelled Air Railcar, Product Design, February 2014
191. Mohamad Syafiq Aizat Hussin, Raja Ariffin Raja Ghazilla, Mirta Widia , Pilot Investigation on the Driving Posture Comfort among Malaysian Drivers, Product Design, Manufacturing and Analysis, December 2012
192. Nor Kamaliana Khamis, Baba Md Deros, Mohd Zaki Nuawi , Understanding the Effect of Discomfort Level towards Motorcycle Riders among Teenagers: A Preliminary Study, Noise, Monitoring, Vibration and Harshness, October 2014
193. Raul Miklos Kulcsar, Ion Borozan, Veronica Argesanu, Inocentiu Maniu, Mihaela Jula, Felicia Streian, Tiberiu Puta, Adrian Nagel, Modeling, Simulation and Experimental Determination of the Spine Muscle's Activities of the Driver, Innovative Techniques of Concurrent Engineering in Process of Product Design , May 2015

194. Kang Hui, Li Jing , Kansei Engineering in Human Engineering Theory and Application, Industrial Design and Engineering Management, October 2013
195. M.S. Syed Mohamed, Muhammad Nur Hakam Basiri, Working Posture Assessment in a Small and Medium Industry (SMI): Automotive Repair Facility, Ergonomics in Design, May 2015
196. Zhuo Li, Yin Jin, J. Hou, Classification Syllogism in the Farm Vehicle Design Based on the Kansei Engineering, June 2008
197. Yue Zeng Xu, The Optimal Design of Mechanical Transmission Reliability, Modeling, Analysis and Simulation of Manufacturing Processes, January 2012
198. Rui Li, Li Xin Guo, The Research of Vehicle Seat Dynamic Comfort Characteristic, Applied Mechanics and Advances in Mechanical Engineering, February 2013
199. Qiu Lei Du, Li Ai Pan , Design Research of Novel Self-Propelled Air Railcar, Product Design, February 2014
200. Mohamad Syafiq Aizat Hussin, Raja Ariffin Raja Ghazilla, Mirta Widia , Pilot Investigation on the Driving Posture Comfort among Malaysian Drivers, Product Design, Manufacturing and Analysis, December 2012
201. Nor Kamaliana Khamis, Baba Md Deros, Mohd Zaki Nuawi , Understanding the Effect of Discomfort Level towards Motorcycle Riders among Teenagers: A Preliminary Study, Noise, Monitoring, Vibration and Harshness, October 2014
202. M.S. Syed Mohamed, Muhammad Nur Hakam Basiri, Working Posture Assessment in a Small and Medium Industry (SMI): Automotive Repair Facility, Ergonomics in Design, May 2015
203. Zhuo Li, Yin Jin, J. Hou, Classification Syllogism in the Farm Vehicle Design Based on the Kansei Engineering, June 2008
204. Yue Zeng Xu, The Optimal Design of Mechanical Transmission Reliability, Modeling, Analysis and Simulation of Manufacturing Processes, January 2012
205. Rui Li, Li Xin Guo, The Research of Vehicle Seat Dynamic Comfort Characteristic, Applied Mechanics and Advances in Mechanical Engineering, February 2013
206. Lei Shen, Xue Huan Jiang , The New Design of Children Safety Device in the Car, April 2011
207. Qiu Lei Du, Xiao Wei Jiang , Virtual Shaping Design of Beach Bike, Industry Technology, Material Engineering and Dynamic System, January 2012
208. Ahmad Kadri Junoh, Zulkifli Mohd Nopiah, Ahmad Kamal Ariffin , Application of Feed-Forward Neural Networks for Classifying Acoustics Levels in Vehicle Cabin, Vehicle Noise, Vibration and Harshness, December 2013
209. Xiao Yang Pan, Xiao Jia Wei , Virtual Reality Technology Applied in Automobile Modeling Design, Industrial Engineering, Product Design, Numerical Modelling and Simulation, August 2014
210. Li Ming Fu, Hai Yang Yu, Ming Yang Sun, Jia Xu Fan , The Automobile Intelligent Dashboard Design to Enhance Driving Safety, Mechanical Engineering, Measurement, Control and Automatisations, December 2014
211. Ramona Nagy, Karoly Menyhardt , Vibration Aspects on Local Light Rail Transportation, Vibration Problems in Industrial Processes, October 2015
212. Yun Liu, Zhi Xiang Hou, Dan Yu, Yi Hu Wu , Research on Forecasting the State of Driver Based on Chaos Theory, February 2011
213. Li Chen, Wei Feng Hu , Multivariate Index Evaluation Model for Product Form by Integration with Manufacturer Performance and its Application in Car Interior, Innovative Design Methodology, May 2013

214. N.K. Khamis, Baba M. Deros, Mohd Zaki Nuawi , A Preliminary Study on Motorcyclists' Perceptions of Fatigue Risk Factors, Comfort and Ergonomics, December 2013
215. Xiao Jing Chen, Chun Hua Qi, Shou Lin Zhu, Ming Xing Gao, Feng Yang , On Study of Driver's Shoulder Fatigue in Manual and Automatic on Grassland Highway, Traffic, Road and Transportation Engineering, September 2014
216. Mihaela Baritz, Balcu Ioan, Cotoros Diana, Stanciu Anca, The Automotive Vibrations effect on the comfort degree determined at the level of foot-shoe composite structure, Materials in product manufacturing, properties and technological characteristics.
217. Muammar Quadafi, Ilyas Rabihah, Fridaus Mohd, Nurulhana Borhan, Review of the Application of Driving Simulators for Research and Training Activities in Malaysia, April 2012
218. P. Vantomme, P. Deprez, A. Placet, D. Gaillot, Friction study of carbon-silicon carbide couples, Proceedings of the Institution of Mechanical Engineers, Journal of Engineering Tribology, Vol.214, No.5, 2000, pp. 485-492.
219. E. V. Wilms, H. Cohen, The motion of two axi-symmetric rigid bodies with friction coupling, Zeitschrift für Angewandte Mathematik und Physik (ZAMP), Vol.53, No.1, 2002, pp. 167-172.
220. M. J. Nunnery, Light and heavy vehicle technology, Elsevier Ltd. , 4th edition, 2007.